

# Low-Speed Wind-Tunnel Investigation of the Stability and Control Characteristics of a Series of Flying Wings With Sweep Angles of $70^\circ$

---

*Holly M. Ross*  
*Langley Research Center • Hampton, Virginia*

*Scott P. Fears*  
*Lockheed Engineering & Sciences Company • Hampton, Virginia*

*Thomas M. Moul*  
*Langley Research Center • Hampton, Virginia*

Available electronically at the following URL address: <http://techreports.larc.nasa.gov/ltrs/ltrs.html>

Printed copies available from the following:

NASA Center for AeroSpace Information  
800 Elkridge Landing Road  
Linthicum Heights, MD 21090-2934  
(301) 621-0390

National Technical Information Service (NTIS)  
5285 Port Royal Road  
Springfield, VA 22161-2171  
(703) 487-4650

## Summary

A wind-tunnel investigation was conducted in the Langley 12-Foot Low-Speed Tunnel to study the low-speed stability and control characteristics of a series of four flying wings over an extended range of angle of attack ( $-8^\circ$  to  $48^\circ$ ). Because of the current emphasis on reducing the radar cross section (RCS) of new military aircraft, the planform of each wing was composed of lines swept at a relatively high angle of  $70^\circ$ , and all the trailing edges and control surface hinge lines were aligned with one of the two leading edges. Three arrow planforms with different aspect ratios and one diamond planform were tested. The models incorporated leading-edge flaps for improved longitudinal characteristics and lateral stability and had three sets of trailing-edge flaps that were deflected differentially for roll control, symmetrically for pitch control, and in a split fashion for yaw control. Three top body widths and two sizes of twin vertical tails were also tested on each model. A large aerodynamic database was compiled that could be used to evaluate some of the trade-offs involved in the design of a configuration with a reduced RCS and good flight dynamic characteristics.

The results of the investigation indicate that the arrow wings experienced a pitch-up that became more severe as aspect ratio was increased. This pitch-up was reduced or delayed by deflecting the leading-edge flaps. When deflected symmetrically, the inboard and middle trailing-edge flaps produced small increments in pitching moment, especially in the nose-down direction. Despite this limited control, each of the wings could be statically trimmed over a large angle-of-attack range, but additional pitch control power would likely be needed to provide these wings with sufficient control margin for dynamic situations such as maneuvering or countering turbulence. An additional limit on the pitch control provided by the flaps may be imposed by the need to budget the amount of flap deflection available for each type of control (pitch, roll, or yaw). For these reasons, these wings would probably require redesigned flaps or additional pitch control devices to achieve desired levels of pitch control.

When the vertical tails were not used, each of the wings exhibited neutral or unstable directional stability and was laterally stable for angles of attack below maximum lift. However, directional and lateral stability were significantly reduced near maximum lift on each of the wings. Increases in aspect ratio reduced lateral stability throughout the test angle-of-attack range. Lateral and directional stability were reduced by adding top bodies or deflecting the leading-edge flaps. Directional stability was improved by adding twin vertical tails.

For each of the wings, differential deflections of the trailing-edge flaps provided small levels of roll control that were relatively invariant with angle of attack, and split deflections of these flaps produced small yawing moments on some of the configurations. On the forward-swept outboard flaps, the side force produced a yawing-moment increment that opposed the yawing moment produced by the drag on the flap. In contrast, the side force generated by split deflection of the rearward-swept middle flaps produced yawing-moment increments in the same direction as the drag, and the middle flaps therefore provided more effective yaw control than the outboard flaps. Supplemental yaw control could be obtained from deflections of the twin vertical tails.

## Introduction

Recent advances in low-observables technology, which increase the effectiveness and survivability of military aircraft, have strongly influenced most new designs. When attempting to achieve low observability, some or all of the aircraft signatures (radar, infrared, visual, or acoustic) may be considered, depending on mission requirements. One primary method of reducing radar observability is to decrease the radar cross section (RCS) of the aircraft by appropriately tailoring the external contours of the configuration. However, when these reduced-RCS shaping constraints are emphasized, the resulting aircraft may have an unconventional forebody shape, wing planform, or tail geometry. Each of these design features can have a large influence on the stability and control characteristics of the configuration; thus, a potential conflict exists between achieving a reduced RCS and achieving good flight dynamic characteristics. If the aircraft is a fighter, the goal to maneuver effectively during close-in engagements will require good stability and control characteristics for angles of attack up to and beyond maximum lift. As a result, designers will be required to balance the attributes of maneuverability and low observability to create a fighter that will be successful in both close-in and beyond-visual-range engagements. For other types of aircraft, the stability and control requirements may be less stringent, and the designs may be more strongly influenced by low-observability considerations.

This study consists of an investigation of flying wing candidates for aircraft with reduced RCS. The wing planforms have highly swept leading and trailing edges, with the trailing edges and control surface hinge lines aligned with one of the two leading edges. The wings were divided into three groups corresponding to the sweep angles of the leading and trailing edges ( $50^\circ$ ,  $60^\circ$ , and  $70^\circ$ ). Each group consisted of a diamond planform and three arrow planforms of different aspect ratio. As a

result of the high sweep angles, some of the planforms were somewhat unconventional in appearance.

This report presents the results of a static low-speed wind-tunnel investigation of the group of flying wings with sweep angles of  $70^\circ$ . The results for the wings with sweep angles of  $60^\circ$  and  $50^\circ$  are reported in references 1 and 2, respectively. Tests were conducted to determine the low-speed stability and control characteristics of the basic wing planforms over a wide range of angle of attack and angle of sideslip. In addition, several control concepts, a broad matrix of control settings, differences in top body width, and two sizes of twin vertical tails were also tested. The data obtained on these wing planforms contribute to an aerodynamic database that could be used in defining some of the trade-offs associated with designing for both reduced RCS and good stability and control characteristics.

## Symbols

All longitudinal forces and moments are referred to the stability-axis system, and all lateral-directional forces and moments are referred to the body-axis system (fig. 1). The longitudinal location of the moment reference center (MRC) varied among the different wings. This position was chosen such that each configuration would have neutral longitudinal stability at angles of attack near  $0^\circ$  when all the controls were undeflected (table I). The MRC vertical position was fixed at 1.87 in. (2.51 percent of root chord) below the wing horizontal plane on all the configurations. The total planform area (table I) was used to nondimensionalize the force and moment data.

$b$	wingspan, ft
$C_D$	drag coefficient, $\frac{\text{Drag force}}{\bar{q}S}$
$C_L$	lift coefficient, $\frac{\text{Lift force}}{\bar{q}S}$
$C_l$	rolling-moment coefficient, $\frac{\text{Rolling moment}}{\bar{q}Sb}$
$C_m$	pitching-moment coefficient, $\frac{\text{Pitching moment}}{\bar{q}S\bar{c}}$
$C_n$	yawing-moment coefficient, $\frac{\text{Yawing moment}}{\bar{q}Sb}$
$C_Y$	side-force coefficient, $\frac{\text{Side force}}{\bar{q}S}$
$\bar{c}$	mean aerodynamic chord (based on entire planform), ft
$\bar{q}$	free-stream dynamic pressure, lb/ft <sup>2</sup>
$S$	reference area (based on entire planform), ft <sup>2</sup>

$X, Y, Z$	longitudinal, lateral, and vertical body axis, respectively
$\alpha$	angle of attack, deg
$\beta$	angle of sideslip, deg
$\Delta C_l$	incremental rolling-moment coefficient, $C_{l,\text{control deflected}} - C_{l,\text{control undeflected}}$
$\Delta C_n$	incremental yawing-moment coefficient, $C_{n,\text{control deflected}} - C_{n,\text{control undeflected}}$
$\Delta C_Y$	incremental side-force coefficient, $C_{Y,\text{control deflected}} - C_{Y,\text{control undeflected}}$
$\delta_{a,IB}$	differential deflection angle of inboard trailing-edge flaps based on equal and opposite deflection, positive with trailing edge down on right wing, measured normal to hinge line, deg
$\delta_{a,MID}$	differential deflection angle of middle trailing-edge flaps based on equal and opposite deflection, positive with trailing edge down on right wing, measured normal to hinge line, deg
$\delta_{a,OB}$	differential deflection angle of outboard trailing-edge flaps based on equal and opposite deflection, positive with trailing edge down on right wing, measured normal to hinge line, deg
$\delta_{bf}$	symmetric deflection angle of body flaps, positive with trailing edge down, measured normal to hinge line, deg
$\delta_{f,IB}$	symmetric deflection angle of inboard trailing-edge flaps, positive with trailing edge down, measured normal to hinge line, deg
$\delta_{f,MID}$	symmetric deflection angle of middle trailing-edge flaps, positive with trailing edge down, measured normal to hinge line, deg
$\delta_{f,OB}$	symmetric deflection angle of outboard trailing-edge flaps, positive with trailing edge down, measured normal to hinge line, deg
$\delta_{LEF}$	leading-edge flap deflection angle, positive with leading edge down, measured normal to hinge line, deg
$\delta_r$	symmetric vertical tail deflection angle, positive with trailing edge left, deg
$\delta_{s,MID}$	split deflection angle of middle trailing-edge flaps, positive when deployed on left wing, measured normal to hinge line, deg

$\delta_{s,OB}$  split deflection angle of outboard trailing-edge flaps, positive when deployed on left wing, measured normal to hinge line, deg

Derivatives:

$$C_{l_\beta} \quad \text{lateral stability parameter, } \frac{\partial C_l}{\partial \beta},$$

$$\frac{(C_l)_{\beta=5} - (C_l)_{\beta=-5}}{10^\circ}, \text{ per deg}$$

$$C_{n_\beta} \quad \text{directional stability parameter, } \frac{\partial C_n}{\partial \beta},$$

$$\frac{(C_n)_{\beta=5} - (C_n)_{\beta=-5}}{10^\circ}, \text{ per deg}$$

$$C_{Y_\beta} \quad \text{side-force parameter, } \frac{\partial C_Y}{\partial \beta},$$

$$\frac{(C_Y)_{\beta=5} - (C_Y)_{\beta=-5}}{10^\circ}, \text{ per deg}$$

Abbreviations:

MRC moment reference center

RCS radar cross section

## Model Description

Four flying-wing models (three arrow-wing planforms and one diamond planform) that each had leading edges, trailing edges, and control surface hinge lines swept at  $70^\circ$  (fig. 2) were tested. Given the relatively high sweep angle, initial sizing analysis indicated that arrow wings with aspect ratios between 2.0 and 3.0 could produce viable configurations. As a result, aspect ratios of 3.0 (Wing 5), 2.5 (Wing 6), and 2.0 (Wing 7) were chosen for the arrow planforms (figs. 3 to 5). A set of arrow wings swept  $60^\circ$  (Wings 1, 2, and 3) and a set of arrow wings swept  $50^\circ$  (Wings 9, 10, and 11) with these same aspect ratios were tested previously (refs. 1 and 2, respectively). Unlike the aerodynamic data that were nondimensionalized with the entire planform area, these aspect ratios were computed by using the trapezoidal areas shown in figure 2(b). For Wing 5, the three aftmost points on the planform extended back the same distance (fig. 3). During formulation of the remaining planforms, the overall length was held constant, and the trapezoidal areas of Wings 6 and 7 were made approximately equal to that of Wing 5. Consequently, as aspect ratio was decreased on the arrow wings, the span was reduced and the tip chord was increased to maintain approximately the same trapezoidal area. The dimensions of the dia-

mond wing (fig. 6) were dictated by the overall length and the leading- and trailing-edge sweep angles and resulted in an aspect ratio of 0.73. From a geometric point of view, the arrow planforms can be considered to be built up from the diamond planform by the addition of outboard panels having the same sweep angles as the diamond planform (fig. 2). Flat plate models of the basic planforms were constructed from 3/4-in. plywood, and the leading and trailing edges were beveled at a  $13^\circ$  half-angle. Table I shows the geometric characteristics for each wing.

All four wings incorporated leading-edge flaps for improved longitudinal characteristics and increased roll stability at high angles of attack. The chord length of these flaps was the same on all the wings, and the hinge line was located along the wing leading-edge bevel line (fig. 2). These flaps were tested at deflection angles of  $15^\circ$ ,  $30^\circ$ ,  $45^\circ$ , and  $60^\circ$ . There were three sets of trailing-edge flaps, designated inboard (IB), middle (MID), and outboard (OB), on each wing for roll, pitch, and yaw control (figs. 3 to 6). For the arrow wings, the chord length of the trailing-edge flaps was 30 percent of the distance between the leading and trailing edges on the outboard section of the wing. For the diamond wing, the trailing-edge flaps had the same chord length as those on the low-aspect-ratio arrow wing (Wing 7). The trailing-edge flaps were deflected symmetrically ( $-30^\circ$ ,  $-15^\circ$ ,  $15^\circ$ , and  $30^\circ$ ) for pitch control and differentially ( $-30^\circ$ ) for roll control. Split deflection of these flaps (to be discussed subsequently) was tested as a means to provide yaw control.

To provide supplemental nose-down pitch control, body flaps were tested by using model parts constructed of sheet metal (fig. 7). The body flaps were mounted on the underside of the wing inboard of the trailing-edge flaps. The inboard corners of the undeflected body flaps were positioned on the centerline with their hinge line coinciding with the hinge line of the trailing-edge flaps (fig. 7). Symmetric downward deflections of  $58^\circ$  and  $73^\circ$  were tested on each wing. The sheet metal part modeled the bottom surface of a beveled body flap (fig. 8). Because these models had a trailing-edge bevel half-angle of  $13^\circ$ , the  $60^\circ$  bend in the sheet metal part represented a  $73^\circ$  deflection of the simulated beveled flap (fig. 8).

As noted previously, to provide yaw control split deflections of the trailing-edge flaps were tested. This concept involves a given flap separating into top and bottom halves such that the top half deflects upward and the bottom half deflects downward. These deflections would be made on the right or left wing only, thereby creating an unbalanced drag force and an associated yawing moment. During these tests, sheet metal pieces were

mounted on the underside of the wing beneath the middle or outboard trailing-edge flaps to represent the lower half of a split deflection. The upper half was simulated by deflecting the trailing-edge flap upward at the same angle (fig. 9). The tested deflections (43° and 73°) were measured similar to the body flap deflections. For these tests, the split trailing-edge flaps were tested on the right wing.

Three top body shapes were tested on the upper surface of each wing in conjunction with a single bottom body that covered the balance (fig. 10). Some testing was done without a top body, but the bottom body was always on the wing to shield the balance from the air-flow. The length and height of the top bodies were kept constant, but the width was varied to obtain the three top shapes (wide, medium, and narrow). The resulting cross-sectional shapes were semielliptical for the wide and narrow bodies and semicircular for the medium body (fig. 10). When installed, the front tip of the top bodies was 5 in. (6.7 percent of root chord) aft of the leading edge of the wing, and the rear tip was the same distance forward of the wing trailing edge. The front tip of the bottom body was also 5 in. behind the leading edge, and the rear tip was 22.43 in. (30.1 percent of root chord) forward of the wing trailing edge.

Two sets of vertical tails (small and medium) were tested (fig. 11). The planform of the tails was a 30°-60°-90° triangle with the leading edge swept 60° (fig. 12). The tails were sized such that the medium tail had twice the area of the small tail (table I). They were mounted in a twin tail configuration with zero cant and toe angle and were deflected as all-moving tails for directional control about a vertical axis located at one-half the vertical tail root chord. On many existing reduced-RCS aircraft (F-117, YF-22, and YF-23), the tails are canted to reduce their contributions to the total aircraft RCS from certain aspects. However, during this study, the tails were uncanted so that the maximum levels of directional stability and control available from the triangular planforms could be determined. The vertical tails were longitudinally positioned on the wing so that the aftmost points of the undeflected tails were at the wing trailing edge (fig. 13).

## Test Techniques and Conditions

The aerodynamic testing was performed in the Langley 12-Foot Low-Speed Tunnel. The model and balance were mounted in the test section on a sting and C-strut arrangement (fig. 14). The tests were conducted at a free-stream dynamic pressure of 4 lb/ft<sup>2</sup>, which cor-

responds to a test Reynolds number of  $1.26 \times 10^6$  for Wing 5,  $1.29 \times 10^6$  for Wing 6,  $1.34 \times 10^6$  for Wing 7, and  $1.52 \times 10^6$  for Wing 8 based on the mean aerodynamic chord of each wing. A six-component, internally mounted strain gauge balance was used to measure the aerodynamic loads. The static force and moment data were measured over an angle-of-attack range of -8° to 48° and over a sideslip range of -15° to 15°. The data at sideslip angles of -5° and 5° were used to calculate the lateral-directional stability derivatives ( $C_{l_\beta}$ ,  $C_{n_\beta}$ , and  $C_{Y_\beta}$ ) by means of a linear fit between these two angles. Flow upwash corrections were included during the angle-of-attack calibration, but no corrections for flow side-wash were needed. Corrections for wall effects or test section blockage were not included.

## Results and Discussion

### Longitudinal Stability Characteristics

The longitudinal stability characteristics of the four flying wings are presented in the following figures.

Figure

Wing planform:	
Top body off, $\delta_{LEF} = 0^\circ$ .....	15
Top body off, $\delta_{LEF} = 45^\circ$ .....	16
Wide top body on, $\delta_{LEF} = 0^\circ$ .....	17
Wide top body on, $\delta_{LEF} = 45^\circ$ .....	18
Top bodies:	
$\delta_{LEF} = 0^\circ$ :	
Wing 5 .....	19
Wing 6 .....	20
Wing 7 .....	21
Wing 8 .....	22
$\delta_{LEF} = 45^\circ$ :	
Wing 5 .....	23
Wing 6 .....	24
Wing 7 .....	25
Wing 8 .....	26
Leading-edge flap deflections:	
Top body off:	
Wing 5 .....	27
Wing 6 .....	28
Wing 7 .....	29
Wing 8 .....	30
Wide top body on:	
Wing 5 .....	31
Wing 6 .....	32
Wing 7 .....	33
Wing 8 .....	34

Vertical tails:

Narrow top body on,  $\delta_{LEF} = 45^\circ$ :

Wing 5.....	35
Wing 6.....	36
Wing 7.....	37
Wing 8.....	38

**Wing planform.** Comparisons of the longitudinal characteristics of the four wings with the leading-edge flaps deflected and undeflected with the wide top body on and off are presented in figures 15 to 18. In general, the maximum lift coefficient was about 1.1 for the arrow wings ( $\alpha \approx 36^\circ$ ) and about 1.0 for the diamond wing ( $\alpha \approx 40^\circ$ ). The lift curve slopes of the arrow wings (trapezoidal aspect ratios of 3.0, 2.5, and 2.0, which correspond to Wings 5, 6, and 7, respectively) were fairly similar. However, the lift curve slope of the diamond wing (aspect ratio of 0.73, Wing 8) was considerably lower at angles of attack below  $8^\circ$ . Therefore, the diamond wing yielded a lower lift coefficient at a given angle of attack than the arrow wings for angles of attack below maximum lift.

As mentioned previously, the moment reference centers (figs. 3 to 6 and table I) were chosen so that each configuration with the wide top body on (fig. 17) would have neutral longitudinal stability at angles of attack near  $0^\circ$  when all the controls were undeflected. The arrow wings experienced a pitch-up for angles of attack between  $10^\circ$  and  $18^\circ$  (depending on planform and leading-edge flap deflection), and the effects of pitch-up became larger as the aspect ratio increased. For these planforms, larger aspect ratios were obtained by adding outboard wing panels of increasing size to the basic diamond shape. Previous studies have shown that the onset of separation on the outboard portions of swept wings contributes to a reduction in longitudinal stability that is sometimes called pitch-up (refs. 3 and 4). For this reason, the wings with the higher aspect ratios were more susceptible to pitch-up effects because the outboard portions of the wings were larger and farther aft (behind the MRC). In contrast, the diamond wing, which did not have these outboard wing panels, actually experienced a slight pitch-down at comparable angles of attack.

**Top bodies.** The effect of the various top bodies (fig. 10) on the longitudinal characteristics of the different wings is shown in figures 19 to 26. With the leading-edge flaps undeflected, the models were tested with the top body off and with the wide body on (figs. 19 to 22). Adding the wide top body generally reduced lift at angles of attack below and near maximum lift. Above maximum lift, lift was increased by adding the wide top body. The angle of attack for maximum lift was also slightly

increased when the wide top body was used. Adding of the wide top body resulted in a nose down increment in pitching moment for each of the wings. As a result, the onset of the pitch-up of the arrow wings was delayed, and the magnitude of the resulting pitching moment was decreased.

With the leading-edge flaps deflected  $45^\circ$ , the models were tested with the top body removed and with each of the three top bodies (figs. 23 to 26). In general, the effect of the bodies on lift and pitching moment were similar to, but smaller in magnitude than, the effects that occurred when the leading-edge flaps were undeflected. As the body width was increased, the magnitude of the nose-down pitching-moment increment increased.

**Leading-edge flap deflections.** The effect of deflections of the leading-edge flaps on the longitudinal characteristics of the different wings is shown in figures 27 to 34. Data are shown for the four planforms with the top body removed in figures 27 to 30 ( $\delta_{LEF} = 0^\circ$  and  $45^\circ$ ) and with the wide top body on in figures 31 to 34 ( $\delta_{LEF} = 0^\circ, 15^\circ, 30^\circ, 45^\circ,$  and  $60^\circ$ ). The data show a typical effect of leading-edge flap deflections on very highly swept wings (ref. 4). For most of the configurations, deflecting these flaps reduced the lift coefficient at angles of attack below maximum lift. A nose-down pitching-moment increment was associated with these reductions in lift, reducing the effects of the pitch-up on the arrow wings. This pitching-moment increment also increased the angle of attack at which the arrow wings began to experience pitch-up effects by about  $8^\circ$ . The effects of leading-edge flap deflections on both lift and pitching moment were increased by using larger deflection angles.

**Vertical tails.** Figures 35 to 38 show the effect of the twin vertical tails (figs. 11 to 13) on the longitudinal characteristics of the four configurations with the narrow top body on and the leading-edge flaps deflected  $45^\circ$ . Adding the vertical tails reduced lift coefficient near maximum lift for each of the wings. This lift reduction was possibly due to the tails interfering with the leading-edge vortical flow on the upper surfaces of the wings, causing these vortices to burst prematurely at the higher angles of attack. A flow field investigation (flow visualization, laser Doppler velocimeter, pressure measurements, etc.) would be required to make this determination. The lift was further reduced as the size of the vertical tails was increased.

### Longitudinal Control Characteristics

The longitudinal control characteristics of the four flying wings are presented in the following figures.

Figure

Inboard trailing-edge flaps:

Wide top body on,  $\delta_{LEF} = 45^\circ$ :

Wing 5..... 39

Wing 6..... 40

Wing 7..... 41

Wing 8..... 42

Middle trailing-edge flaps:

Wide top body on,  $\delta_{LEF} = 45^\circ$ :

Wing 5..... 43

Wing 6..... 44

Wing 7..... 45

Wing 8..... 46

Inboard and middle trailing-edge flaps:

Wide top body on:

Wing 5,  $\delta_{LEF} = 0^\circ$ ..... 47

Wing 5,  $\delta_{LEF} = 45^\circ$ ..... 48

Wing 6,  $\delta_{LEF} = 45^\circ$ ..... 49

Wing 7,  $\delta_{LEF} = 0^\circ$ ..... 50

Wing 7,  $\delta_{LEF} = 45^\circ$ ..... 51

Wing 8,  $\delta_{LEF} = 0^\circ$ ..... 52

Wing 8,  $\delta_{LEF} = 45^\circ$ ..... 53

Maximum nose-down control:

Wide top body on,  $\delta_{LEF} = 45^\circ$ :

Wing 5..... 54

Wing 6..... 55

Wing 7..... 56

Wing 8..... 57

**Inboard trailing-edge flaps.** The longitudinal control effectiveness of symmetric deflections of the inboard trailing-edge flaps is shown in figures 39 to 42. At angles of attack below  $8^\circ$ , these flaps were essentially ineffective for longitudinal control. Above this angle of attack, these flaps produced small nose-up control increments on the arrow wings and small amounts of nose-up and nose-down control on the diamond wing. These results indicated a potential pitch-up problem for these configurations. The lack of nose-down control effectiveness could limit the maximum trim angle of attack if nose-down control was required for trim at the higher angles of attack, depending on the longitudinal stability level of the final design. The aforementioned insufficient control power combined with a stable, deep stall trim condition could result in a hung stall (fig. 41).

**Middle trailing-edge flaps.** Figures 43 to 46 show the longitudinal control effectiveness of symmetric deflections of the middle trailing-edge flaps. As with the inboard flaps, the middle flaps were essentially ineffective for longitudinal control at low angles of attack, but small amounts of nose-up control were produced by negative deflections at the higher angles of attack. These

control increments were smaller than those produced by the marginally effective inboard flaps on the arrow wings, despite the fact that the middle flaps were larger than the inboard flaps and had a longer longitudinal moment arm. For the diamond wing, the middle flaps produced slightly more lift than the inboard flaps, but there was less longitudinal control because the longitudinal moment arm of the middle flaps was shorter than that of the inboard flaps.

**Inboard and middle trailing-edge flaps.** The longitudinal control effectiveness produced when the inboard and middle trailing-edge flaps were deflected symmetrically is shown in figures 47 to 53. As with the individual deflections, these combined flap deflections produced minimal effectiveness at the lower angles of attack and moderate nose-up control effectiveness at the higher angles of attack. Nose-up control effectiveness at the intermediate deflections tested was relatively linear over most of the angle-of-attack range. For Wings 5, 7, and 8, multiple trailing-edge flap deflections were tested with the leading-edge flaps undeflected and deflected  $45^\circ$ . Deflecting the leading-edge flaps  $45^\circ$  did not significantly affect the control effectiveness produced by multiple deflections of the inboard and middle trailing-edge flaps.

Multiple symmetric deflections of the inboard and middle trailing-edge flaps involved moving a significant portion of the total wing area allocated for control. Despite this large area, the longitudinal control effectiveness was very small, especially in the nose-down direction. It should be noted that each of the wings could be statically trimmed over a large angle-of-attack range when the effect of the pitch-up was reduced by leading-edge flap deflections. However, additional pitch control power would likely be needed to provide these wings with sufficient control margin for situations such as maneuvering or countering turbulence (ref. 5). An additional limit on the pitch control provided by the flaps may be imposed by the need to budget the amount of flap deflection available for each type of control (pitch, roll, or yaw). If some portion of the total flap travel must be reserved for roll or yaw control, the remaining amount available for pitch control will be less than the maximum. For these reasons, these configurations would probably require redesigned flaps or additional pitch control devices to achieve desired levels of pitch control.

**Maximum nose-down control.** In addition to the trailing-edge flaps, each configuration also had body flaps on the bottom surface of the wing (fig. 8) that were intended to provide supplemental nose-down pitch control. The body flaps were deflected in combination with nose-down deflections of the trailing-edge flaps, and the

data are presented in figures 54 to 57. Deflections of the body flaps provided a small nose-down pitching increment that was relatively constant throughout the angle-of-attack range. Deflecting the body flaps from 58° to 73° did not produce any additional nose-down control. Symmetric deflections of the relatively small outboard trailing-edge flaps did not significantly increase the overall level of longitudinal control.

### Lateral-Directional Stability Characteristics

The lateral-directional aerodynamics and stability characteristics of the four flying wings are presented in the following figures.

	Figure
<b>Sideslip:</b>	
Wing 5, wide top body on:	
$\delta_{LEF} = 0^\circ$ , low angles of attack . . . . .	58
$\delta_{LEF} = 0^\circ$ , high angles of attack . . . . .	59
$\delta_{LEF} = 45^\circ$ , low angles of attack . . . . .	60
$\delta_{LEF} = 45^\circ$ , high angles of attack . . . . .	61
Wing 6, wide top body on:	
$\delta_{LEF} = 0^\circ$ , low angles of attack . . . . .	62
$\delta_{LEF} = 0^\circ$ , high angles of attack . . . . .	63
$\delta_{LEF} = 45^\circ$ , low angles of attack . . . . .	64
$\delta_{LEF} = 45^\circ$ , high angles of attack . . . . .	65
Wing 7, wide top body on:	
$\delta_{LEF} = 0^\circ$ , low angles of attack . . . . .	66
$\delta_{LEF} = 0^\circ$ , high angles of attack . . . . .	67
$\delta_{LEF} = 45^\circ$ , low angles of attack . . . . .	68
$\delta_{LEF} = 45^\circ$ , high angles of attack . . . . .	69
Wing 8, wide top body on:	
$\delta_{LEF} = 0^\circ$ , low angles of attack . . . . .	70
$\delta_{LEF} = 0^\circ$ , high angles of attack . . . . .	71
$\delta_{LEF} = 45^\circ$ , low angles of attack . . . . .	72
$\delta_{LEF} = 45^\circ$ , high angles of attack . . . . .	73
<b>Wing planform:</b>	
Top body off, $\delta_{LEF} = 0^\circ$ . . . . .	74
Top body off, $\delta_{LEF} = 45^\circ$ . . . . .	75
Wide top body on, $\delta_{LEF} = 0^\circ$ . . . . .	76
Wide top body on, $\delta_{LEF} = 45^\circ$ . . . . .	77
<b>Top bodies:</b>	
$\delta_{LEF} = 0^\circ$ :	
Wing 5 . . . . .	78
Wing 6 . . . . .	79
Wing 7 . . . . .	80
Wing 8 . . . . .	81
$\delta_{LEF} = 45^\circ$ :	
Wing 5 . . . . .	82
Wing 6 . . . . .	83
Wing 7 . . . . .	84
Wing 8 . . . . .	85

Leading-edge flap deflections:

Top body off:

Wing 5 . . . . .	86
Wing 6 . . . . .	87
Wing 7 . . . . .	88
Wing 8 . . . . .	89

Wide top body on:

Wing 5 . . . . .	90
Wing 6 . . . . .	91
Wing 7 . . . . .	92
Wing 8 . . . . .	93

Vertical tails:

Narrow top body on,  $\delta_{LEF} = 45^\circ$ :

Wing 5 . . . . .	94
Wing 6 . . . . .	95
Wing 7 . . . . .	96
Wing 8 . . . . .	97

**Sideslip.** The lateral-directional force and moment coefficients of the four wings with the wide top body on are presented in figures 58 to 73 as a function of sideslip at various angles of attack and leading-edge flap deflections. In general, for each of the wings the coefficients varied linearly with sideslip for angles between  $-5^\circ$  and  $5^\circ$ . At sideslip angles outside of this range, the variation in the lateral-directional coefficients became less linear on many of the configurations, especially at the higher angles of attack where some portion of the wings was most likely experiencing extensive flow separation. These trends were not significantly affected by leading-edge flap deflections.

**Wing planform.** Comparisons of the lateral-directional stability characteristics (computed between sideslip angles of  $-5^\circ$  and  $5^\circ$ ) of the four wings with the leading-edge flaps deflected and undeflected with the wide top body on and off are presented in figures 74 to 77. Note that the data are for the configurations without vertical tails, and therefore each of these wings possessed unstable or essentially neutral values of directional stability ( $C_{n_\beta}$ ) at angles of attack below maximum lift. At angles of attack near maximum lift, a region of directional instability of larger magnitude occurred on each of the wings.

Each of these wings was laterally stable (negative  $C_{l_\beta}$ ) for most of the angles of attack tested. However, the lateral stability was reduced at angles of attack near maximum lift, and configurations with leading-edge flap deflections of  $45^\circ$  were laterally unstable for part of this range of angle of attack. This phenomenon is a well-documented characteristic of highly swept wings that is due primarily to asymmetric breakdown of the wing leading-edge vortices at sideslip (ref. 6). Changes in

wing planform had a significant effect on the magnitude of lateral stability throughout the test angle-of-attack range. In general, increases in aspect ratio reduced lateral stability, and the diamond wing was typically more laterally stable than the arrow wings. These results indicate that the outboard panels added to the basic diamond planform caused the resulting arrow wings to experience reduced lateral stability.

**Top bodies.** The effect of the various top bodies (fig. 10) on the lateral-directional stability characteristics of the four wings is shown in figures 78 to 85. With the leading-edge flaps undeflected, the wings were tested with the top body off and with the wide top body on (figs. 78 to 81). Each of the top bodies (wide, medium, and narrow) was tested on the wings when the leading-edge flaps were deflected  $45^\circ$  (figs. 82 to 85).

Adding the top bodies caused small reductions in directional stability on all of the wings at the lower angles of attack, with the largest reduction occurring on the diamond wing. Reduction of directional stability due to addition of the bodies was not unexpected, because the majority of the body side area was ahead of the moment reference center. At angles of attack near and beyond maximum lift, adding the top bodies caused more significant reductions in directional stability on each of the wings, especially when the leading-edge flaps were undeflected. In general, the wide and medium bodies caused larger reductions in directional stability than the narrow body.

Adding the top bodies also reduced lateral stability for each of the wings. When the leading-edge flaps were undeflected, the reductions in lateral stability for the arrow wings occurred at two ranges of angle of attack ( $\alpha = 16^\circ$  to  $28^\circ$  and  $\alpha = 36^\circ$  to  $48^\circ$ ). For the diamond wing, adding the top bodies decreased lateral stability throughout the test angle-of-attack range. When the leading-edge flaps were deflected  $45^\circ$ , the results were less consistent. In general, the reductions in lateral stability occurred at similar angles of attack, but the magnitudes of these reductions were lower on many of the configurations when the leading-edge flaps were deflected.

**Leading-edge flaps.** The effect of leading-edge flap deflections on the lateral-directional stability characteristics of the four wings is shown in figures 86 to 93. Data are shown for the four planforms without a top body in figures 86 to 89 and with the wide top body in figures 90 to 93. Without a top body, leading-edge flap deflections caused small changes in directional stability for each of the wings that varied between stabilizing and destabilizing increments. When the wide top body was added,

leading-edge flap deflections generally reduced directional stability. For the  $60^\circ$  swept and  $50^\circ$  swept wings discussed in references 1 and 2, leading-edge flap deflections significantly improved lateral stability, especially near maximum lift. But for the  $70^\circ$  swept wings discussed in this report, leading-edge flap deflections generally reduced lateral stability throughout the angle-of-attack range.

**Vertical tails.** The effect of the small and medium twin vertical tails (figs. 11 to 13) on the lateral-directional stability characteristics of the four wings with the narrow top body on and the leading-edge flaps deflected  $45^\circ$  is shown in figures 94 to 97. Use of the narrow top body for the tails-on testing enabled the tails to be deflected through larger angles before they interfered with the body.

Adding the tails produced expected increases in directional stability for each of the wings at angles of attack below maximum lift, with the medium tails providing the larger increments. At angles of attack above maximum lift, the tails were located in the low-energy wake above the wings and thus became less effective. Despite these improvements in directional stability, some of the higher-aspect-ratio configurations were directionally unstable for a significant portion of the test angle-of-attack range.

The effects of the tails on lateral stability were more varied. Even though they produced side forces and yawing moments, adding the tails did not significantly change the lateral stability of the arrow wings at angles of attack below  $12^\circ$  (figs. 94 to 96). The presence of the vertical tails caused an induced load on the aft sections of the wing (ref. 7). This induced load resulted in a rolling moment in the opposite direction to the rolling moment generated by the vertical tails in sideslip. Because these two rolling moments are typically of similar magnitudes, they tend to cancel each other, and adding of the tails therefore had minimal effect on the lateral stability of the arrow wings at the lower angles of attack. For the diamond wing (fig. 97), the vertical tails produced a small increase in lateral stability at these angles of attack. The tails produced a different change in lateral stability for this wing because the induced loads were most likely smaller. The tails decreased lateral stability at angles of attack between  $24^\circ$  and  $36^\circ$  but improved lateral stability at angles of attack above maximum lift.

### Lateral Control Characteristics

The lateral control characteristics of the four flying wings are presented in the following figures.

	Figure
Inboard, middle, and outboard trailing-edge flaps:	
Wide top body on, $\delta_{LEF} = 45^\circ$ :	
Wing 5 . . . . .	98
Wing 6 . . . . .	99
Wing 7 . . . . .	100
Wing 8 . . . . .	101

The lateral controls tested consisted of differential deflections of the inboard, middle, and outboard trailing-edge flaps. On each of the wings, the middle and outboard flaps were tested deflected separately and in combination. The inboard flaps were deflected separately on Wings 5 and 8, and deflected with the middle flaps on Wings 5, 6, and 7. Figures 98 to 101 show the lateral control effectiveness of various differential flap deflections on each of the wings with the leading-edge flaps deflected  $45^\circ$  and the wide top body on.

Differential deflections of the trailing-edge flaps on each of the wings produced small rolling-moment increments that were fairly invariant with changes in angle of attack. Comparison of the control effectiveness generated by the various flaps showed that the roll-control effectiveness did not vary significantly among the flaps, despite the relatively large differences in flap area and lateral moment arm. In general, for high angles of attack the total roll control available from multiple flap deflections was equal to or less than that required to trim out the adverse rolling moments induced by vertical tail deflections. As a result, the lateral-directional maneuvering capability of these wings could possibly be limited by this relatively low level of total roll-control effectiveness. More in-depth dynamic analysis, which was beyond the scope of this study, would be required to make this determination.

For the arrow wings, differential deflections of the inboard and outboard trailing-edge flaps yielded negligible yawing moments. But beginning at an angle of attack of approximately  $4^\circ$ , deflections of the middle flaps produced adverse yawing moments that became quite large at the higher angles of attack. For the diamond wing, all the differential deflections produced small proverse yawing moments. These results show that the flaps with a forward-swept hinge line (inboard and outboard flaps on the arrow wings and all the flaps on the diamond wing) produced predominantly small proverse yawing moments, but flaps with a rearward-swept hinge line (middle flaps on the arrow wings) produced significant adverse yawing moments.

### Directional Control Characteristics

The directional control characteristics of the four flying wings are presented in the following figures.

	Figure
Split trailing-edge flaps:	
Wide top body on, $\delta_{LEF} = 45^\circ$ :	
Outboard flaps:	
Wing 5 . . . . .	102
Wing 6 . . . . .	103
Wing 8 . . . . .	104
Middle flaps:	
Wing 5 . . . . .	105
Wing 6 . . . . .	106
Wing 7 . . . . .	107
Wing 8 . . . . .	108
Small vertical tails:	
Narrow top body on, $\delta_{LEF} = 45^\circ$ :	
Wing 5 . . . . .	109
Wing 6 . . . . .	110
Wing 7 . . . . .	111
Wing 8 . . . . .	112
Medium vertical tails:	
Narrow top body on, $\delta_{LEF} = 45^\circ$ :	
Wing 5 . . . . .	113
Wing 6 . . . . .	114
Wing 7 . . . . .	115
Wing 8 . . . . .	116

Two types of directional controls, split trailing-edge flaps (figs. 7 and 9) and vertical tail deflections (figs. 12 and 13), were tested on these models. As discussed in the section "Model Description" (p. 3), the split trailing-edge flaps were designed to separate into a top half that would deflect upward and a bottom half that would deflect downward at the same angle, and they would be deflected on only one wing at a time. The resulting geometry would result in an unbalanced incremental drag force on the wing that would produce an associated yawing moment. The all-moving twin vertical tails were deflected about an unswept hinge post located at the midpoint of the tail root chord.

**Split trailing-edge flaps.** The control effectiveness of split deflections of the right outboard trailing-edge flaps for Wings 5, 6, and 8 with the wide top body on and a leading-edge flap deflection of  $45^\circ$  is shown in figures 102 to 104. Split deflections of the outboard flaps produced small yawing moments that were opposite to those that would be expected to be generated by the drag on the split flaps. This result was due to the strong contribution of side force to the net yawing moments produced by these deflections (fig. 117). The forward sweep of the hinge lines on the outboard flaps and their location aft of the moment reference center caused these surfaces to function as a left rudder deflection when deflected on the right wing. For this reason, split deflections of a surface with a forward-swept hinge line produced rudder-like

side forces that generated yawing moments in the opposite direction to the yawing moments generated by the drag on the device, resulting in the observed yawing moments (fig. 117). The data for different deflection angles showed that the  $-73^\circ$  deflection produced larger yawing moments than the  $-43^\circ$  deflection, but this control effectiveness was not linear with deflection angle. For the highest-aspect-ratio wing (Wing 5), split deflections of the outboard flaps produced negligible rolling moments. For the other wings, these deflections produced rolling moments towards the wing on which the flap was split that were due to a spoiler-like loss of lift on the wing containing the split flap.

Figures 105 to 108 show the control effectiveness of split deflections of the middle trailing-edge flaps for each of the wings with the wide top body on and a leading-edge flap deflection of  $45^\circ$ . As with the outboard flaps, the middle flaps were deflected on the right wing. Split deflections of the middle flaps on the arrow wings produced yawing moments in the opposite direction to those produced by split deflections of the outboard flaps because of the difference in the sweep of the hinge lines between the middle and outboard flaps. In contrast to the forward sweep on the outboard flaps, the rearward sweep of the middle flaps on the arrow wings caused split deflections of these flaps to produce side forces in the opposite direction to those produced by comparable deflections of the outboard flaps. These side forces produced yawing moments in the same direction as the yawing moments produced by the drag forces, resulting in higher net yawing moments for many of the angles of attack (fig. 117).

For the diamond wing, the forward-swept middle flaps produced larger yawing moments than those produced by the outboard flaps because the middle flaps had a longer side-force moment arm. As with the outboard flaps, the data for different deflection angles showed that the  $-73^\circ$  deflection produced larger yawing moments than the  $-43^\circ$  deflection at some of the angles of attack tested, but this control effectiveness was not linear with deflection angle. Also, these deflections produced proverse rolling moments towards the wing on which the flap was split because of a spoiler-like loss of lift on that wing.

Despite the improved effectiveness relative to the outboard flaps, the levels of yaw control produced by split deflections of the middle flaps were relatively small, especially at the lower angles of attack. Because of this low level of yaw-control effectiveness, the lateral-directional maneuvering potential of these configurations could be limited. More in-depth dynamic analysis, which was beyond the scope of this study, would be required to

determine whether these configurations could obtain adequate yaw control from split deflections of the trailing-edge flaps.

**Vertical tails.** Figures 109 to 112 show the control effectiveness of the small twin vertical tails for each of the wings when the narrow top body was used and the leading-edge flaps were deflected  $45^\circ$ . For each of the wings, deflections of the small tails produced yaw-control effectiveness that was relatively invariant at angles of attack below maximum lift. Above maximum lift, the yaw-control effectiveness decreased with increasing angle of attack as the tails became located in the low-energy wake behind the stalled wing. The  $-30^\circ$  deflection of the small tails produced approximately twice the yaw-control effectiveness of the  $-10^\circ$  deflection on many of the configurations. This shows that the yaw-control effectiveness of the small tails was not linear with deflection angle for deflections between  $10^\circ$  and  $30^\circ$ . The rolling moments produced by deflections of the small tails were negligible at low angles of attack on the arrow wings, but adverse rolling moments were generated at these same angles of attack on the diamond wing. For each of the wings, larger adverse rolling moments occurred near maximum lift.

The control effectiveness of deflections of the medium twin vertical tails for each of the wings with the narrow top body on and the leading-edge flaps deflected  $45^\circ$  is shown in figures 113 to 116. The yaw-control effectiveness produced by deflections of the medium tails was generally larger than that generated by the small tails. As with the small tails, the level of effectiveness generated on a given arrow wing was relatively invariant at angles of attack below maximum lift, and this effectiveness decayed at angles of attack above maximum lift. For the diamond wing, the medium tails began to lose effectiveness at a lower angle of attack (approximately  $20^\circ$ ) than the small tails. The data for deflection angles of  $-10^\circ$  and  $-21^\circ$  (the lower maximum deflection angle for the medium tails resulted from body interference) indicate that the yaw-control effectiveness of the medium tails was linear with deflection angle for deflection angles below approximately  $21^\circ$ . The rolling moments produced by deflections of the medium tails were also similar in character to, but larger in magnitude than, the rolling moments produced by deflections of the small tails. For the arrow wings, negligible rolling moments were produced at the lower angles of attack, and significant adverse rolling moments were produced near maximum lift. For the diamond wing, adverse rolling moments were produced throughout the angle-of-attack range with larger moments occurring near maximum lift.

## Conclusions

A wind-tunnel investigation was conducted in the Langley 12-Foot Low-Speed Tunnel to study the low-speed stability and control characteristics of a series of four flying wings over an extended range of angle of attack. Because of the current emphasis on reducing the radar cross section (RCS) of new military aircraft, the planform of each wing was composed of lines swept at a relatively high angle of  $70^\circ$ , and all the trailing edges and control surface hinge lines were aligned with one of the two leading edges. Three arrow planforms with different aspect ratios and one diamond planform were tested. The models incorporated leading-edge flaps for improved longitudinal characteristics and lateral stability and had three sets of trailing-edge flaps that were deflected symmetrically for pitch control, differentially for roll control, and in a split fashion for yaw control. Three top body widths and two sizes of twin vertical tails were also tested on each model. A large aerodynamic database was compiled that could be used to evaluate some of the trade-offs involved in the design of a configuration with a reduced RCS and good flight dynamic characteristics. The results of this investigation may be summarized as follows:

1. The maximum lift coefficient was approximately 1.1 for the three arrow wings and about 1.0 for the diamond wing. This value occurred at an angle of attack of  $36^\circ$  for the arrow wings and  $40^\circ$  for the diamond wing.
2. Without vertical tails, the configurations exhibited neutral or unstable directional stability at most of the angles of attack tested. Each of these wings was laterally stable for most of the angles of attack tested. However, the lateral stability was reduced at angles of attack near maximum lift, and some of the configurations were laterally unstable for part of this range of angle of attack. In general, the diamond wing was the most laterally stable of the four wings.
3. The onset of separation on the outboard wing panels that were added to the basic diamond planform to create the arrow wings caused the arrow wings to experience a pitch-up. These planform additions also significantly reduced lateral stability.
4. Adding top bodies to the wings resulted in a nose-down pitching-moment increment that increased as top body width increased. The top bodies reduced directional stability over most of the test angle-of-attack range. When the leading-edge flaps were not deflected, lateral stability was decreased by adding the wide body. These reductions in lateral-directional stability were largest for the diamond wing.
5. For the arrow wings, leading-edge flap deflections improved the pitching-moment characteristics by reduc-

ing or delaying the pitch-up but reduced lift coefficient over most of the angle-of-attack range. One reason for including leading-edge flaps in these designs was to improve lateral stability, but deflections of these flaps actually degraded the lateral stability.

6. The addition of vertical tails provided expected increases in directional stability.
7. The inboard and middle trailing-edge flaps were deflected symmetrically for pitch control on each wing. The longitudinal control effectiveness produced was very small, especially in the nose-down direction. Despite this limited control, each of the wings could be statically trimmed over a large angle-of-attack range, but additional pitch control power would likely be needed to provide these wings with sufficient control margin for dynamic situations such as maneuvering or countering turbulence. An additional limit on the pitch control provided by the flaps may be imposed by the need to budget the amount of flap deflection available for each type of control (pitch, roll, or yaw). For these reasons, these configurations would probably require redesigned flaps or additional pitch control devices to achieve the desired levels of pitch control.
8. Differential deflections of the trailing-edge flaps for roll control produced rolling moments that were relatively invariant with angle of attack. The total levels of roll control generated by multiple deflections of more than one set of flaps were small, and this ineffectiveness may limit the lateral-directional maneuvering capabilities of these wings.
9. Split deflections of the middle and outboard trailing-edge flaps were tested for yaw control. The forward-swept outboard trailing-edge flaps were not effective at providing yaw control when split. This is because the yawing moment developed by the drag on these flaps was in the opposite direction to the yawing moment developed by the side force. For the arrow wings, the middle trailing-edge flaps were swept aft, and the yawing moment due to side force on these flaps acted in the same direction as the drag force. Therefore, the summation of the yawing moments due to the drag and side forces on these flaps resulted in larger net yawing moments. Despite this effect, the levels of yaw control produced by split deflections of the middle flaps were small, especially at the lower angles of attack. Because of a spoiler-like loss of lift, these deflections caused rolling moments towards the wing on which the flap was split.
10. Deflection of all-moving twin vertical tails was effective for yaw control below maximum lift but ineffective at angles of attack above maximum lift, where they became immersed in the low-energy wake of the stalled wing. Significant adverse rolling moments were

created near maximum lift by deflection of the vertical tail.

NASA Langley Research Center  
Hampton, VA 23681-0001  
May 26, 1995

## References

1. Moul, Thomas M.; Fears, Scott P.; Ross, Holly M.; and Foster, John V.: *Low-Speed Wind-Tunnel Investigation of the Stability and Control Characteristics of a Series of Flying Wings With Sweep Angles of 60°*. NASA TM-4649, 1995.
2. Fears, Scott P.; Ross, Holly M.; and Moul, Thomas M.: *Low-Speed Wind-Tunnel Investigation of the Stability and Control Characteristics of a Series of Flying Wings With Sweep Angles of 50°*. NASA TM-4640, 1995.
3. Hom, K. W.; Morris, O. A.; and Hahne, D. E.: *Low-Speed Investigation of the Maneuver Capability of Supersonic Fighter Wings*. AIAA-83-0426, Jan. 1983.
4. Freeman, Delma C., Jr.: *Low Subsonic Flight and Force Investigation of a Supersonic Transport Model With a Highly Swept Arrow Wing*. NASA TN D-3887, 1967.
5. Ogburn, Marilyn E.; Foster, John V.; Nguyen, Luat T.; Breneman, Kevin P.; McNamara, William G.; Clark, Christopher M.; Rude, Dennis D.; Draper, Marjorie G.; Wood, Craig A.; and Hynes, Marshall S.: *High-Angle-of-Attack Nose-Down Pitch Control Requirements for Relaxed Static Stability Combat Aircraft. High-Angle-of-Attack Technology, Volume I*, Joseph R. Chambers, William P. Gilbert, and Luat T. Nguyen, eds., NASA CP-3149, Part 2, 1992, pp. 639–658.
6. Johnson, Joseph L., Jr.; Grafton, Sue B.; and Yip, Long P.: *Exploratory Investigation of the Effects of Vortex Bursting on the High-Angle-of-Attack Lateral-Directional Stability Characteristics of Highly-Swept Wings. A Collection of Technical Papers—AIAA 11th Aerodynamic Testing Conference*, Mar. 1980, pp. 282–297. (Available as AIAA-80-0463.)
7. Queijo, M. J.; and Riley, Donald R.: *Calculated Subsonic Span Loads and Resulting Stability Derivatives of Unswept and 45° Sweptback Tail Surfaces in Sideslip and in Steady Roll*. NACA TN 3245, 1954.

Table I. Model Geometric Characteristics

	Wing 5	Wing 6	Wing 7	Wing 8
<b>Wing:</b>				
Area (reference), in <sup>2</sup> . . . . .	1366.03	1327.09	1272.63	1009.20
Area (trapezoidal), in <sup>2</sup> . . . . .	766.20	767.50	768.91	1009.20
Span, in. . . . .	48.00	43.82	39.18	27.10
Mean aerodynamic chord, in. . . . .	41.15	42.30	43.88	49.65
Root chord, in. . . . .	74.48	74.48	74.48	74.48
Tip chord, in. . . . .	0	0	0	0
Aspect ratio (based on total planform) . . . . .	1.69	1.45	1.21	.73
Aspect ratio (based on trapezoidal area) . . . . .	3.00	2.50	2.00	.73
Leading-edge sweep, deg. . . . .	70	70	70	70
Trailing-edge sweep, deg. . . . .	±70	±70	±70	±70
Dihedral, deg . . . . .	0	0	0	0
Incidence, deg . . . . .	0	0	0	0
<b>Moment reference centers:</b>				
Longitudinal (X-axis), percent $\bar{c}$ . . . . .	39.71	40.00	37.97	36.48
Longitudinal (X-axis, back from nose), in. . . . .	37.88	36.90	34.82	28.48
Vertical (Z-axis, below wing centerline), in. . . . .	1.87	1.87	1.87	1.87
<b>Leading-edge flaps:</b>				
Area (per side), in <sup>2</sup> . . . . .	88.57	78.80	67.35	39.40
Span (per side), in. . . . .	19.92	17.82	15.35	9.33
Chord, in. . . . .	4.64	4.64	4.64	4.64
<b>Trailing-edge flaps:</b>				
<b>Inboard:</b>				
Area (per side), in <sup>2</sup> . . . . .	33.16	36.48	35.41	20.84
Span (per side), in. . . . .	7.42	7.44	6.59	4.37
Chord, in. . . . .	5.11	5.69	6.58	6.58
<b>Middle:</b>				
Area (per side), in <sup>2</sup> . . . . .	53.40	47.58	39.66	20.84
Span (per side), in. . . . .	11.37	9.40	7.24	4.37
Chord, in. . . . .	5.11	5.69	6.58	6.58
<b>Outboard:</b>				
Area (per side), in <sup>2</sup> . . . . .	11.14	13.81	18.27	20.84
Span (per side), in. . . . .	3.11	3.46	3.97	4.37
Chord, in. . . . .	5.11	5.69	6.58	6.58
<b>Body flaps:</b>				
Area (per side), in <sup>2</sup> . . . . .	13.99	17.14	19.80	18.53
Span (per side), in. . . . .	3.96	3.69	4.19	4.01
Chord, in. . . . .	5.11	5.69	6.58	6.58
<b>Split trailing-edge flaps:</b>				
<b>Middle:</b>				
Area (per side), in <sup>2</sup> . . . . .	53.40	47.58	39.66	20.84
Span (per side), in. . . . .	11.37	9.40	7.24	4.37
Chord, in. . . . .	5.11	5.69	6.58	6.58
<b>Outboard:</b>				
Area (per side), in <sup>2</sup> . . . . .	11.14	13.81	18.27	20.84
Span (per side), in. . . . .	3.11	3.46	3.97	4.37
Chord, in. . . . .	5.11	5.69	6.58	6.58

Table I. Concluded

	Wide Top	Medium Top	Narrow Top	Bottom
Bodies:				
Length, in. ....	64.40	64.40	64.40	47.05
Width, in. ....	9.50	6.40	4.60	9.50
Height, in. ....	3.20	3.20	3.20	3.00
			Medium	Small
Vertical tails:				
Area, in <sup>2</sup> .....			50.47	25.27
Root chord, in. ....			15.27	10.80
Tip chord, in. ....			0	0
Height, in. ....			6.61	4.68
Aspect ratio .....			.87	.87
Leading-edge sweep, deg. ....			60	60
Hinge line location, percent chord. ....			50	50

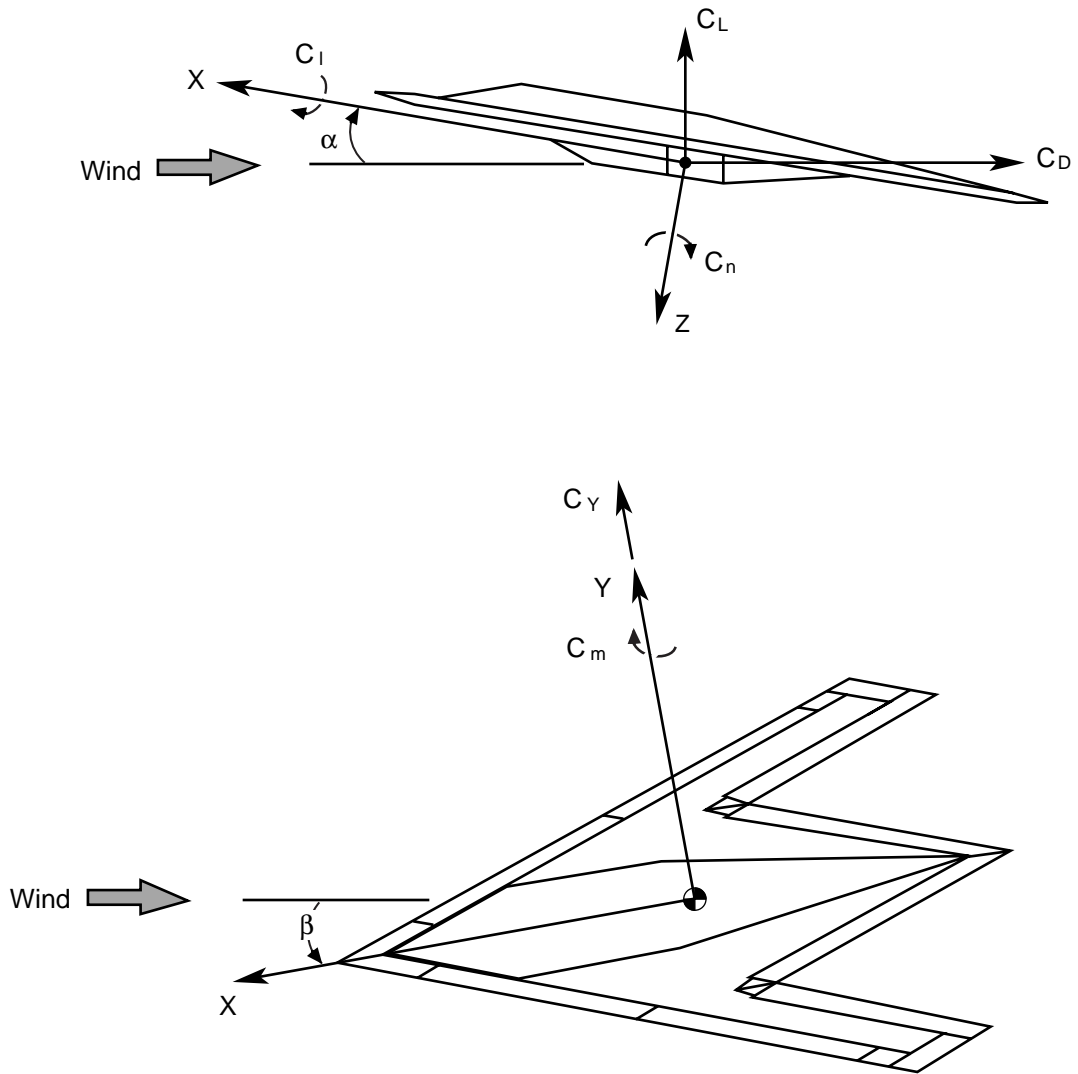
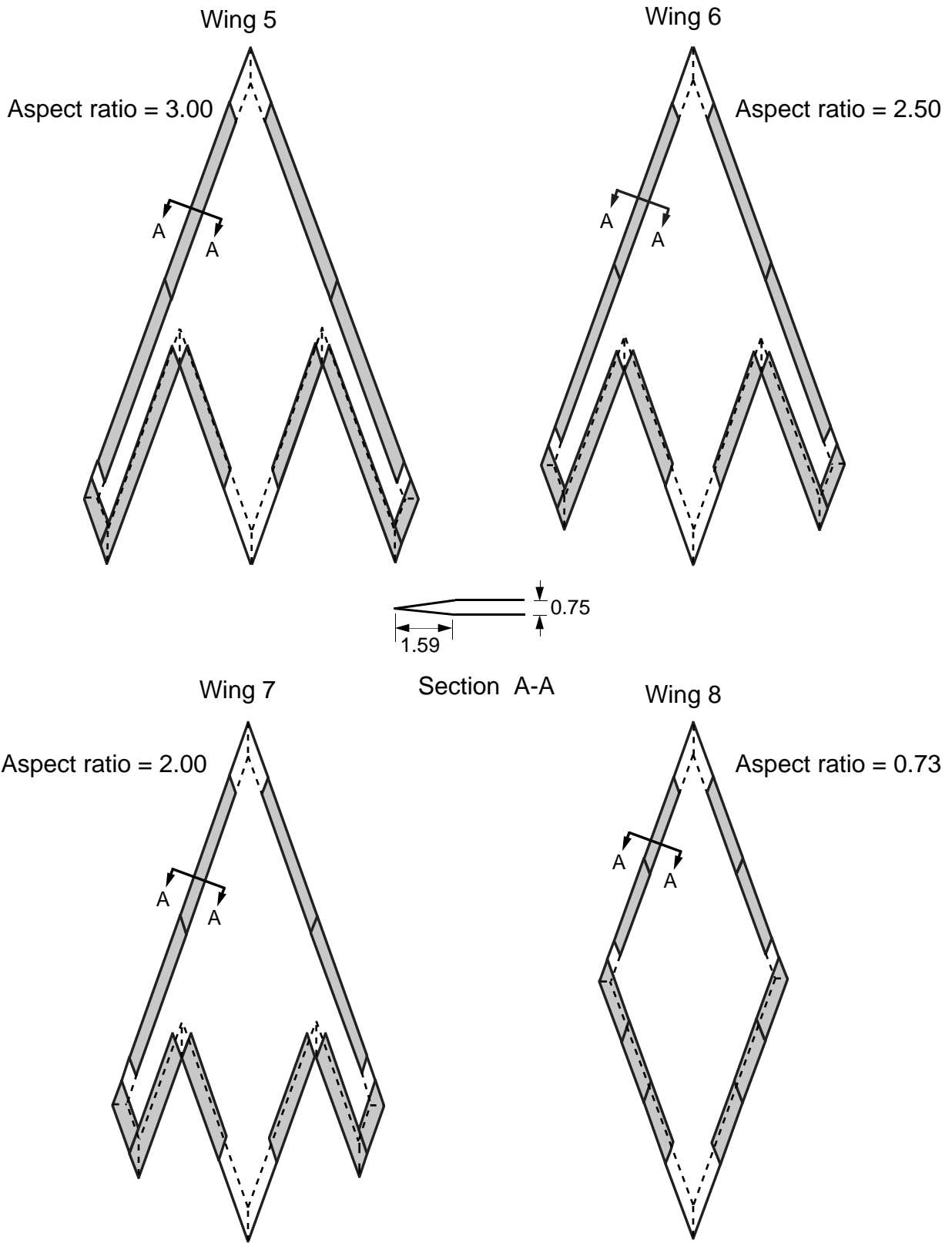
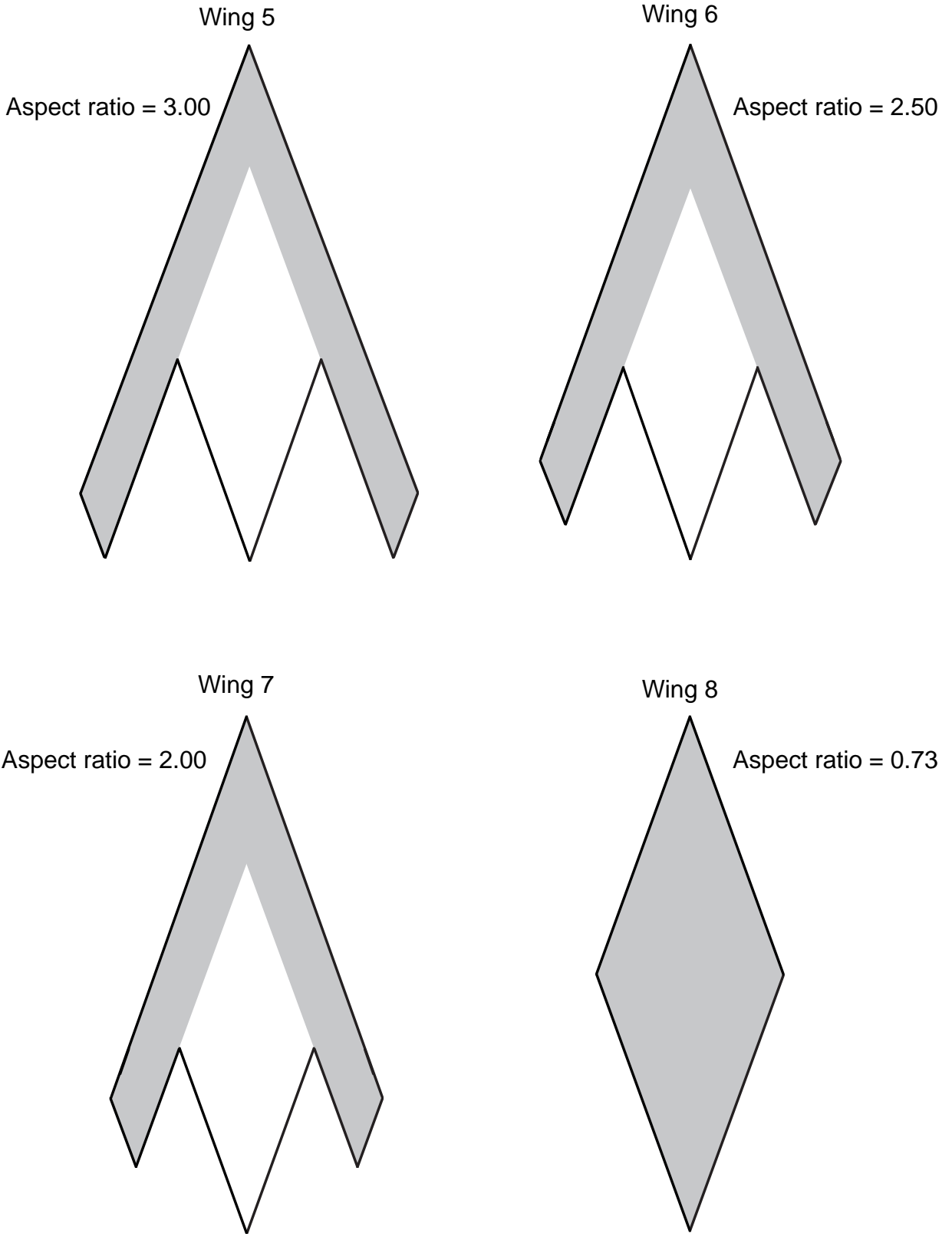


Figure 1. System of axes and angular notation.



(a) Control surfaces (shaded areas) and bevel lines (dashed lines).

Figure 2. Wing planforms.



(b) Trapezoidal wing areas (shaded areas).

Figure 2. Concluded.

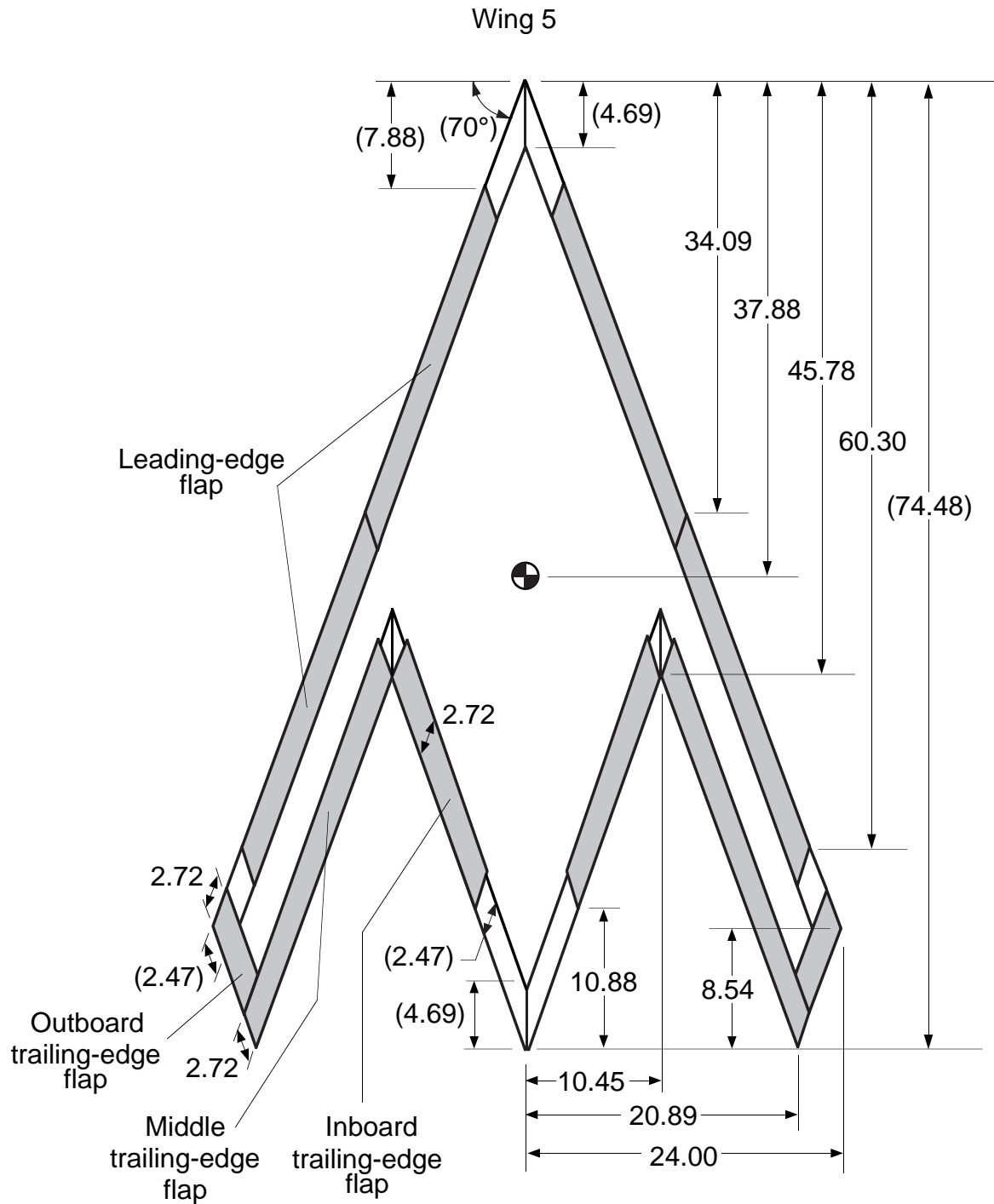


Figure 3. Wing 5. Linear dimensions are in inches. Dimensions in parentheses are common for all wings. Shaded areas indicate control surfaces.

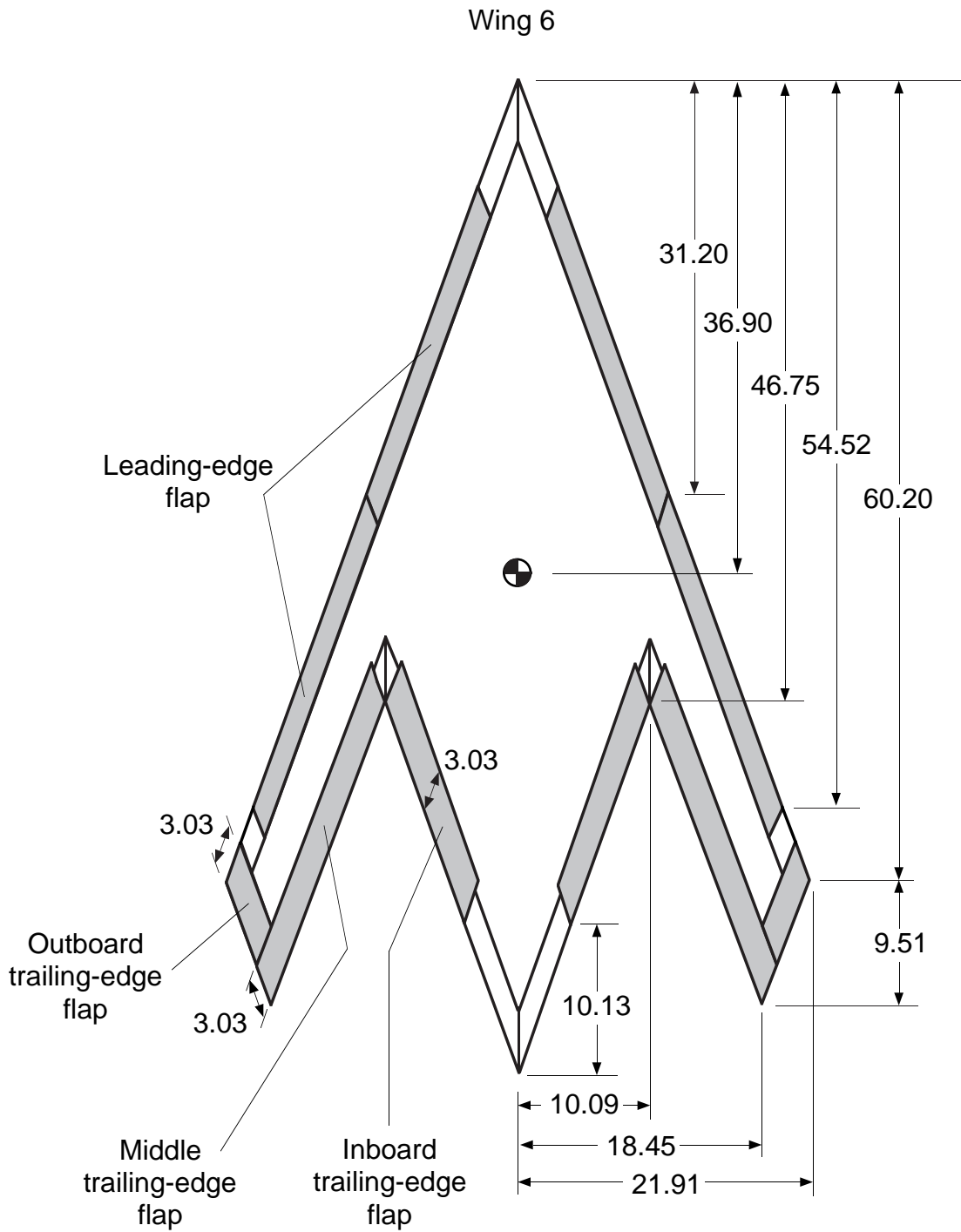


Figure 4. Wing 6. All dimensions are in inches. Shaded areas indicate control surfaces.

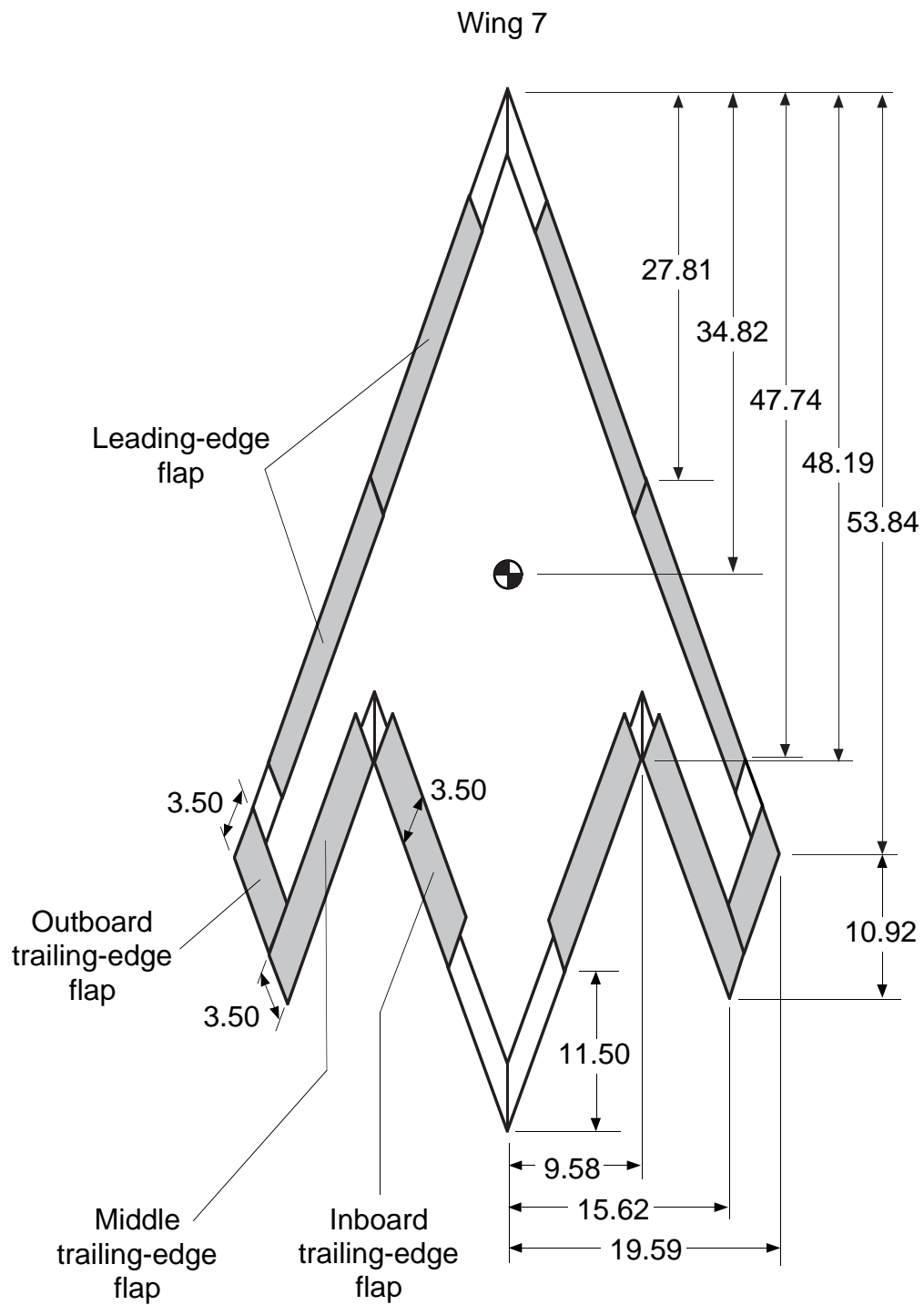


Figure 5. Wing 7. All dimensions are in inches. Shaded areas indicate control surfaces.

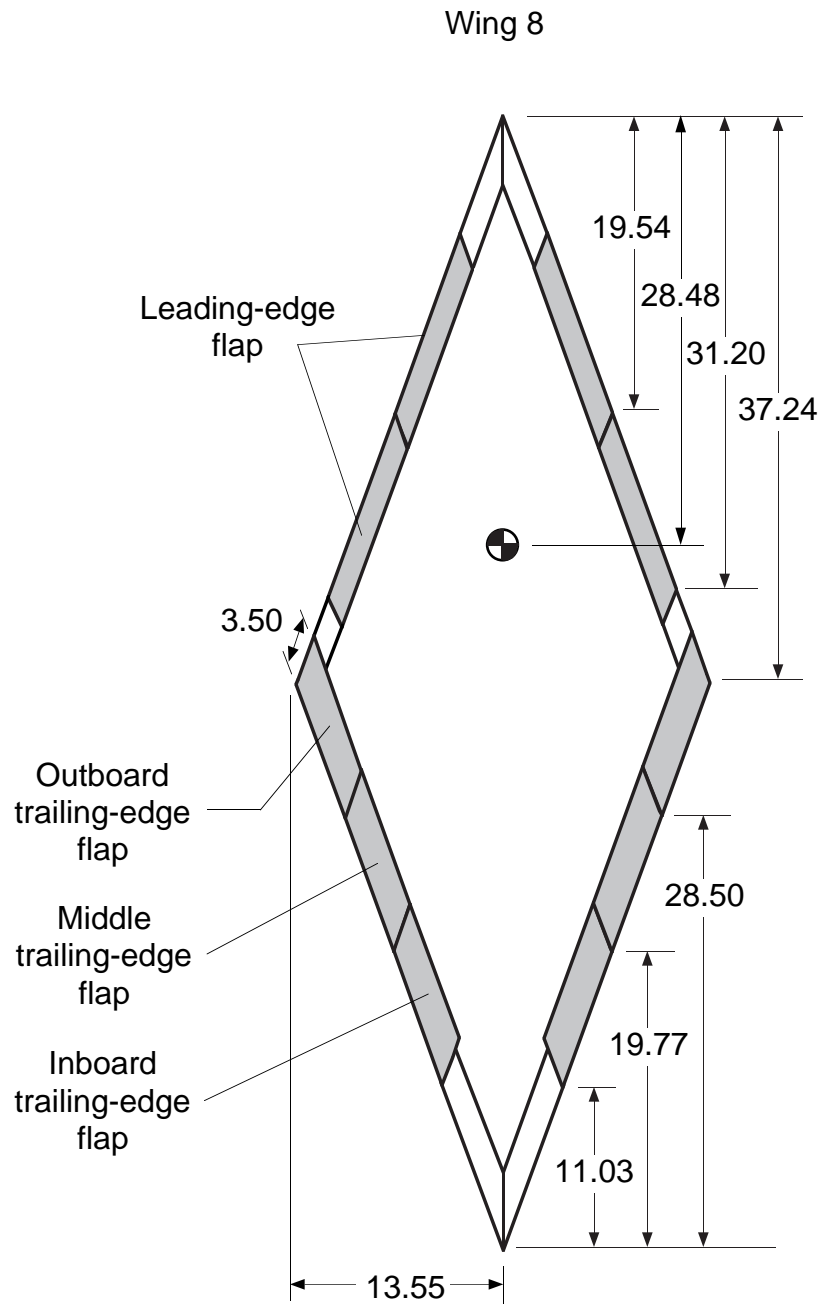
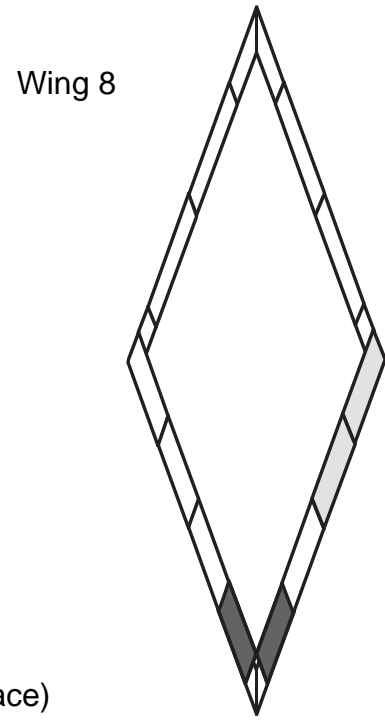
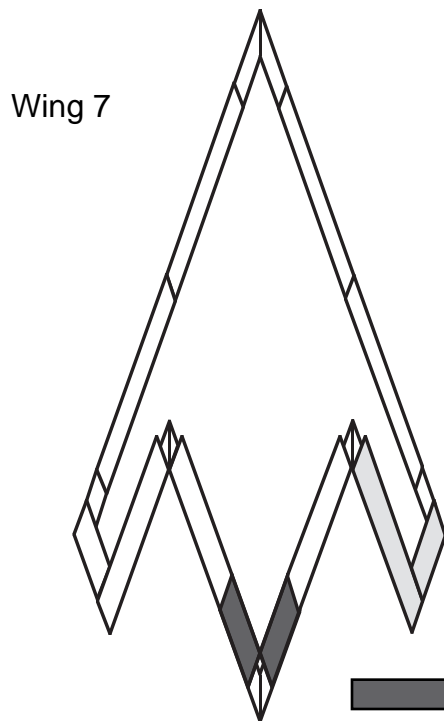
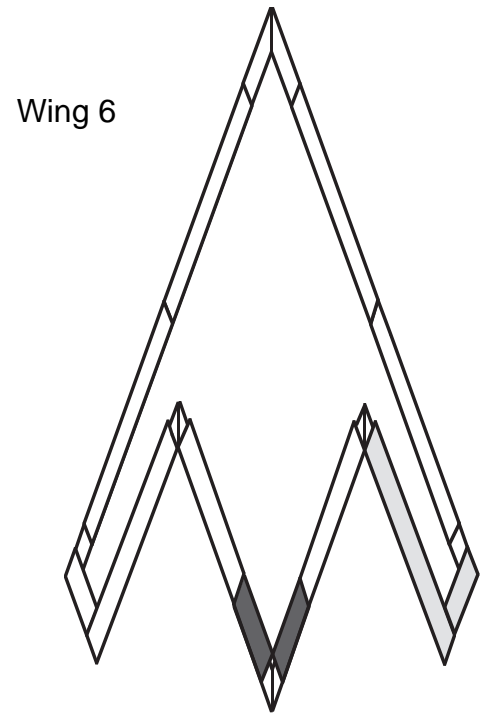
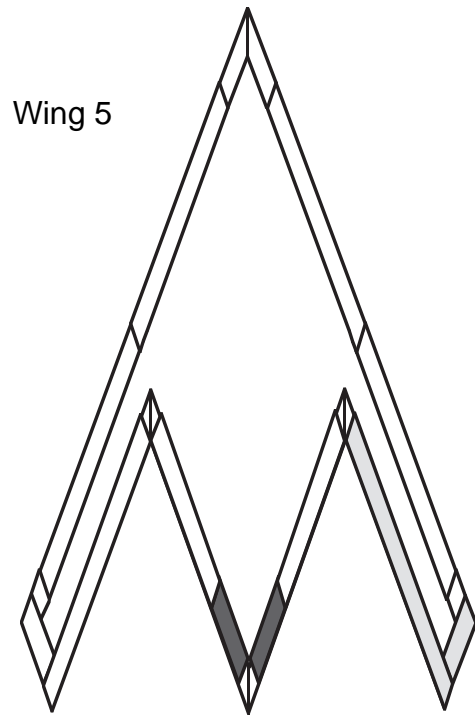
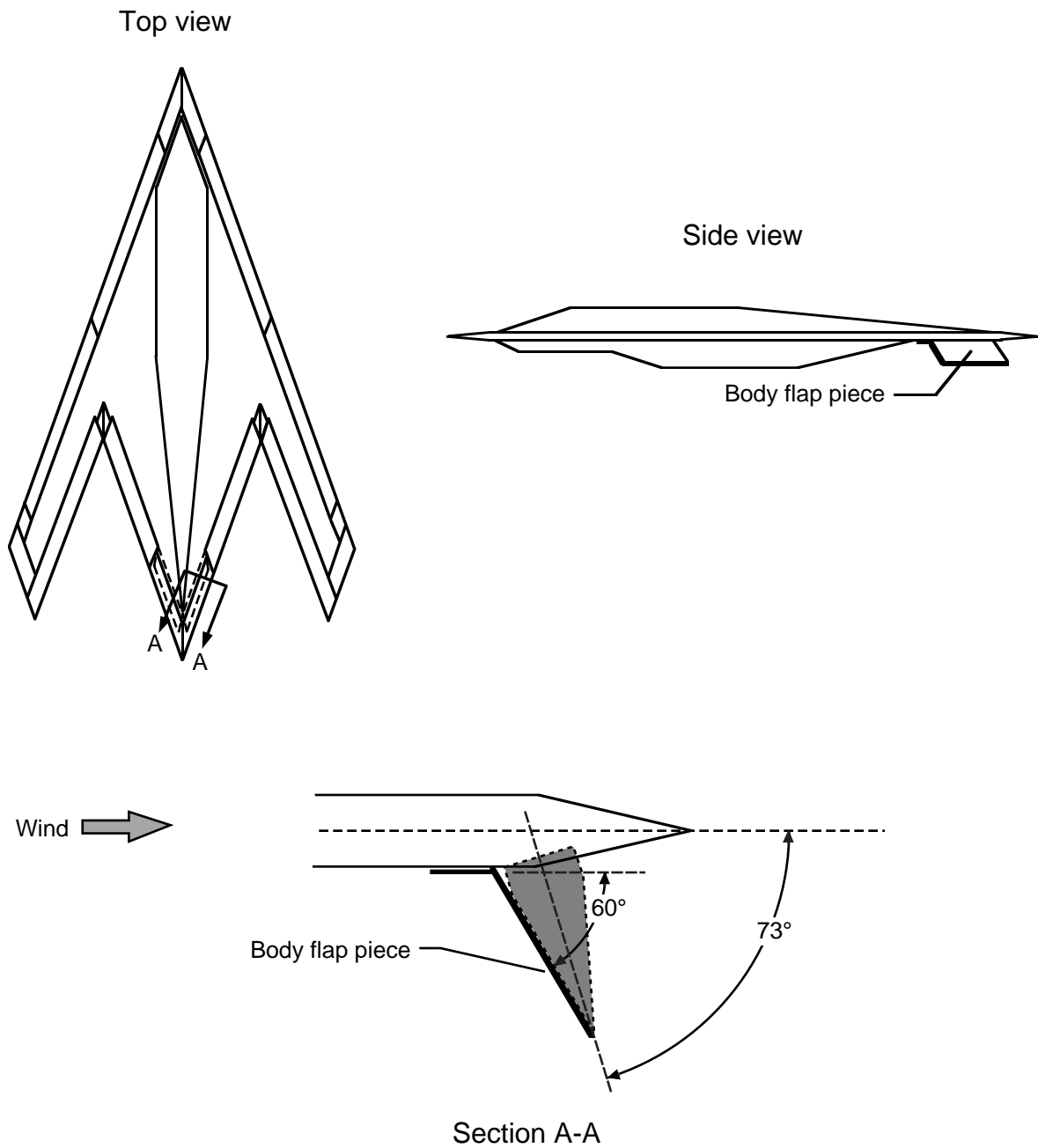


Figure 6. Wing 8. All dimensions are in inches. Shaded areas indicate control surfaces.



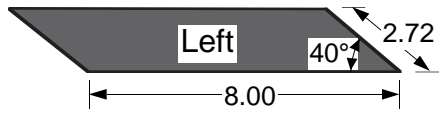
■ Body flaps (bottom surface)  
□ Split trailing-edge flaps (bottom surface)

Figure 7. Top view showing locations of undeflected body flaps and split trailing-edge flaps on bottom surfaces of wings.

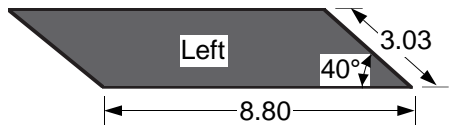
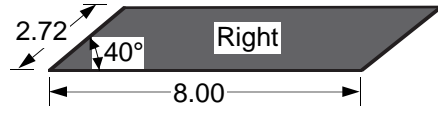


(a) Typical body flap location and mounting for deflection angle of  $73^\circ$ . Shaded area represents simulated flap.

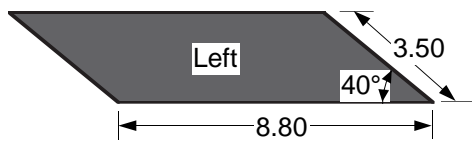
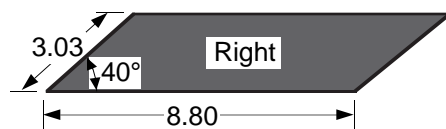
Figure 8. Body flap locations, dimensions, and deflection angles.



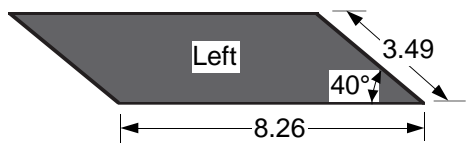
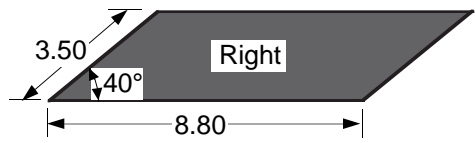
Wing 5



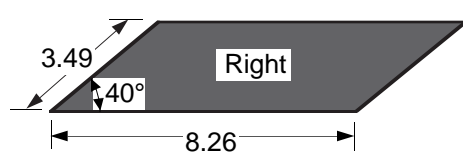
Wing 6



Wing 7

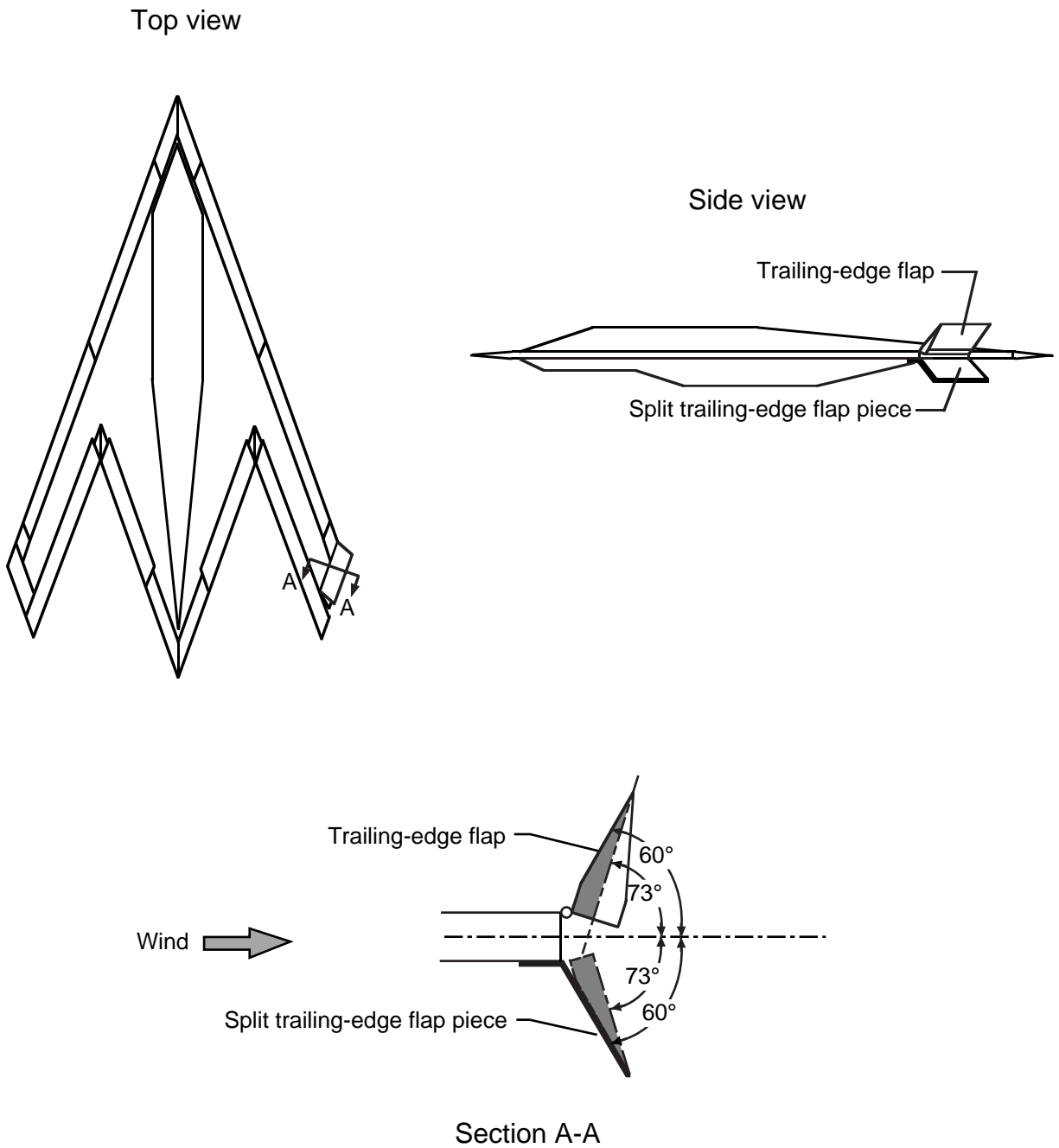


Wing 8



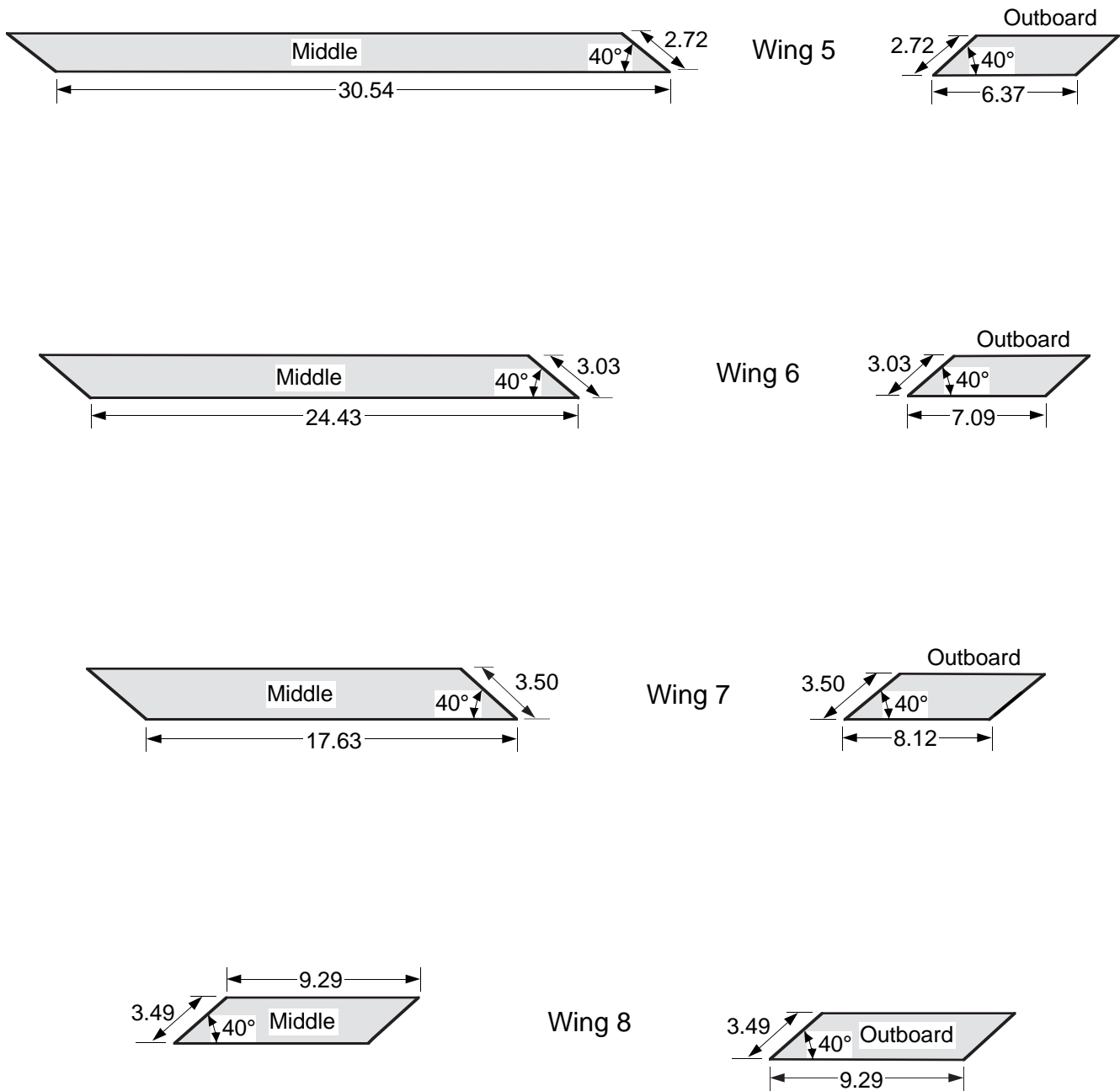
(b) Planforms of body flaps. All dimensions are in inches.

Figure 8. Concluded.



(a) Typical split trailing-edge flap location and mounting for deflection angle of 73°. Shaded areas represent simulated upper and lower halves of split flaps.

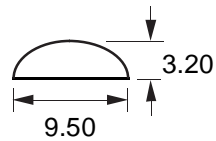
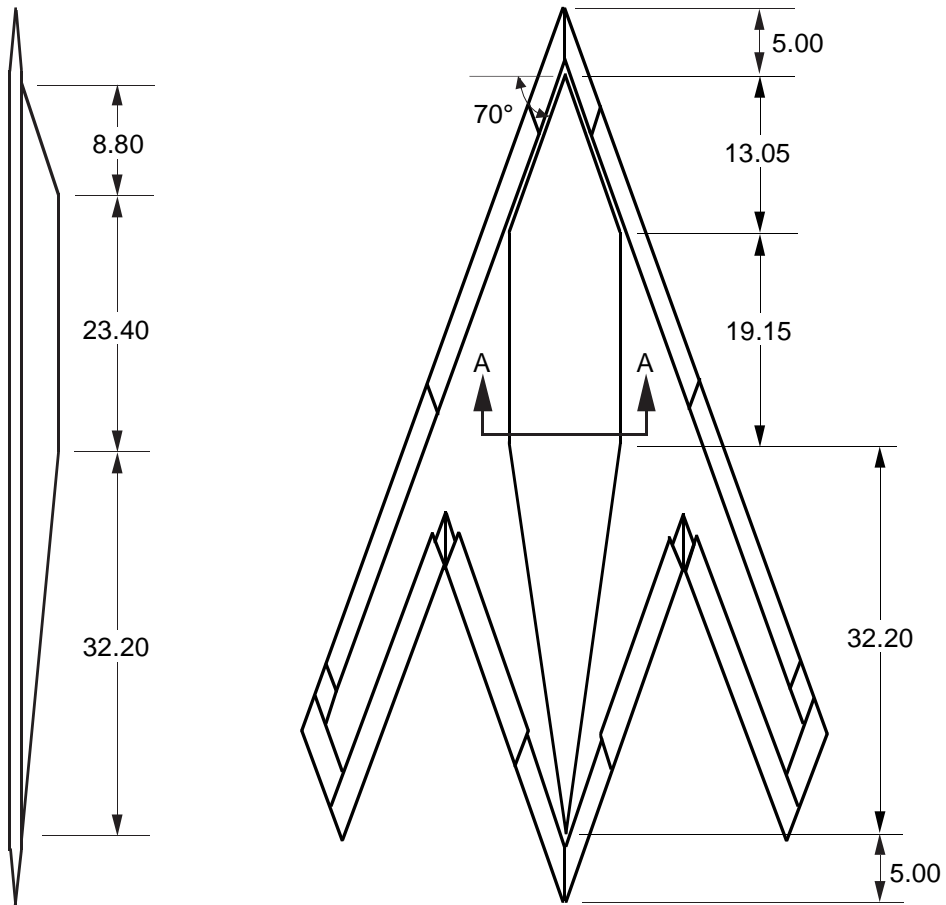
Figure 9. Split trailing-edge flap locations, dimensions, and deflection angles.



(b) Planforms of split trailing-edge flaps. All dimensions are in inches.

Figure 9. Concluded.

Wide body

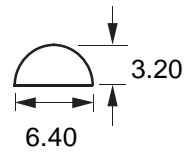
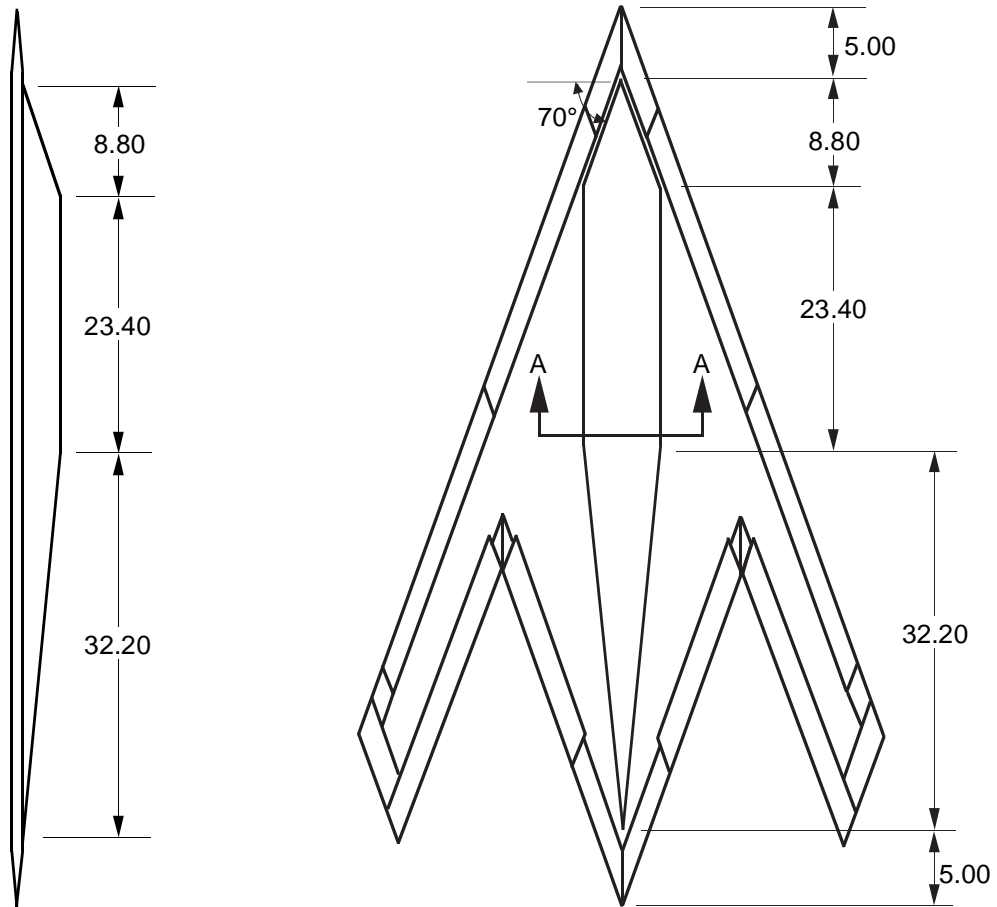


Section A-A

(a) Wide top body.

Figure 10. Top bodies and bottom balance cover. All dimensions are in inches.

Medium body

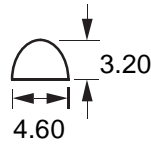
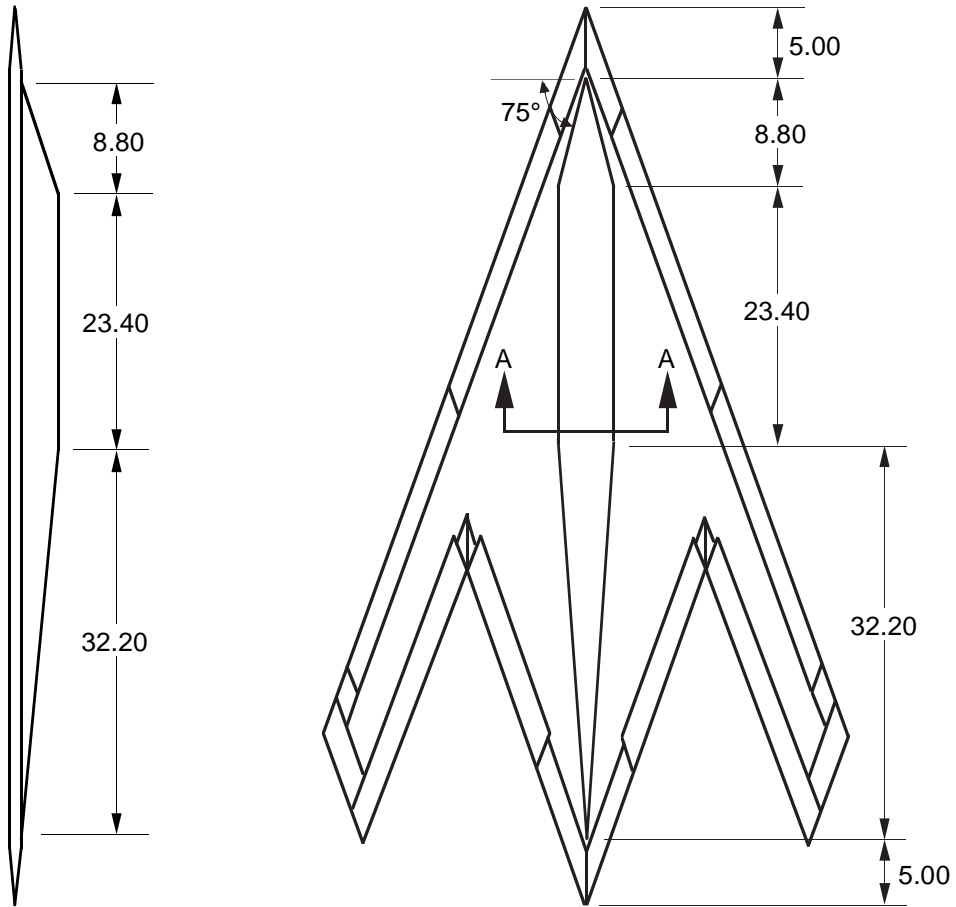


Section A-A

(b) Medium top body.

Figure 10. Continued.

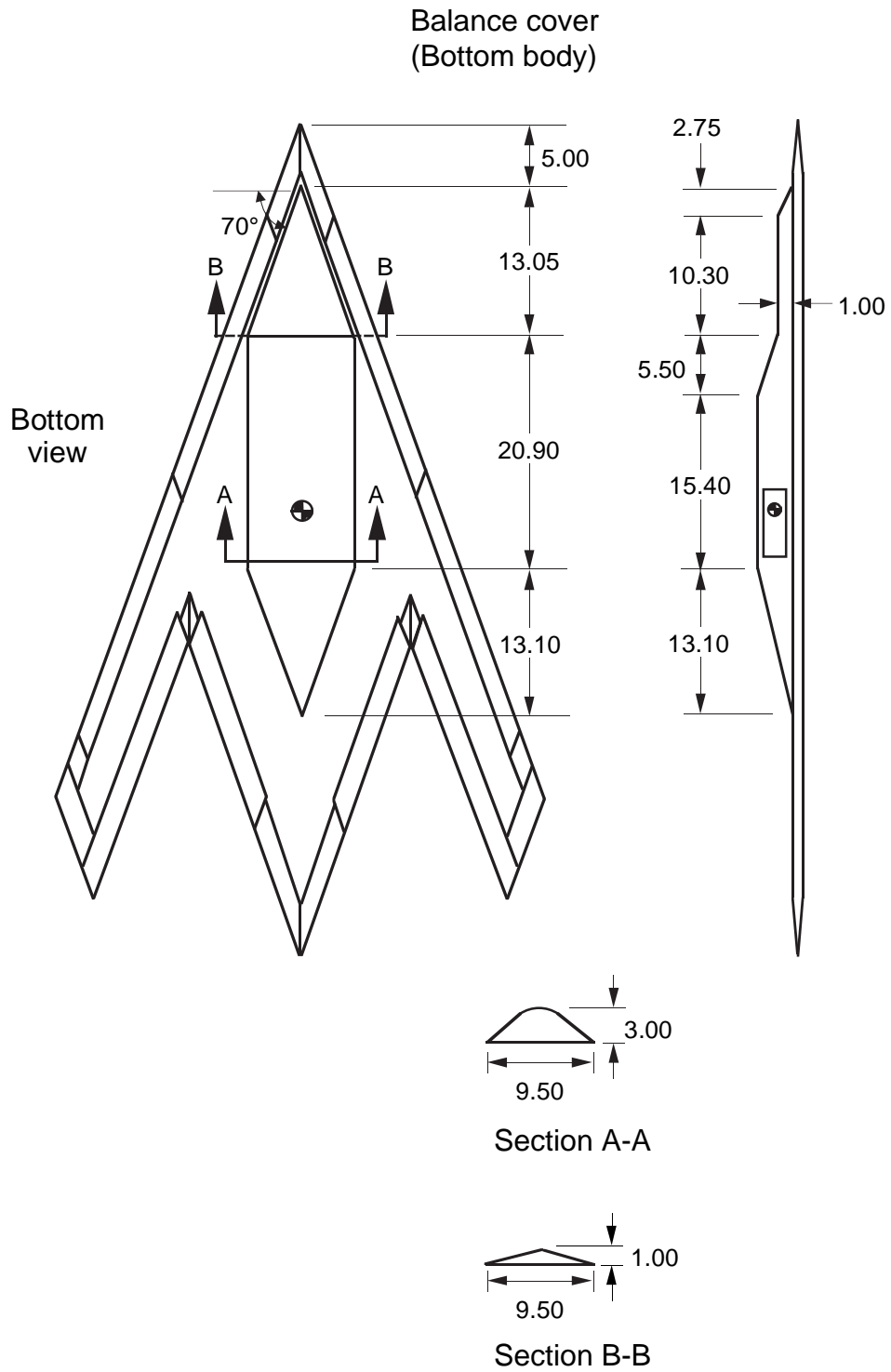
Narrow body



Section A-A

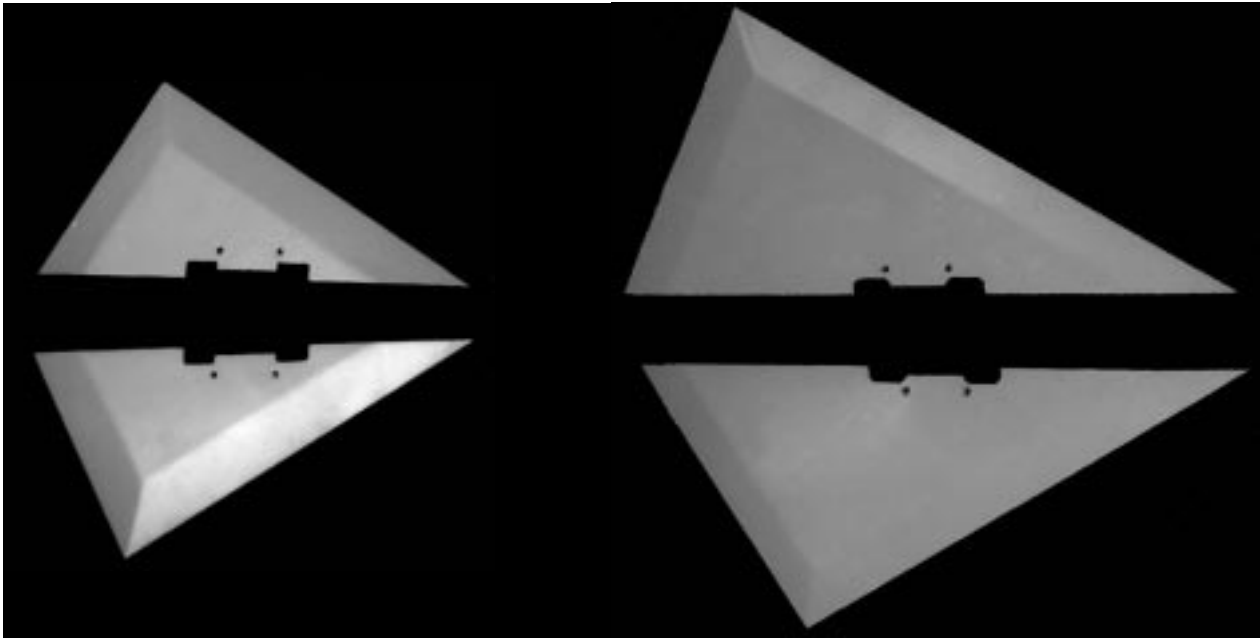
(c) Narrow top body.

Figure 10. Continued.



(d) Bottom balance cover.

Figure 10. Concluded.



Small

Medium

Figure 11. Vertical tails.

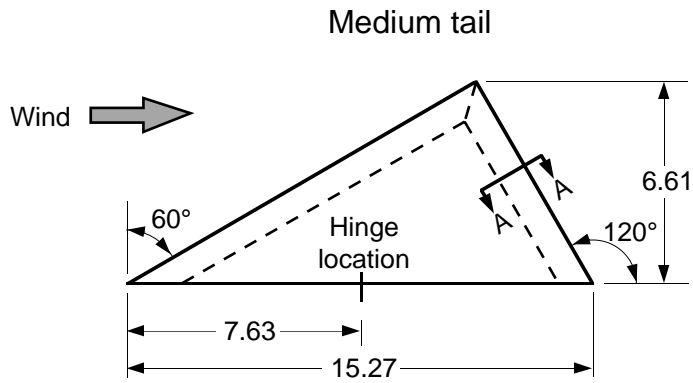
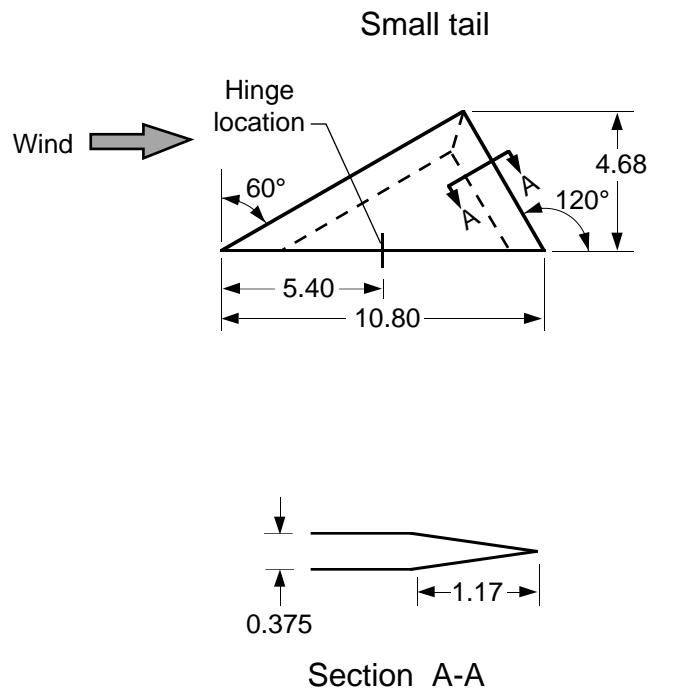
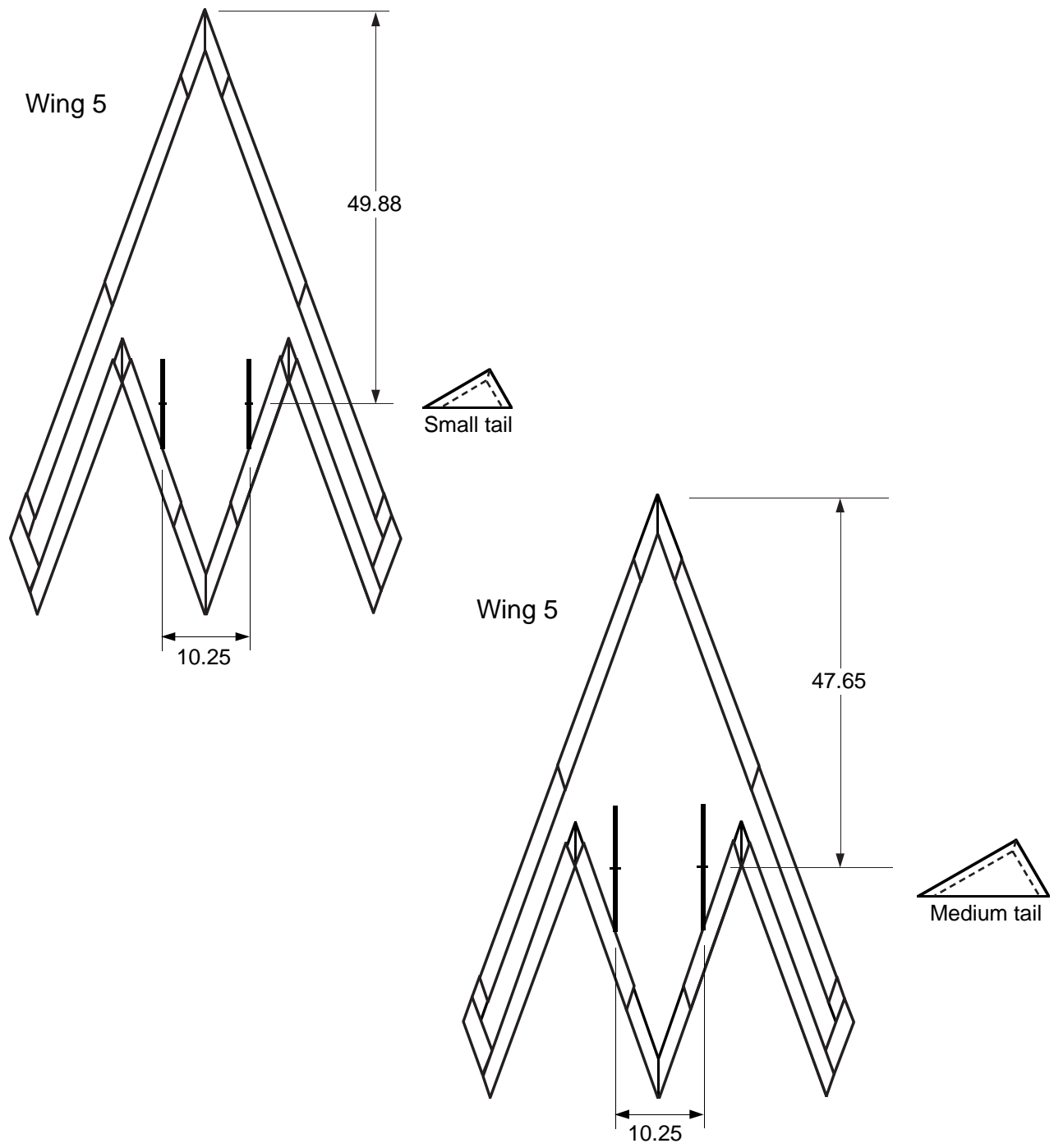
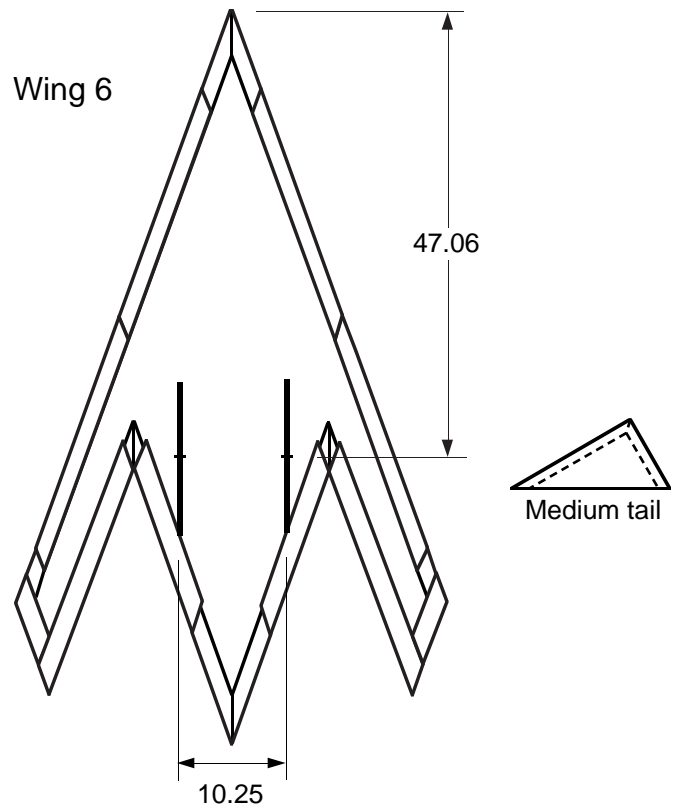
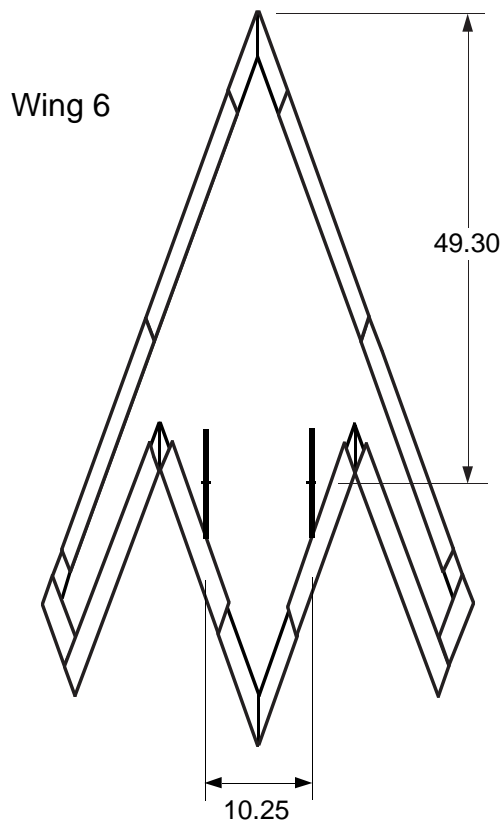


Figure 12. Medium and small vertical tails. All dimensions are in inches. Dashed lines indicate bevel lines.



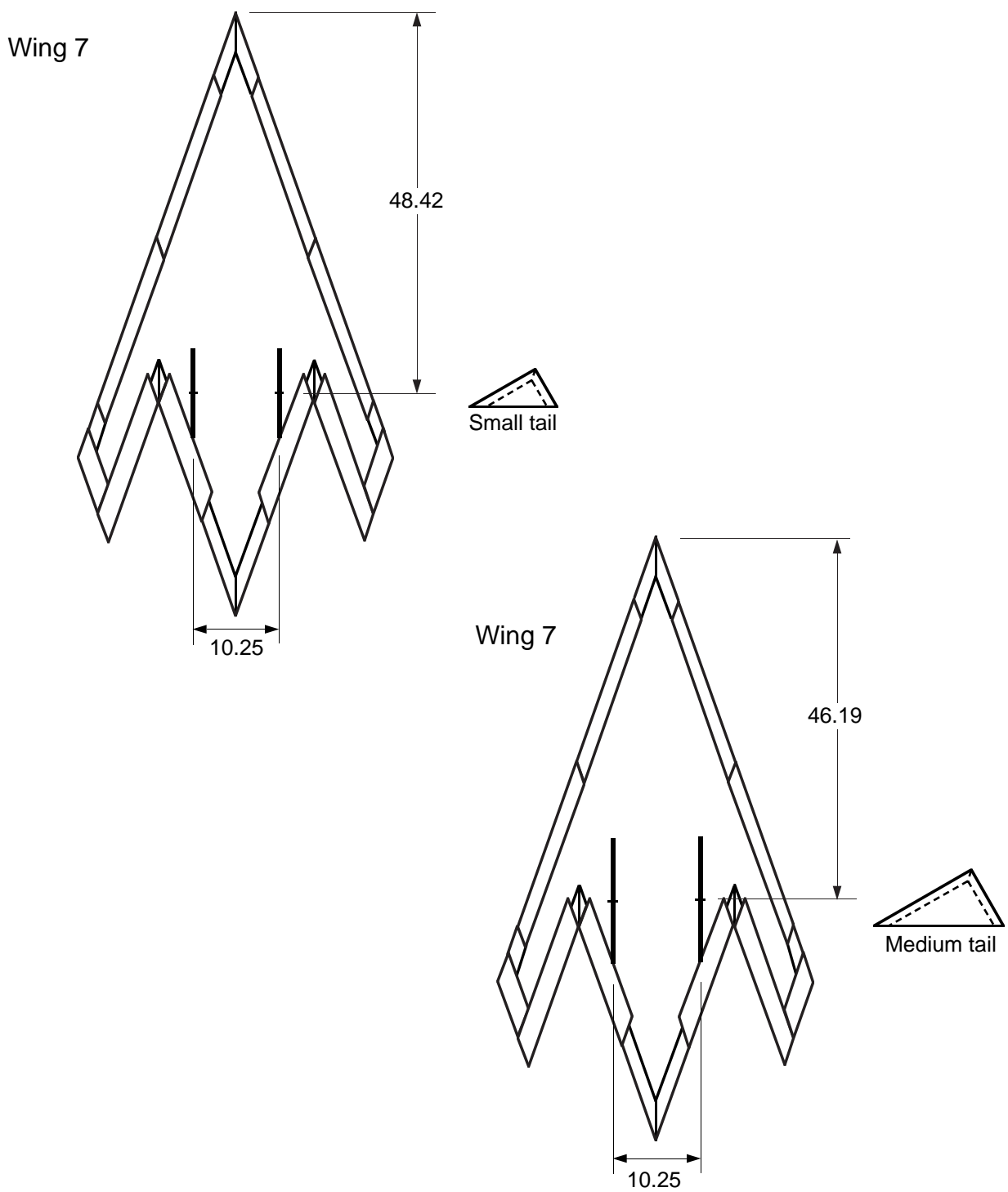
(a) Small and medium tails on Wing 5.

Figure 13. Vertical tail locations. All dimensions are in inches.



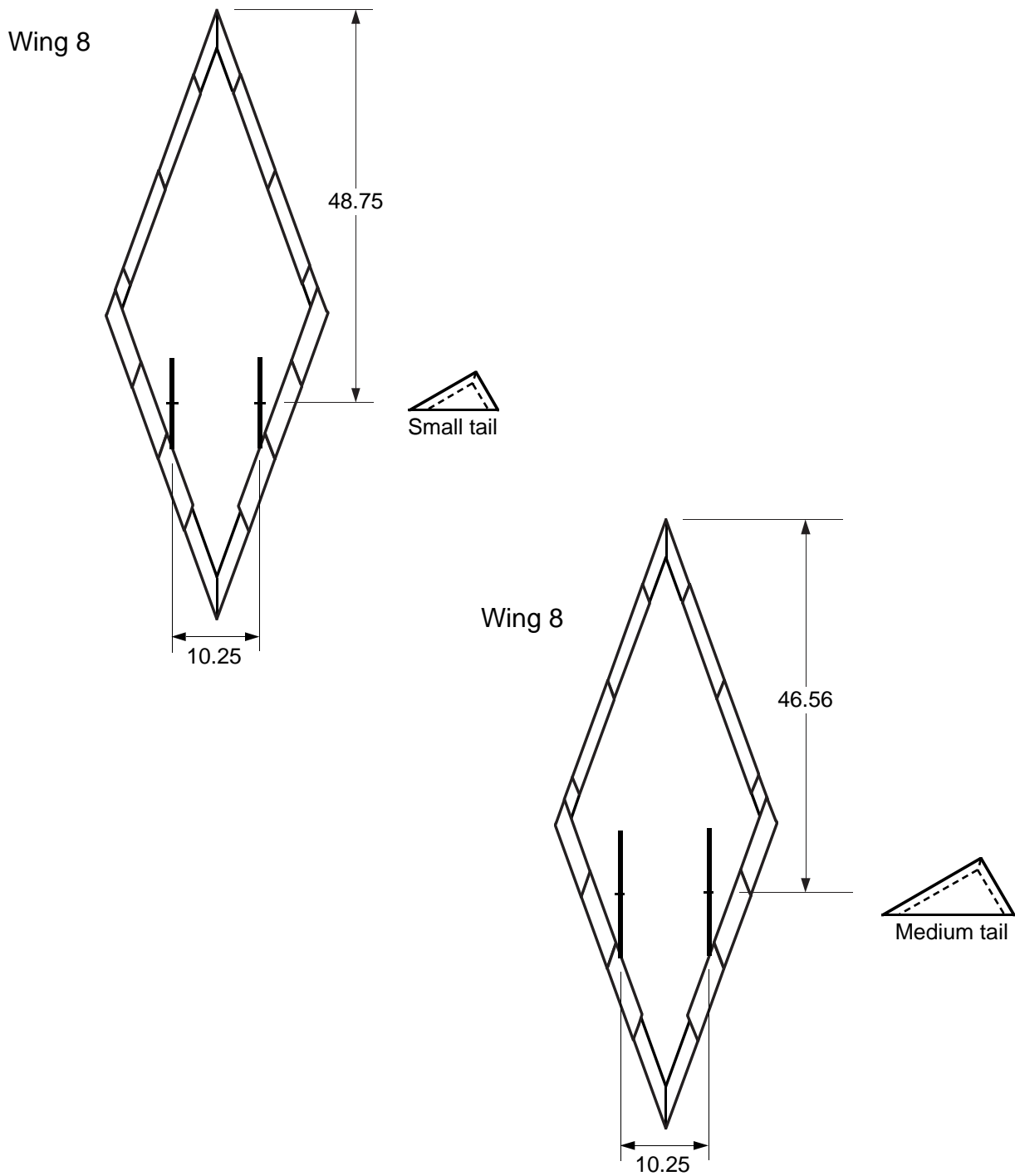
(b) Small and medium tails on Wing 6.

Figure 13. Continued.



(c) Small and medium tails on Wing 7.

Figure 13. Continued.



(d) Small and medium tails on Wing 8.

Figure 13. Concluded.

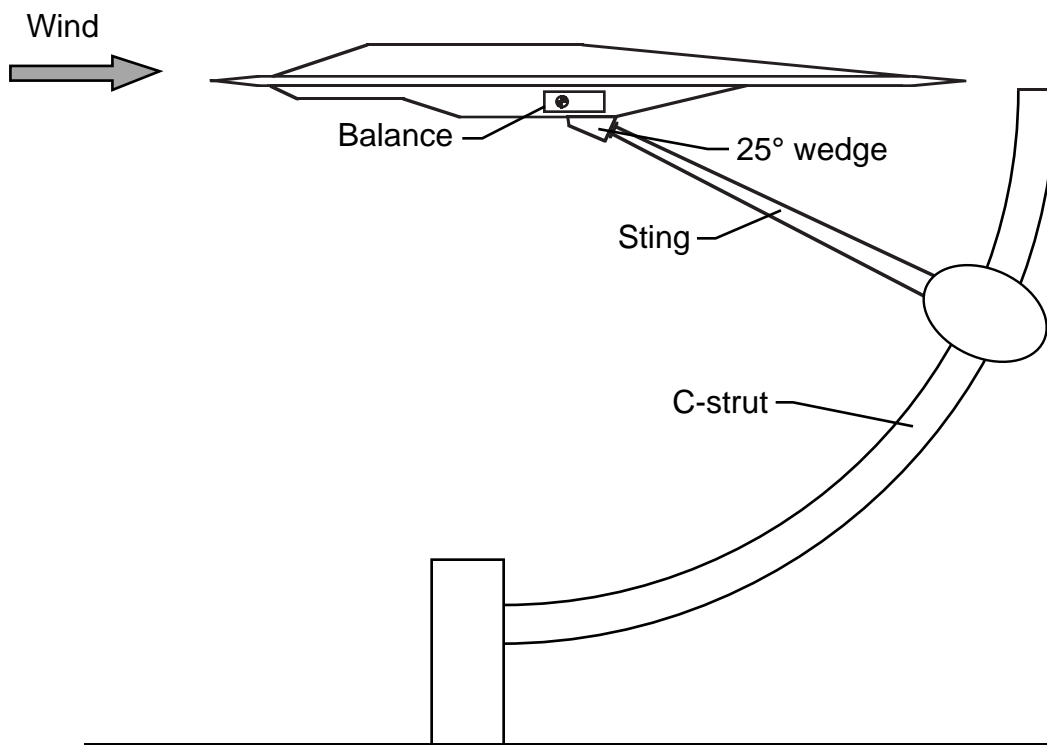


Figure 14. Typical configuration mounted on sting and C-strut arrangement in wind-tunnel test section. Not to scale.

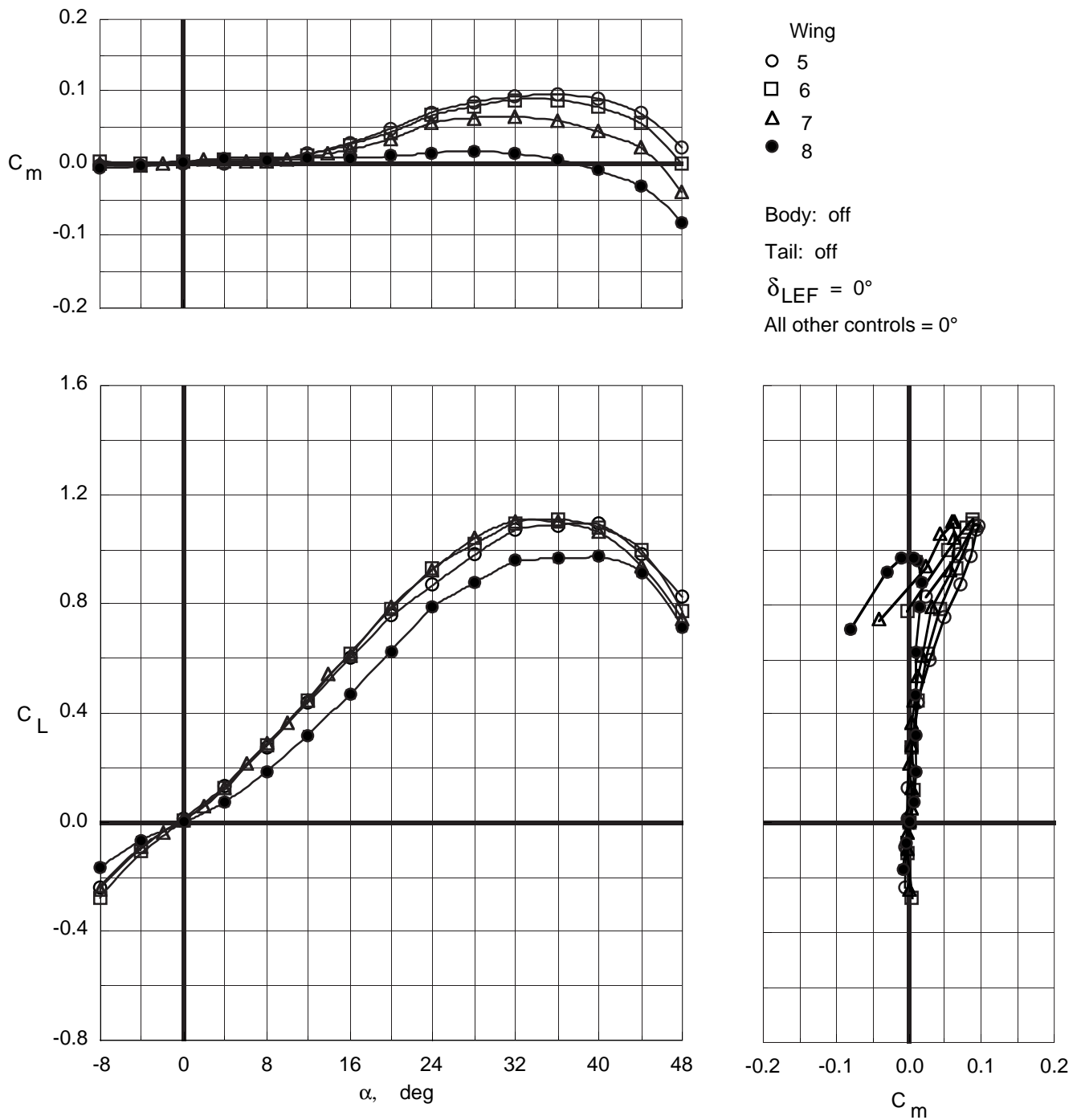


Figure 15. Longitudinal characteristics of wing planforms with top body off.

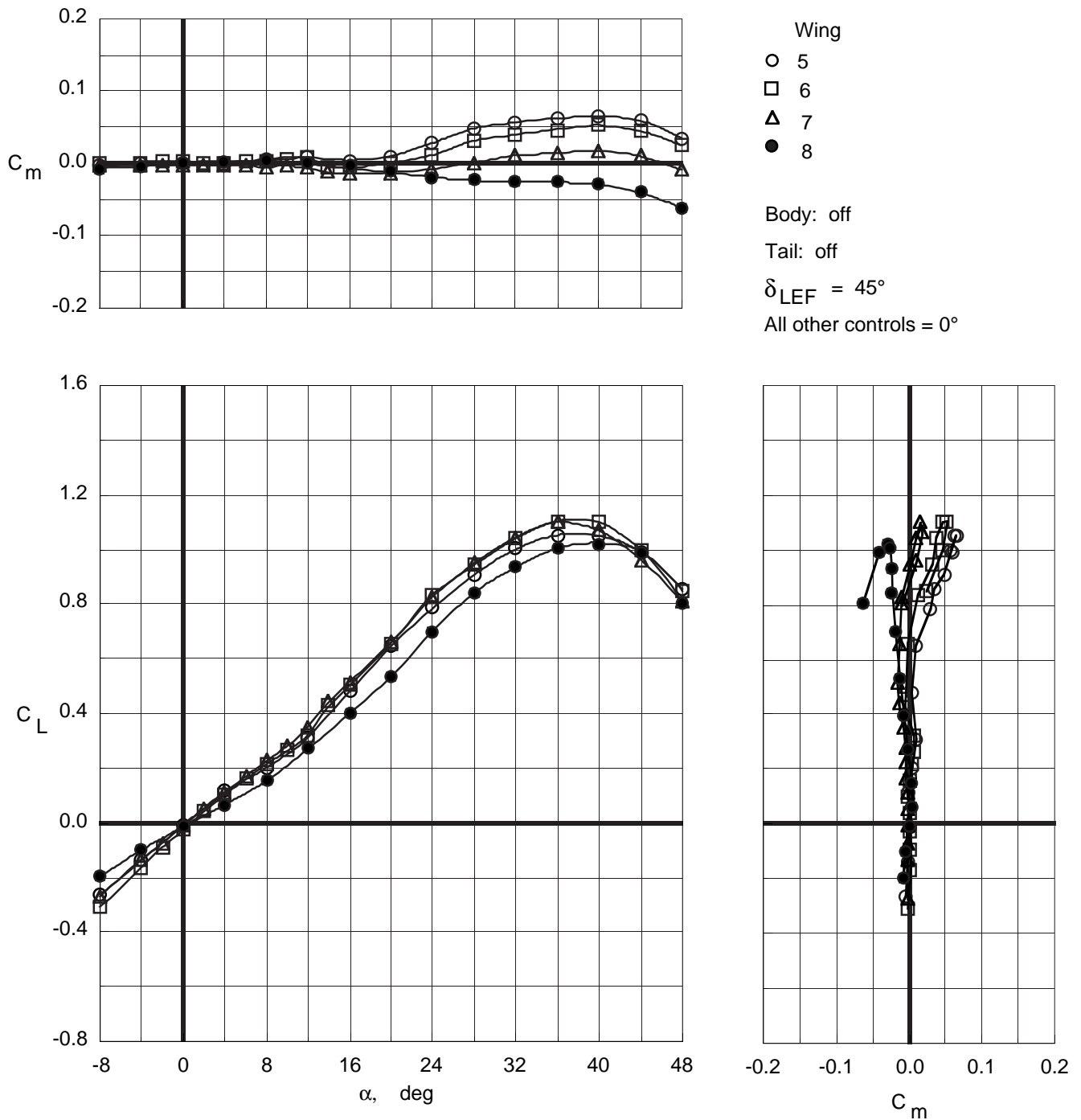


Figure 16. Longitudinal characteristics of wing planforms with top body off and leading-edge flaps deflected.

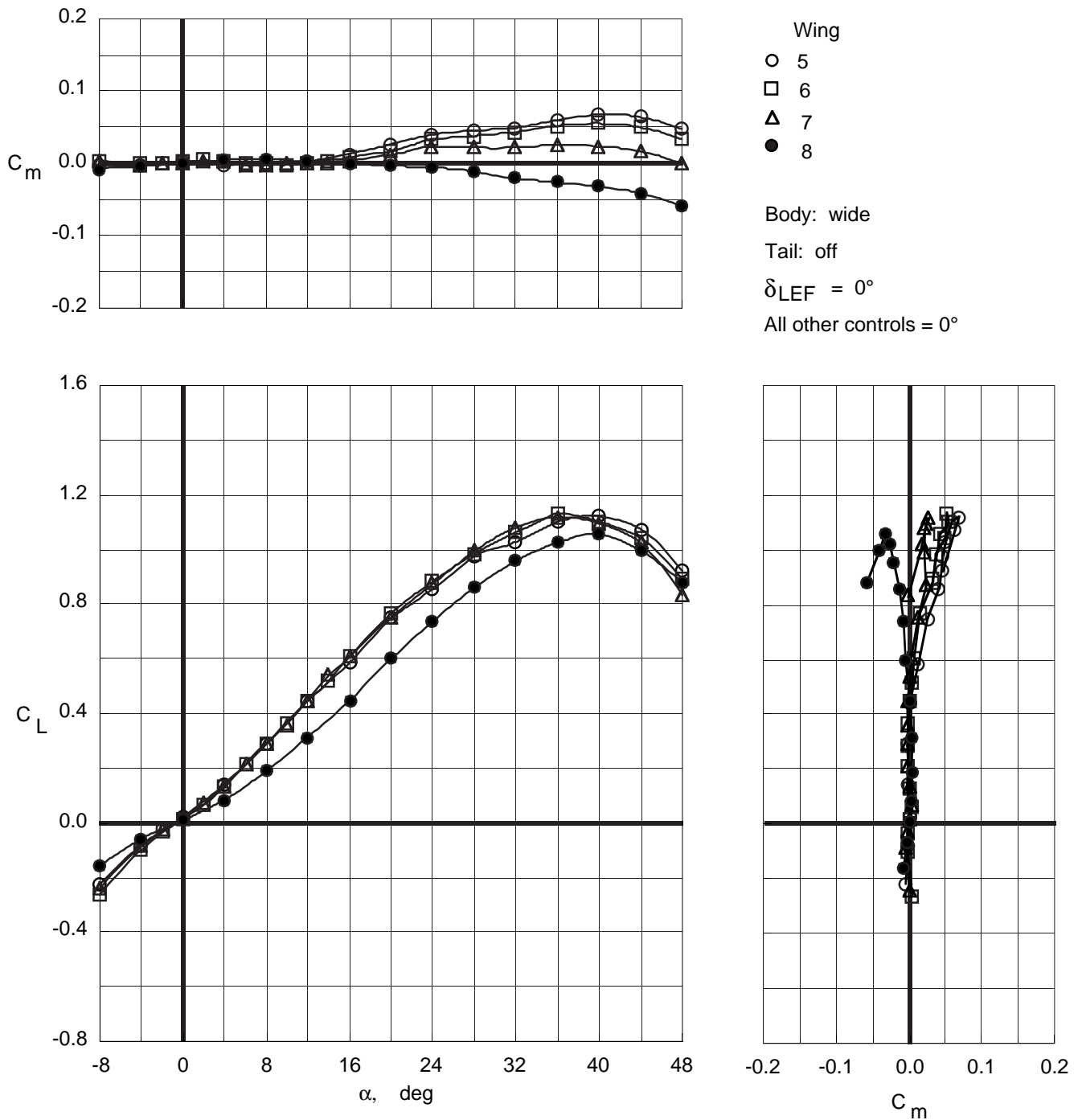


Figure 17. Longitudinal characteristics of wing planforms with wide top body on.

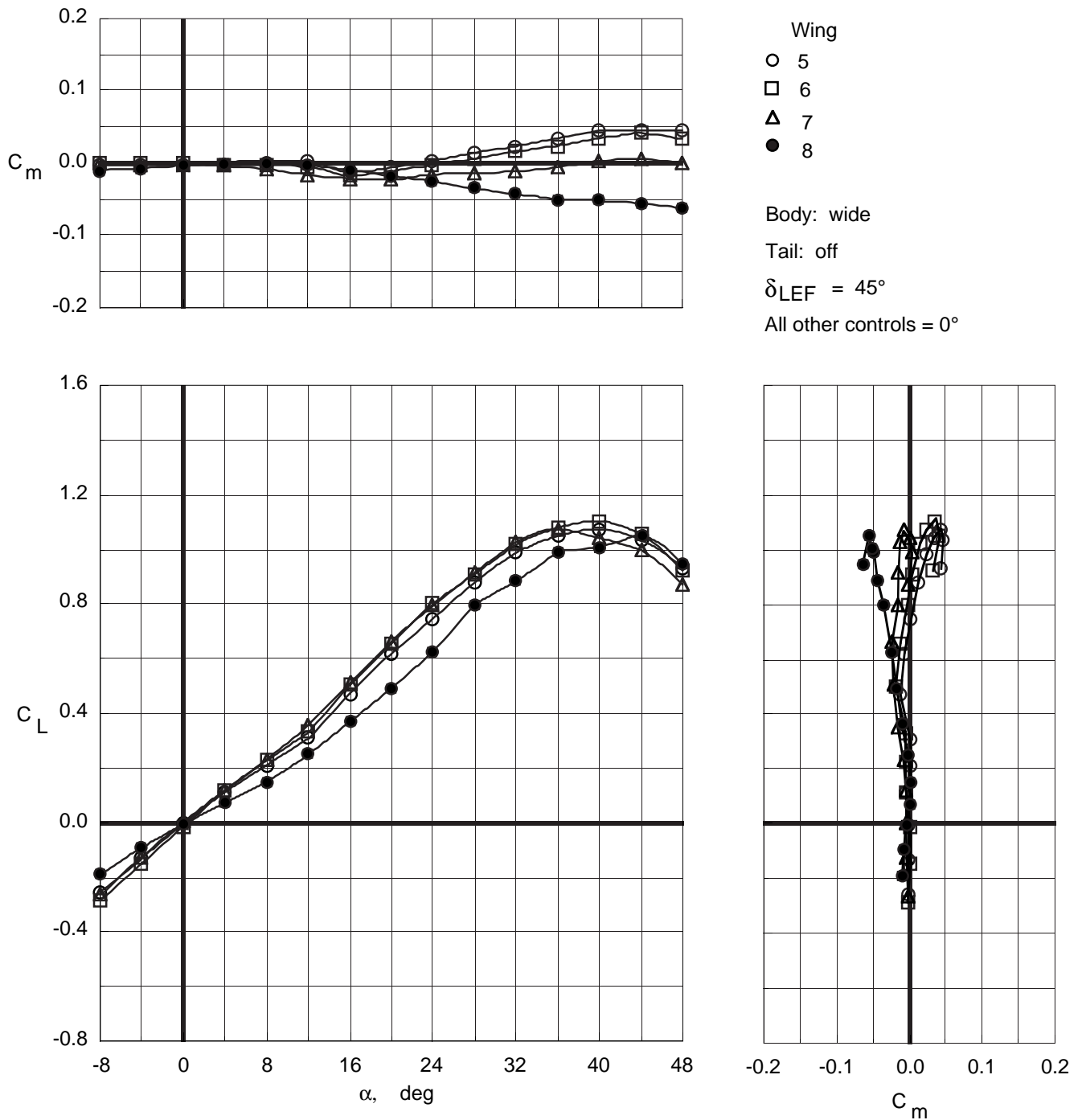


Figure 18. Longitudinal characteristics of wing planforms with wide top body on and leading-edge flaps deflected.

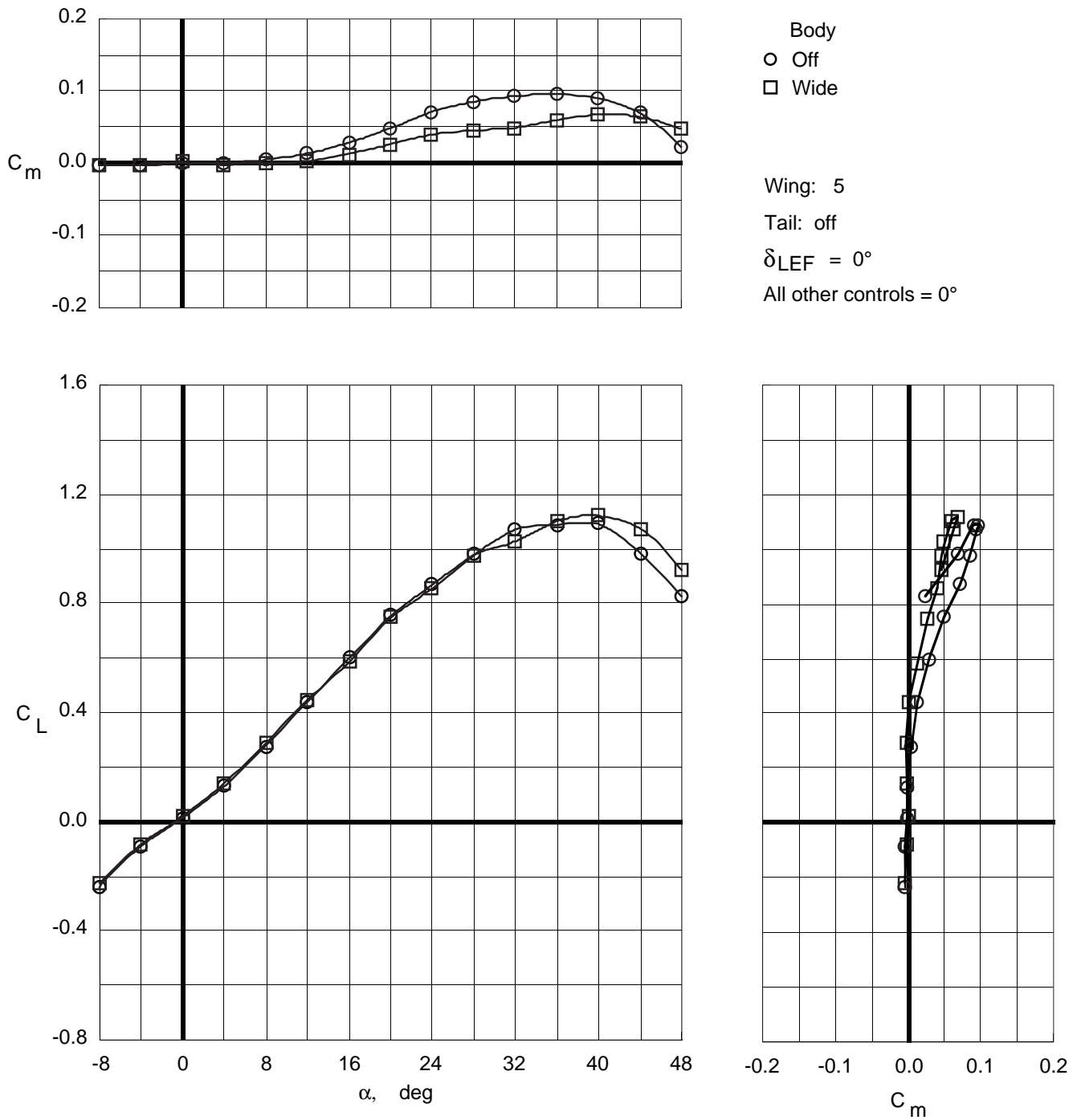


Figure 19. Effect of wide top body on longitudinal characteristics of Wing 5.

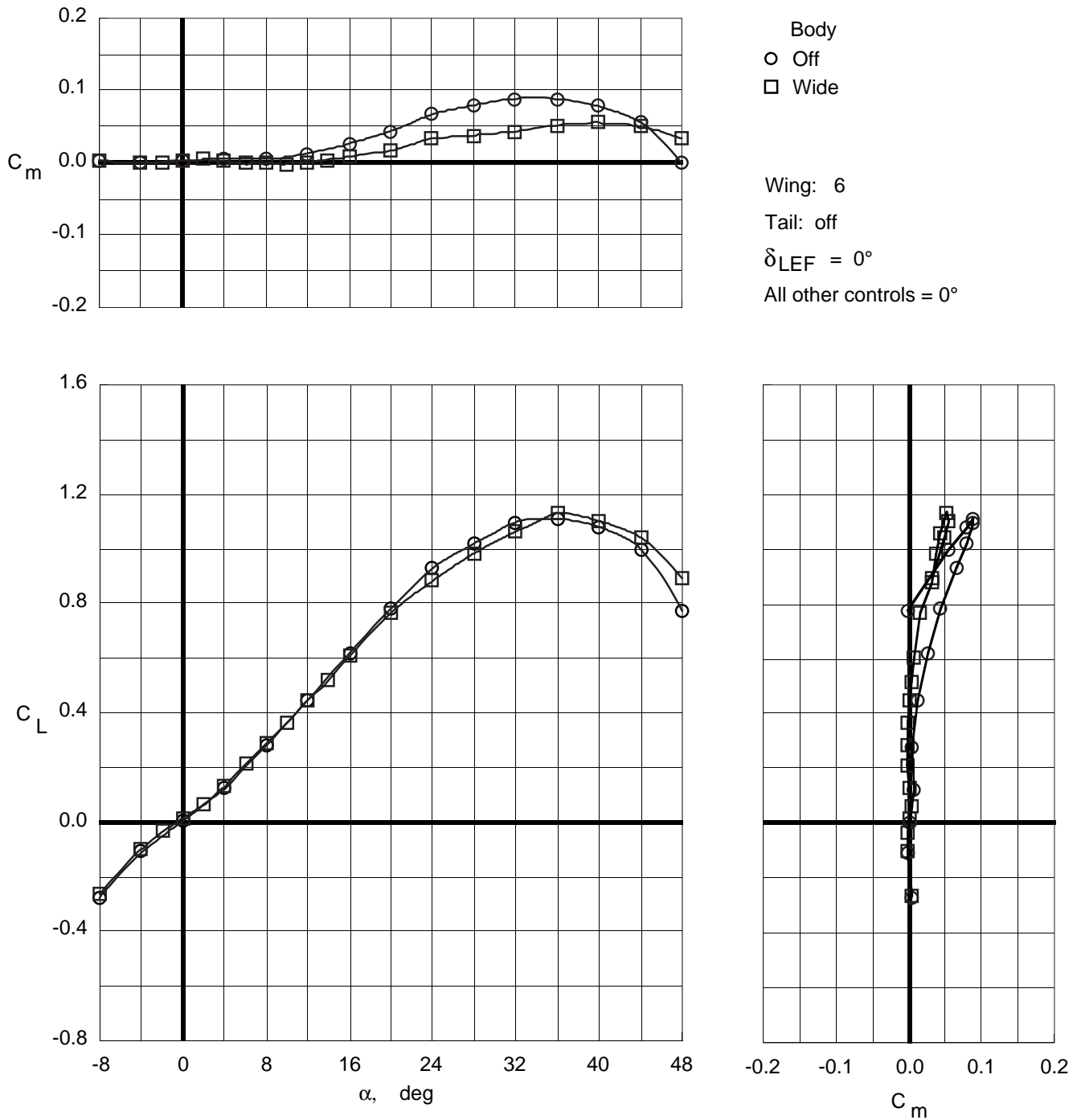


Figure 20. Effect of wide top body on longitudinal characteristics of Wing 6.

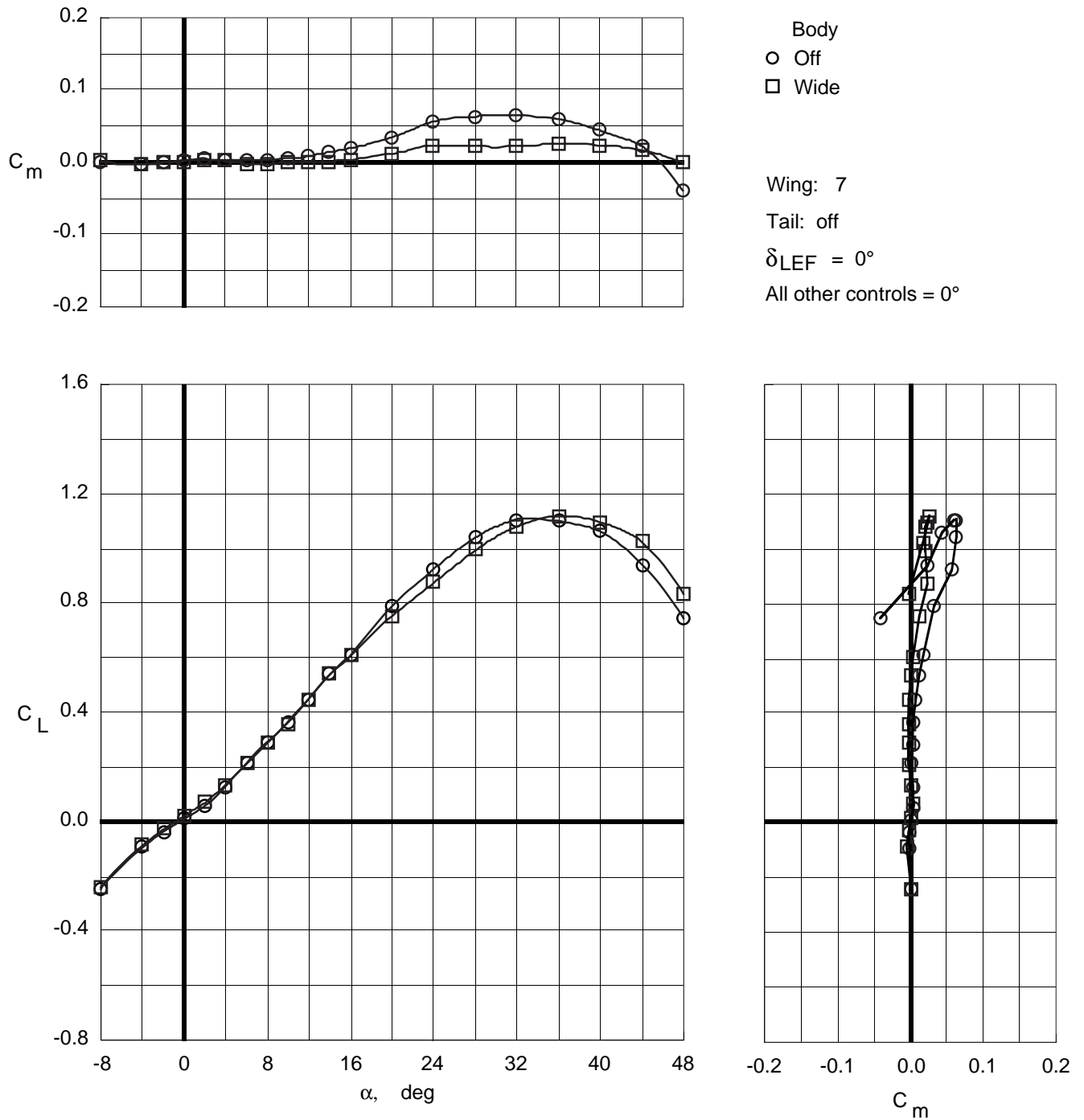


Figure 21. Effect of wide top body on longitudinal characteristics of Wing 7.

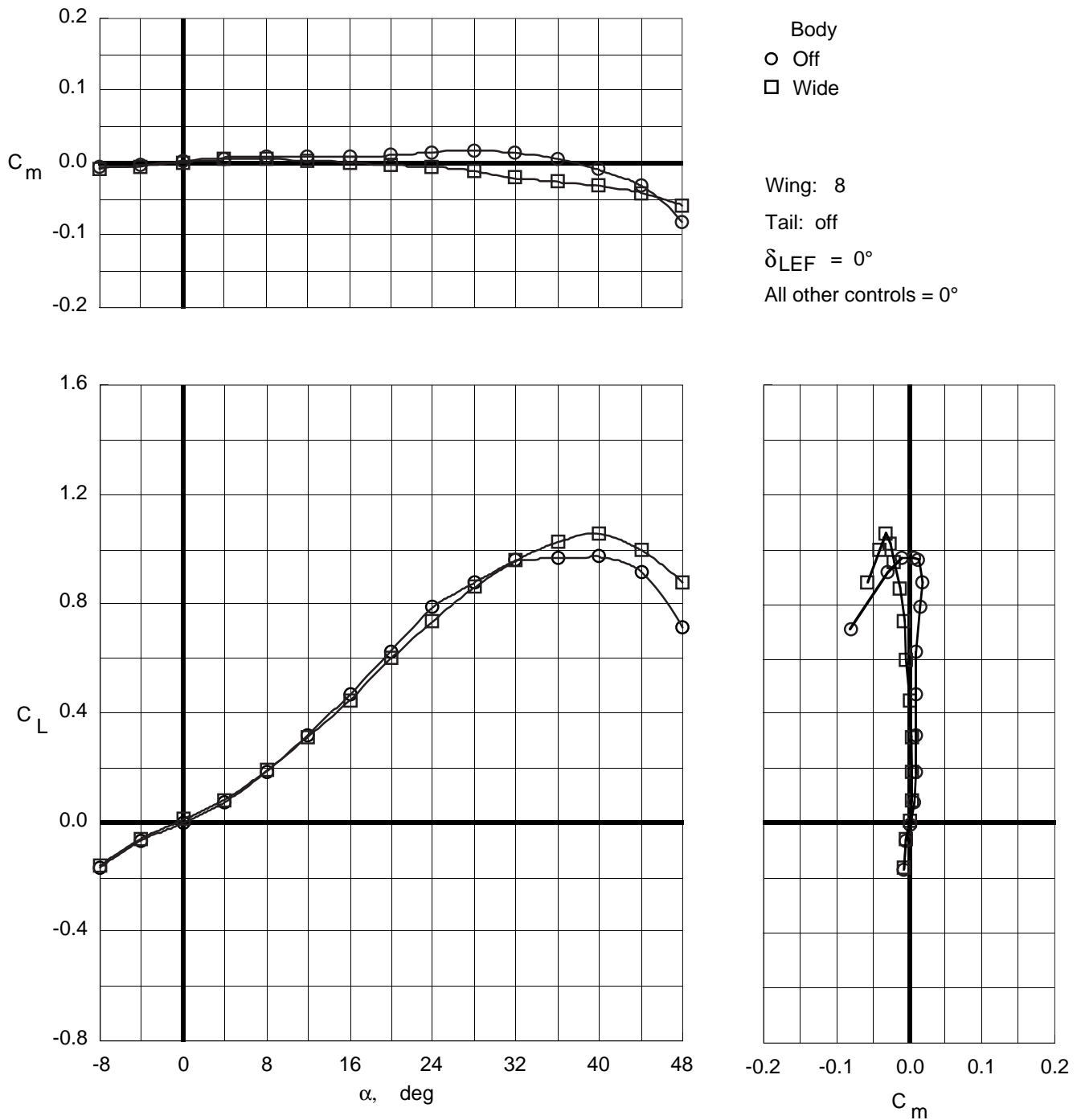


Figure 22. Effect of wide top body on longitudinal characteristics of Wing 8.

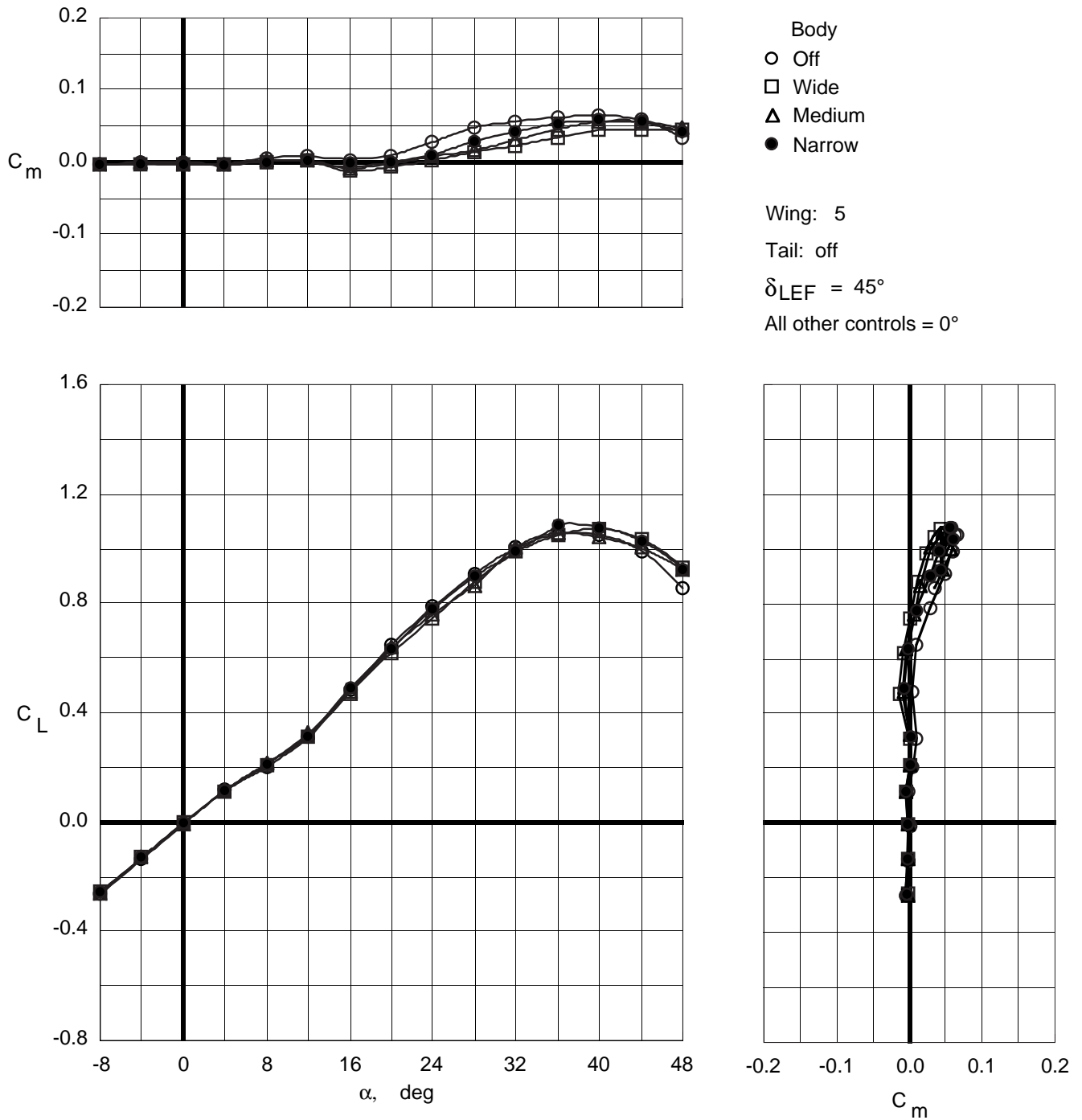


Figure 23. Effect of top body on longitudinal characteristics of Wing 5 with leading-edge flaps deflected.

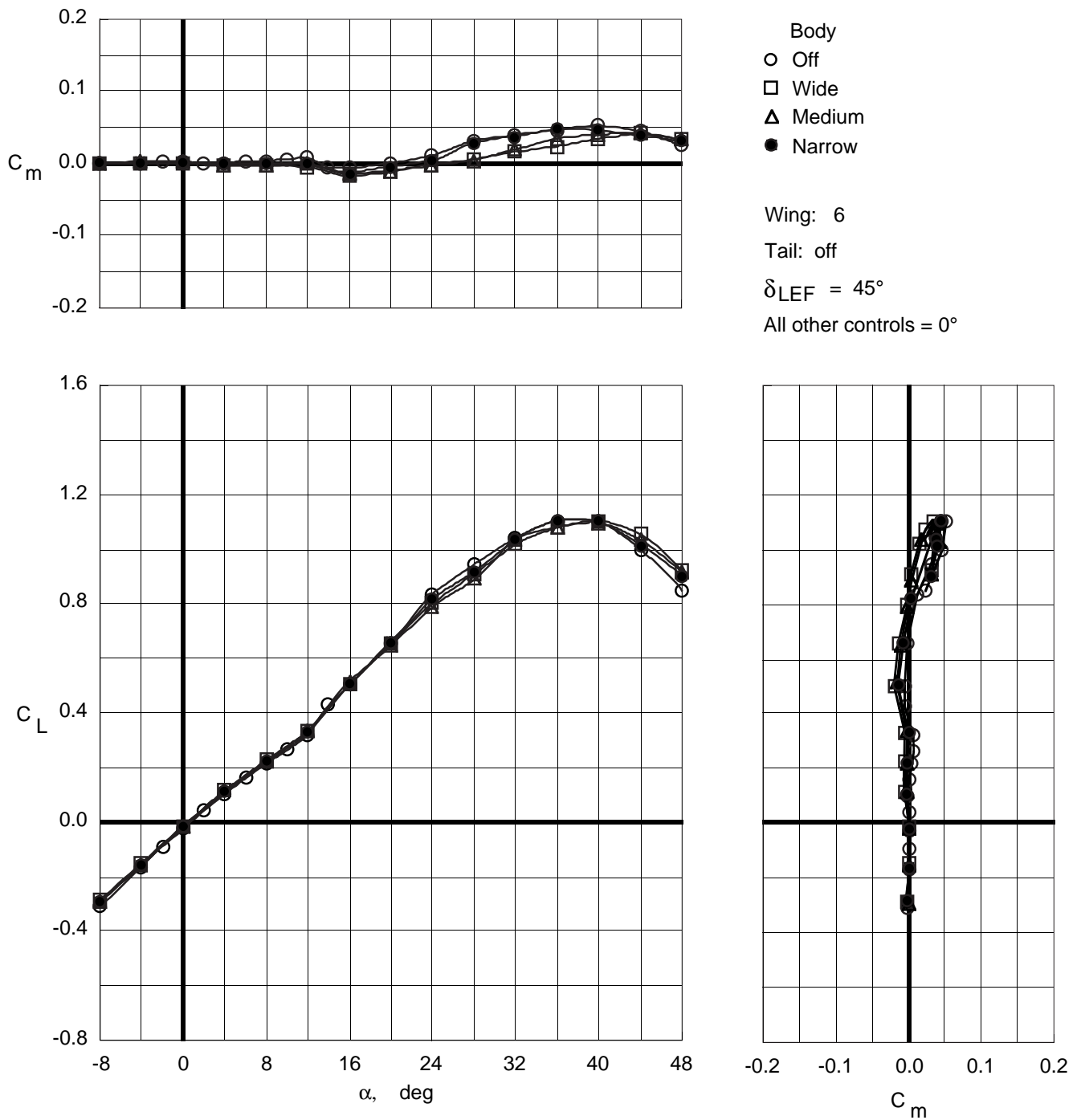


Figure 24. Effect of top body width on longitudinal characteristics of Wing 6 with leading-edge flaps deflected.

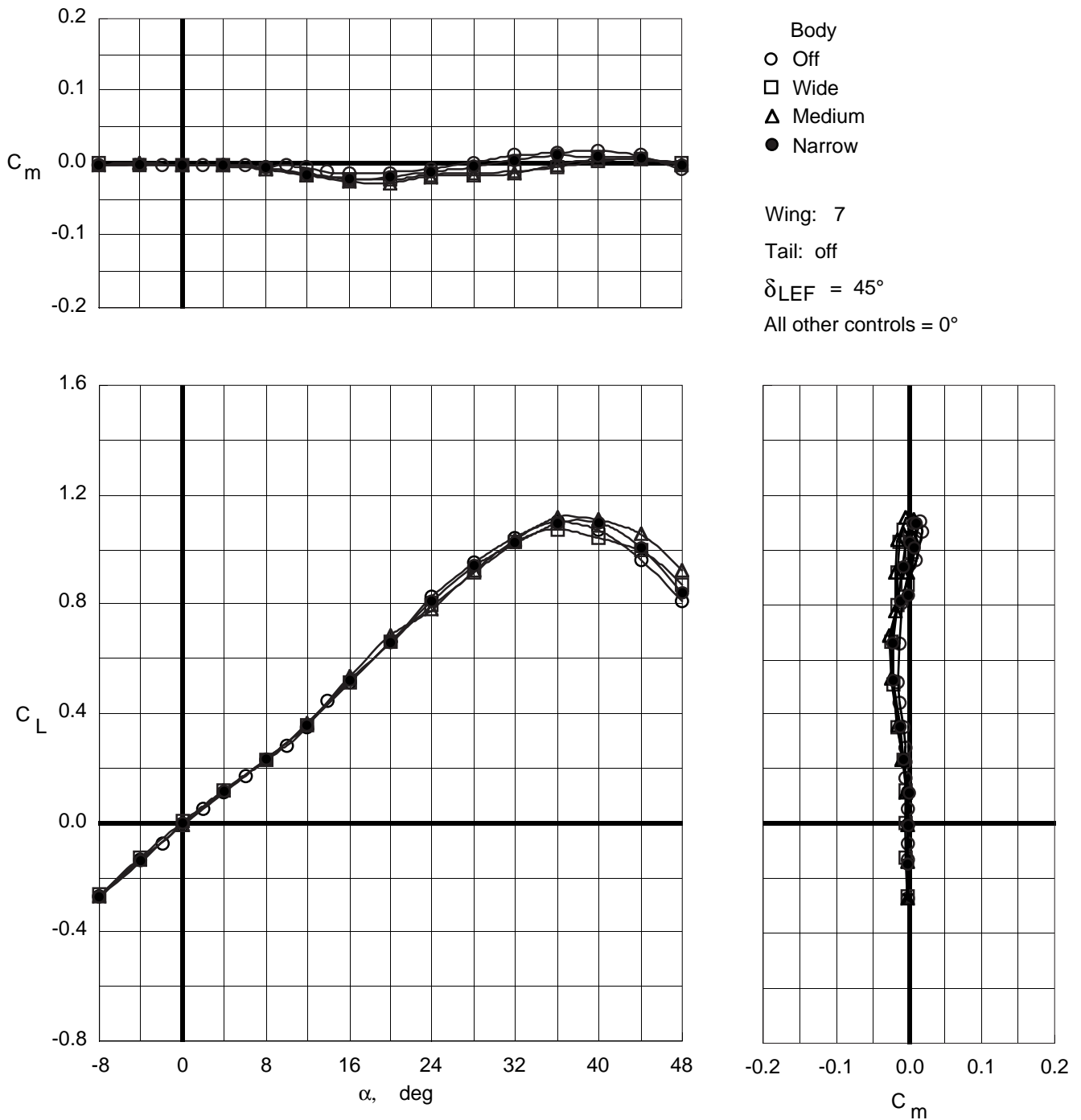


Figure 25. Effect of top body width on longitudinal characteristics of Wing 7 with leading-edge flaps deflected.

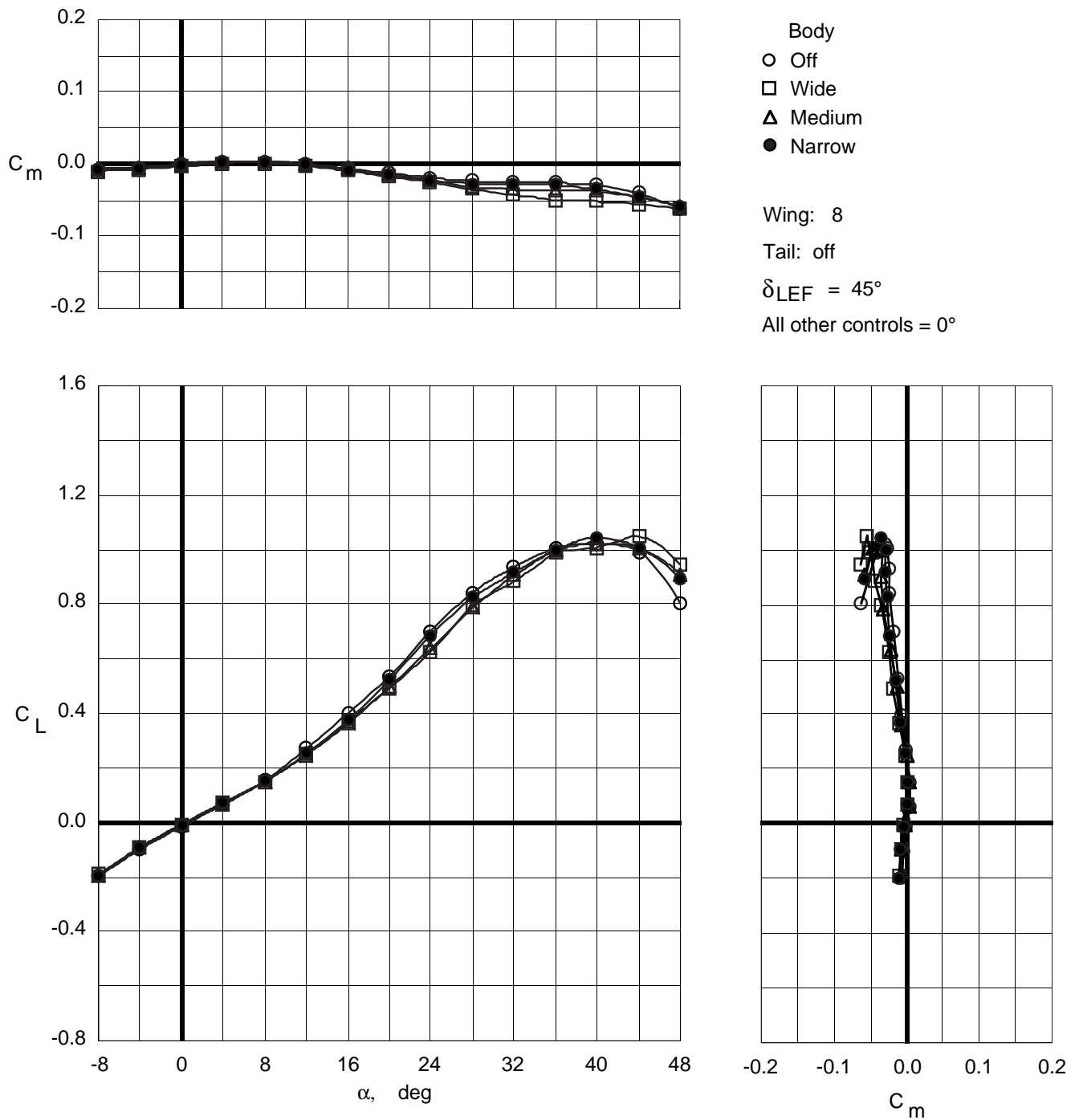


Figure 26. Effect of top body width on longitudinal characteristics of Wing 8 with leading-edge flaps deflected.

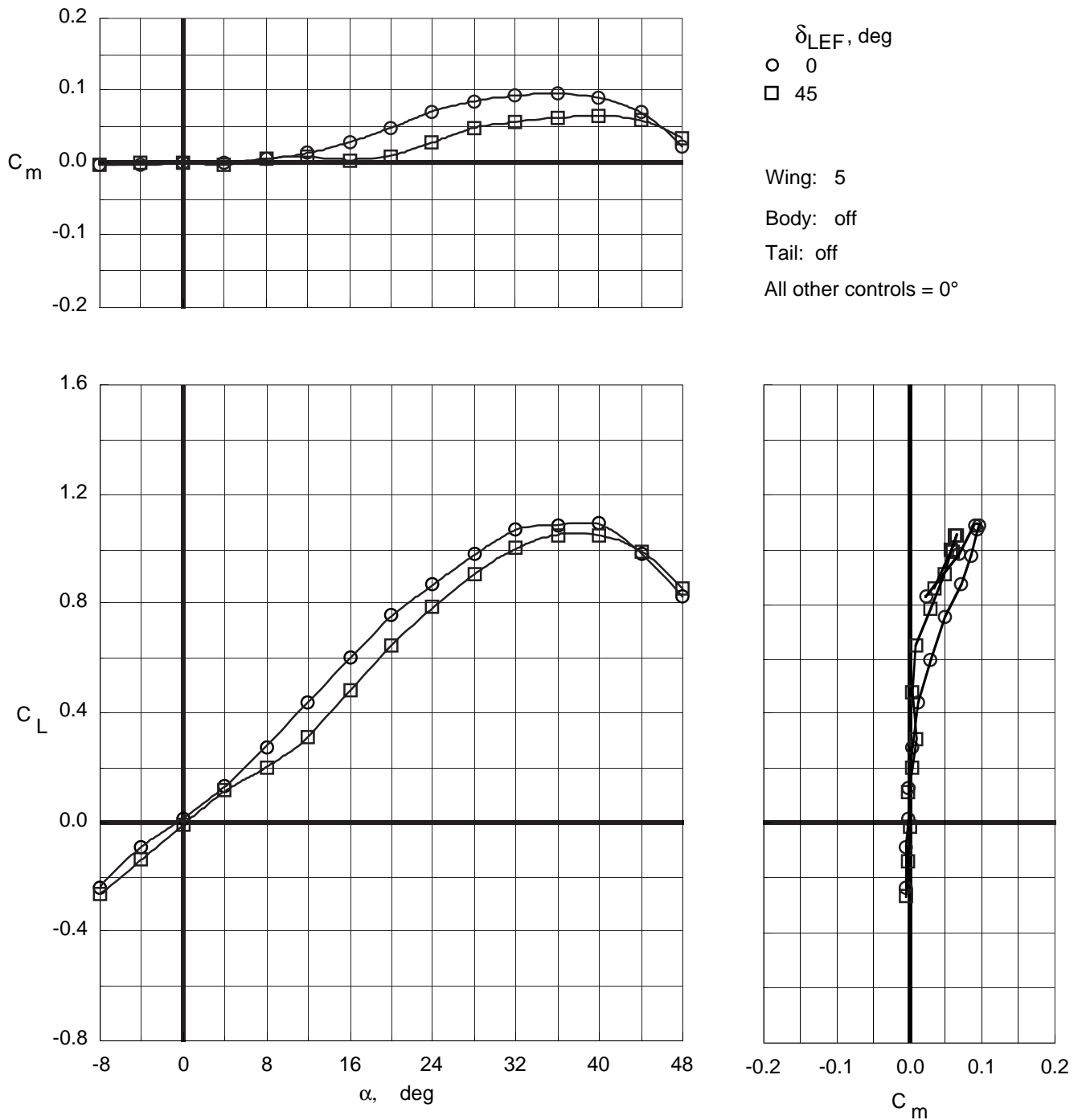


Figure 27. Effect of leading-edge flap deflection on longitudinal characteristics of Wing 5 with top body off.

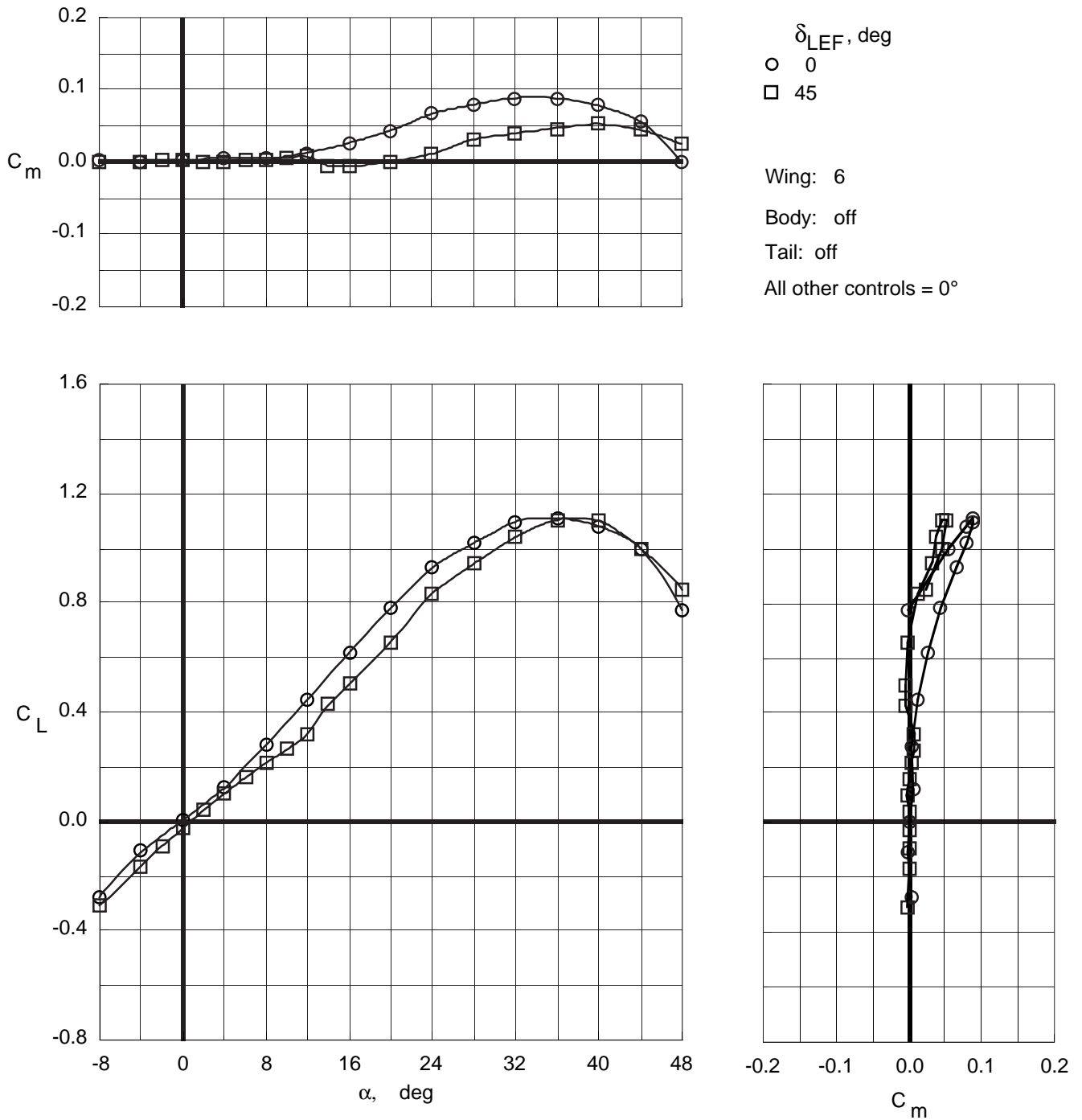


Figure 28. Effect of leading-edge flap deflection on longitudinal characteristics of Wing 6 with top body off.

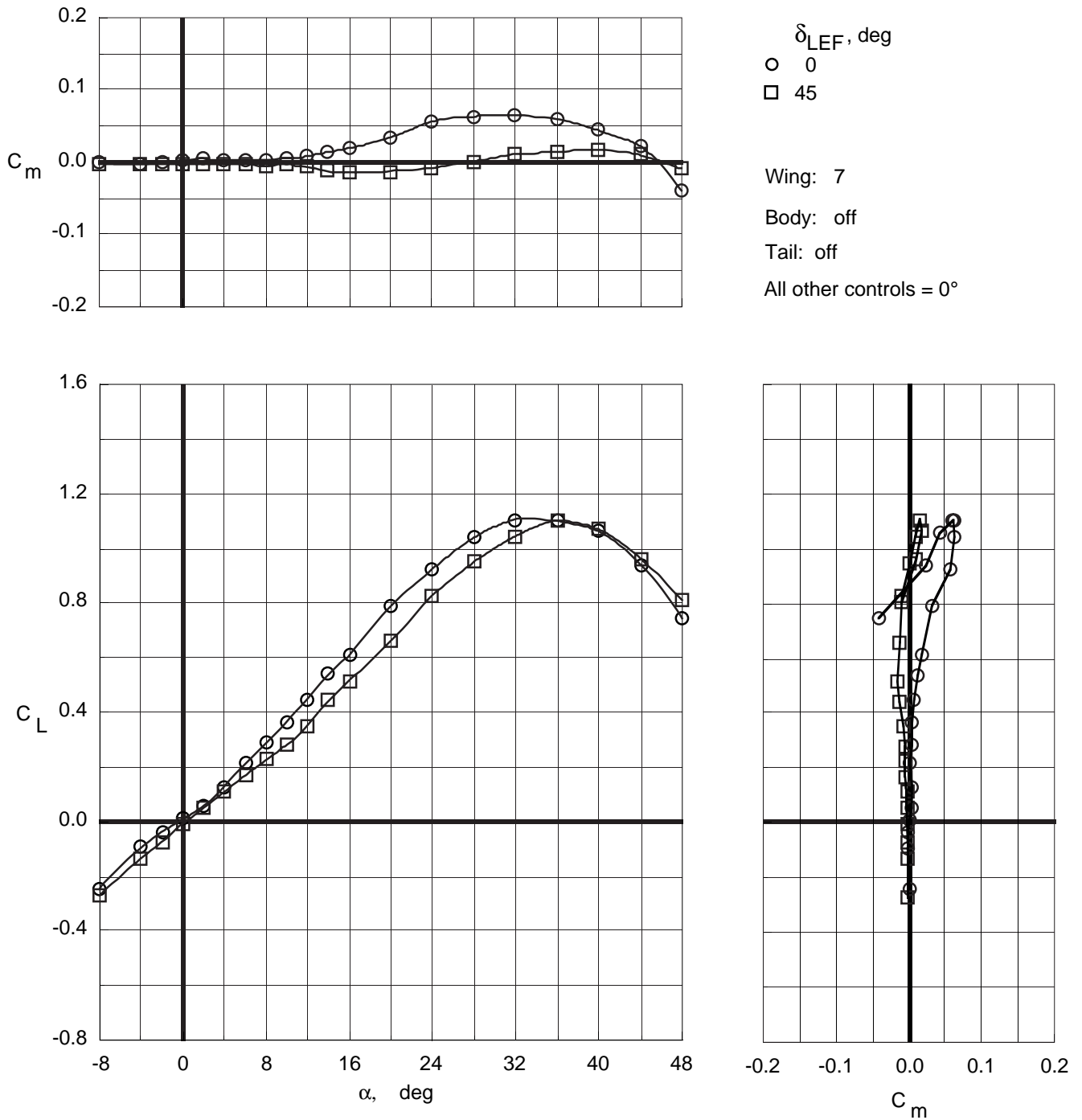


Figure 29. Effect of leading-edge flap deflection on longitudinal characteristics of Wing 7 with top body off.

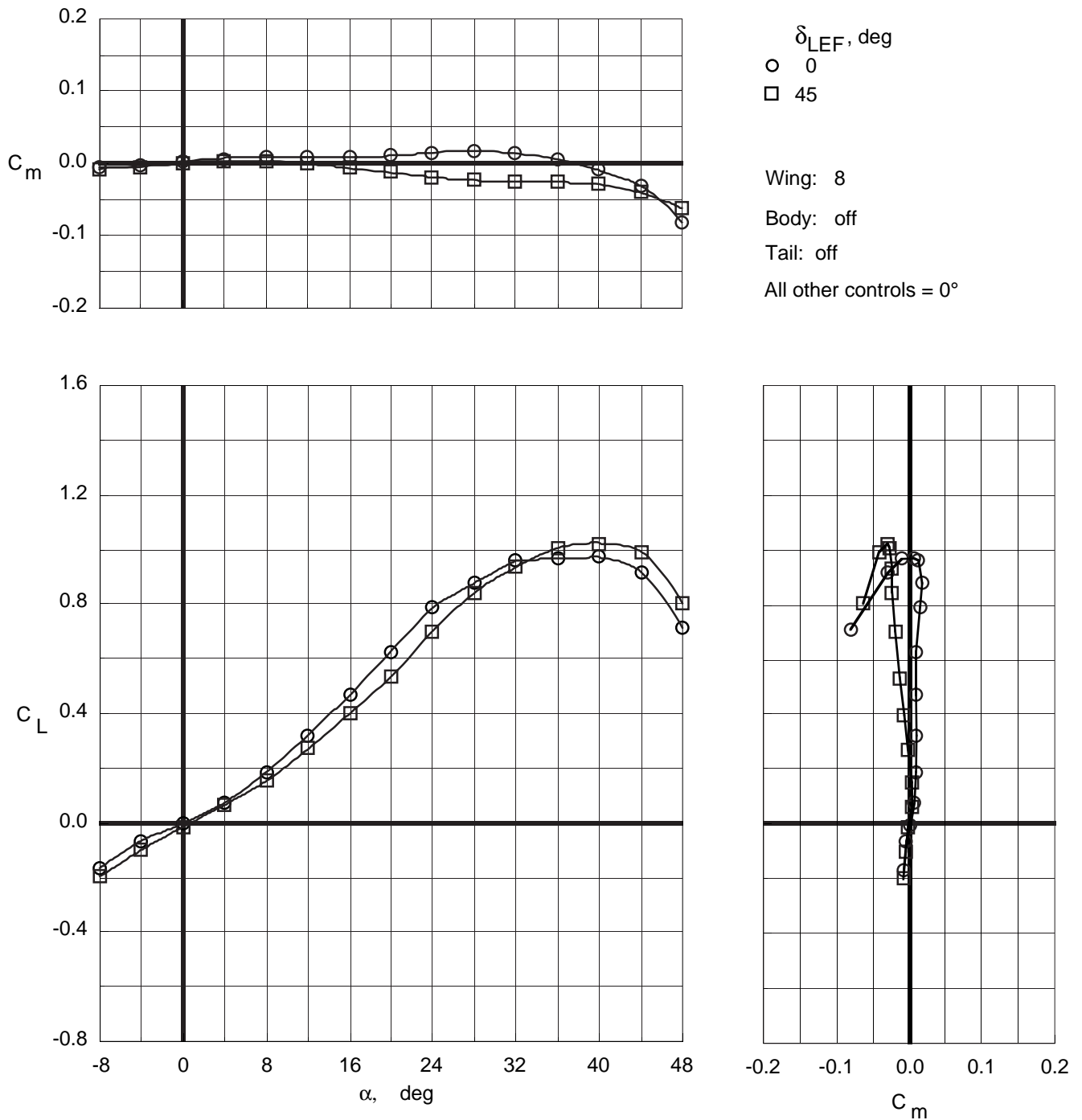


Figure 30. Effect of leading-edge flap deflection on longitudinal characteristics of Wing 8 with top body off.

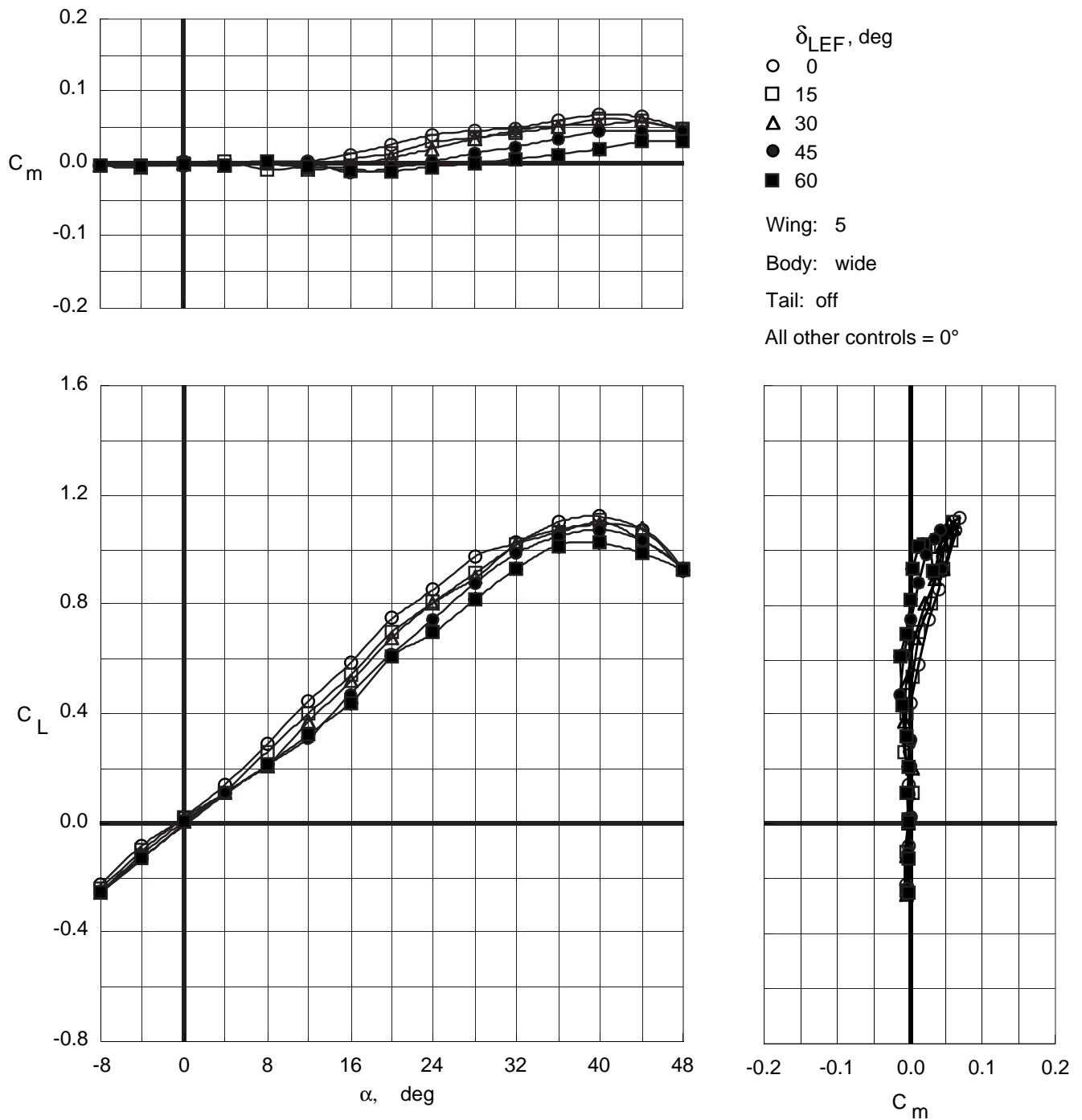


Figure 31. Effect of leading-edge flap deflections on longitudinal characteristics of Wing 5 with wide top body on.

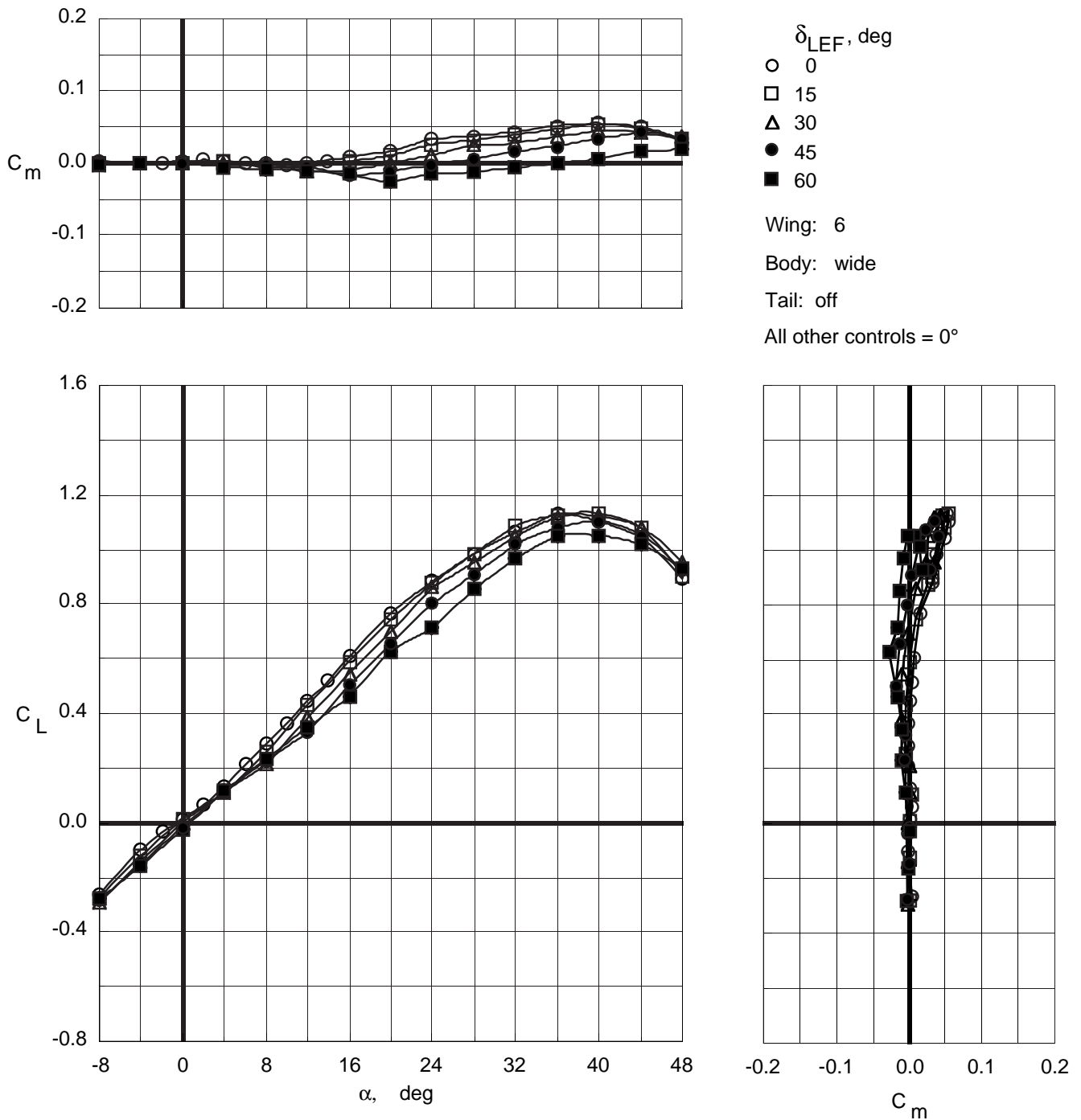


Figure 32. Effect of leading-edge flap deflections on longitudinal characteristics of Wing 6 with wide top body on.

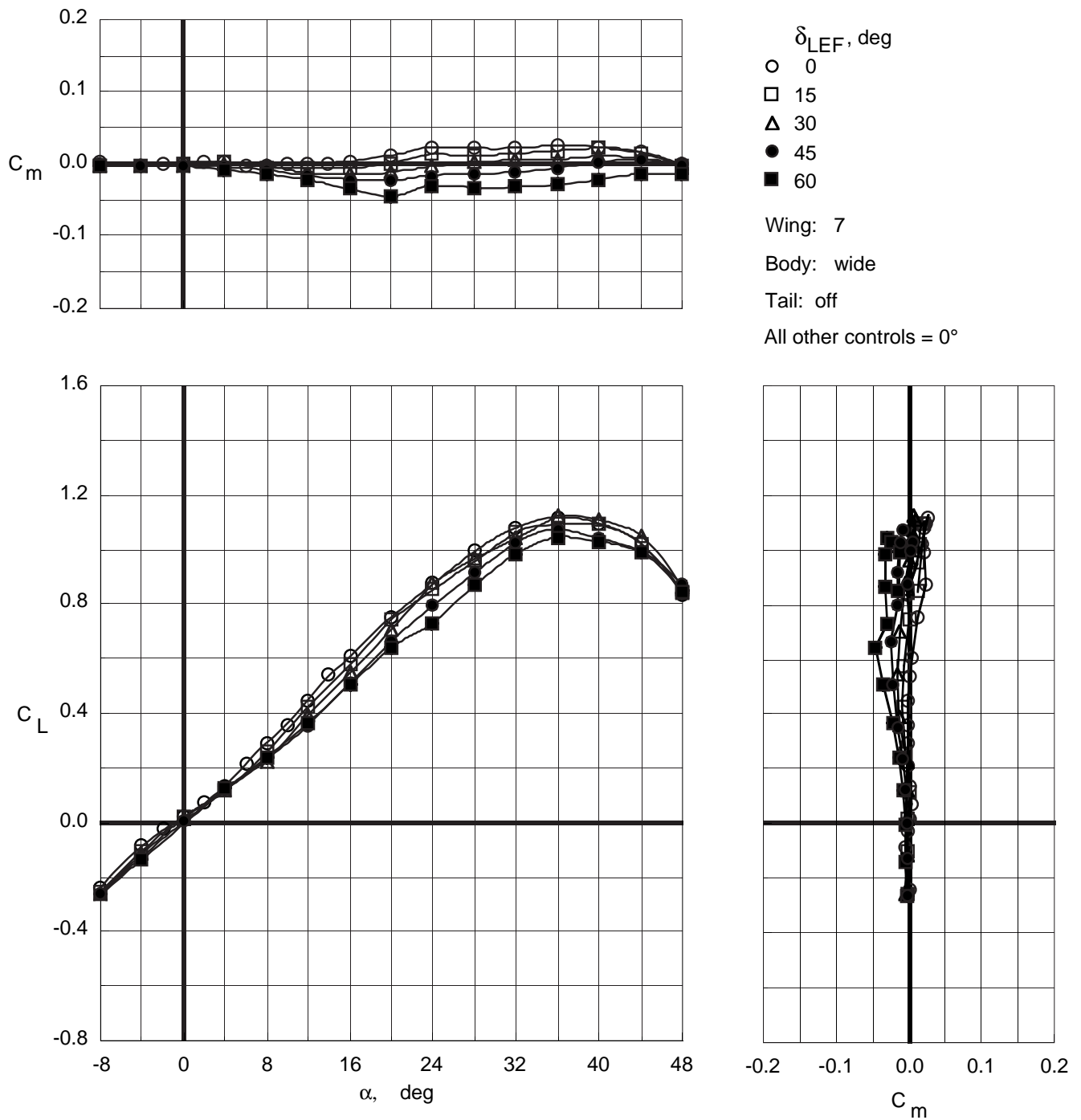


Figure 33. Effect of leading-edge flap deflections on longitudinal characteristics of Wing 7 with wide top body on.

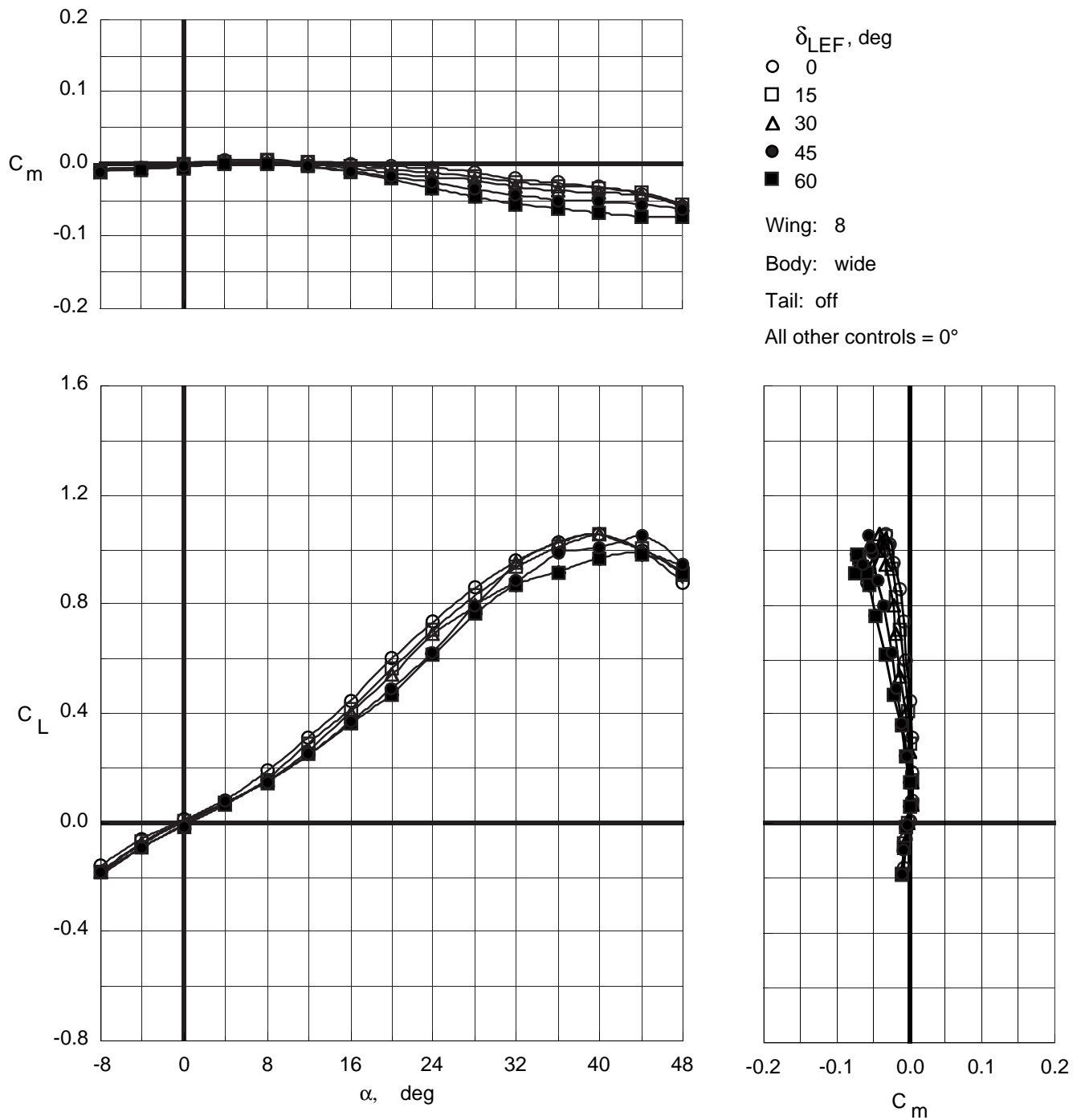


Figure 34. Effect of leading-edge flap deflections on longitudinal characteristics of Wing 8 with wide top body on.

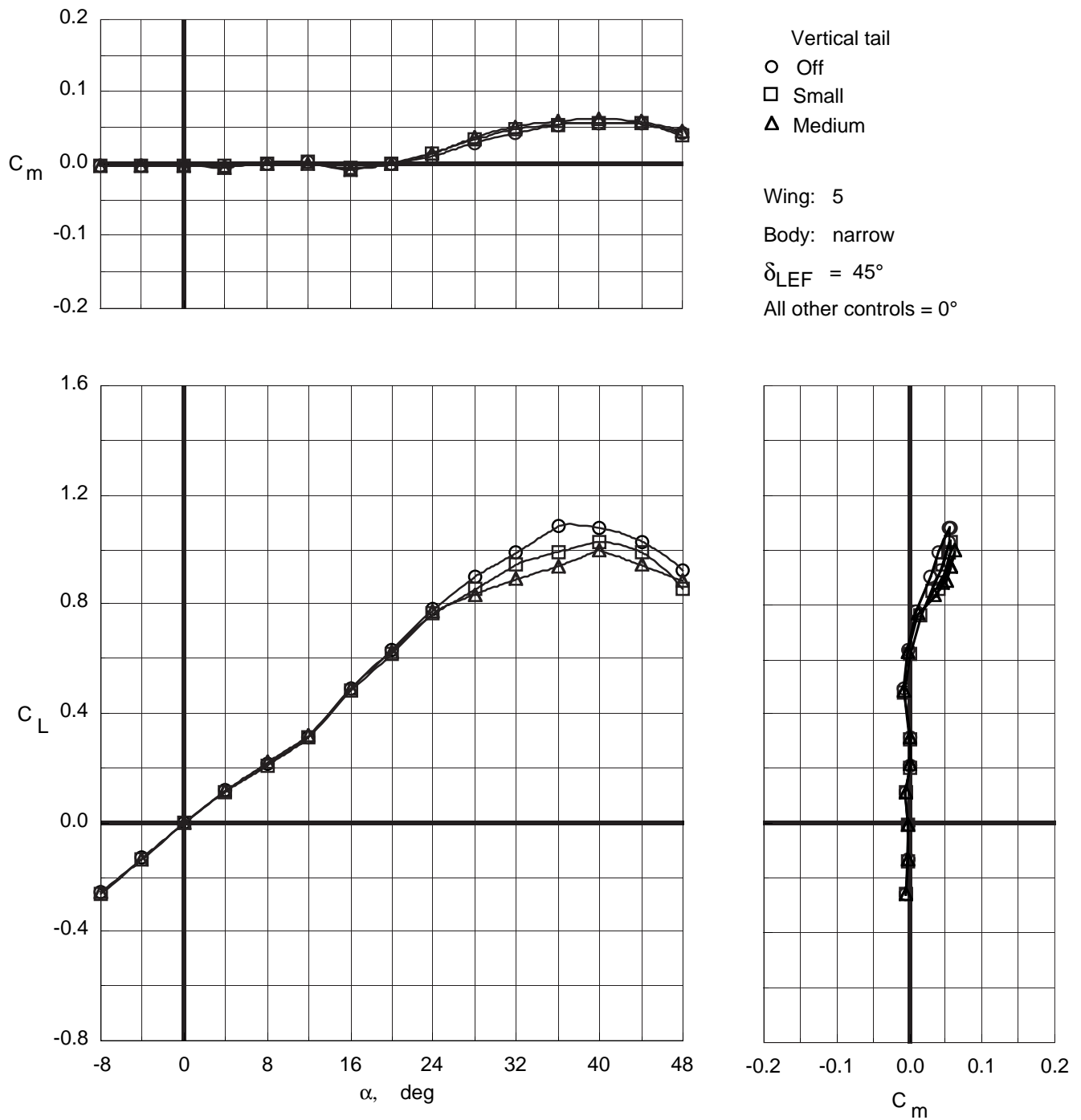


Figure 35. Effect of vertical tail size on longitudinal characteristics of Wing 5 with narrow top body on and leading-edge flaps deflected.

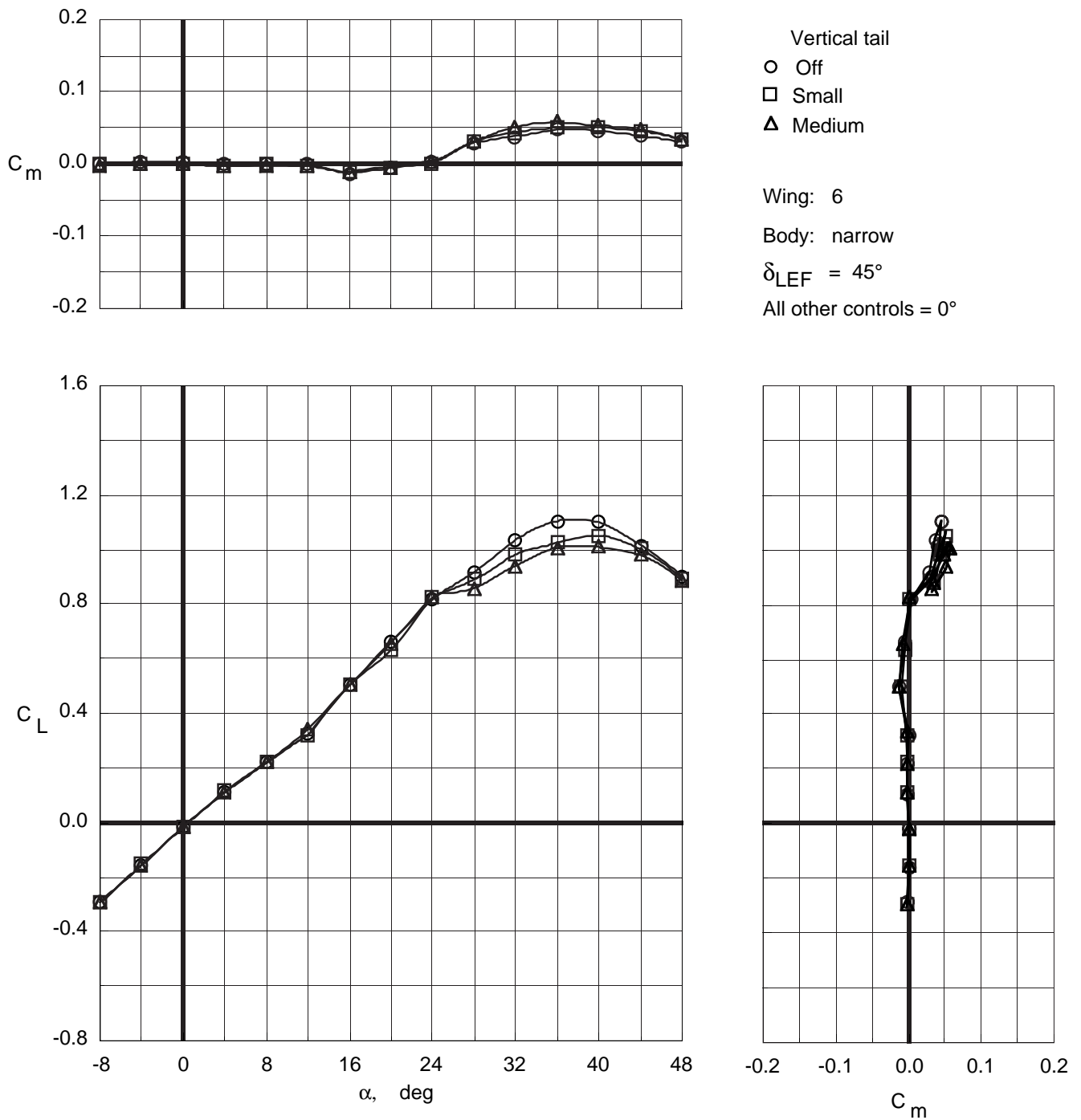


Figure 36. Effect of vertical tail size on longitudinal characteristics of Wing 6 with narrow top body on and leading-edge flaps deflected.

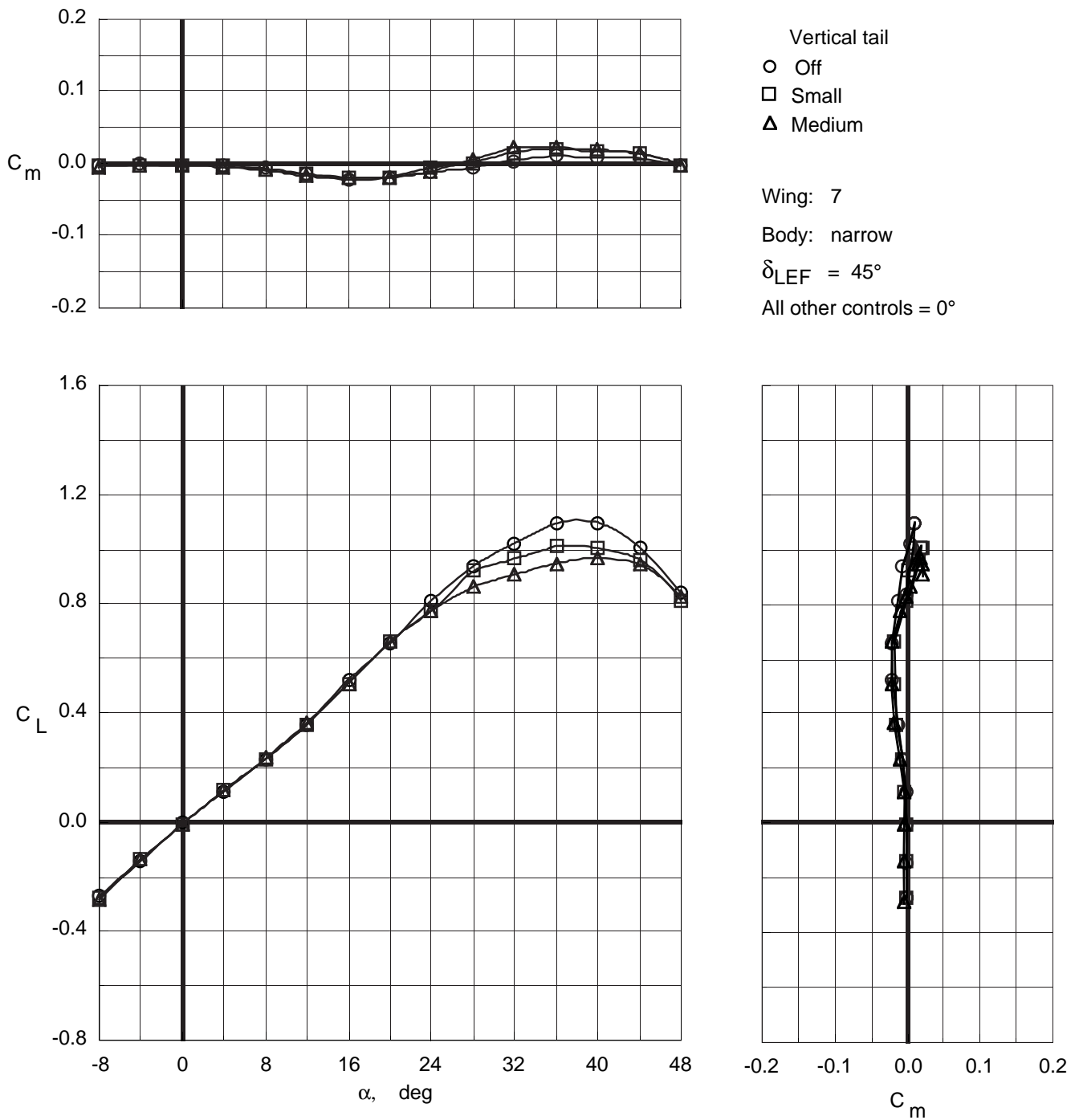


Figure 37. Effect of vertical tail size on longitudinal characteristics of Wing 7 with narrow top body on and leading-edge flaps deflected.

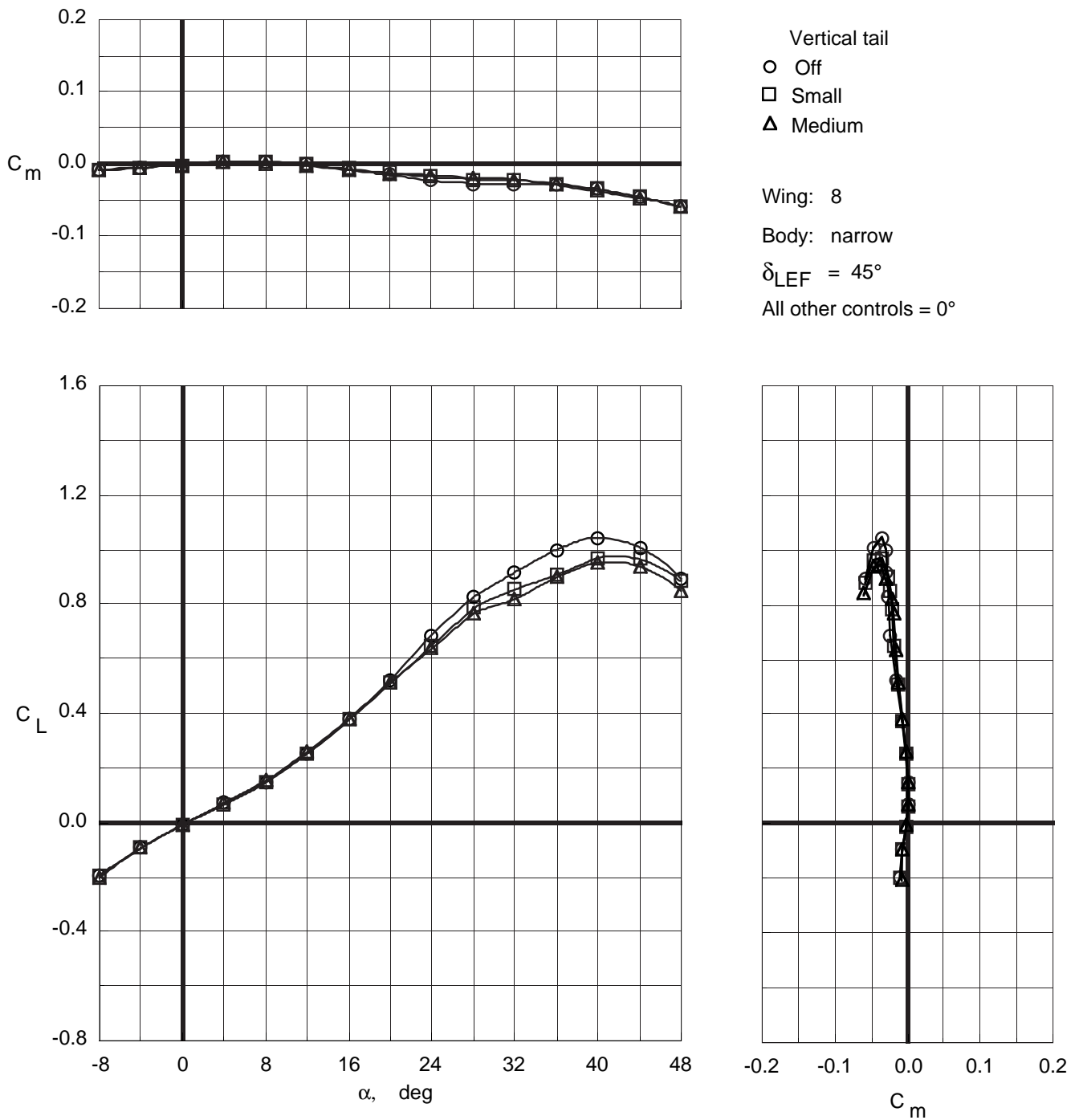


Figure 38. Effect of vertical tail size on longitudinal characteristics of Wing 8 with narrow top body on and leading-edge flaps deflected.

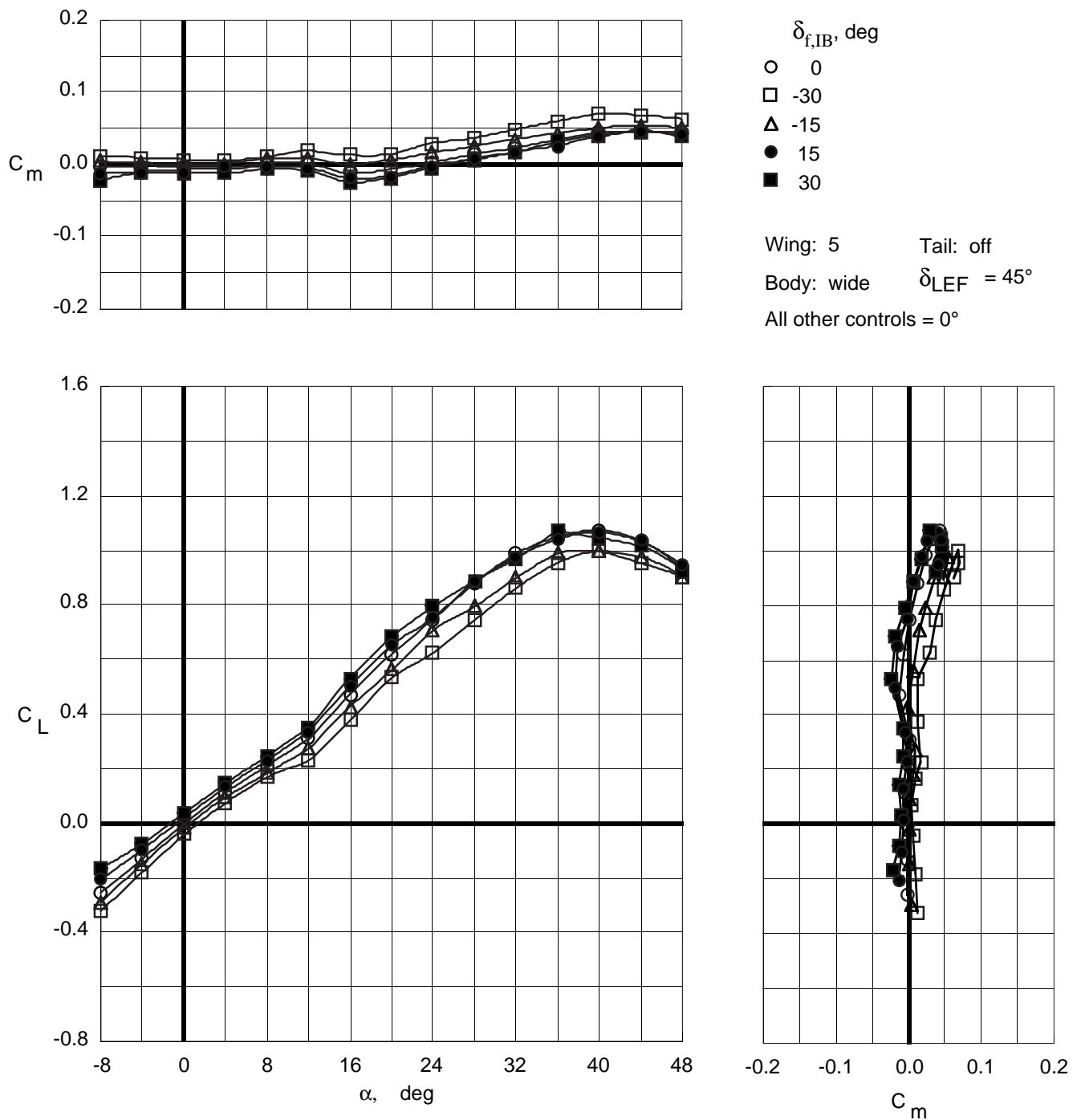


Figure 39. Control effectiveness of symmetric deflections of inboard trailing-edge flaps on Wing 5 with wide top body on and leading-edge flaps deflected.

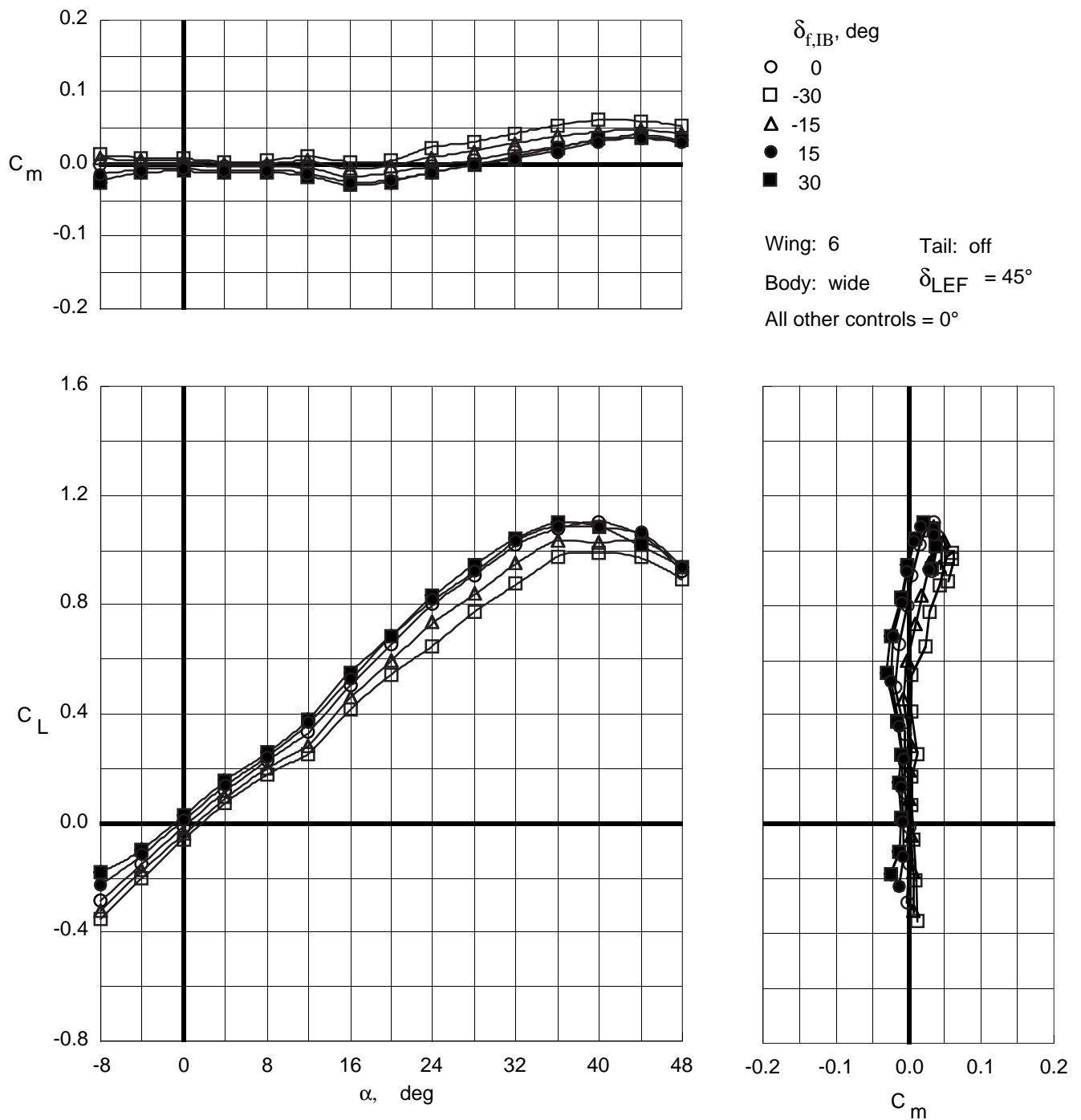


Figure 40. Control effectiveness of symmetric deflections of inboard trailing-edge flaps on Wing 6 with wide top body on and leading-edge flaps deflected.

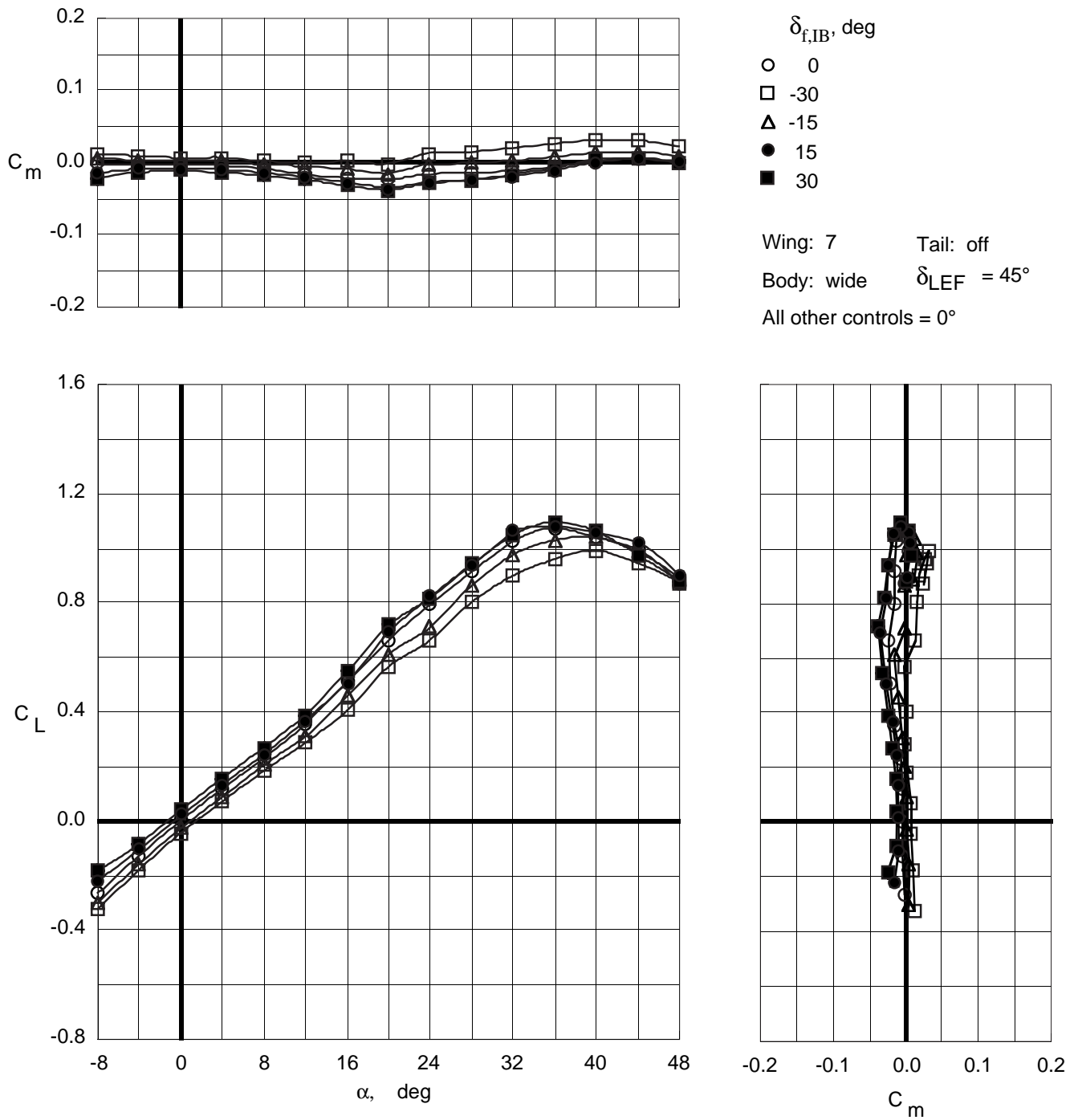


Figure 41. Control effectiveness of symmetric deflections of inboard trailing-edge flaps on Wing 7 with wide top body on and leading-edge flaps deflected.

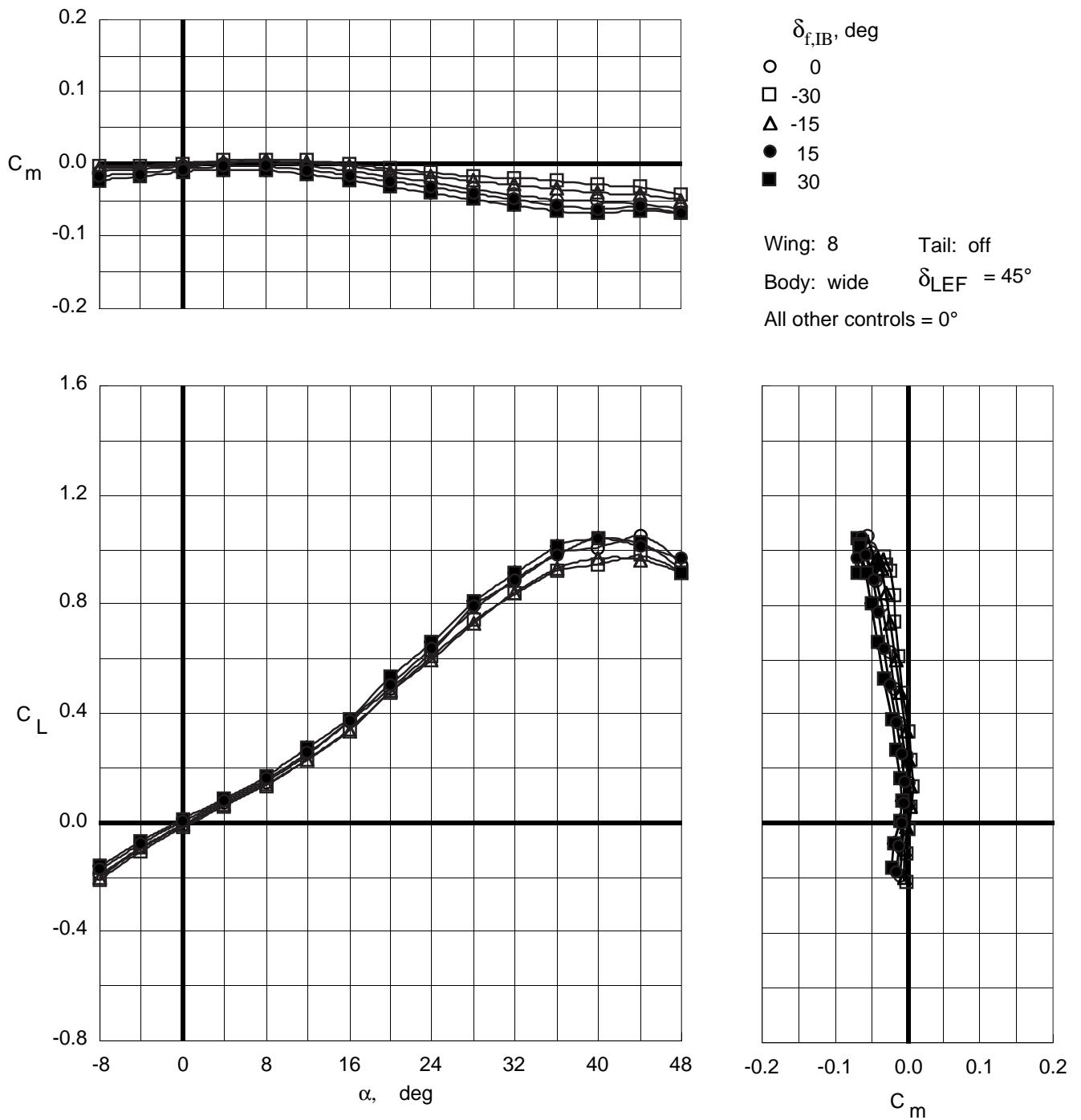


Figure 42. Control effectiveness of symmetric deflections of inboard trailing-edge flaps on Wing 8 with wide top body on and leading-edge flaps deflected.

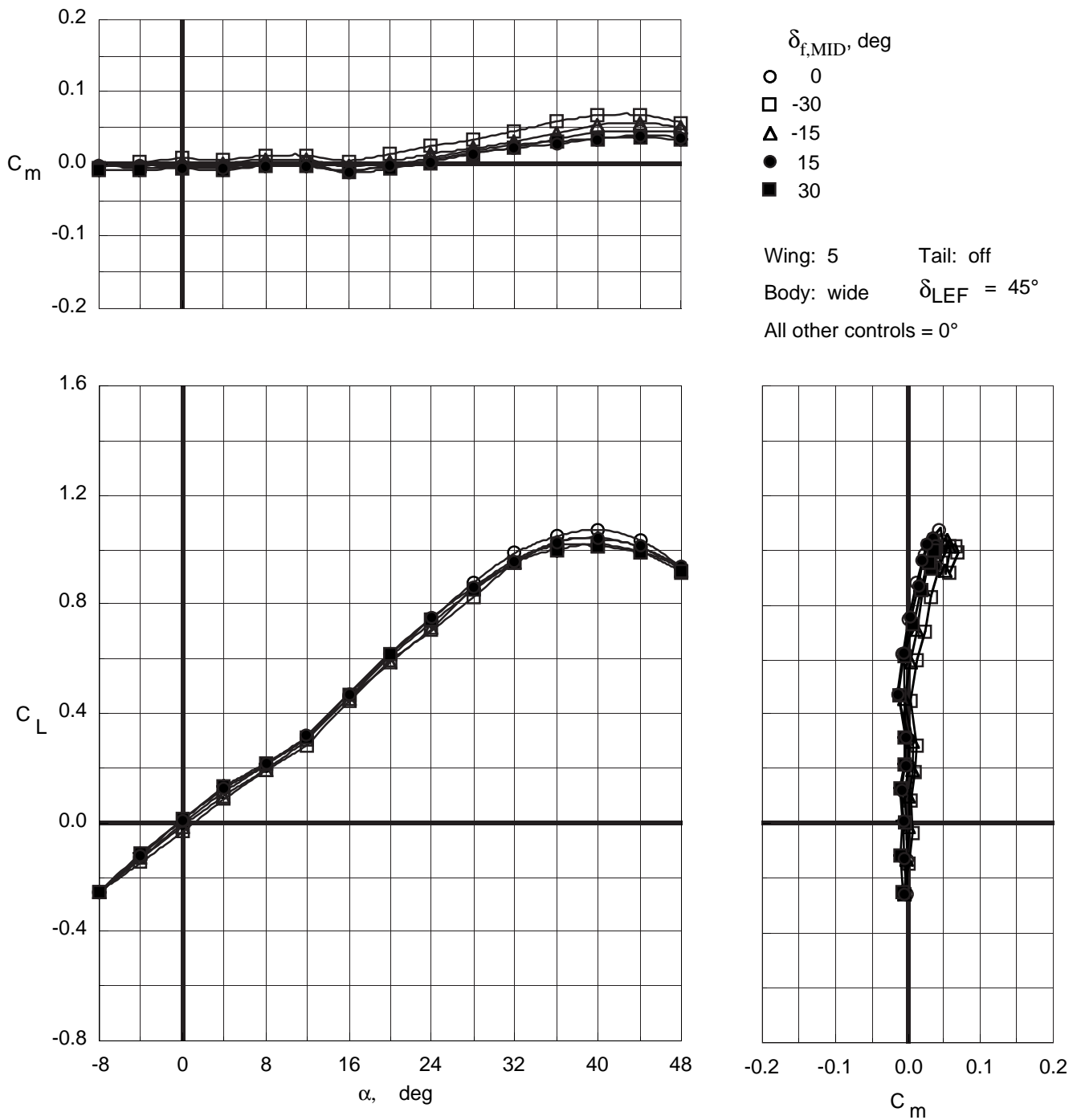


Figure 43. Control effectiveness of symmetric deflections of middle trailing-edge flaps on Wing 5 with wide top body on and leading-edge flaps deflected.

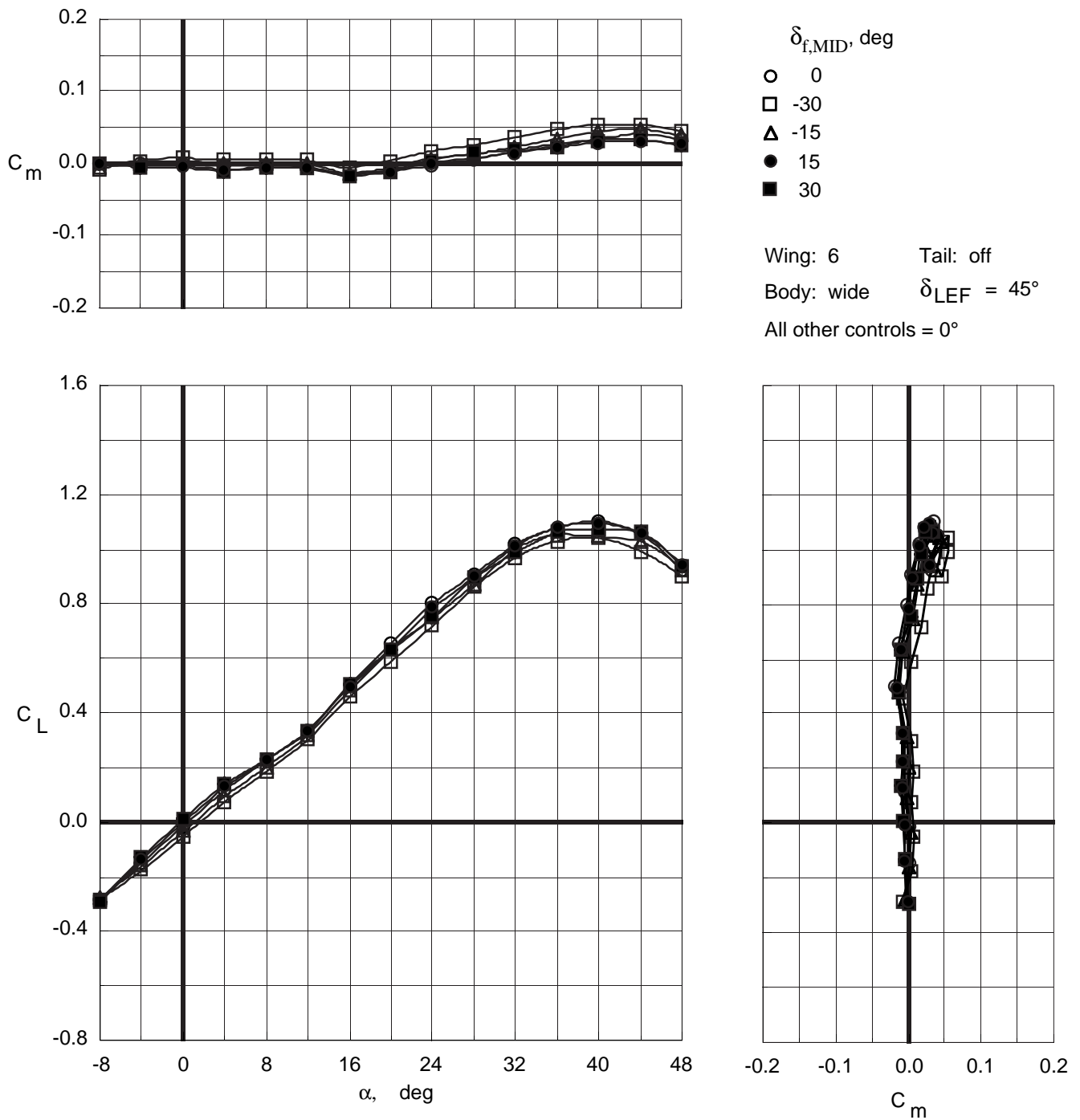


Figure 44. Control effectiveness of symmetric deflections of middle trailing-edge flaps on Wing 6 with wide top body on and leading-edge flaps deflected.

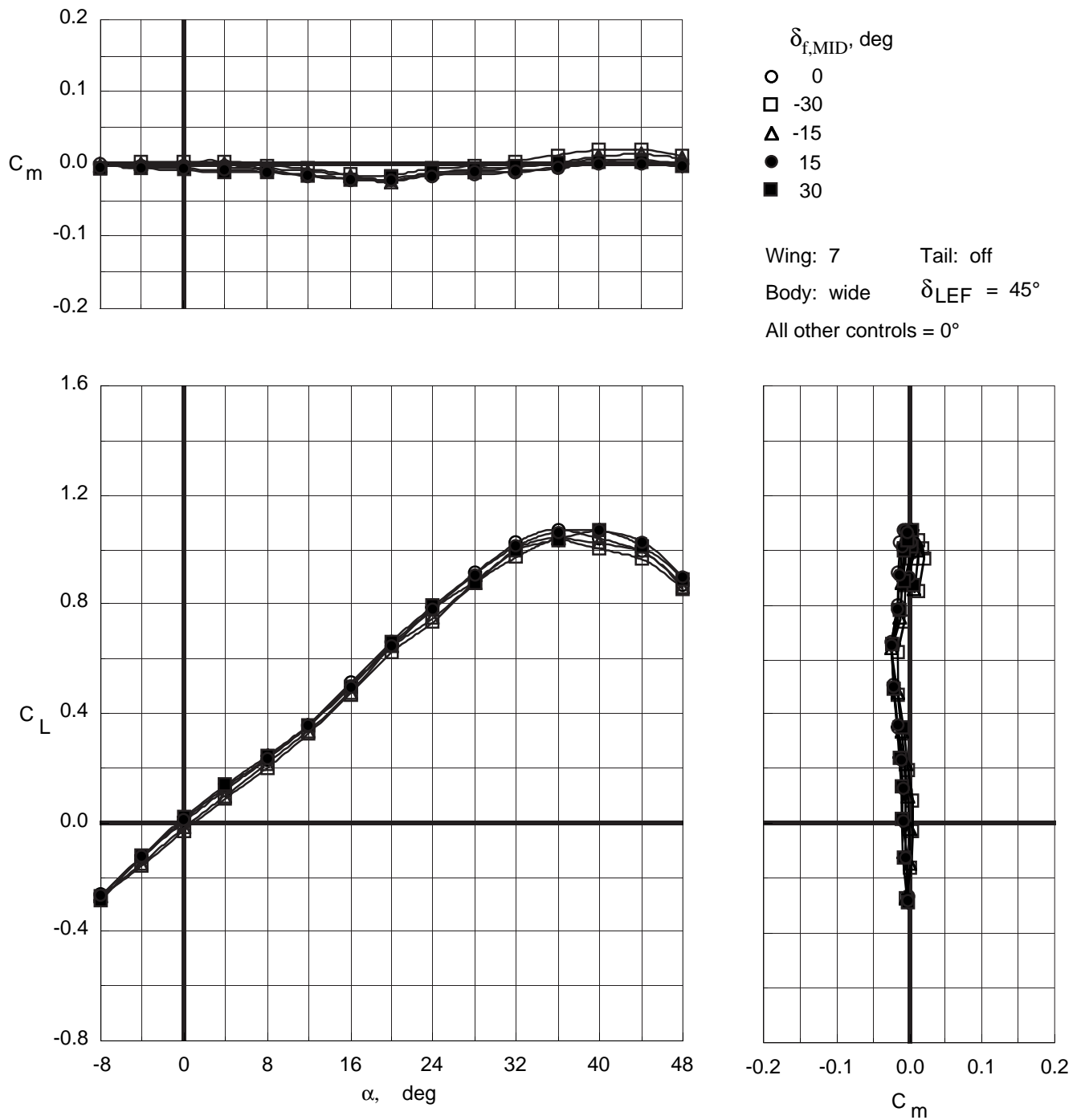


Figure 45. Control effectiveness of symmetric deflections of middle trailing-edge flaps on Wing 7 with wide top body on and leading-edge flaps deflected.

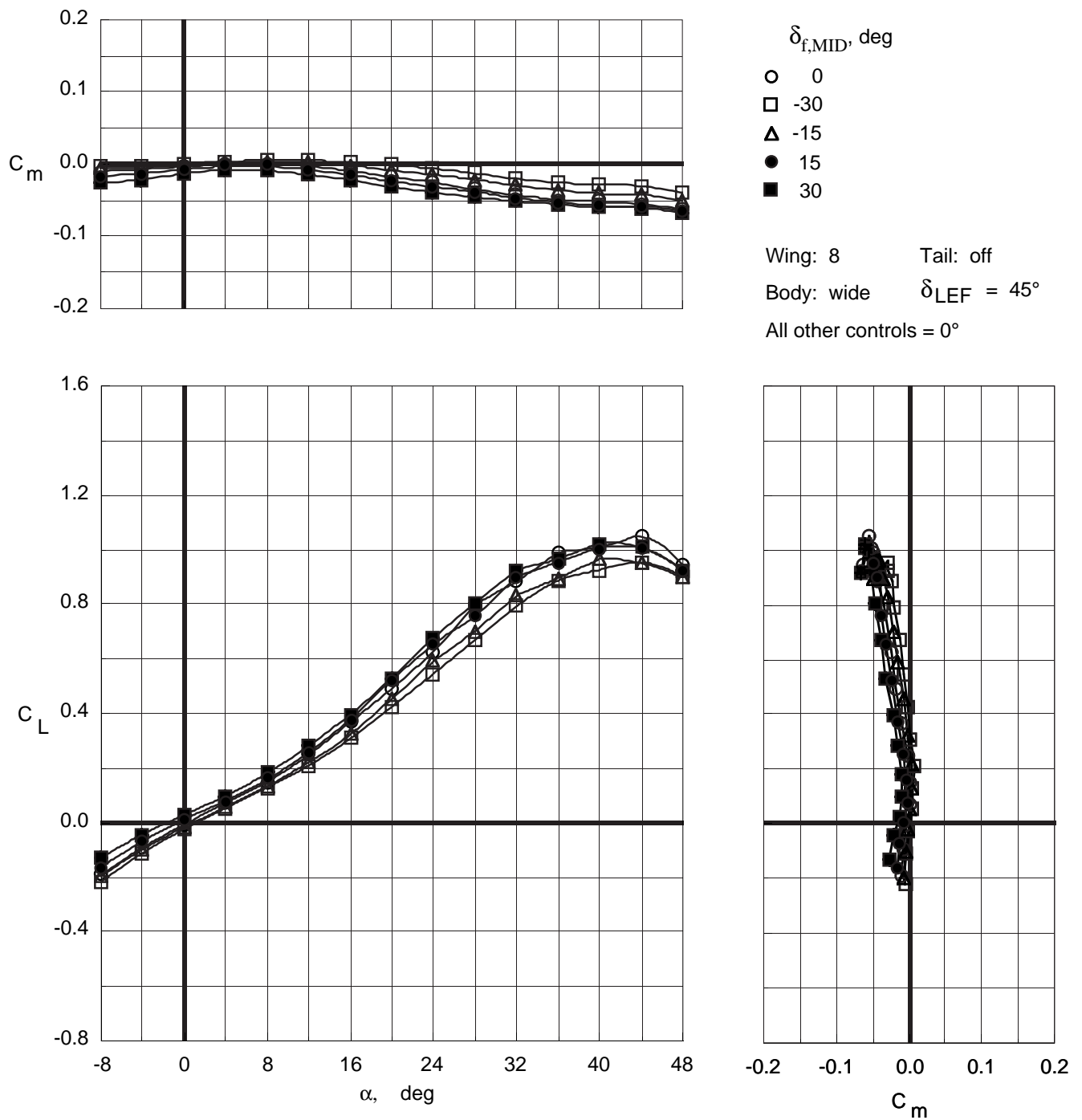


Figure 46. Control effectiveness of symmetric deflections of middle trailing-edge flaps on Wing 8 with wide top body on and leading-edge flaps deflected.

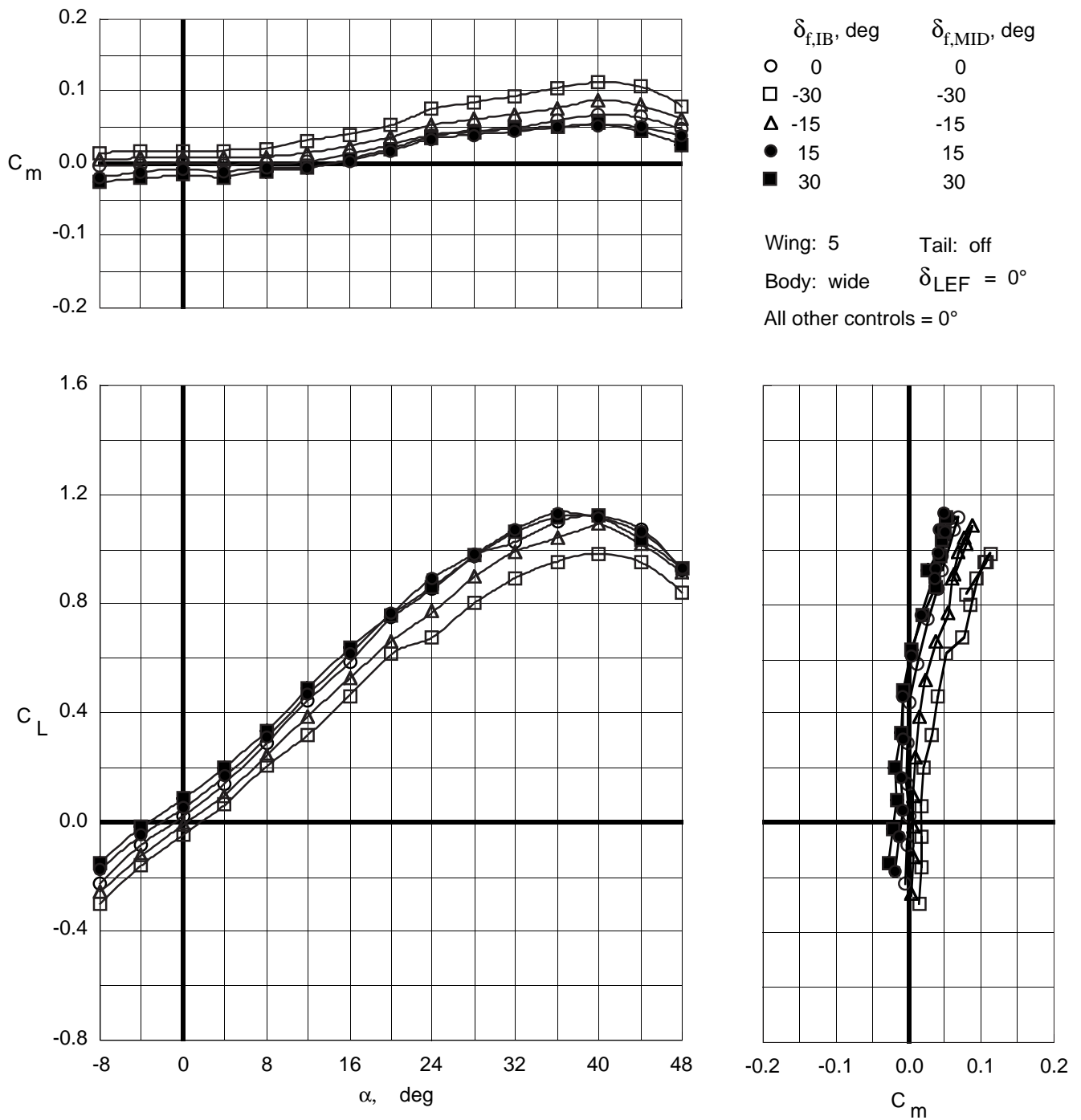


Figure 47. Control effectiveness of symmetric deflections of inboard and middle trailing-edge flaps on Wing 5 with wide top body on.

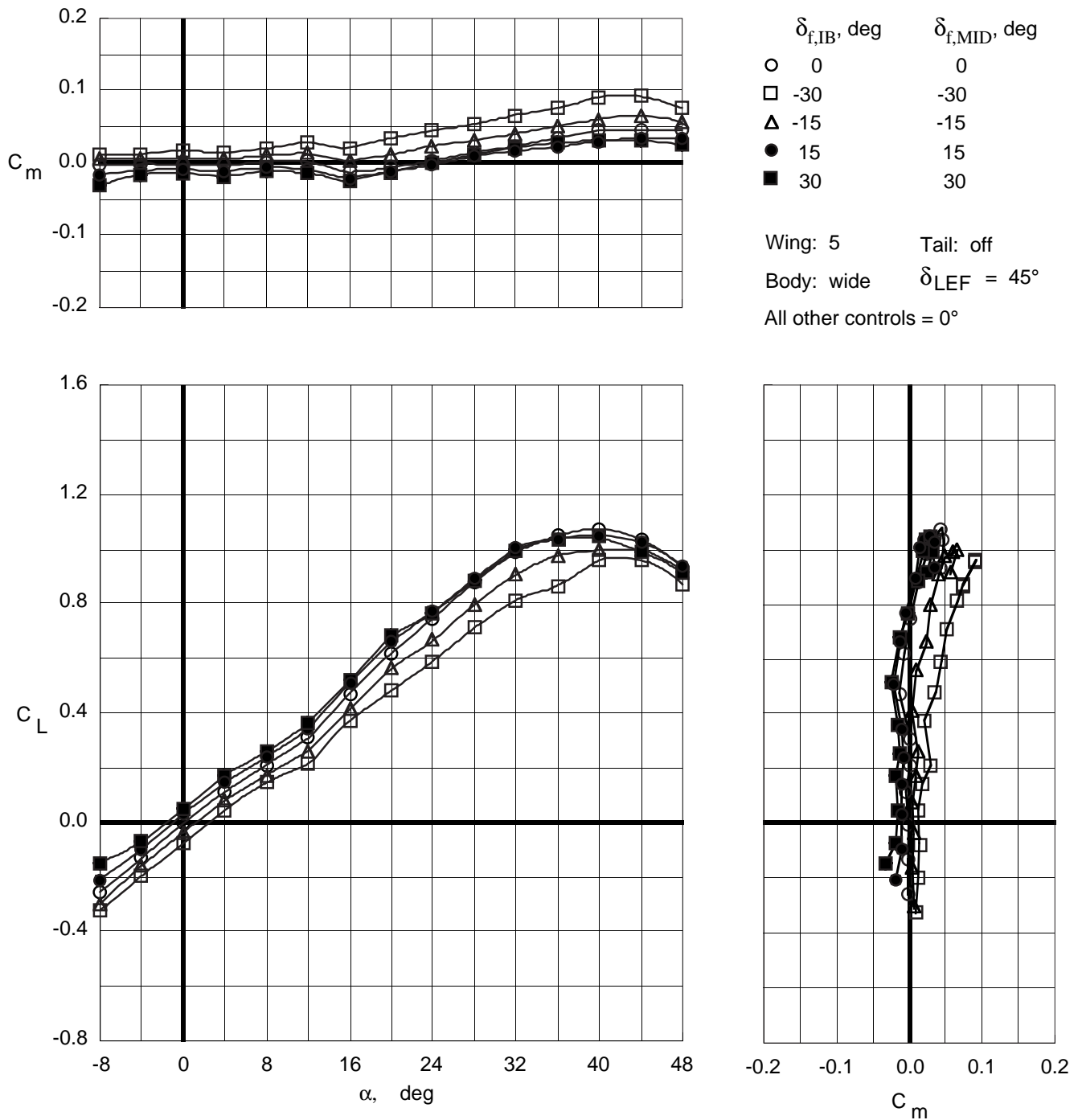


Figure 48. Control effectiveness of symmetric deflections of inboard and middle trailing-edge flaps on Wing 5 with wide top body on and leading-edge flaps deflected.

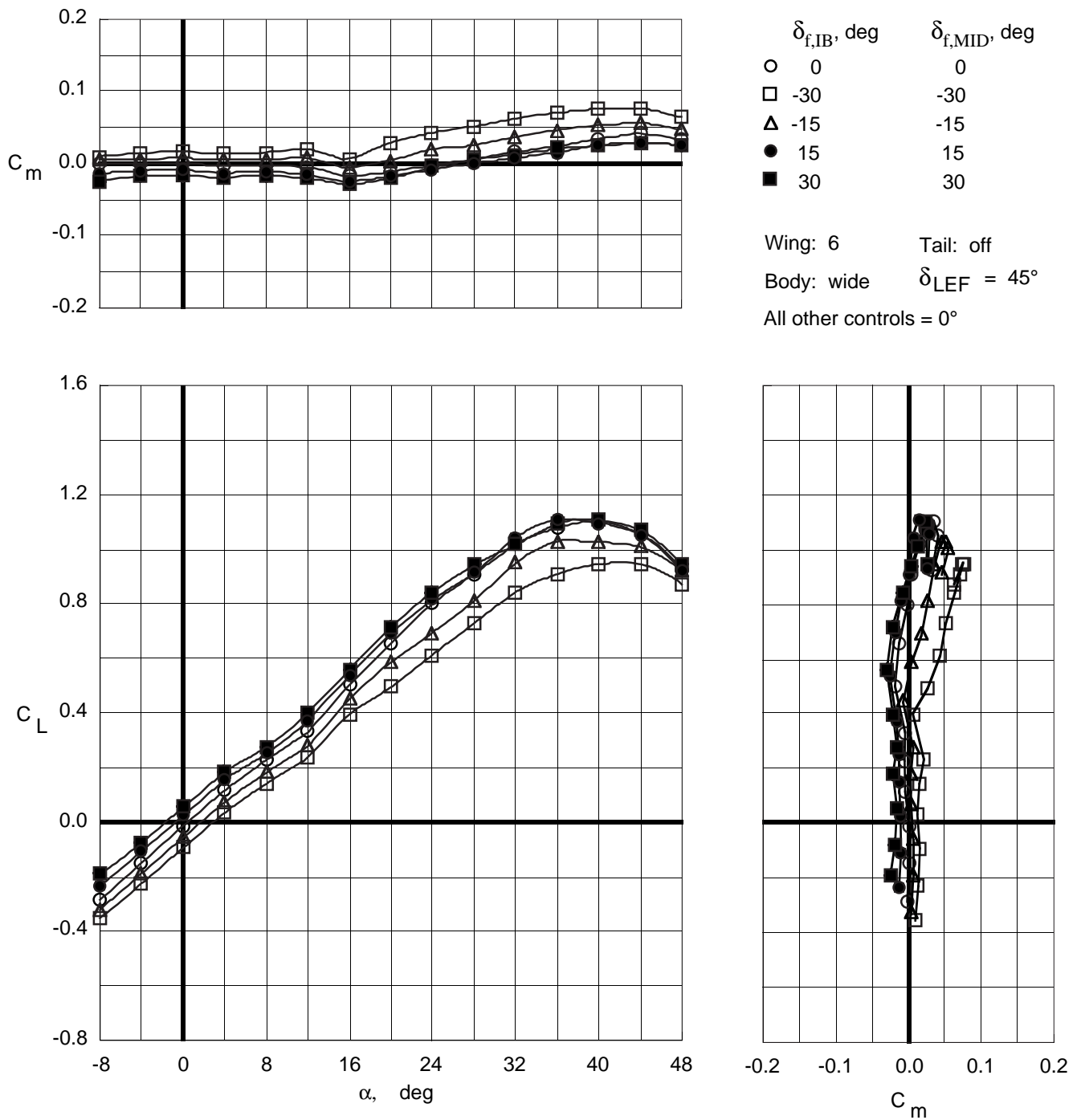


Figure 49. Control effectiveness of symmetric deflections of inboard and middle trailing-edge flaps on Wing 6 with wide top body on and leading-edge flaps deflected.

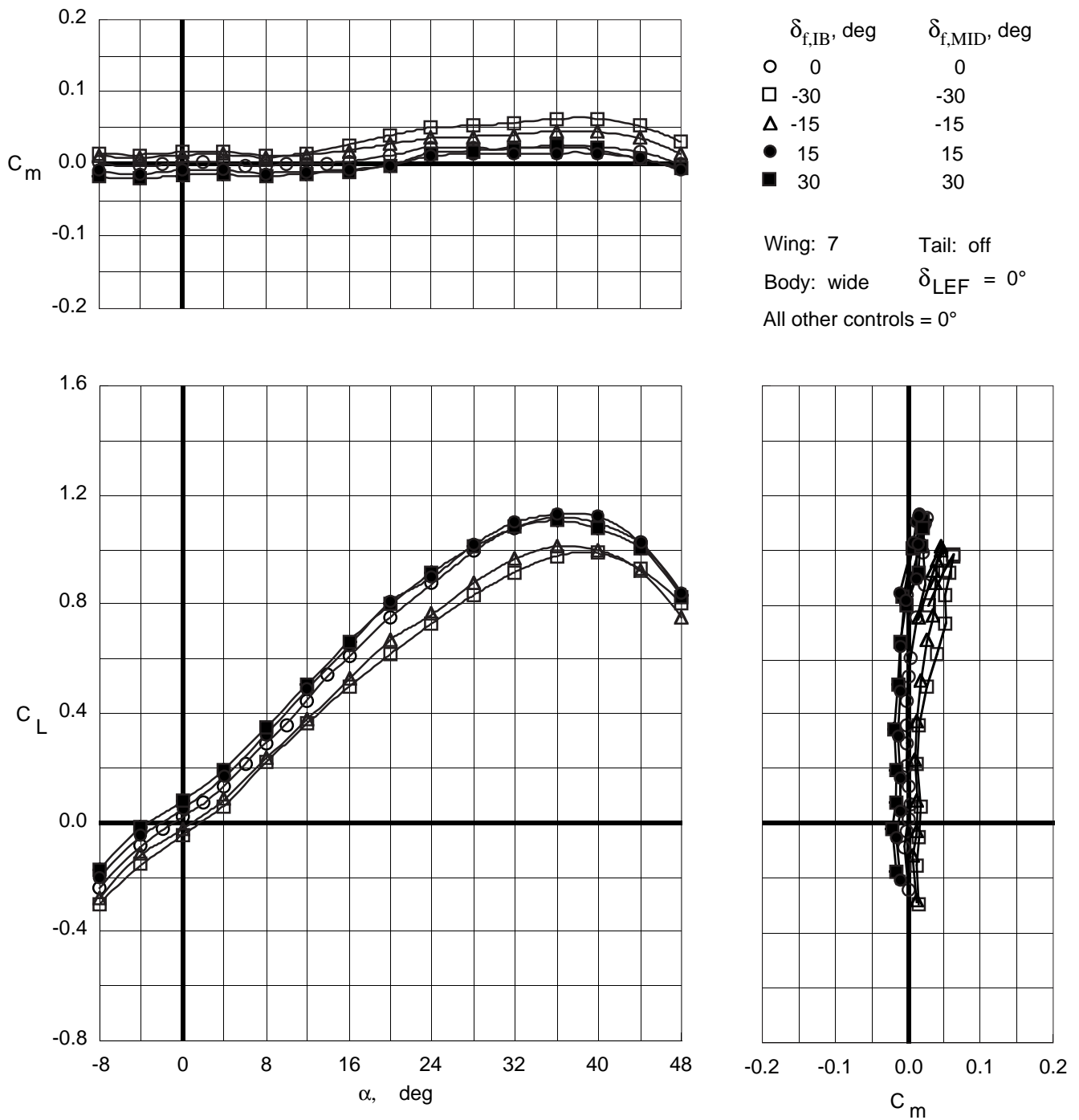


Figure 50. Control effectiveness of symmetric deflections of inboard and middle trailing-edge flaps on Wing 7 with wide top body on.

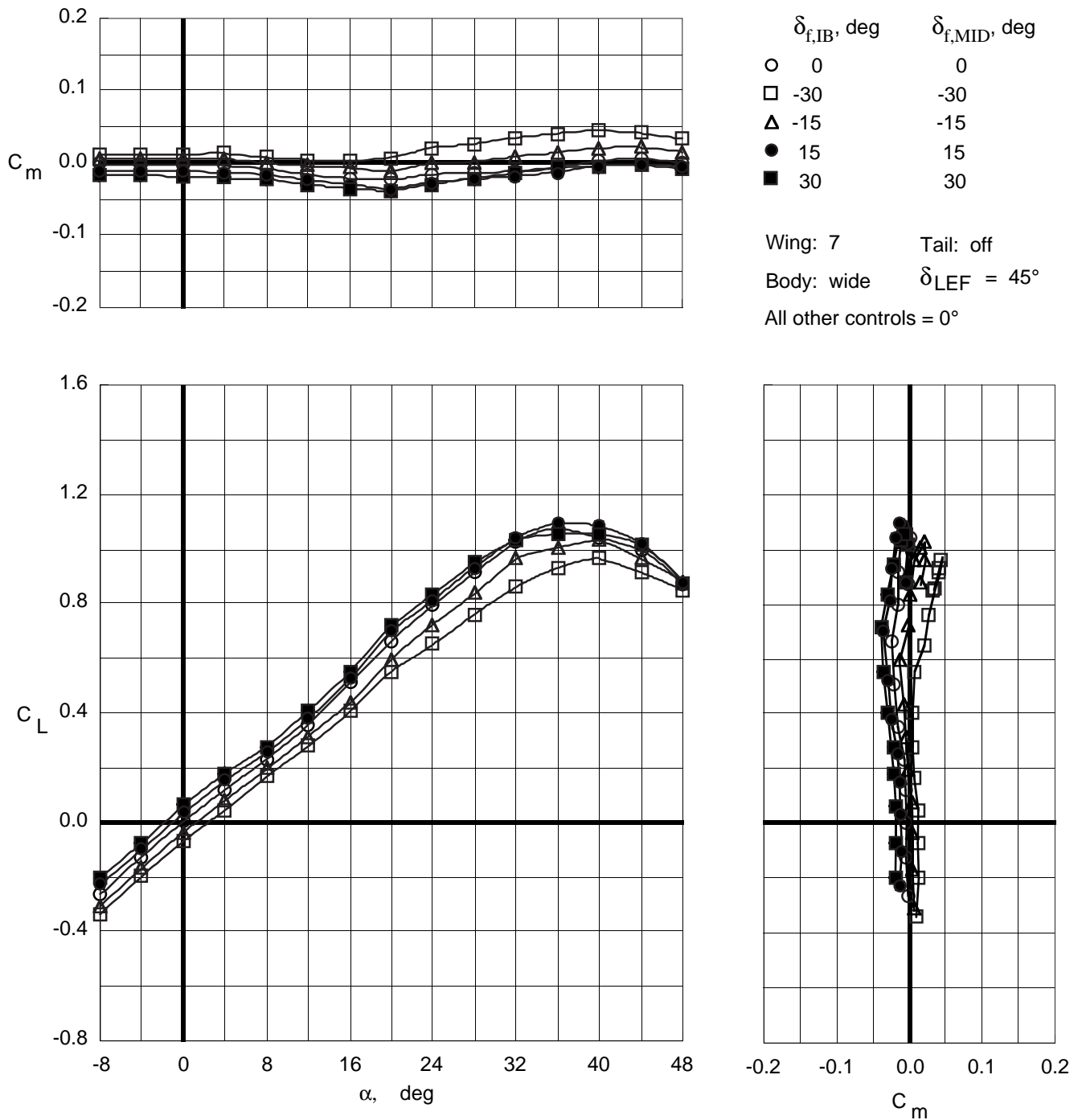


Figure 51. Control effectiveness of symmetric deflections of inboard and middle trailing-edge flaps on Wing 7 with wide top body on and leading-edge flaps deflected.

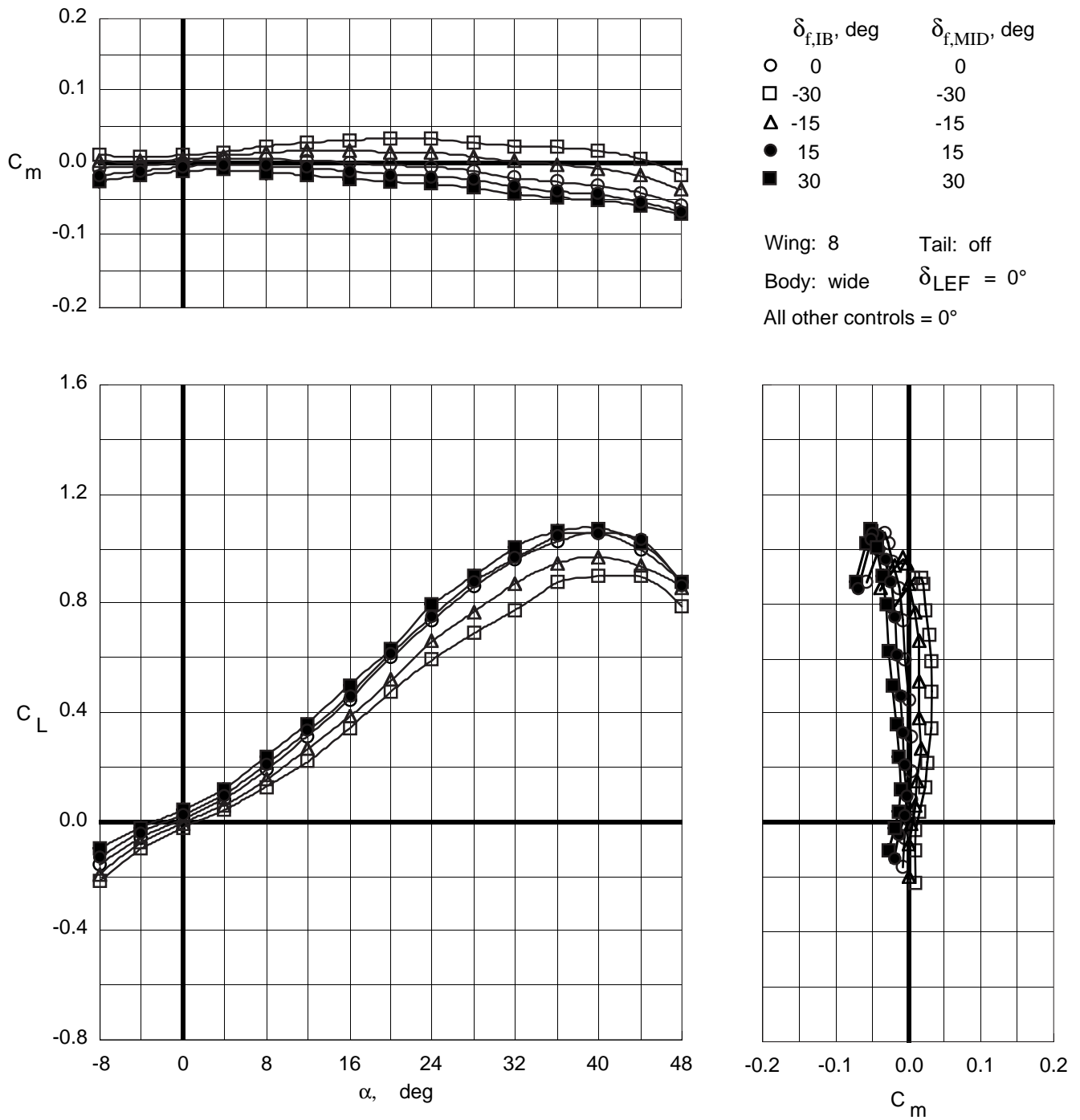


Figure 52. Control effectiveness of symmetric deflections of inboard and middle trailing-edge flaps on Wing 8 with wide top body on.

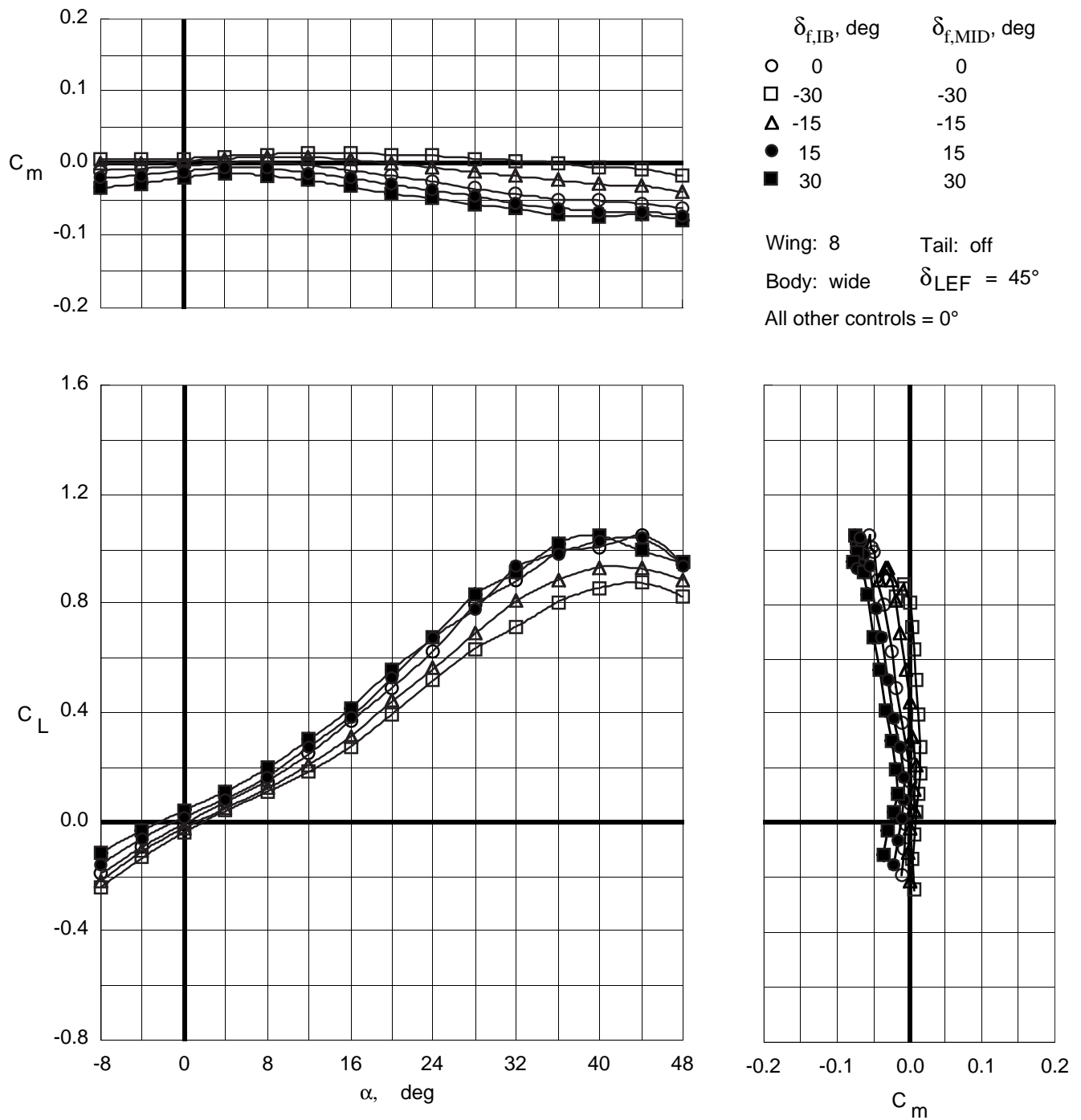
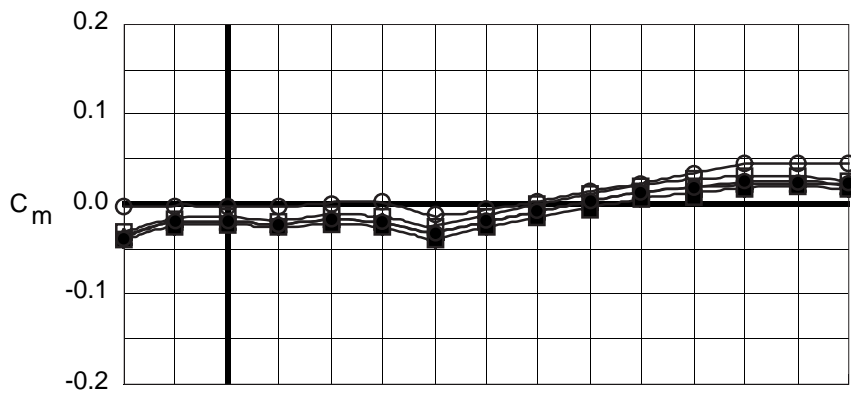


Figure 53. Control effectiveness of symmetric deflections of inboard and middle trailing-edge flaps on Wing 8 with wide top body on and leading-edge flaps deflected.



	$\delta_{f,IB}$ , deg	$\delta_{f,MID}$ , deg	$\delta_{f,OB}$ , deg	$\delta_{bf}$ , deg
○	0	0	0	0
□	30	30	0	0
△	30	30	0	58
●	30	30	0	73
■	30	30	30	73

Wing: 5       $\delta_{LEF} = 45^\circ$   
 Body: wide    Tail: off  
 All other controls =  $0^\circ$

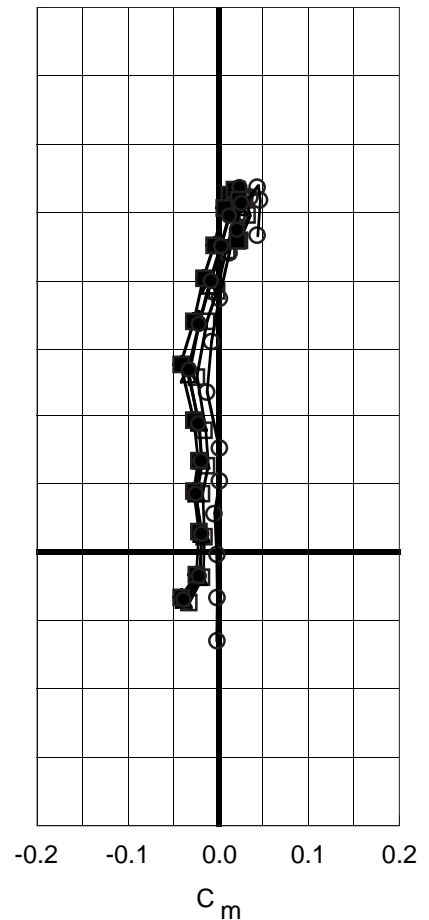
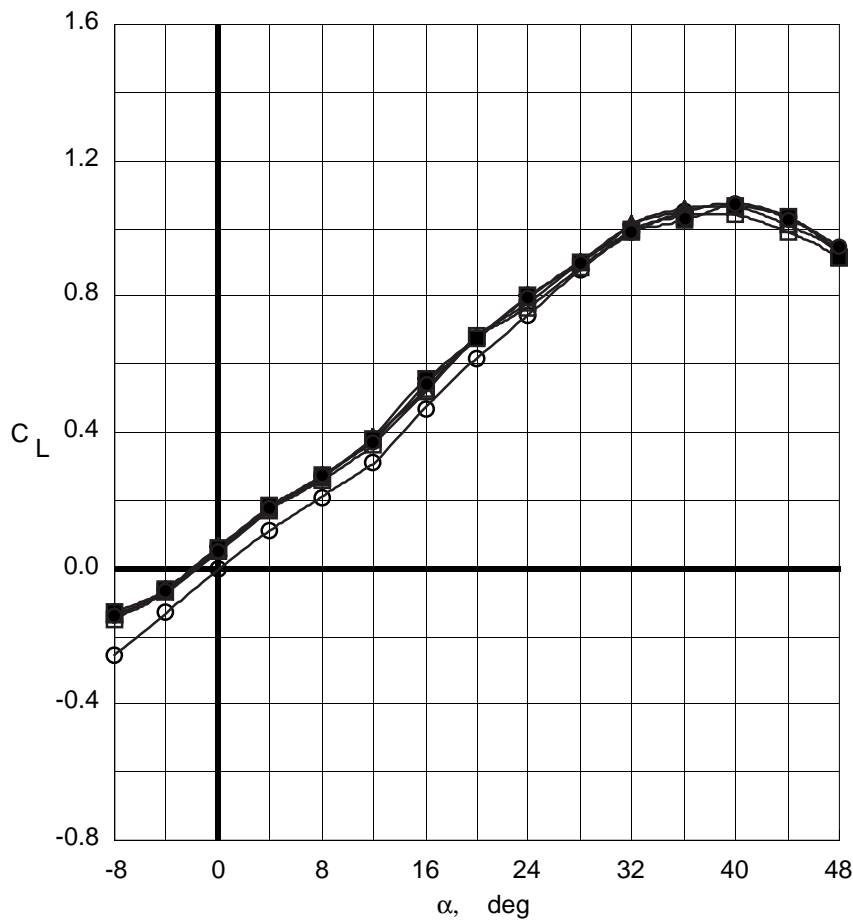
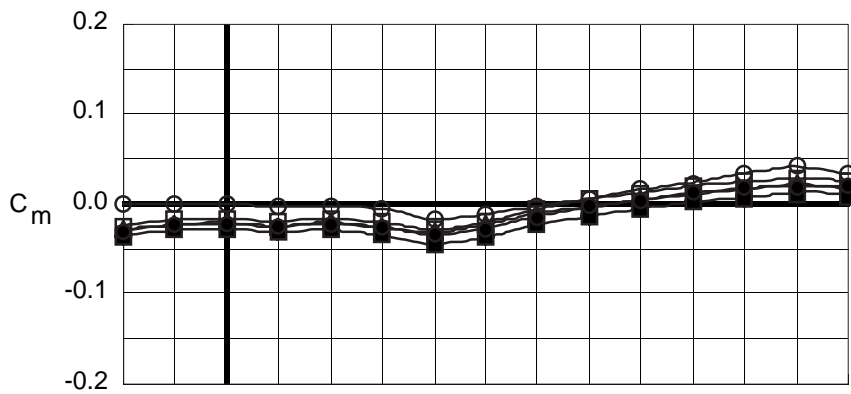


Figure 54. Control effectiveness of symmetric deflections of trailing-edge flaps and body flaps on Wing 5 with wide top body on and leading-edge flaps deflected.



	$\delta_{f,IB}$ , deg	$\delta_{f,MID}$ , deg	$\delta_{f,OB}$ , deg	$\delta_{bf}$ , deg
○	0	0	0	0
□	30	30	0	0
△	30	30	0	58
●	30	30	0	73
■	30	30	30	73

Wing: 6       $\delta_{LEF} = 45^\circ$   
 Body: wide      Tail: off  
 All other controls =  $0^\circ$

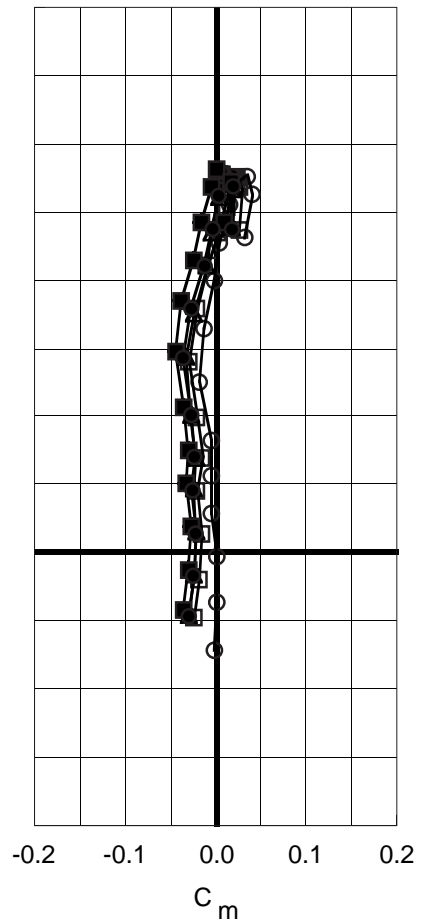
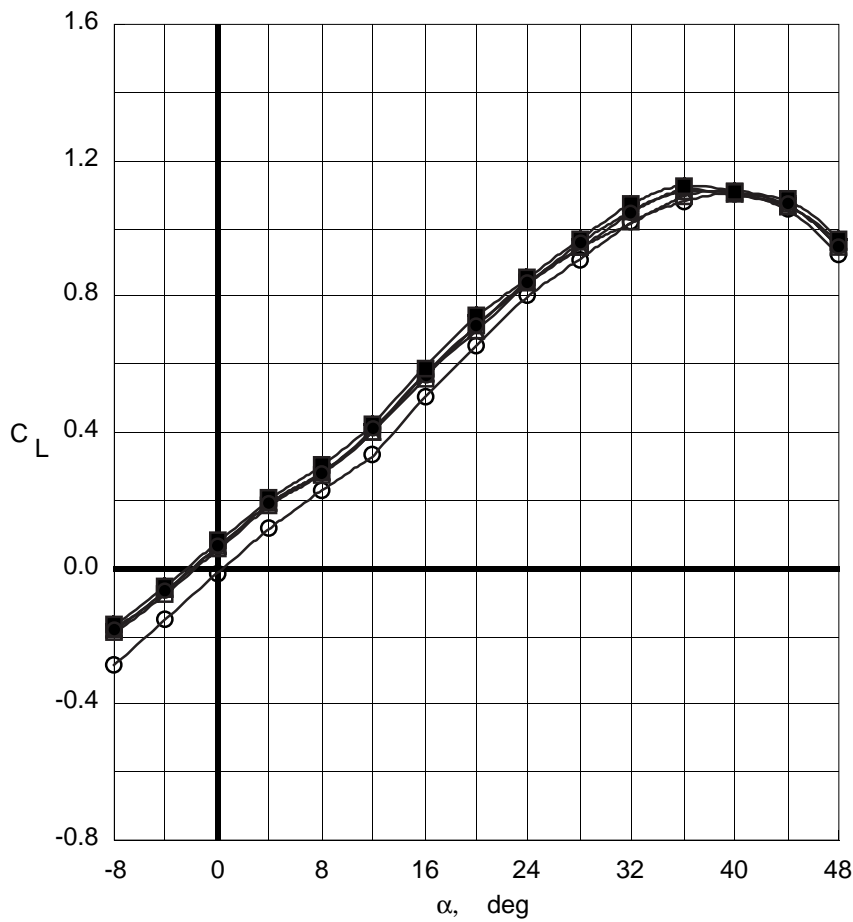
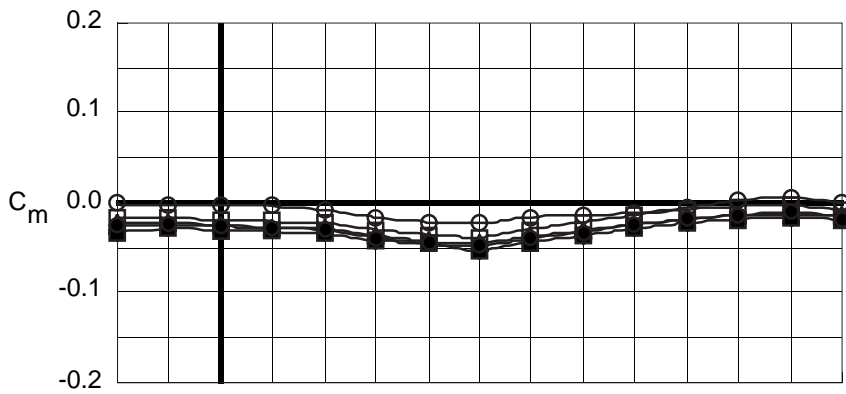


Figure 55. Control effectiveness of symmetric deflections of trailing-edge flaps and body flaps on Wing 6 with wide top body on and leading-edge flaps deflected.



	$\delta_{f,IB}$ , deg	$\delta_{f,MID}$ , deg	$\delta_{f,OB}$ , deg	$\delta_{bf}$ , deg
○	0	0	0	0
□	30	30	0	0
△	30	30	0	58
●	30	30	0	73
■	30	30	30	73

Wing: 7       $\delta_{LEF} = 45^\circ$   
 Body: wide    Tail: off  
 All other controls =  $0^\circ$

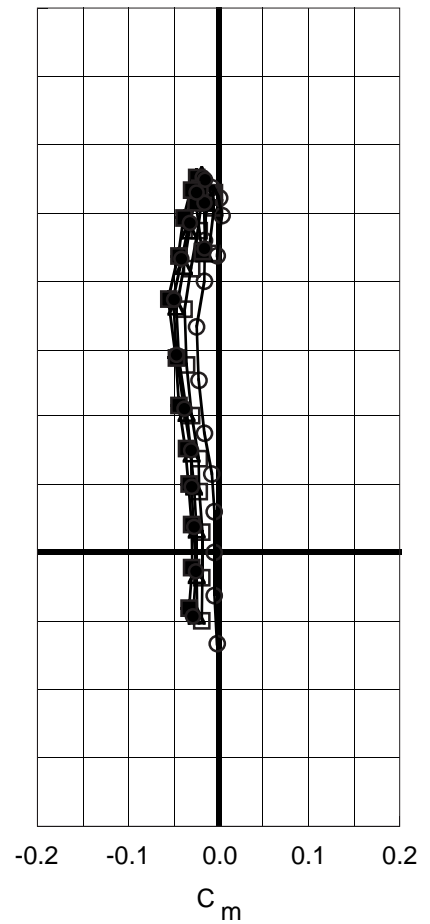
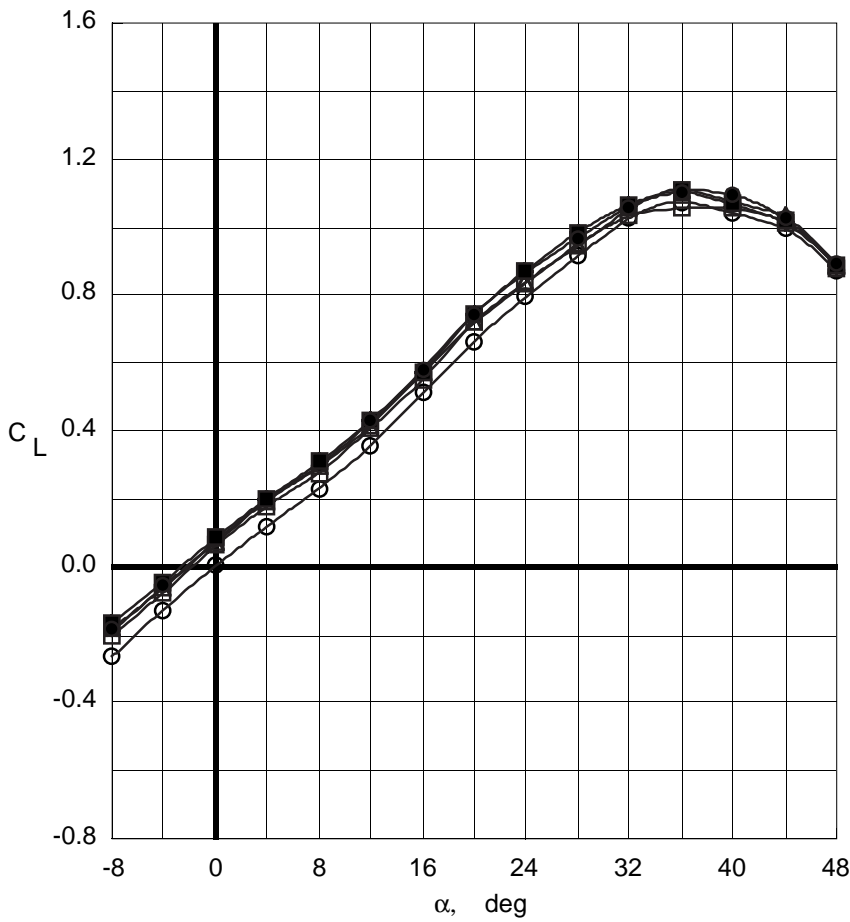


Figure 56. Control effectiveness of symmetric deflections of trailing-edge flaps and body flaps on Wing 7 with wide top body on and leading-edge flaps deflected.

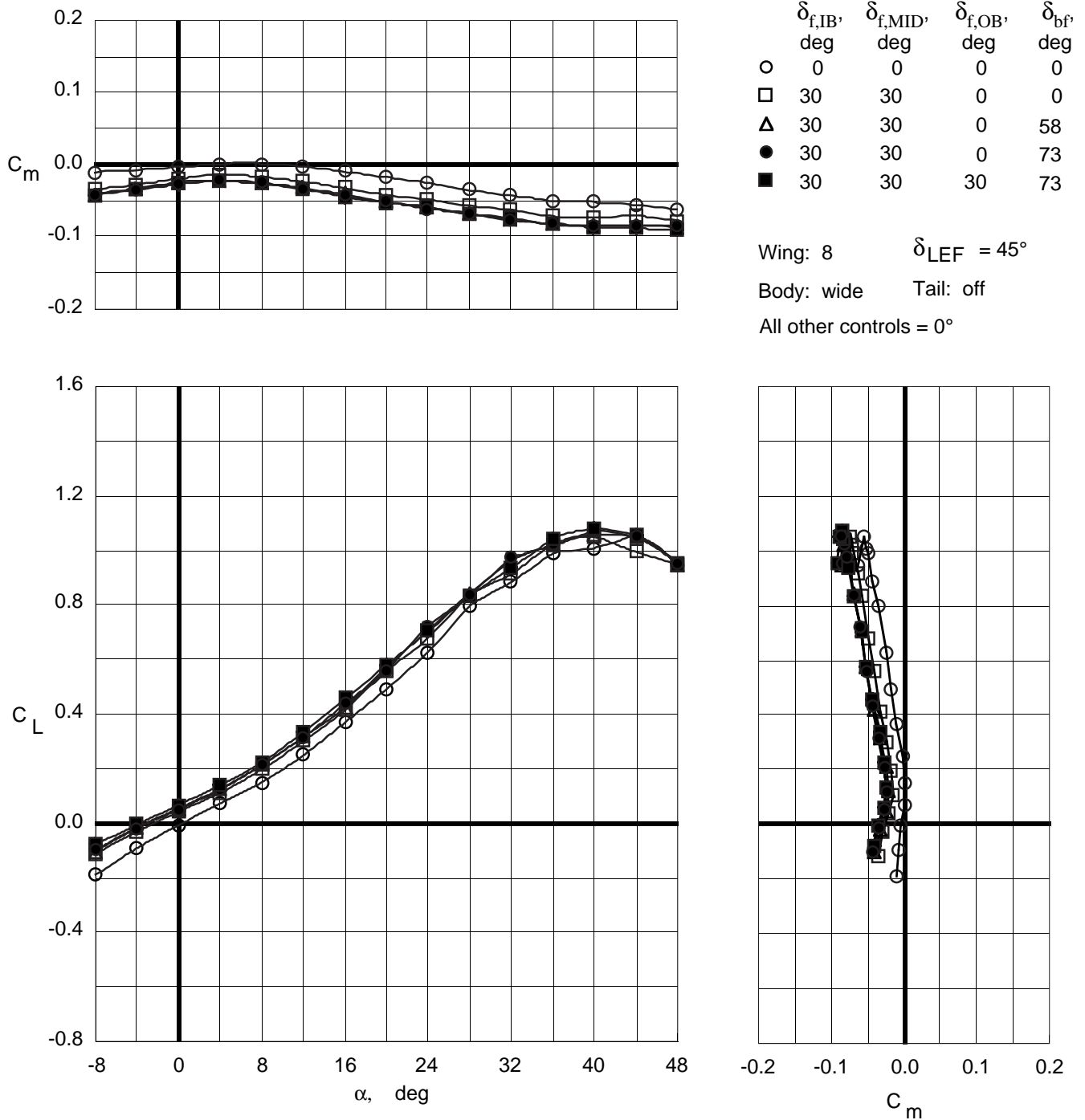


Figure 57. Control effectiveness of symmetric deflections of trailing-edge flaps and body flaps on Wing 8 with wide top body on and leading-edge flaps deflected.

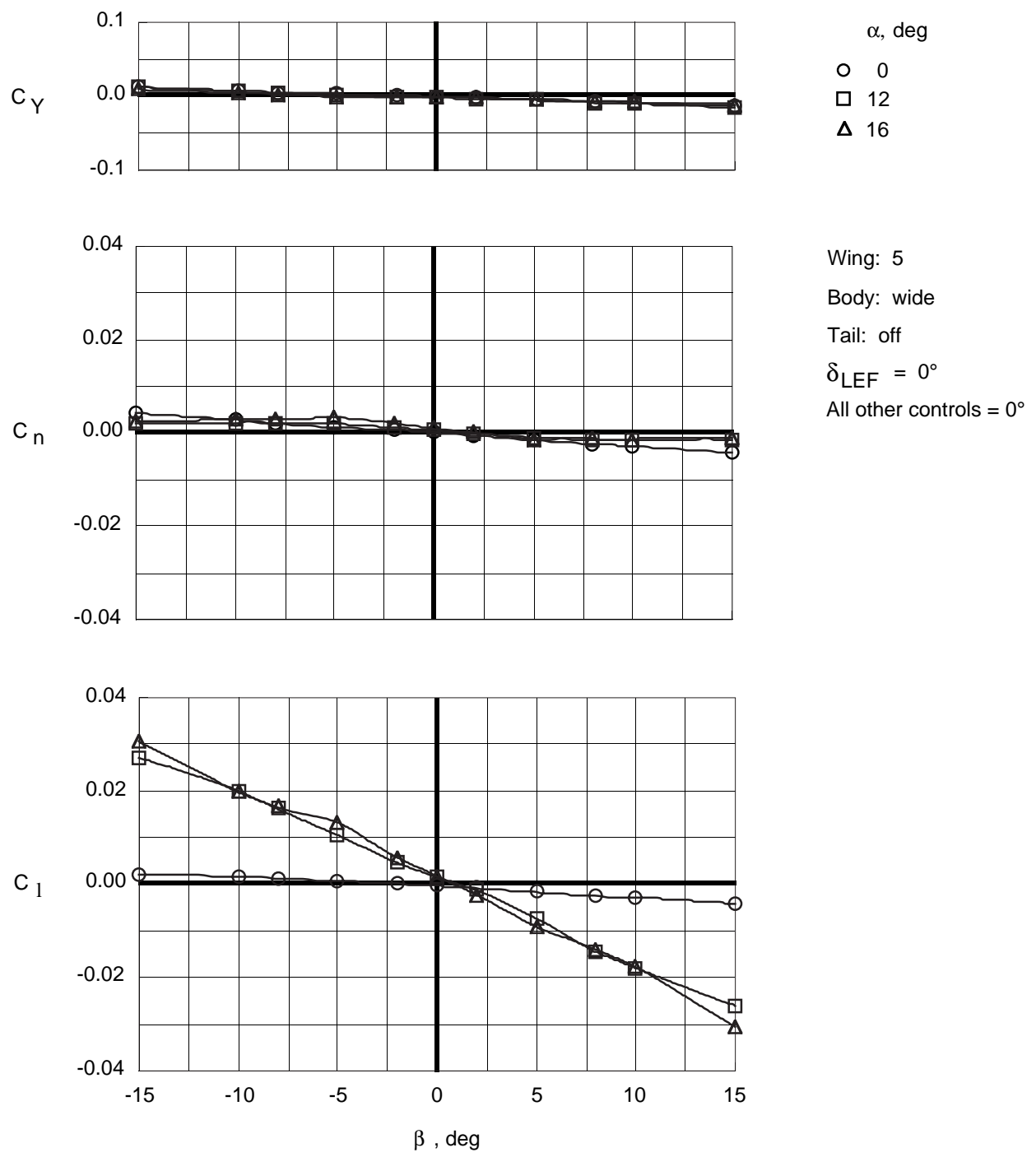


Figure 58. Variation of lateral-directional coefficients with sideslip at low angles of attack for Wing 5 with wide top body on.

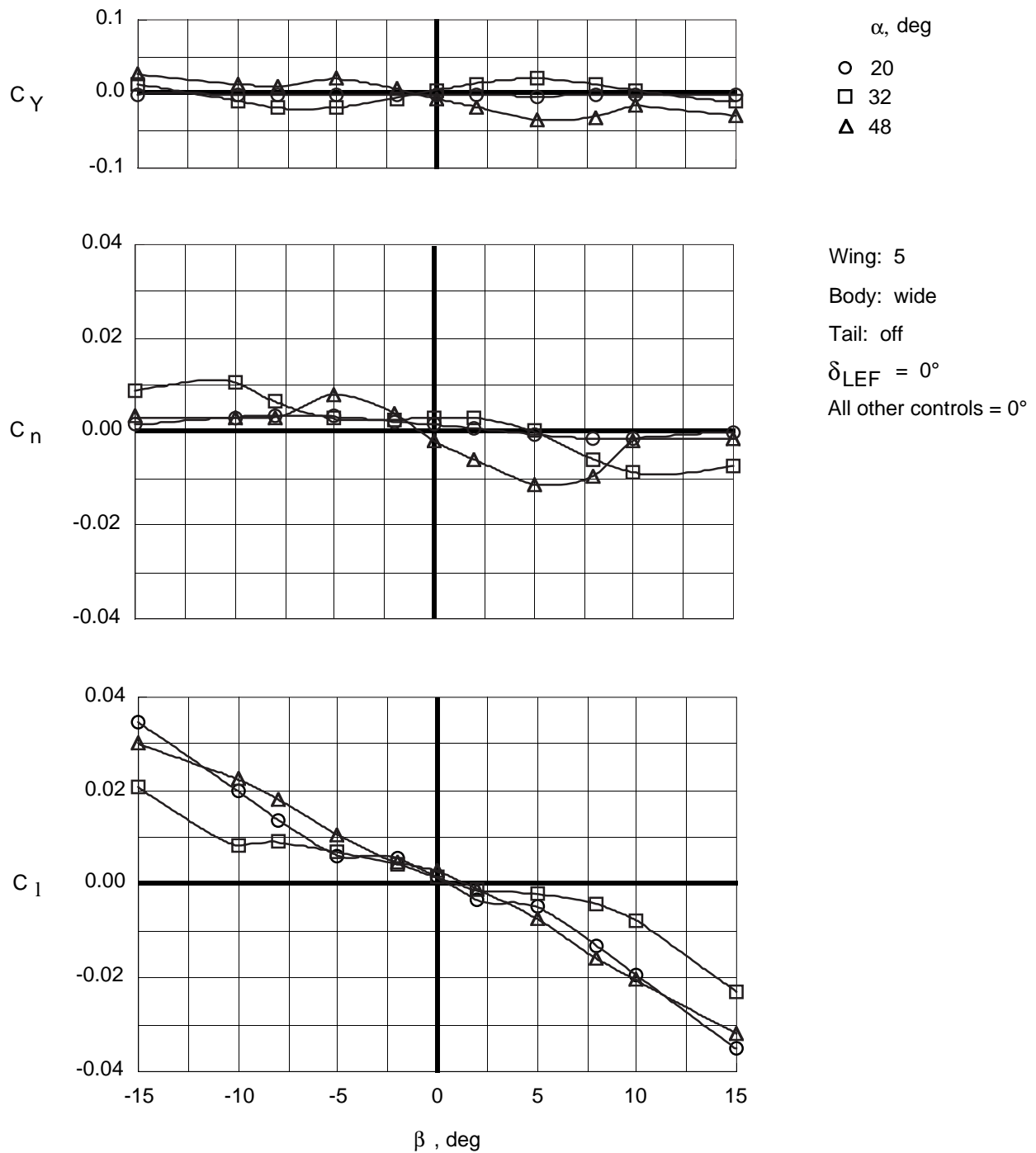


Figure 59. Variation of lateral-directional coefficients with sideslip at high angles of attack for Wing 5 with wide top body on.

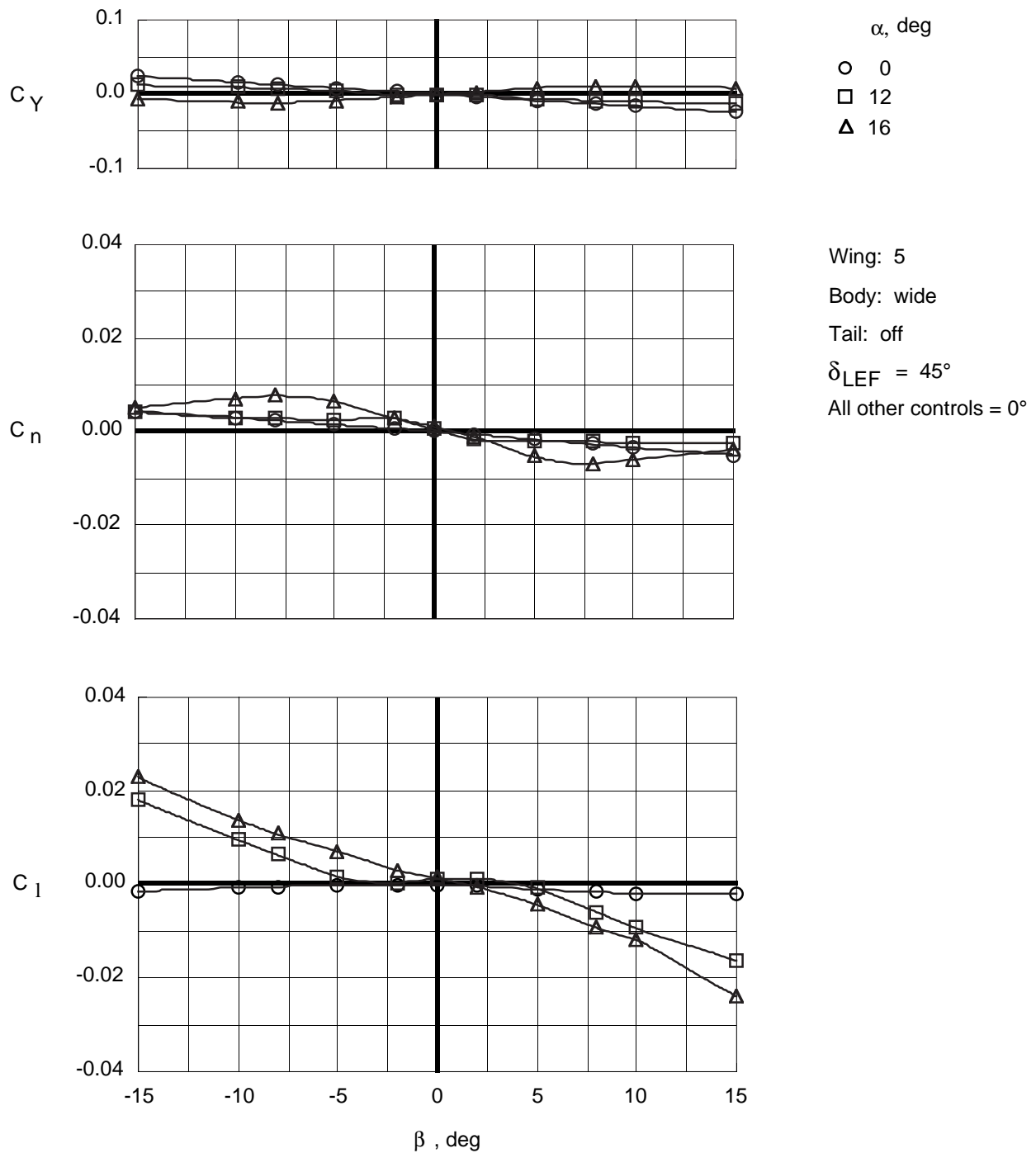


Figure 60. Variation of lateral-directional coefficients with sideslip at low angles of attack for Wing 5 with wide top body on and leading-edge flaps deflected.

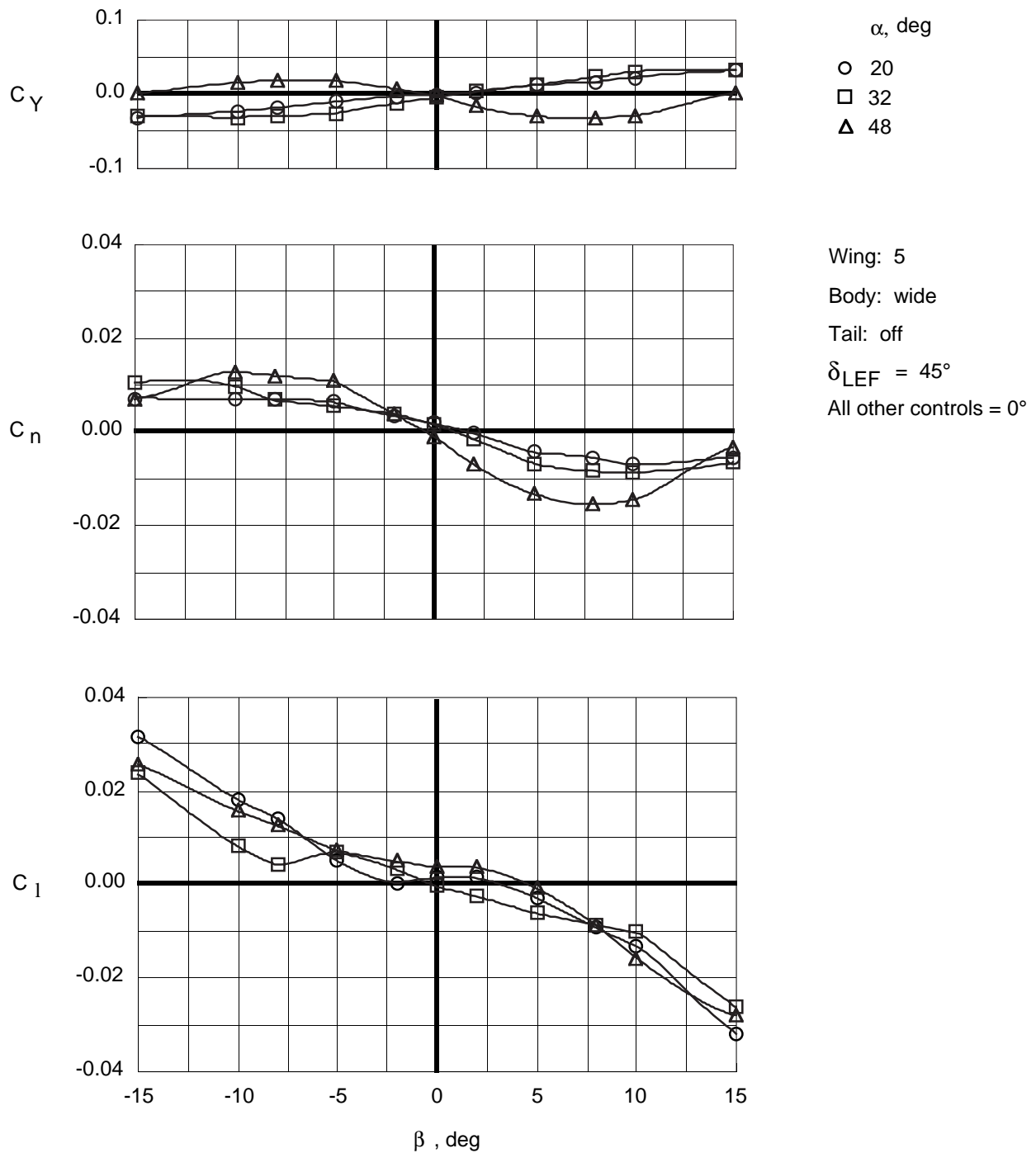


Figure 61. Variation of lateral-directional coefficients with sideslip at high angles of attack for Wing 5 with wide top body on and leading-edge flaps deflected.

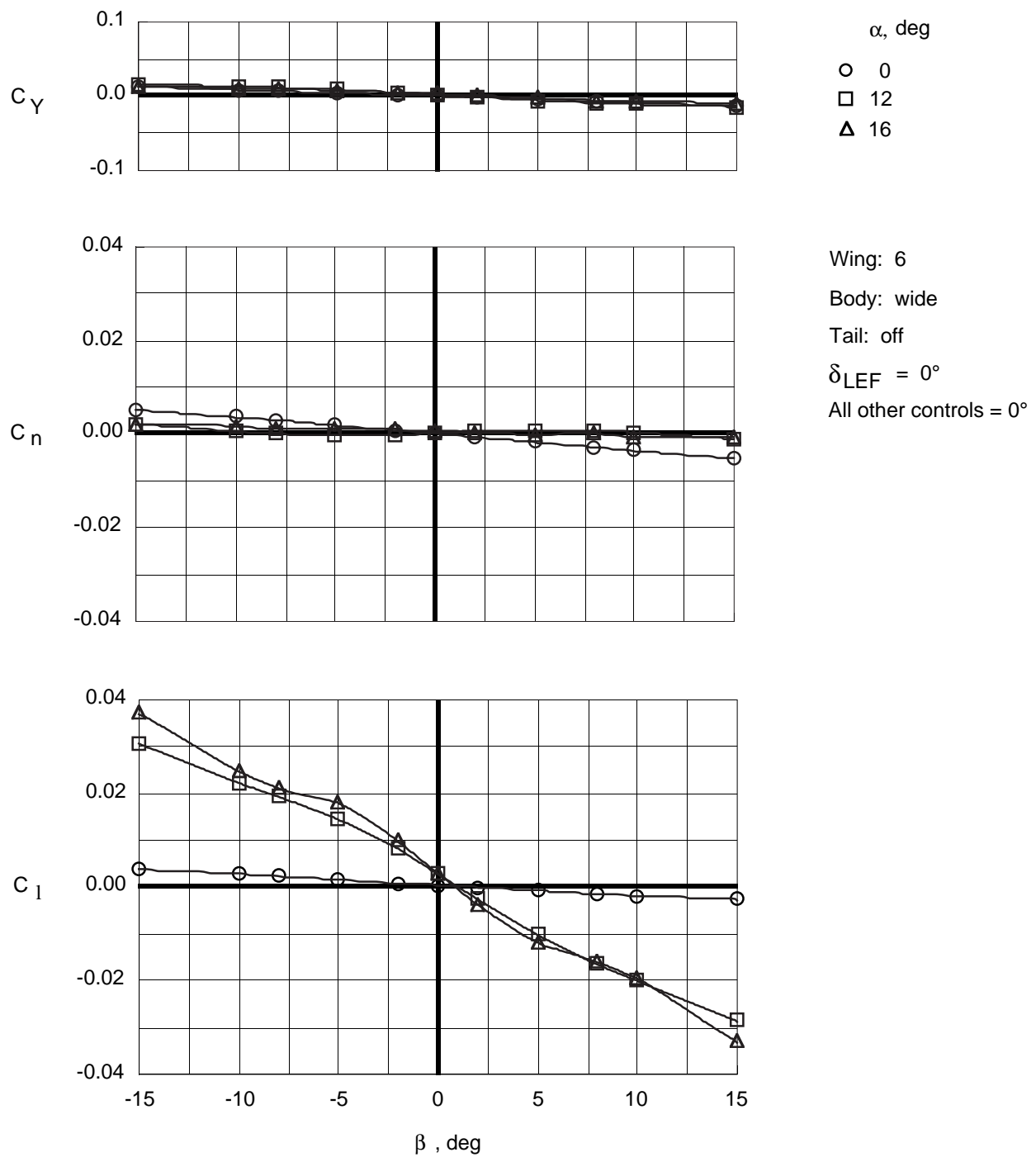


Figure 62. Variation of lateral-directional coefficients with sideslip at low angles of attack for Wing 6 with wide top body on.

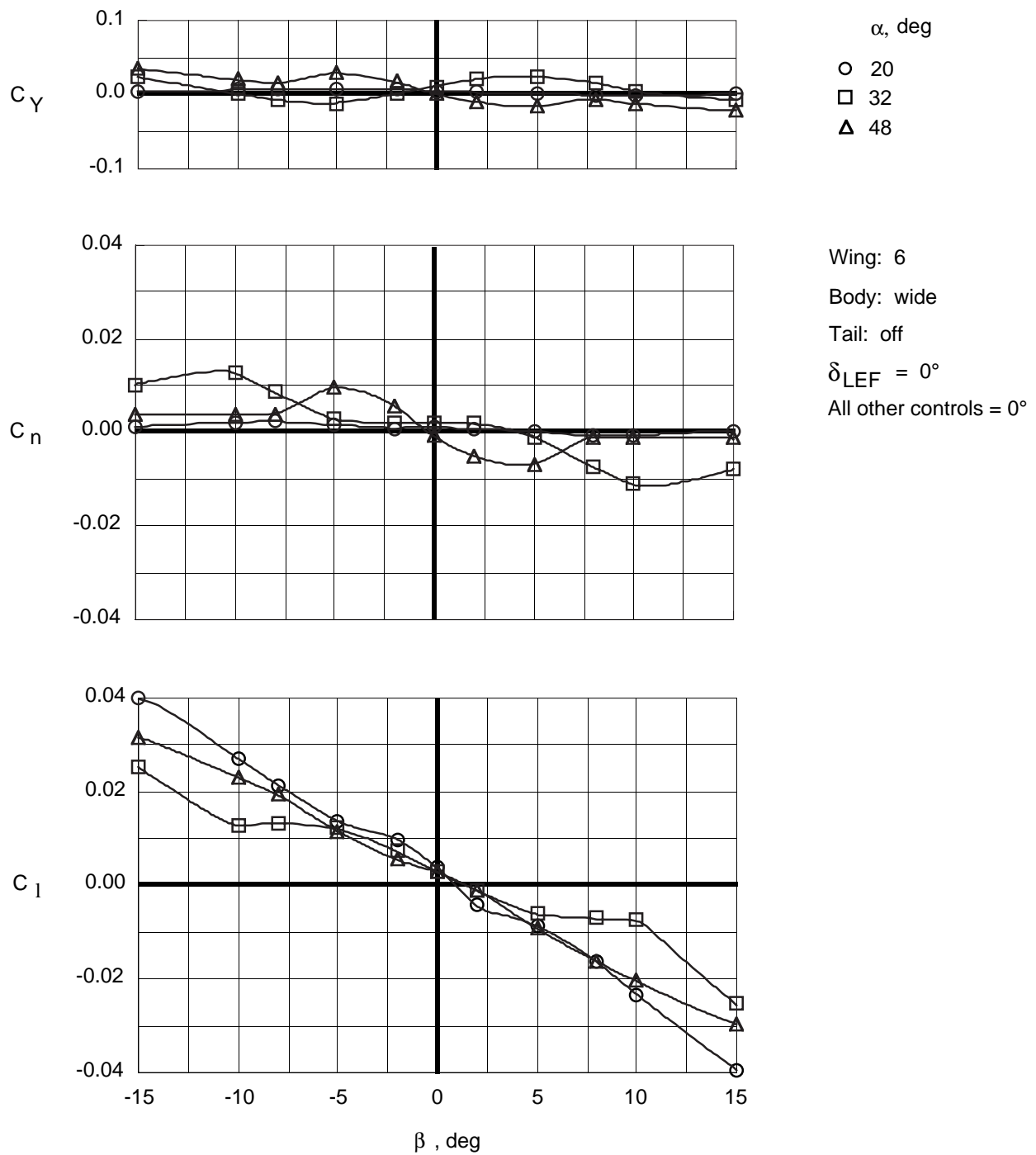


Figure 63. Variation of lateral-directional coefficients with sideslip at high angles of attack for Wing 6 with wide top body on.

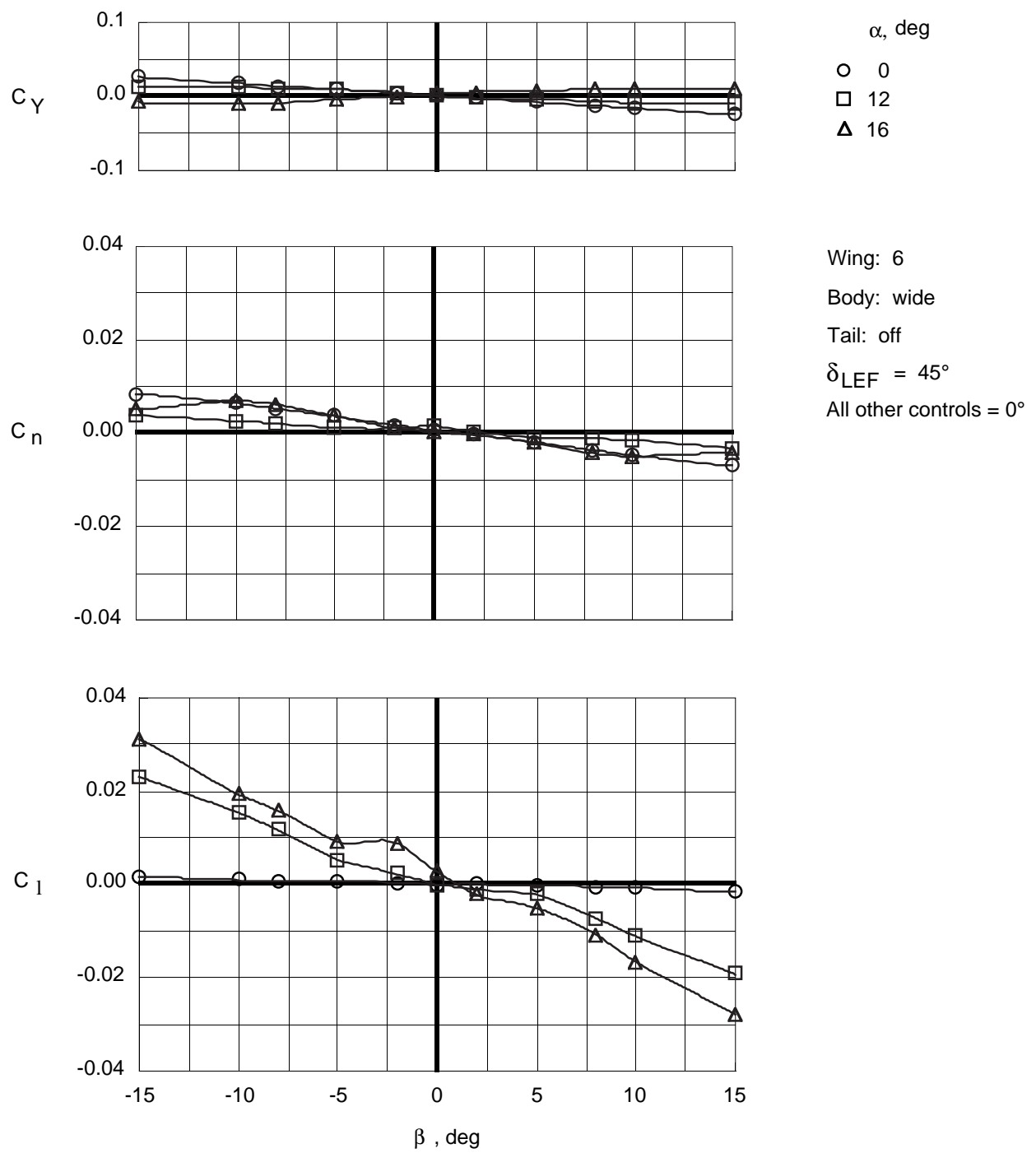


Figure 64. Variation of lateral-directional coefficients with sideslip at low angles of attack for Wing 6 with wide top body on and leading-edge flaps deflected.

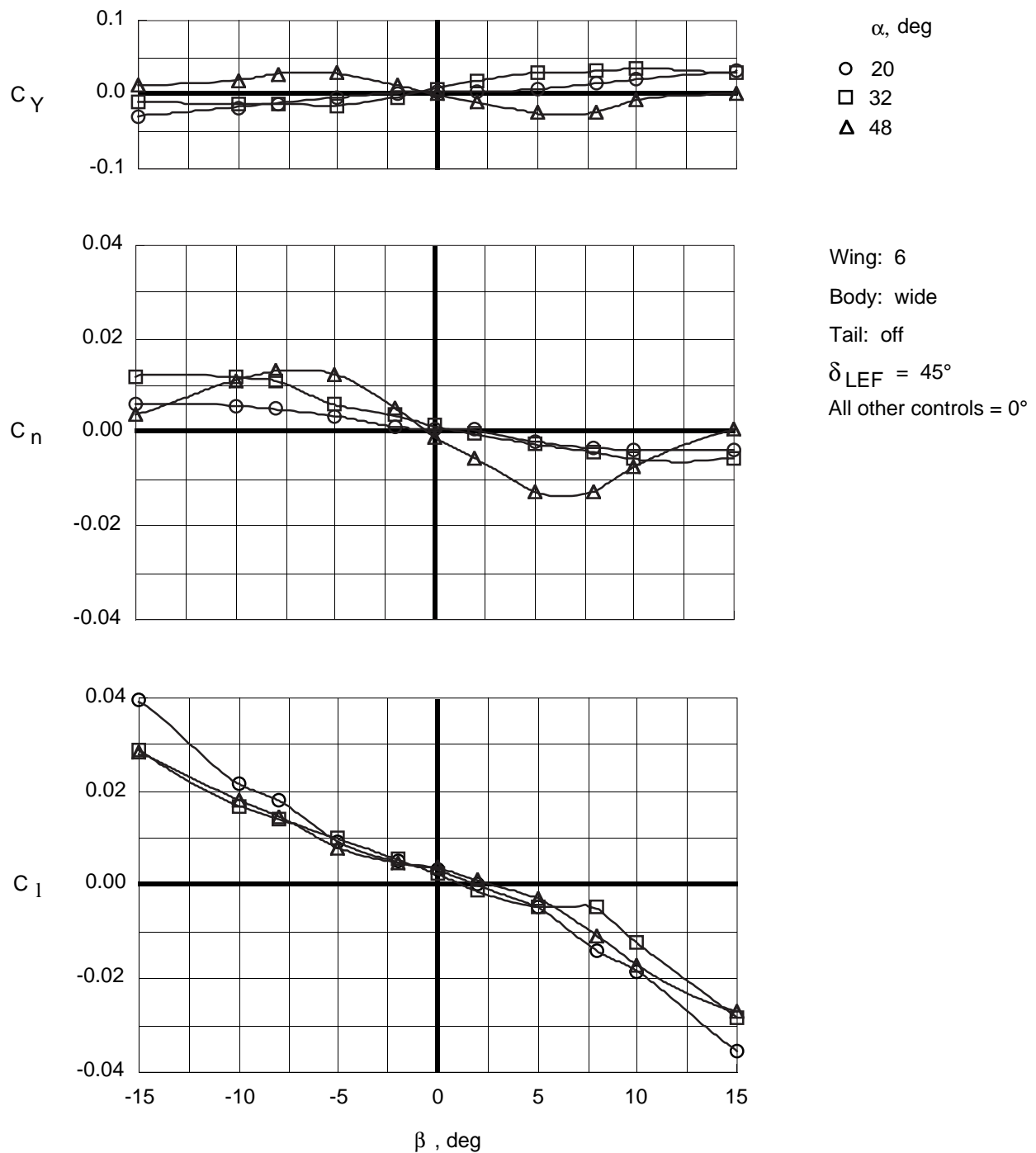


Figure 65. Variation of lateral-directional coefficients with sideslip at high angles of attack for Wing 6 with wide top body on and leading-edge flaps deflected.

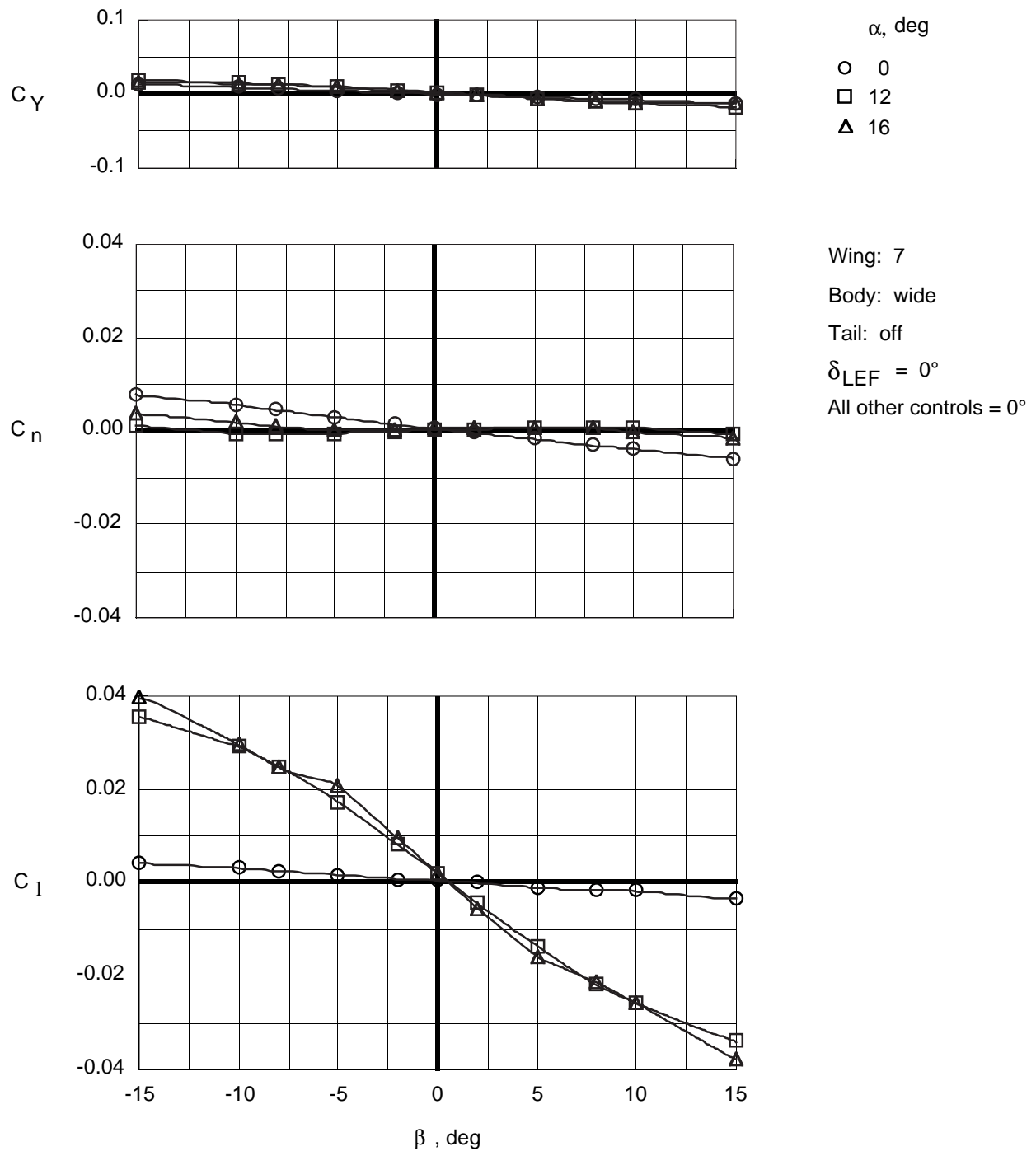


Figure 66. Variation of lateral-directional coefficients with sideslip at low angles of attack for Wing 7 with wide top body on.

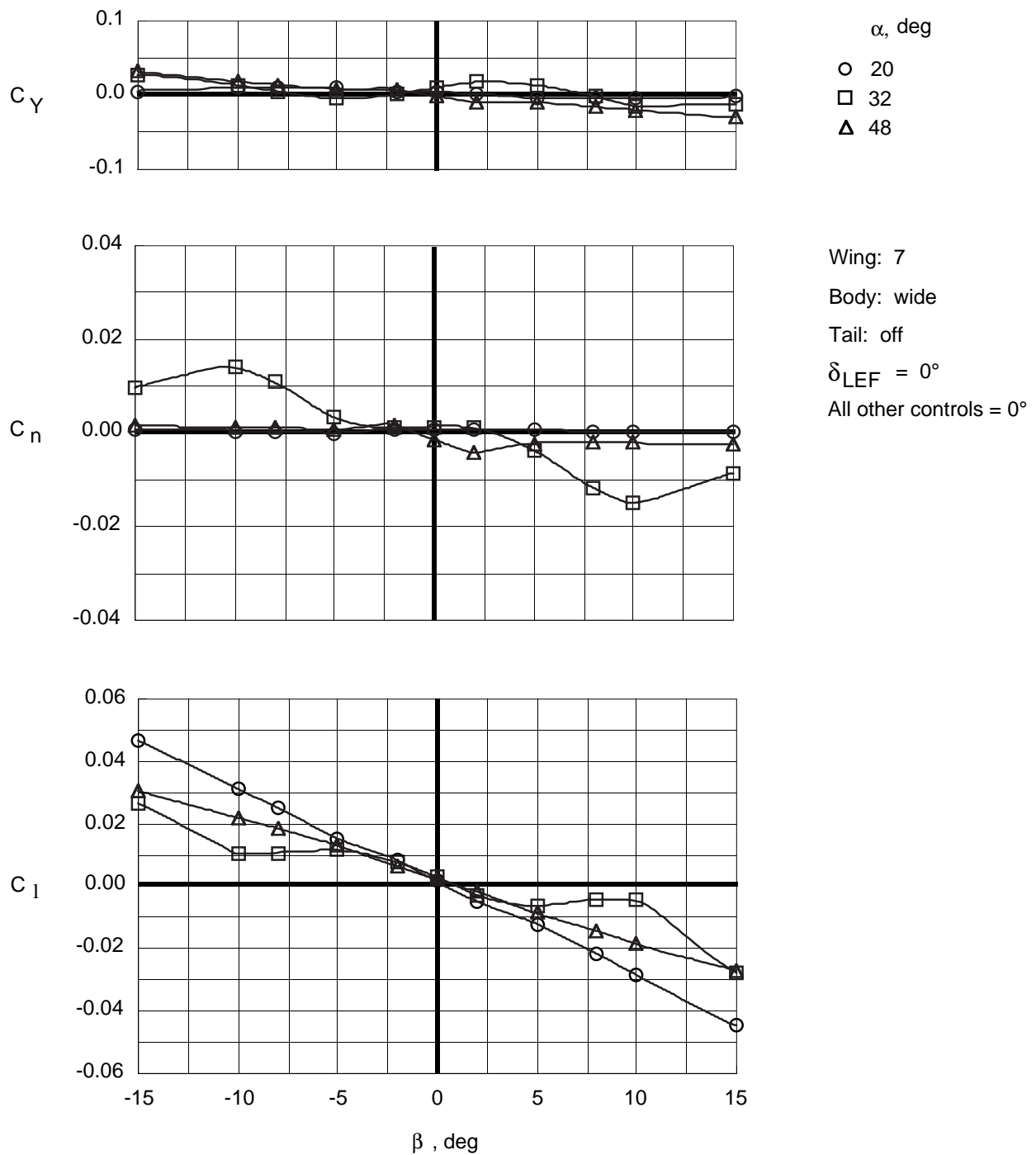


Figure 67. Variation of lateral-directional coefficients with sideslip at high angles of attack for Wing 7 with wide top body on.

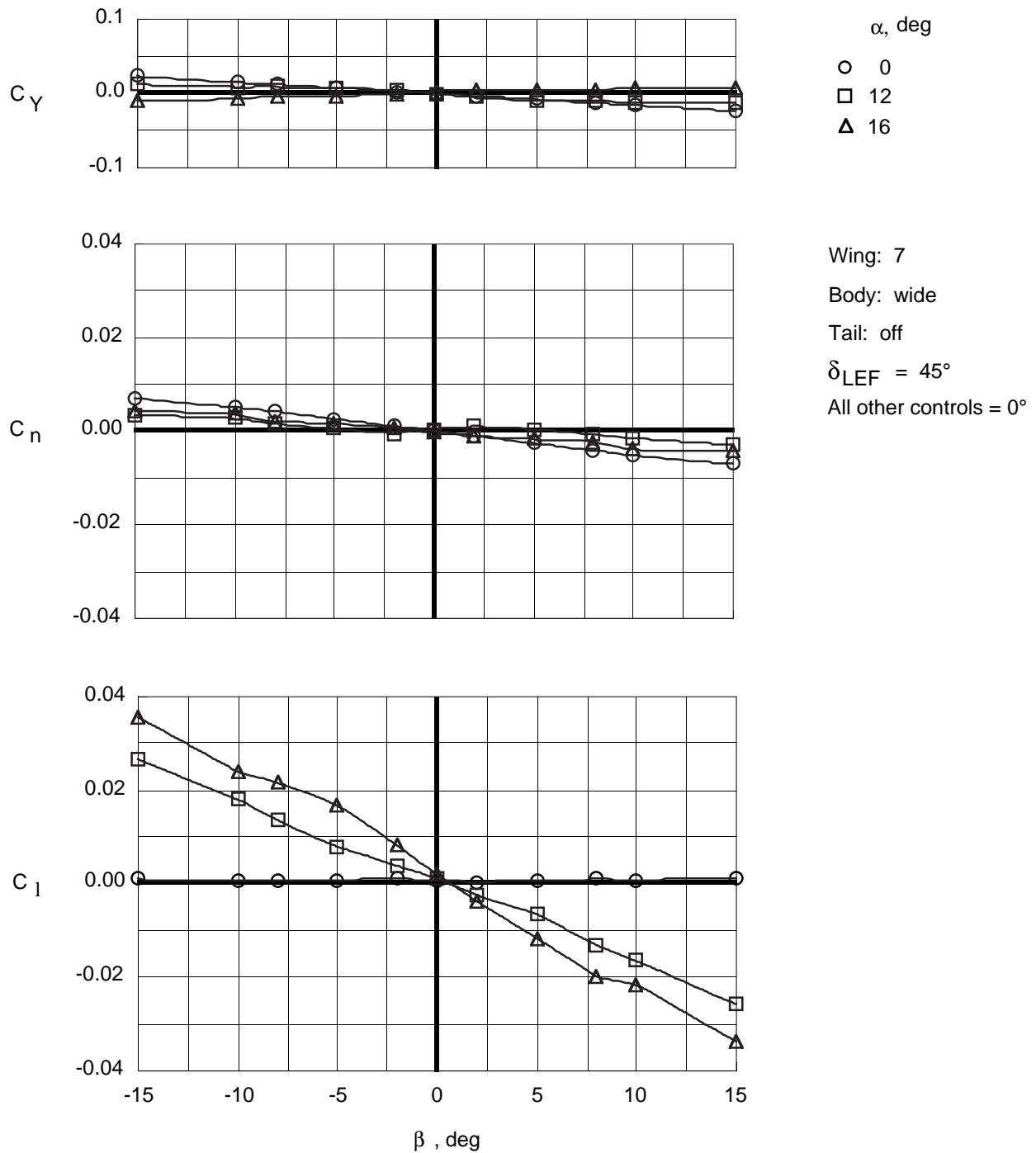


Figure 68. Variation of lateral-directional coefficients with sideslip at low angles of attack for Wing 7 with wide top body on and leading-edge flaps deflected.

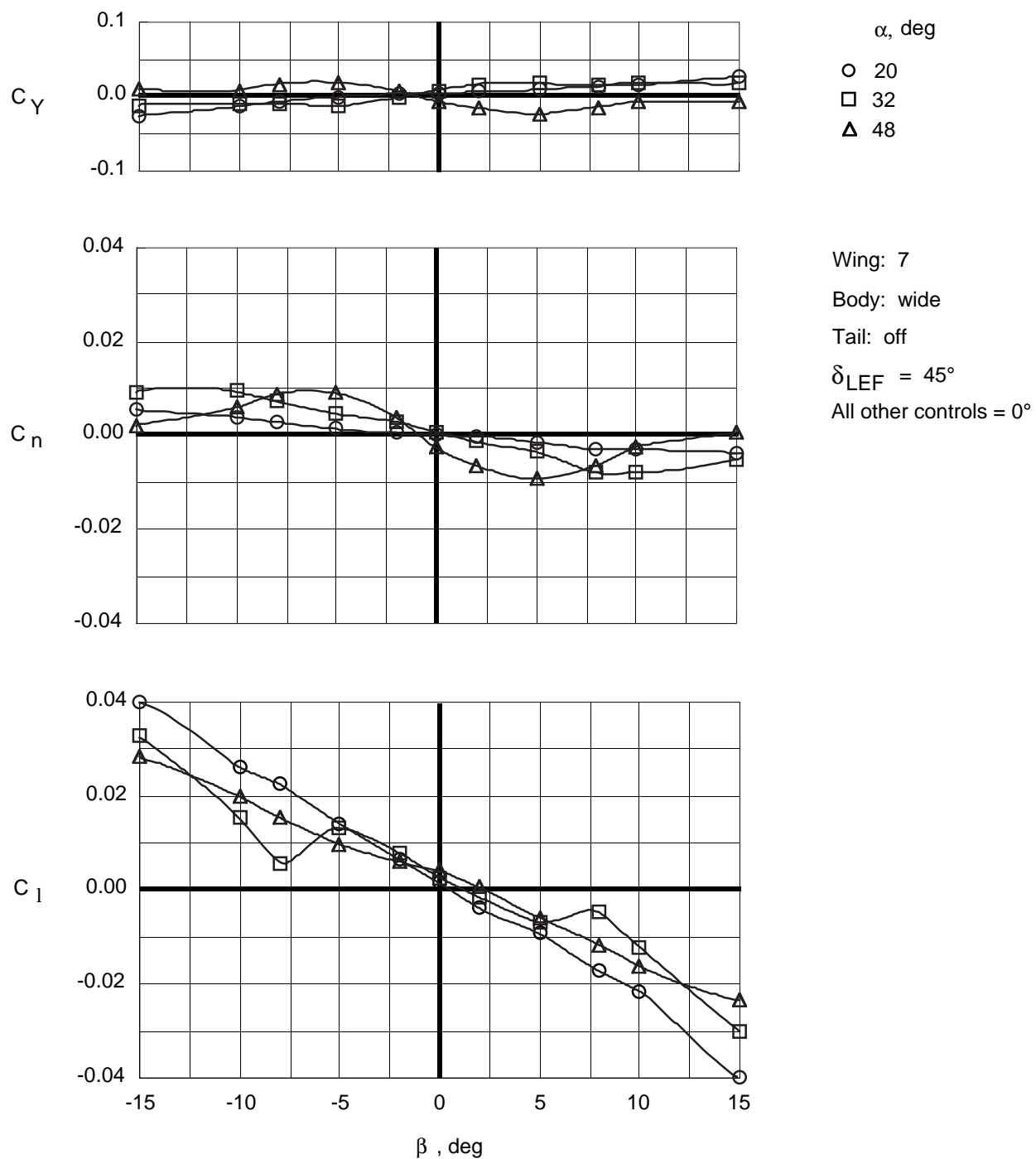


Figure 69. Variation of lateral-directional coefficients with sideslip at high angles of attack for Wing 7 with wide top body on and leading-edge flaps deflected.

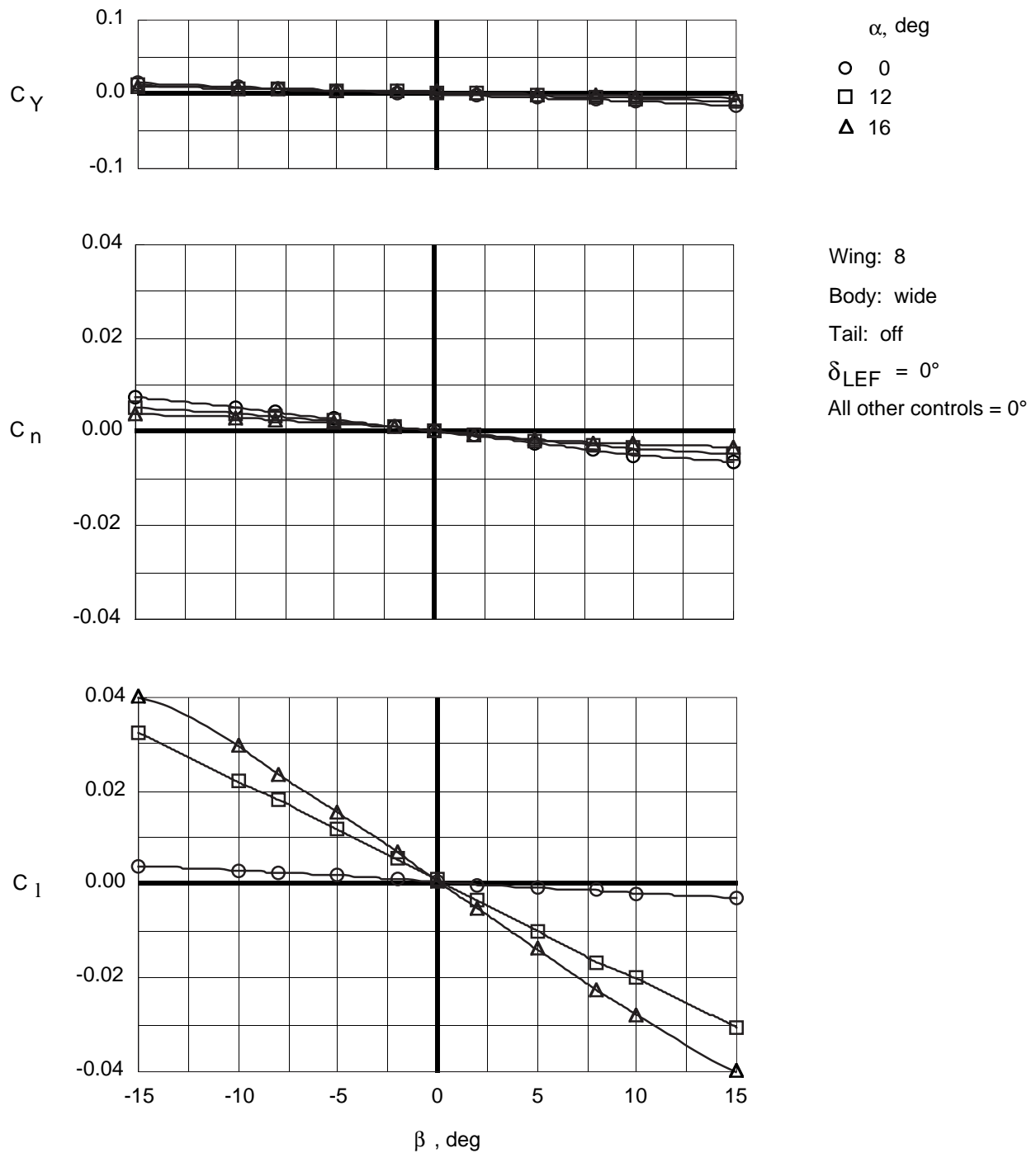


Figure 70. Variation of lateral-directional coefficients with sideslip at low angles of attack for Wing 8 with wide top body on.

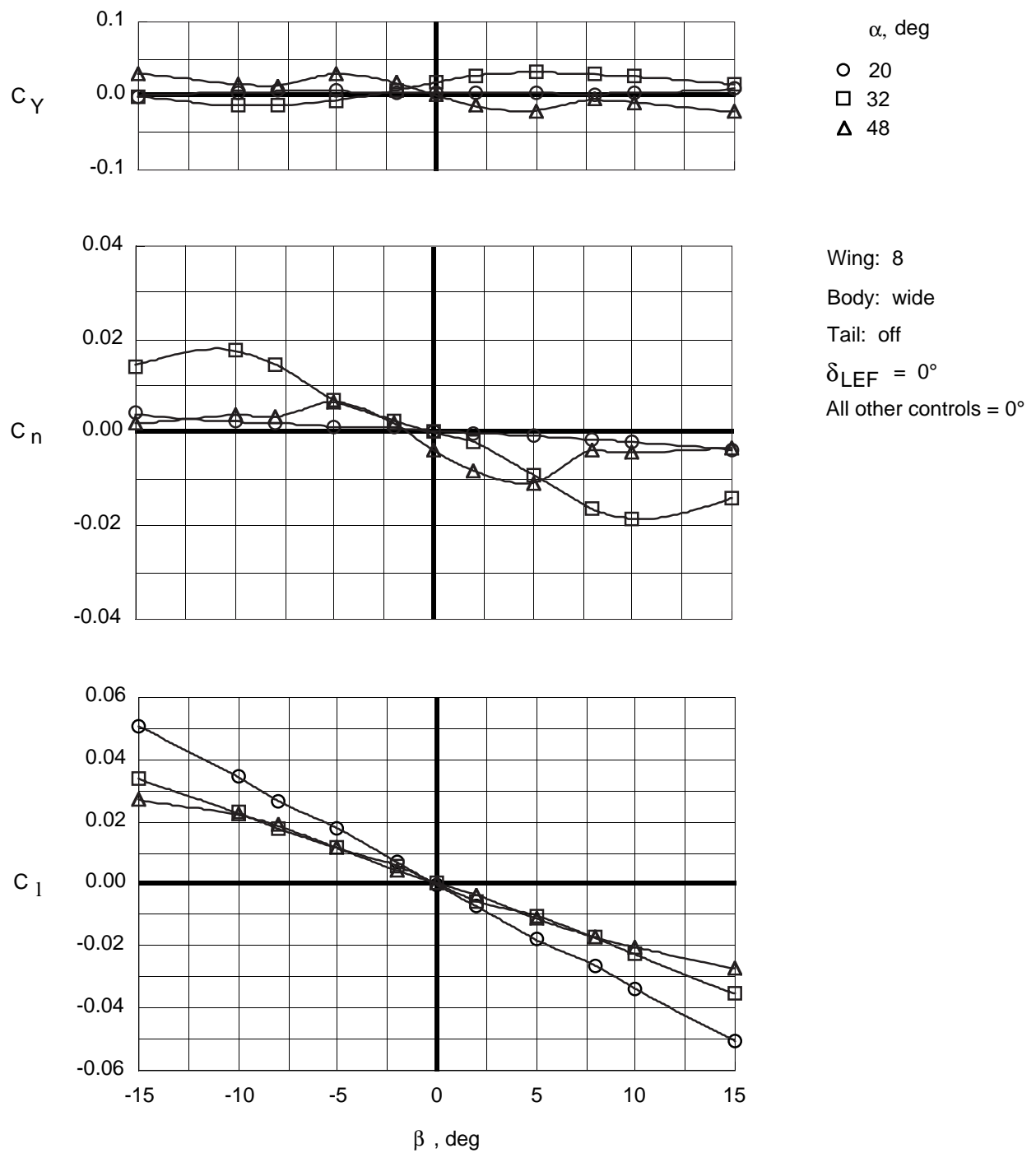


Figure 71. Variation of lateral-directional coefficients with sideslip at high angles of attack for Wing 8 with wide top body on.

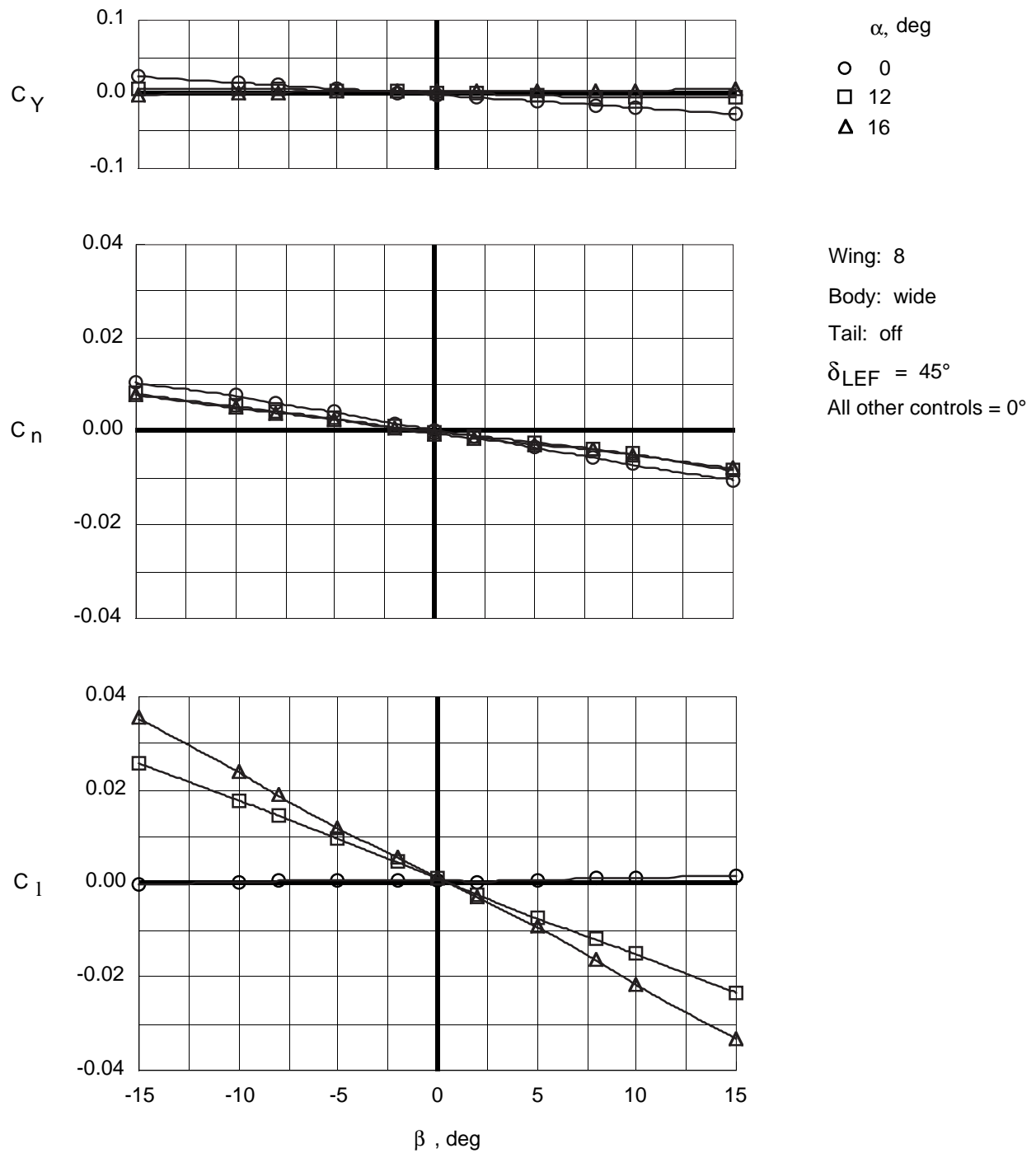


Figure 72. Variation of lateral-directional coefficients with sideslip at low angles of attack for Wing 8 with wide top body on and leading-edge flaps deflected.

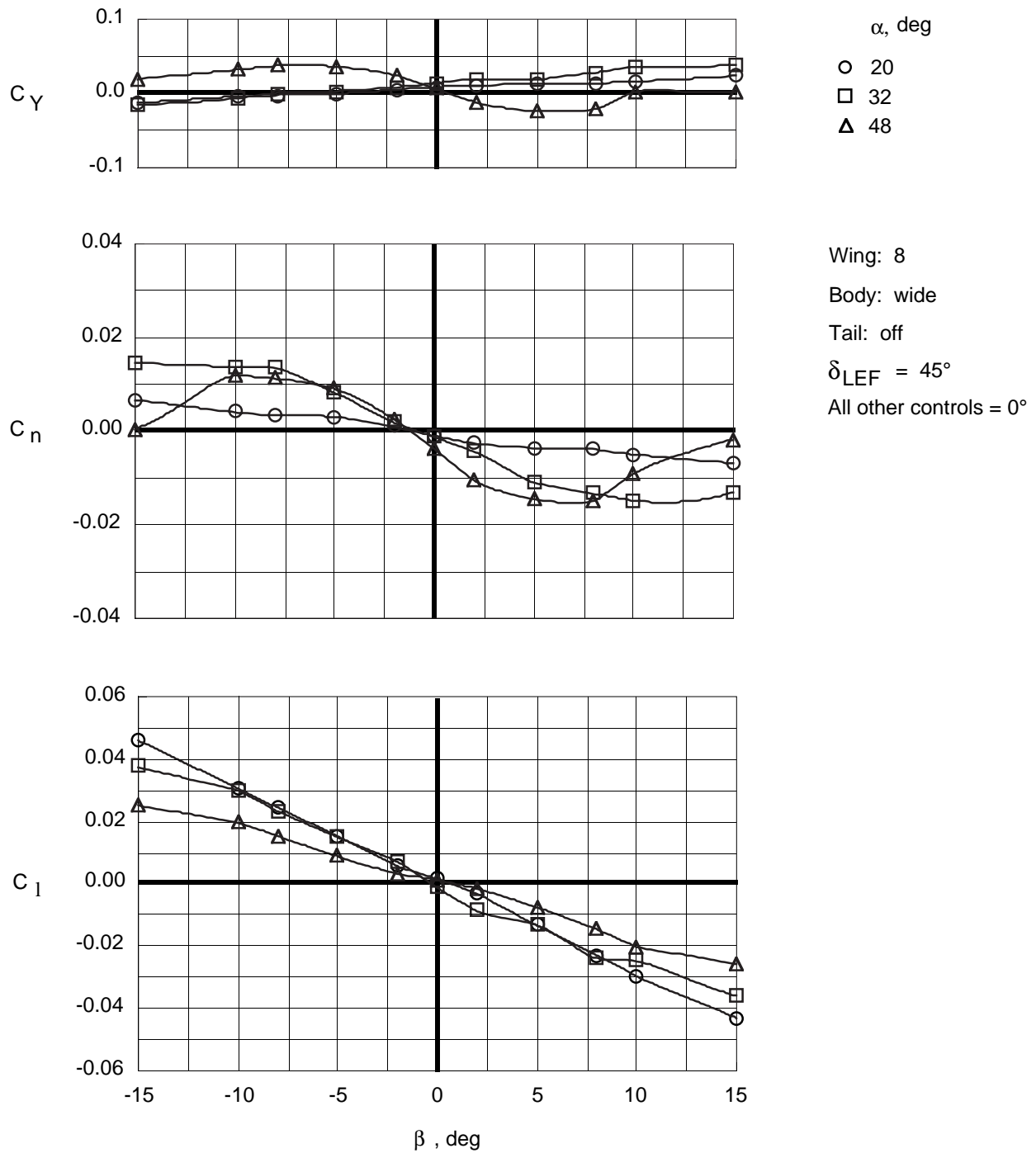


Figure 73. Variation of lateral-directional coefficients with sideslip at high angles of attack for Wing 8 with wide top body on and leading-edge flaps deflected.

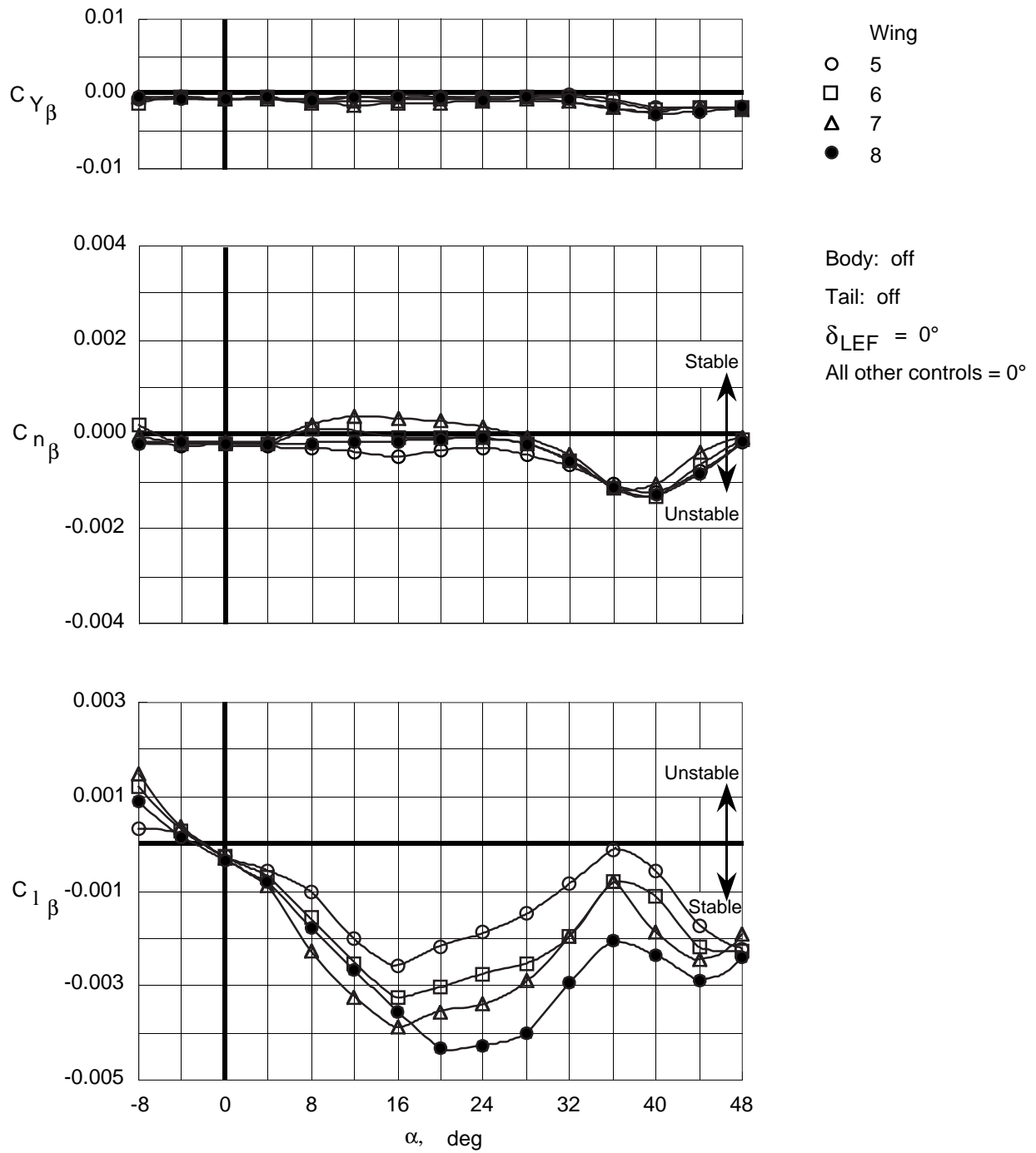


Figure 74. Lateral-directional stability characteristics of wing planforms with top body off.

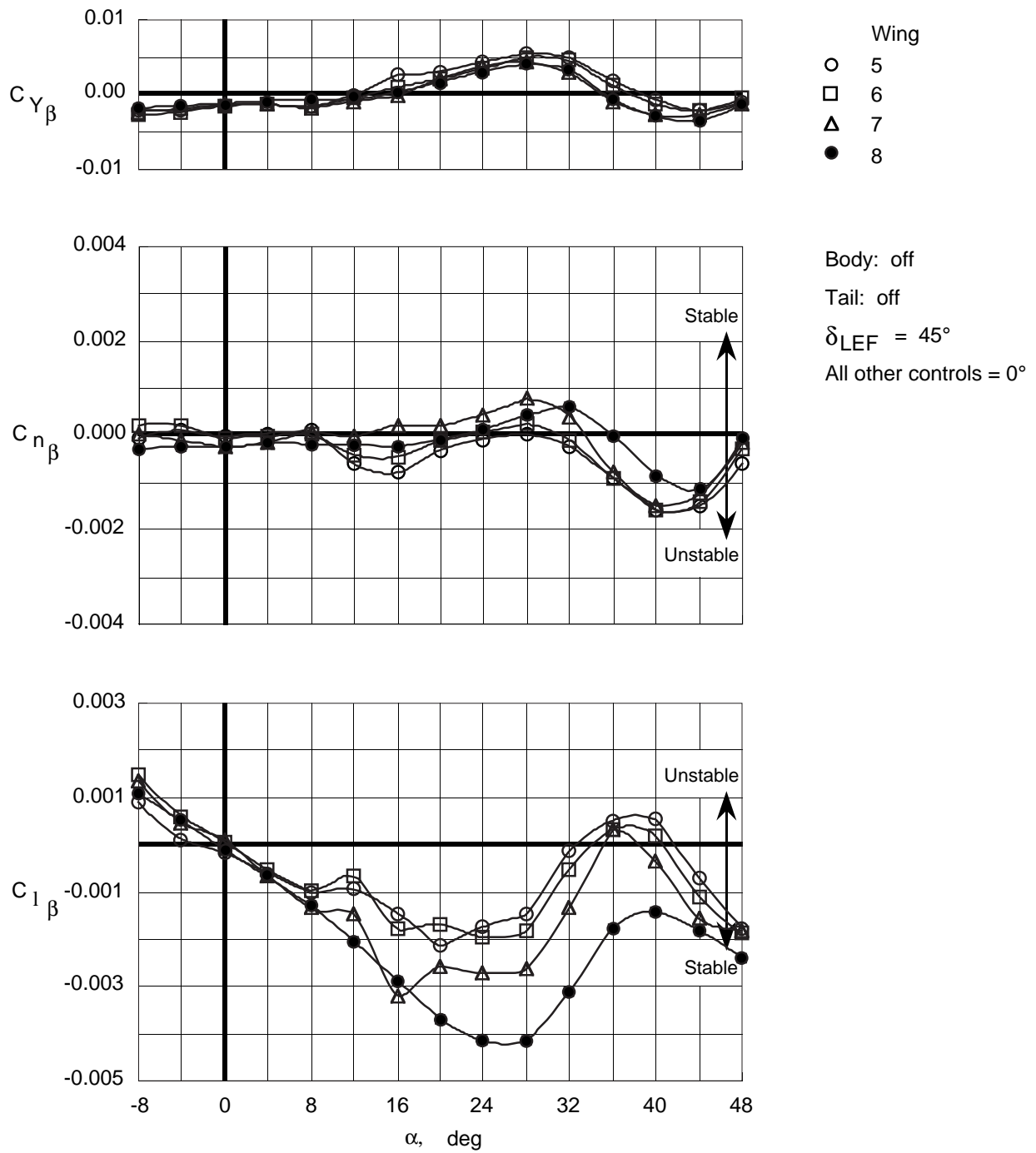


Figure 75. Lateral-directional stability characteristics of wing planforms with top body off and leading-edge flaps deflected.

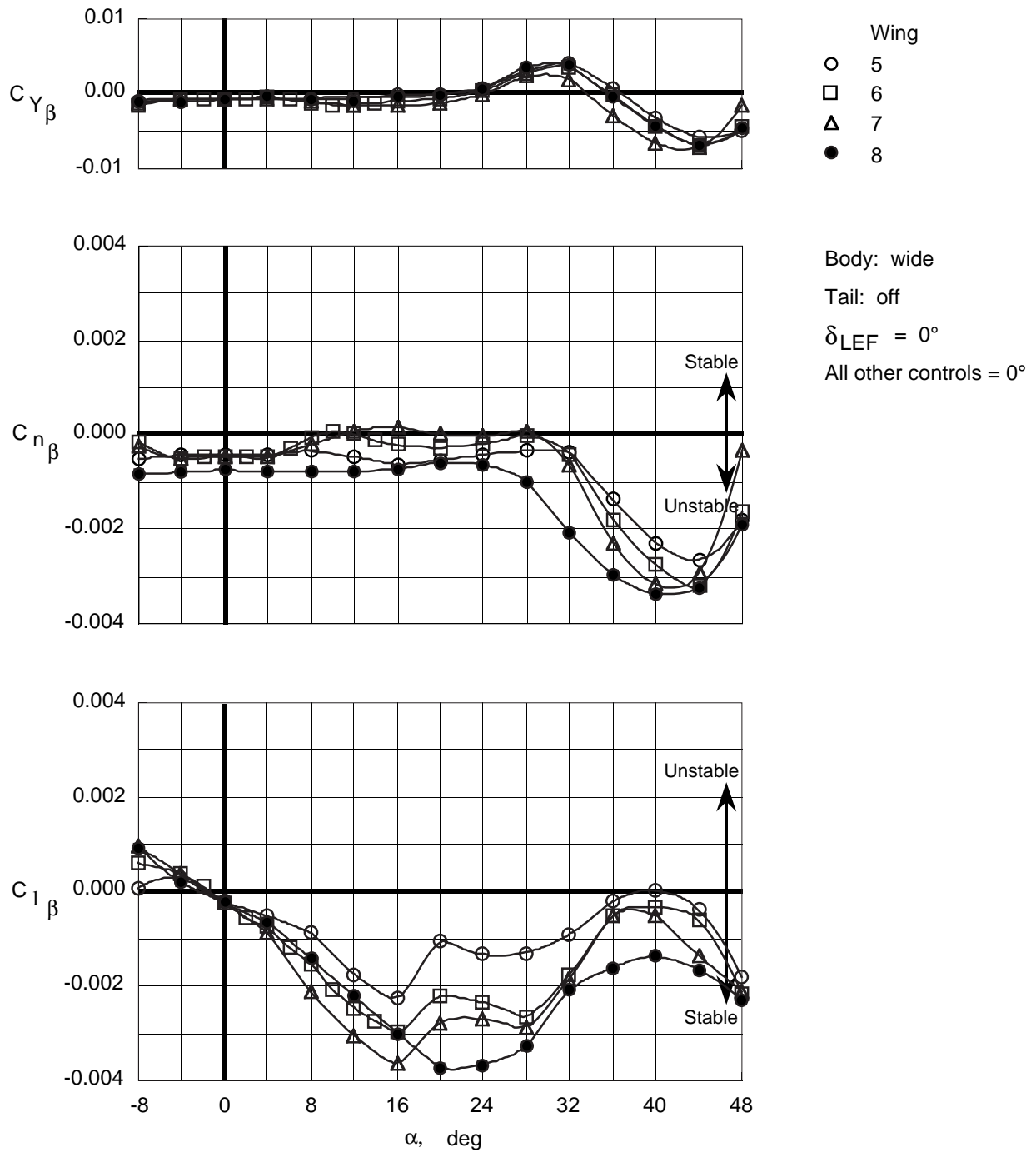


Figure 76. Lateral-directional stability characteristics of wing planforms with wide top body on.

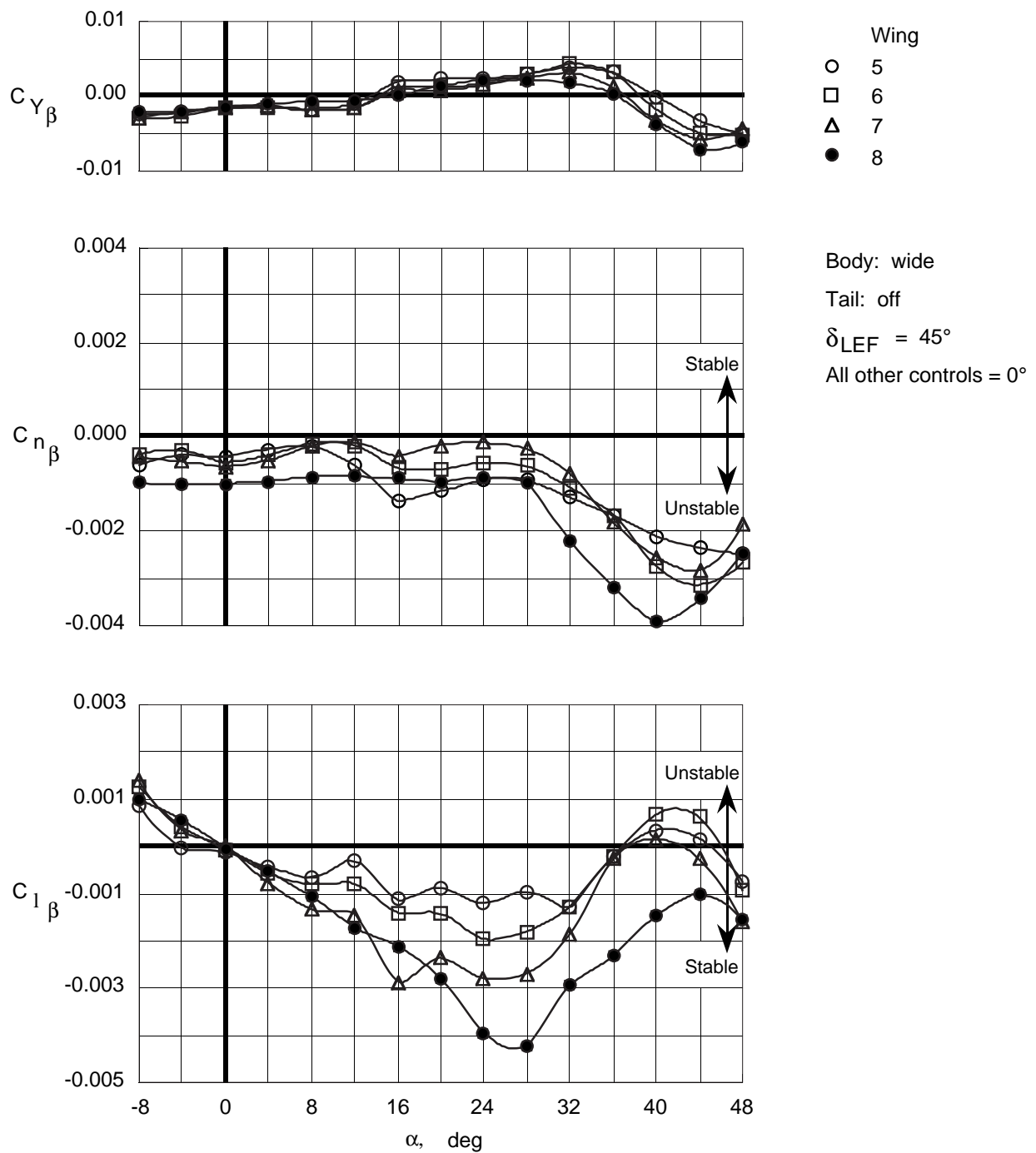


Figure 77. Lateral-directional stability characteristics of wing planforms with wide top body on and leading-edge flaps deflected.

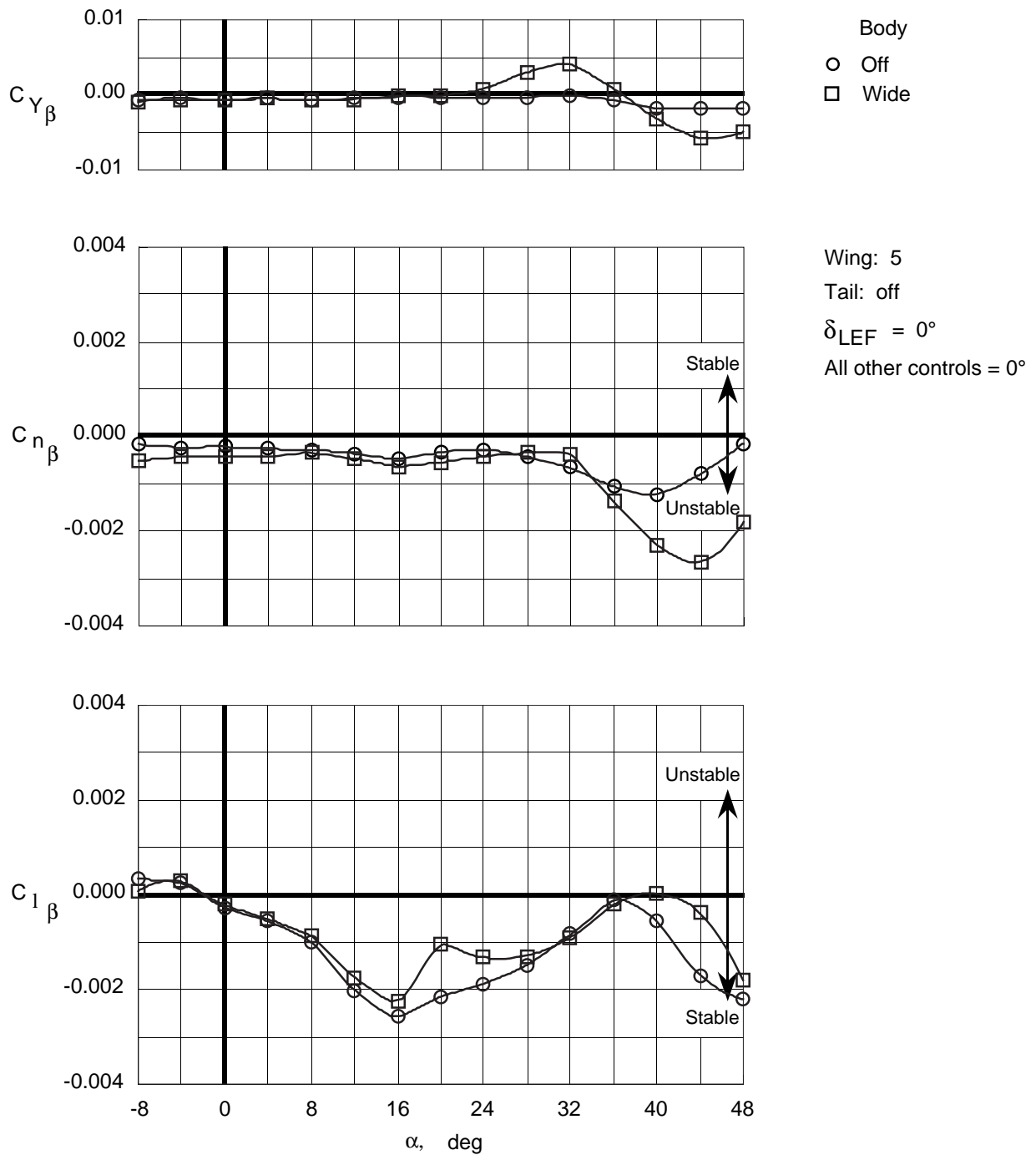


Figure 78. Effect of wide top body on lateral-directional stability characteristics of Wing 5.

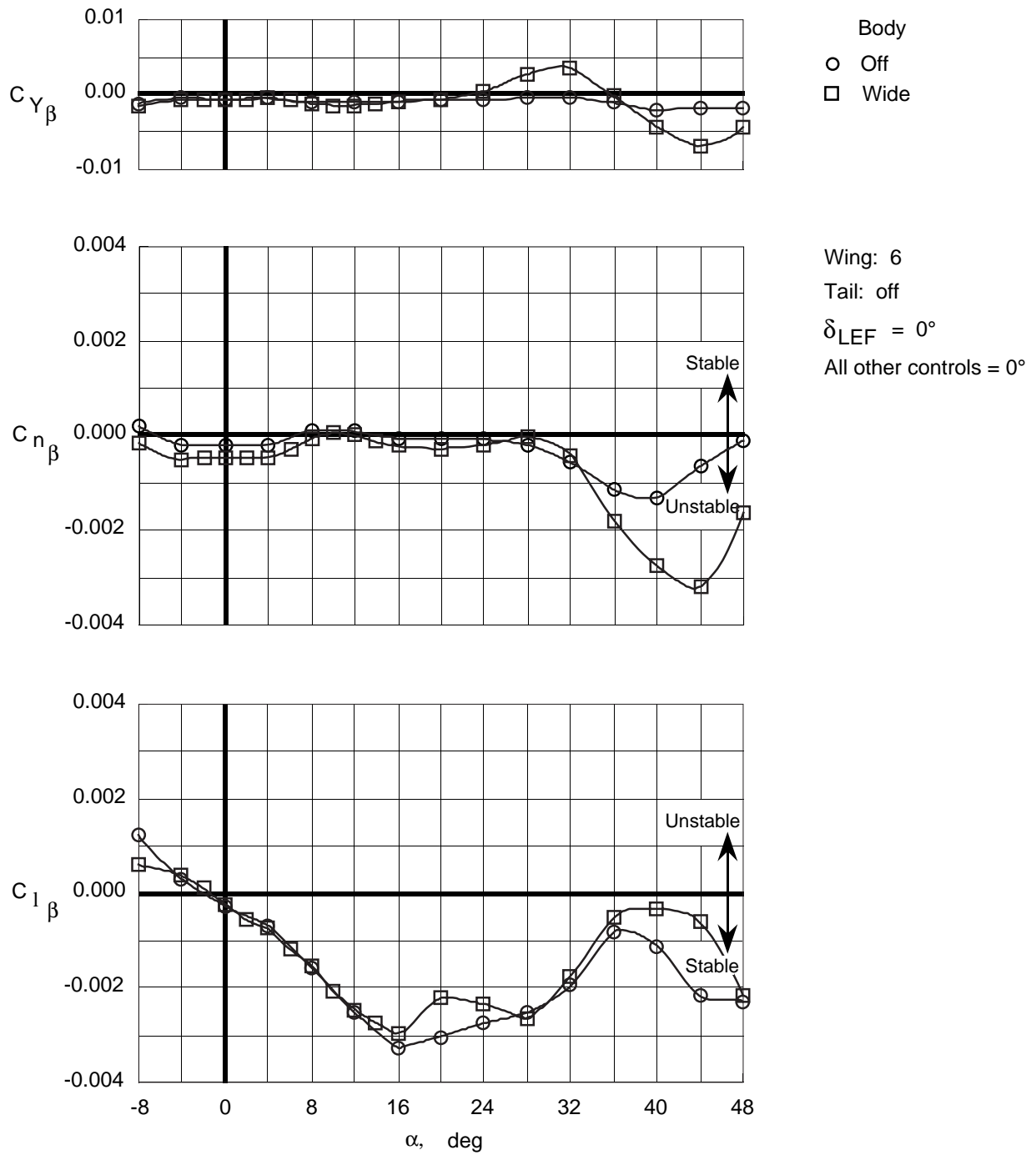


Figure 79. Effect of wide top body on lateral-directional stability characteristics of Wing 6.

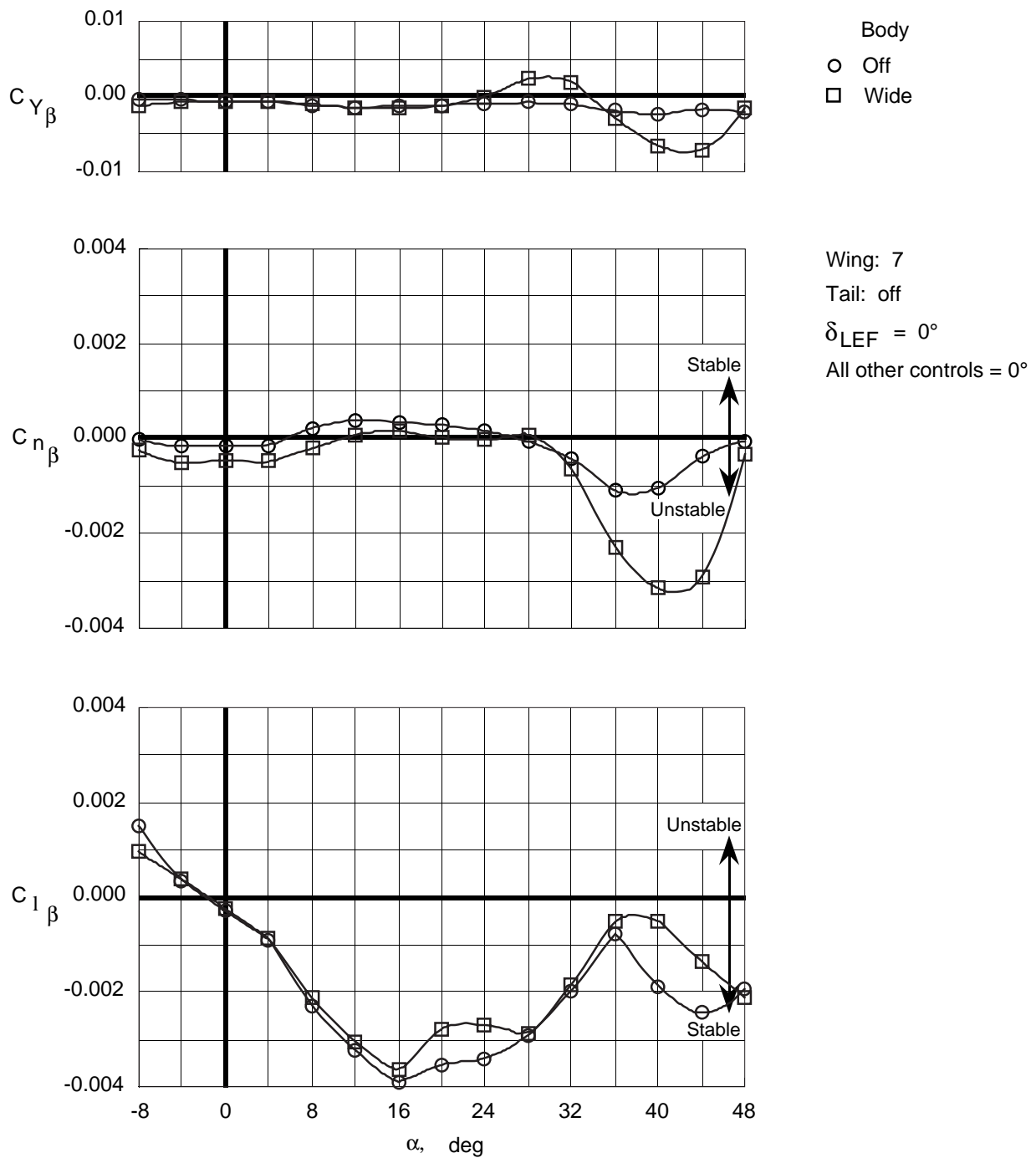


Figure 80. Effect of wide top body on lateral-directional stability characteristics of Wing 7.

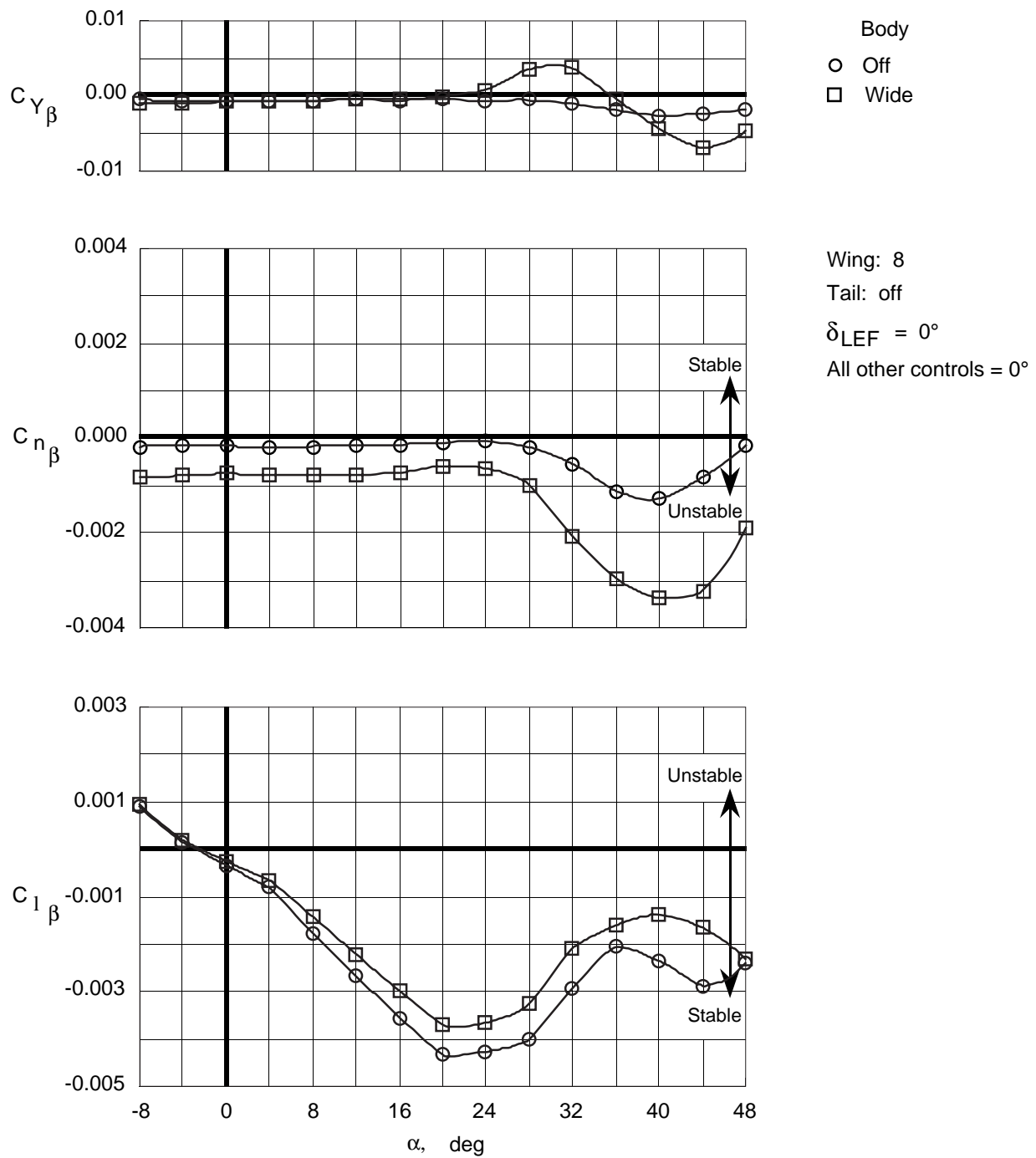


Figure 81. Effect of wide top body on lateral-directional stability characteristics of Wing 8.

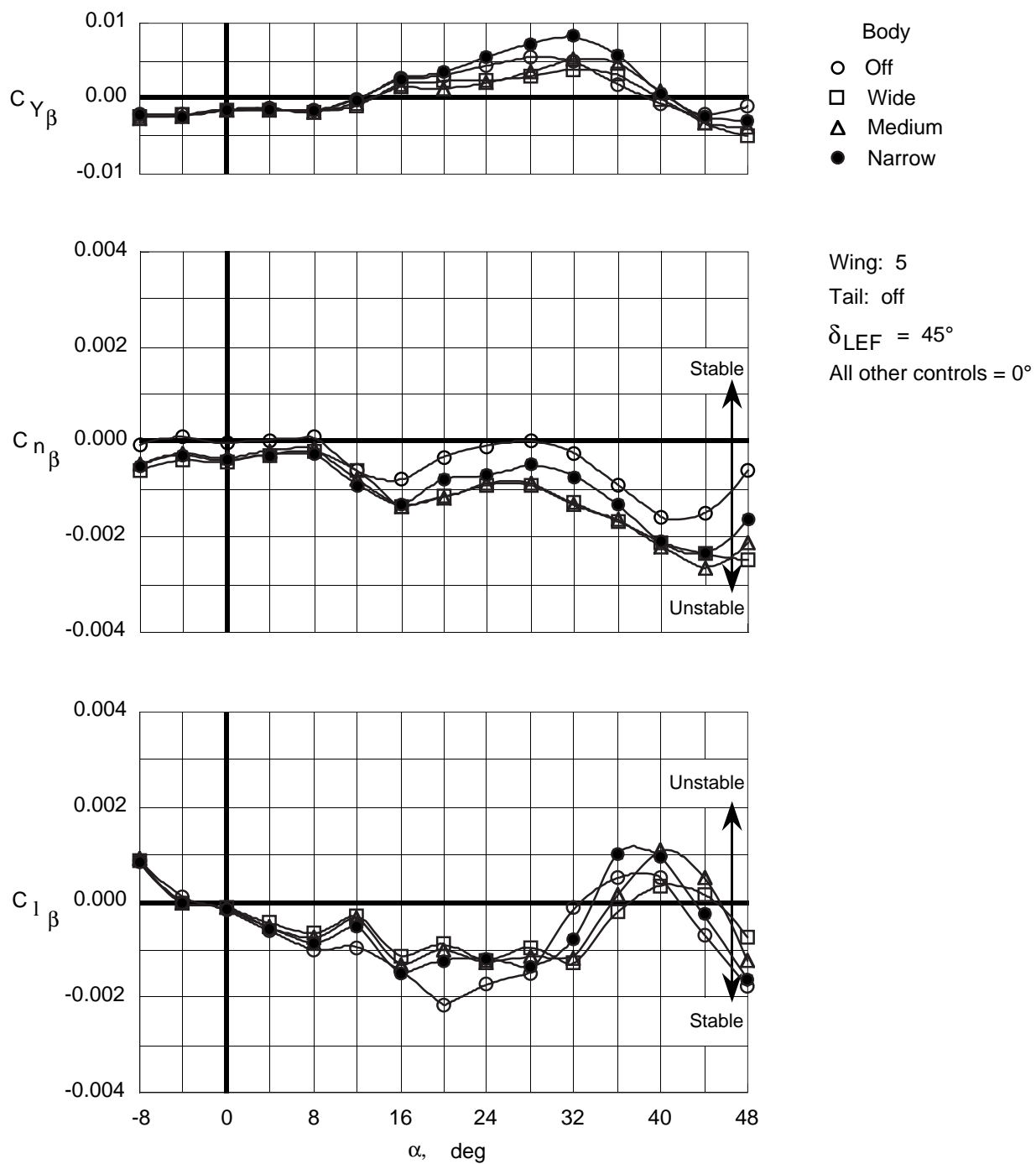


Figure 82. Effect of top body width on lateral-directional stability characteristics of Wing 5 with leading-edge flaps deflected.

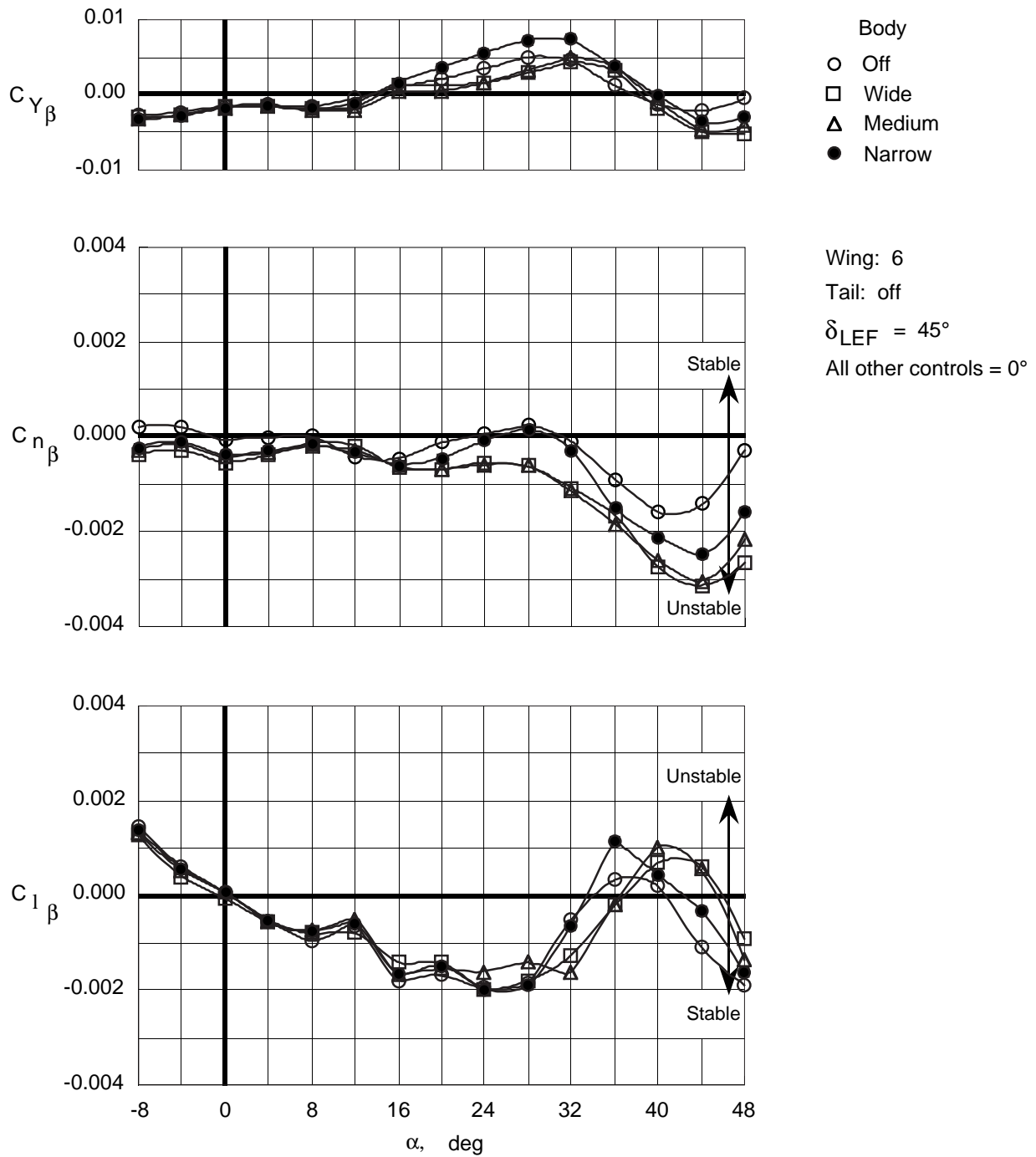


Figure 83. Effect of top body width on lateral-directional stability characteristics of Wing 6 with leading-edge flaps deflected.

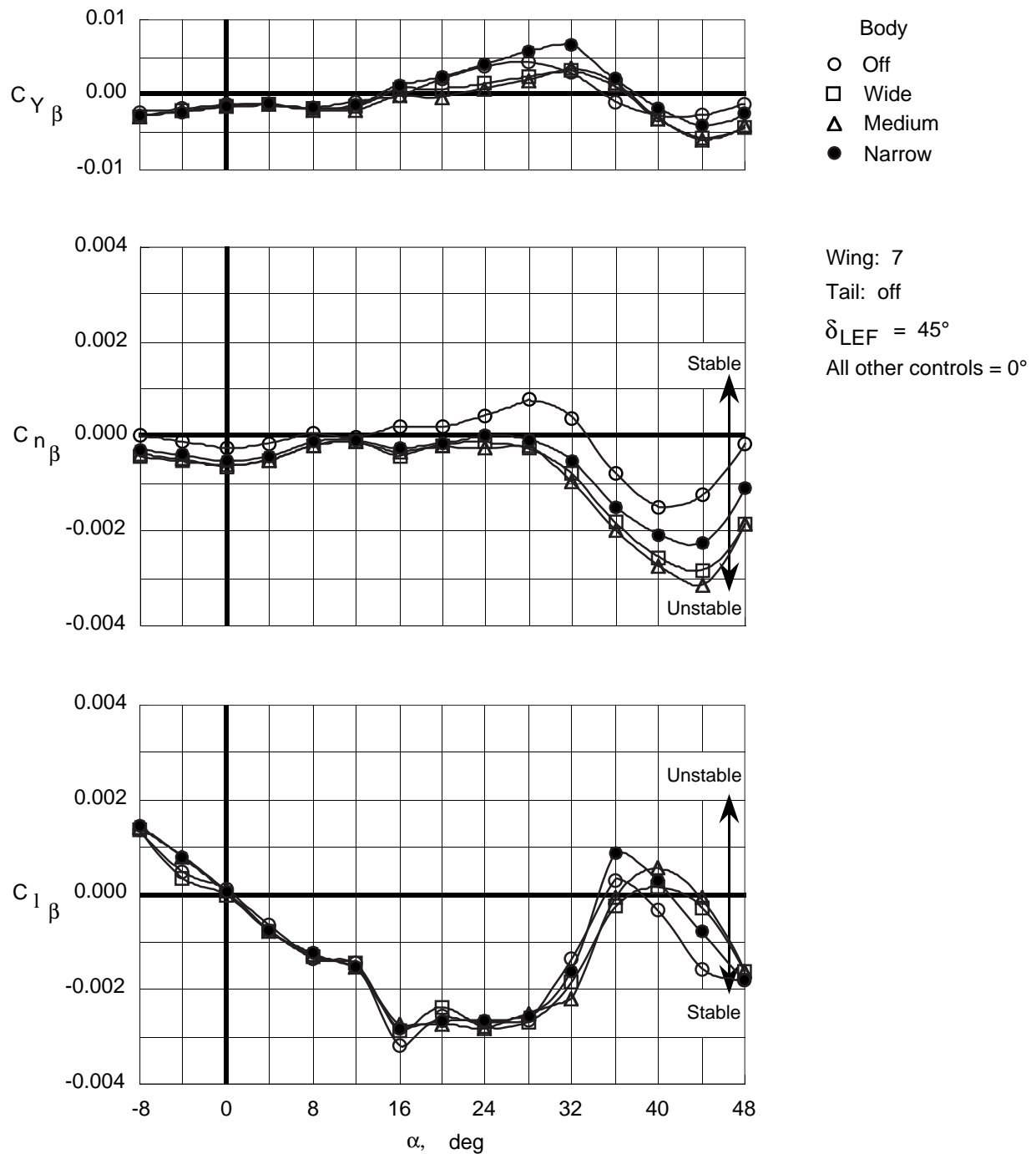


Figure 84. Effect of top body width on lateral-directional stability characteristics of Wing 7 with leading-edge flaps deflected.

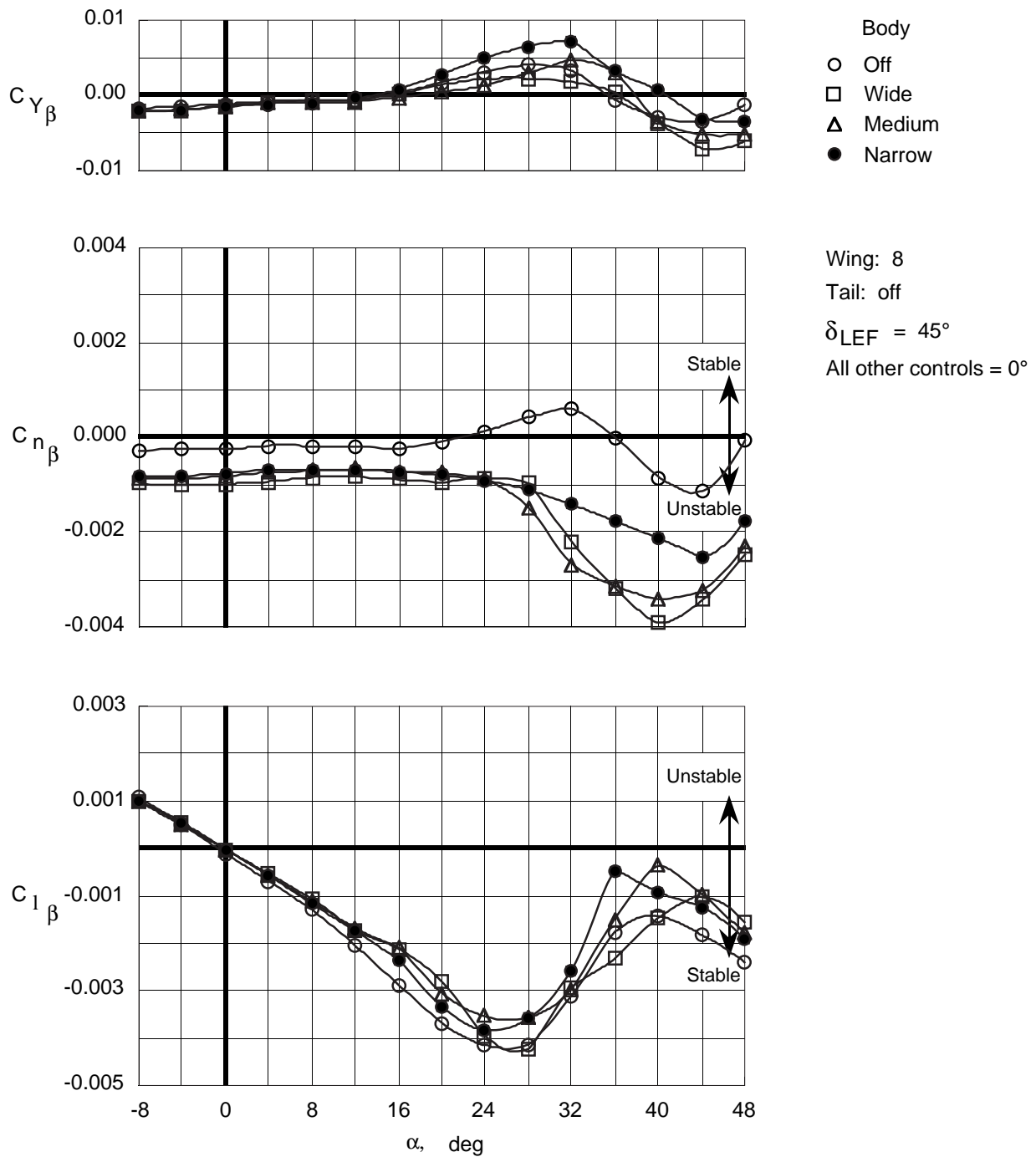


Figure 85. Effect of top body width on lateral-directional stability characteristics of Wing 8 with leading-edge flaps deflected.

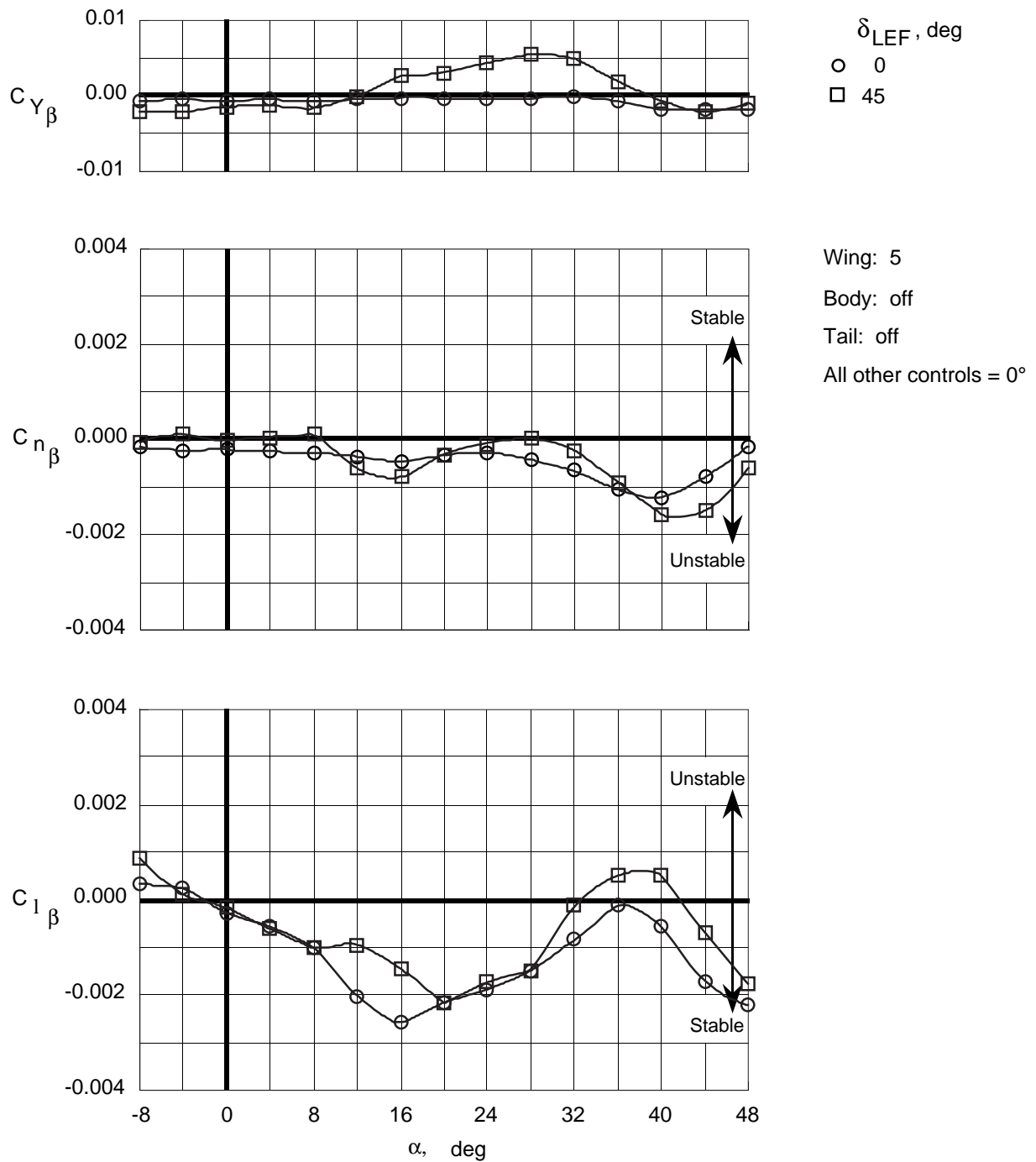


Figure 86. Effect of leading-edge flap deflection on lateral-directional stability characteristics of Wing 5 with top body off.

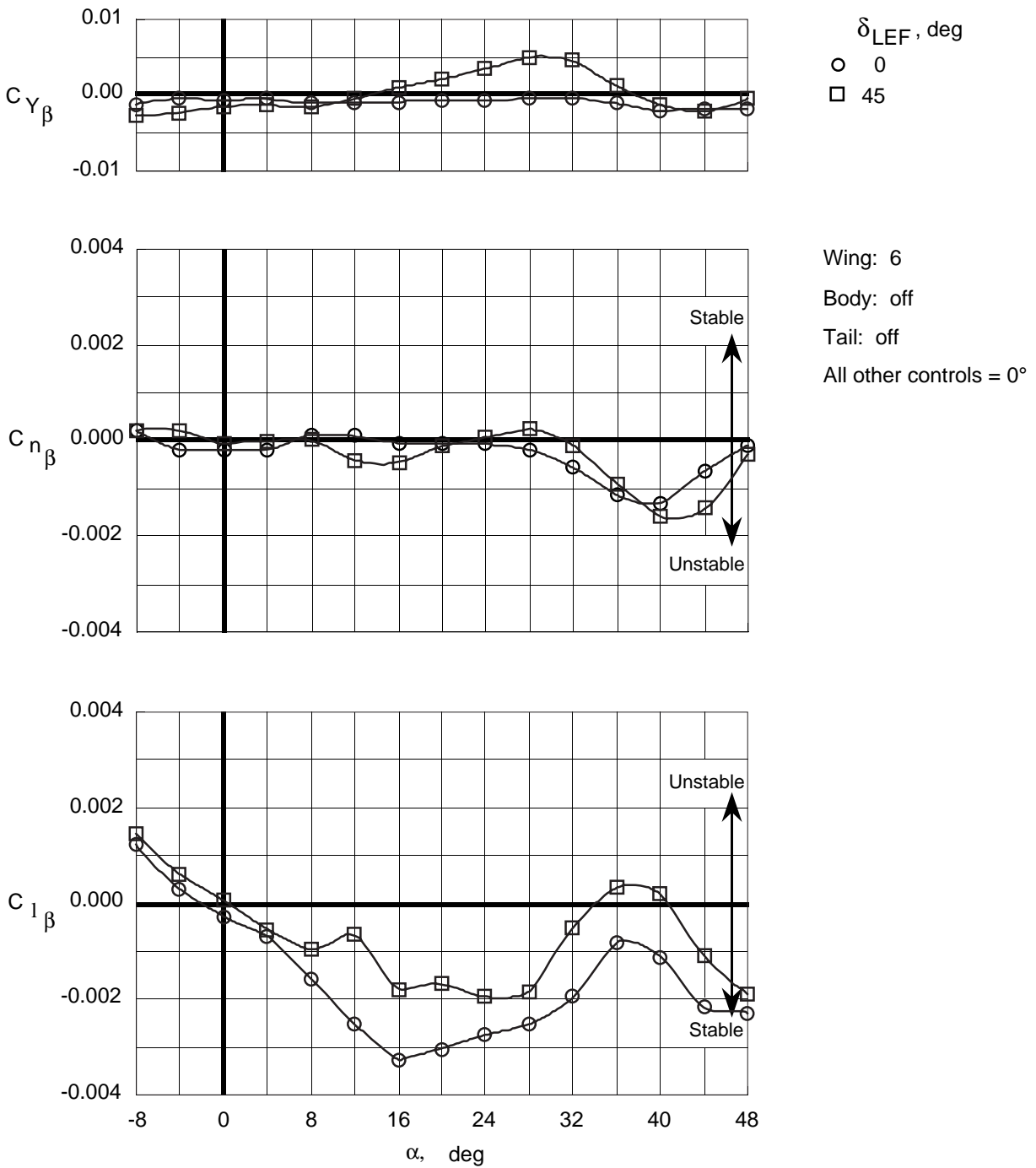


Figure 87. Effect of leading-edge flap deflection on lateral-directional stability characteristics of Wing 6 with top body off.

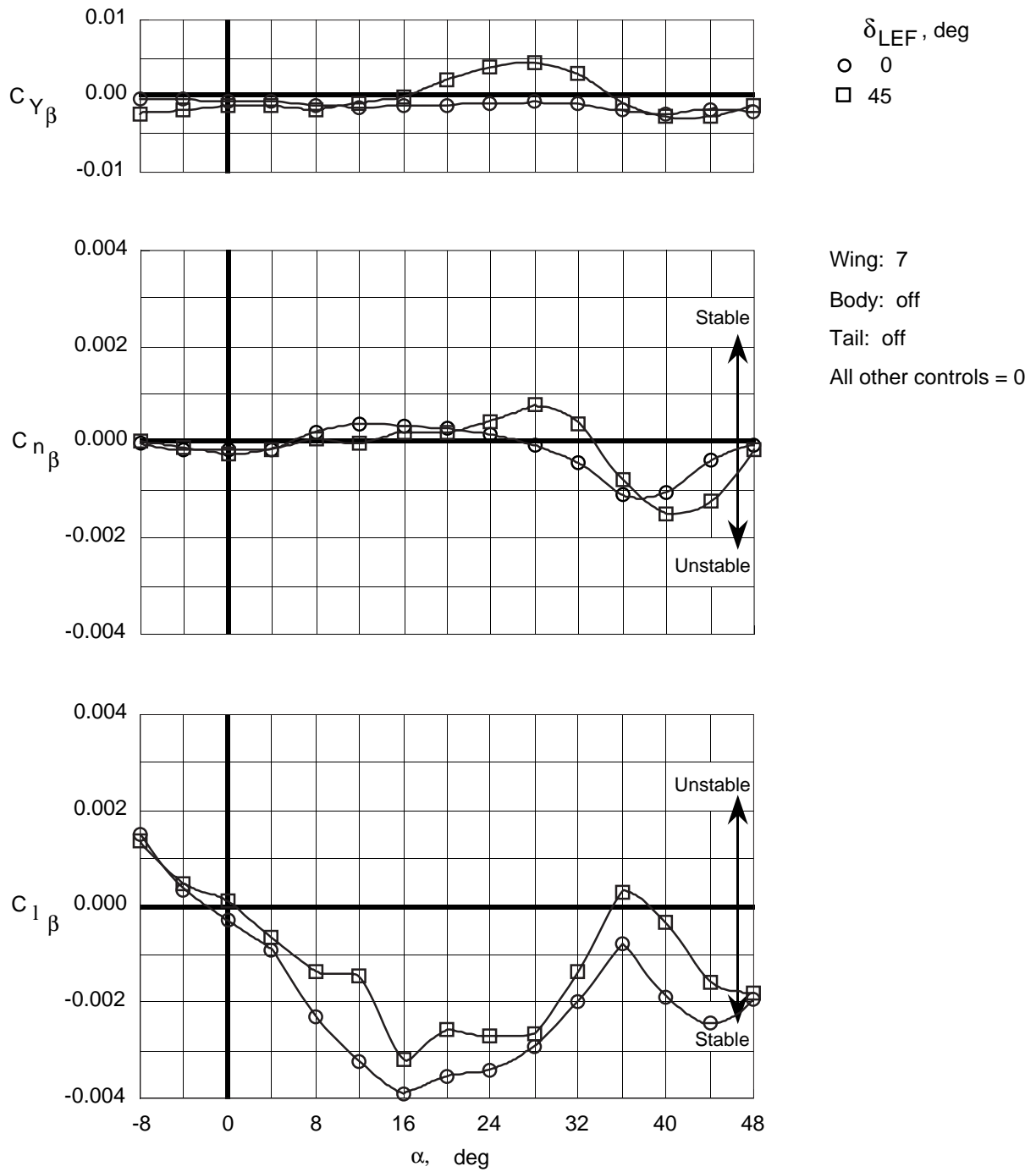


Figure 88. Effect of leading-edge flap deflection on lateral-directional stability characteristics of Wing 7 with top body off.

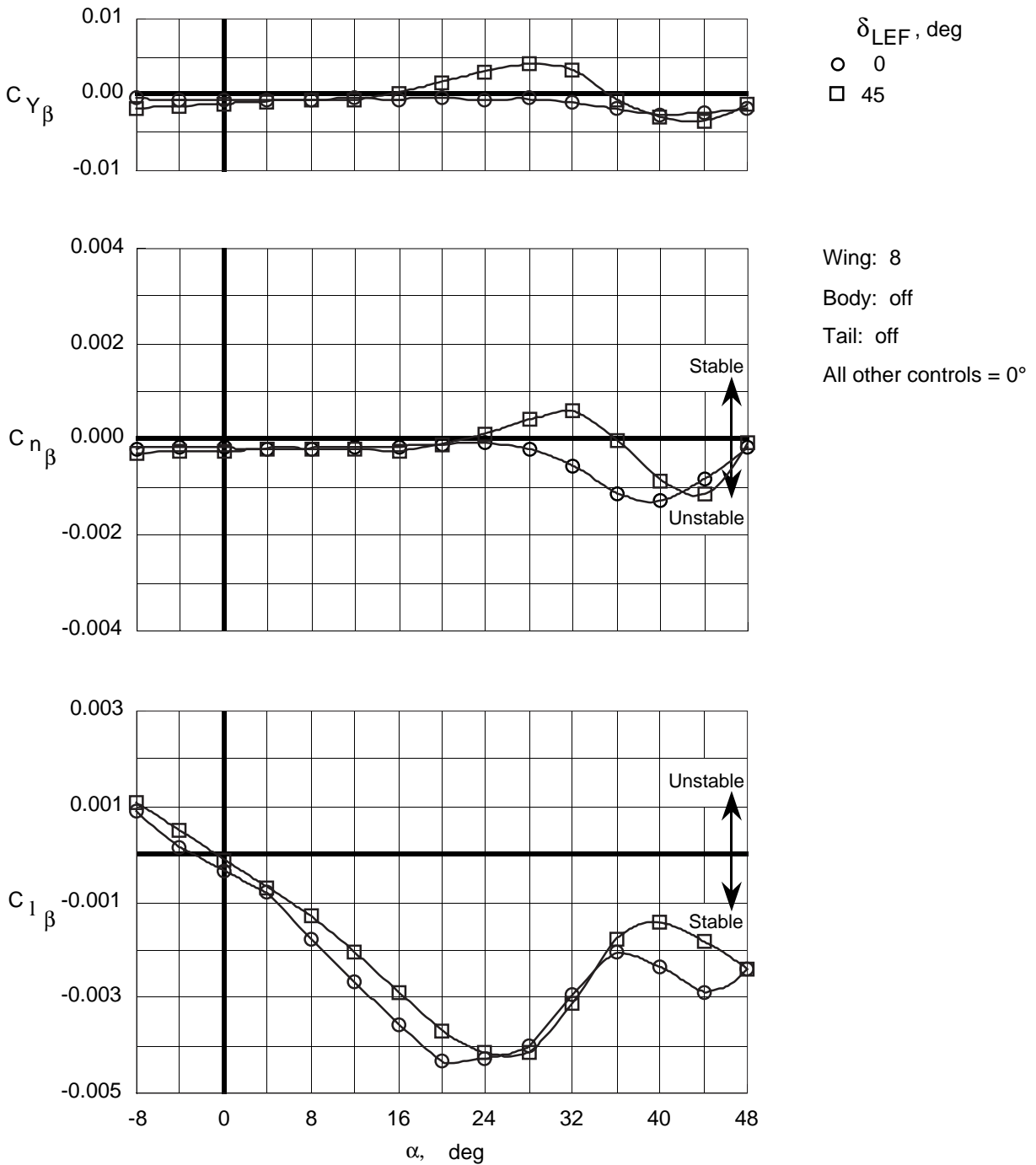


Figure 89. Effect of leading-edge flap deflection on lateral-directional stability characteristics of Wing 8 with top body off.

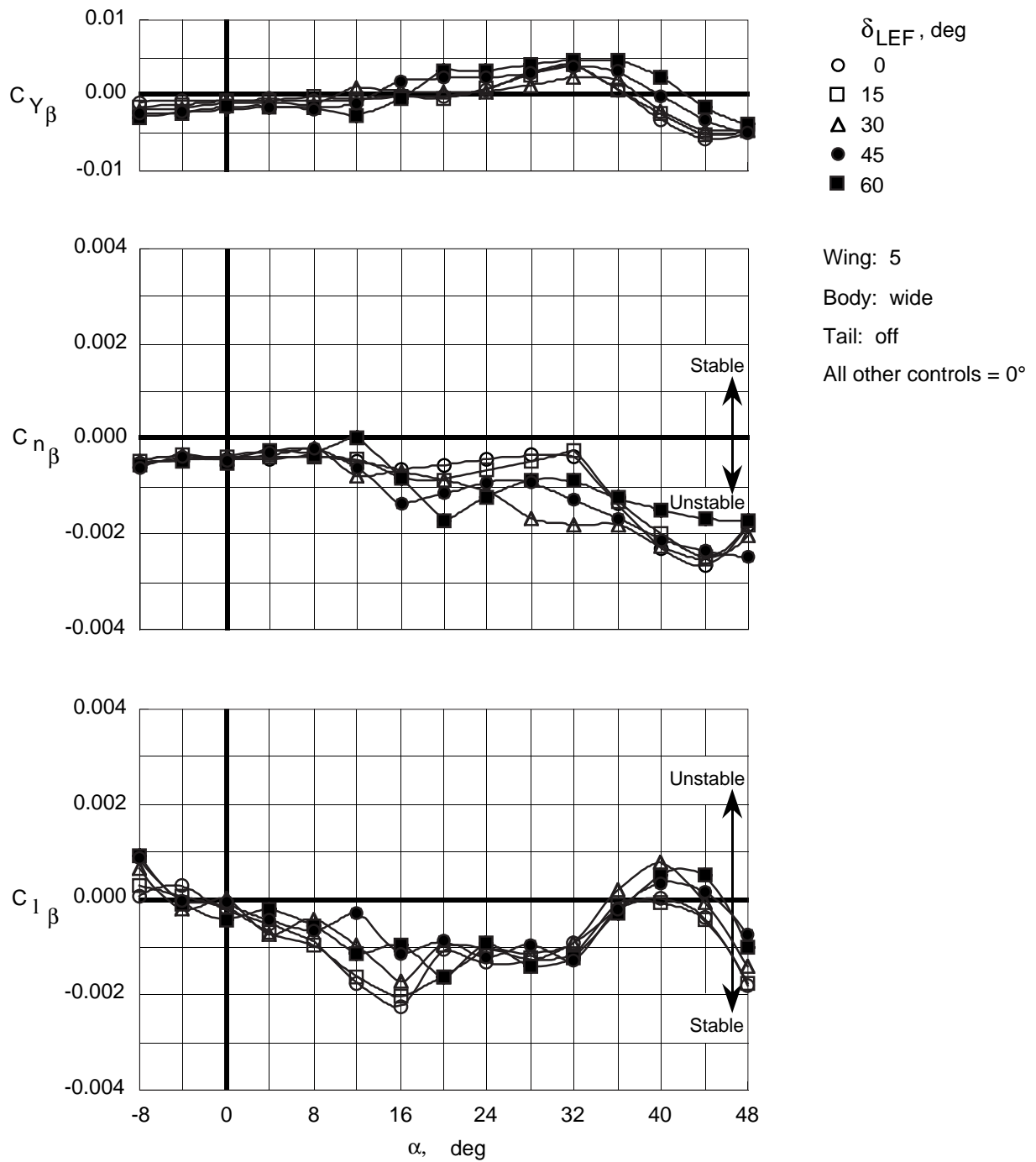


Figure 90. Effect of leading-edge flap deflections on lateral-directional stability characteristics of Wing 5 with wide top body on.

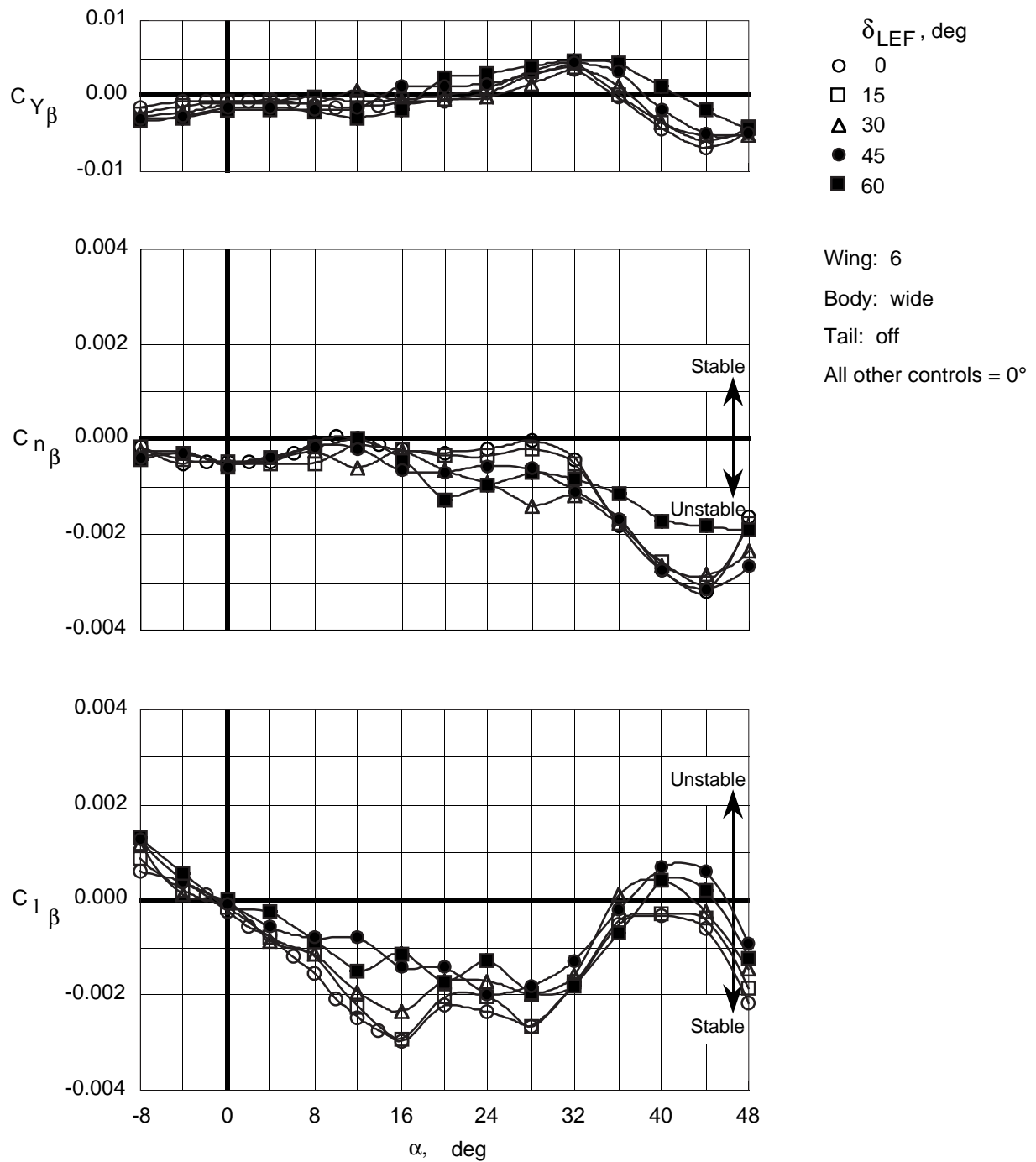


Figure 91. Effect of leading-edge flap deflections on lateral-directional stability characteristics of Wing 6 with wide top body on.

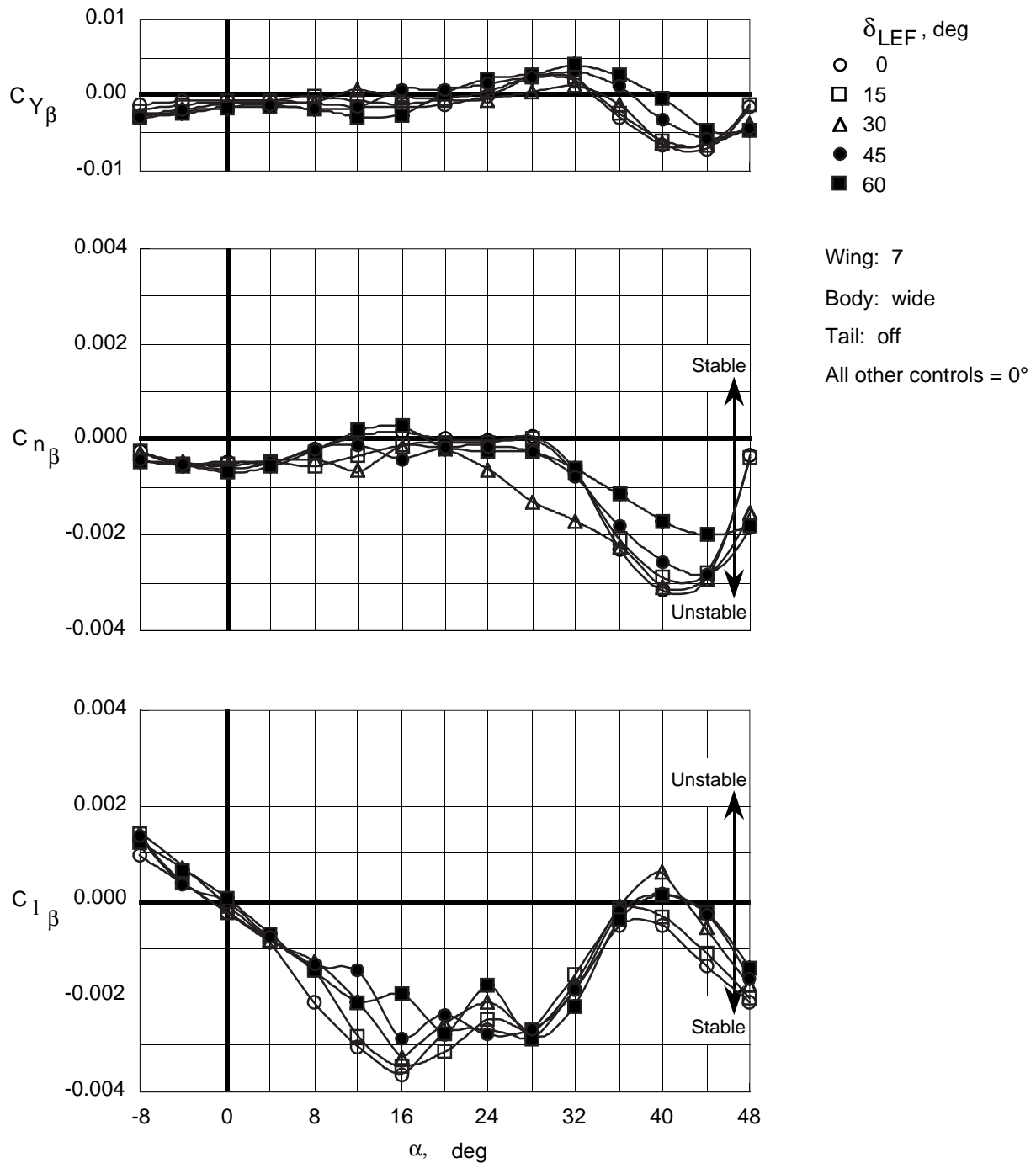


Figure 92. Effect of leading-edge flap deflections on lateral-directional stability characteristics of Wing 7 with wide top body on.

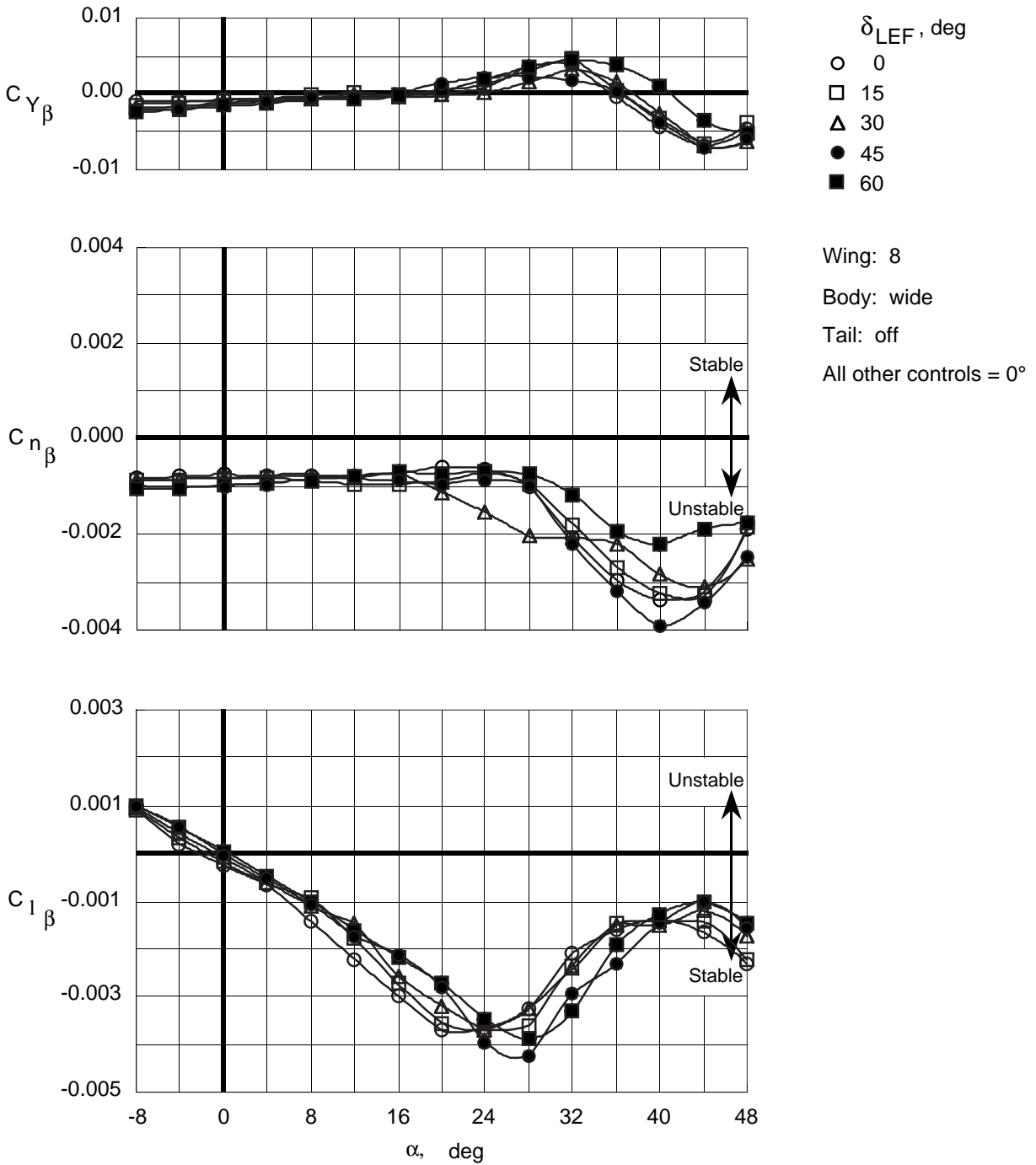


Figure 93. Effect of leading-edge flap deflections on lateral-directional stability characteristics of Wing 8 with wide top body on.

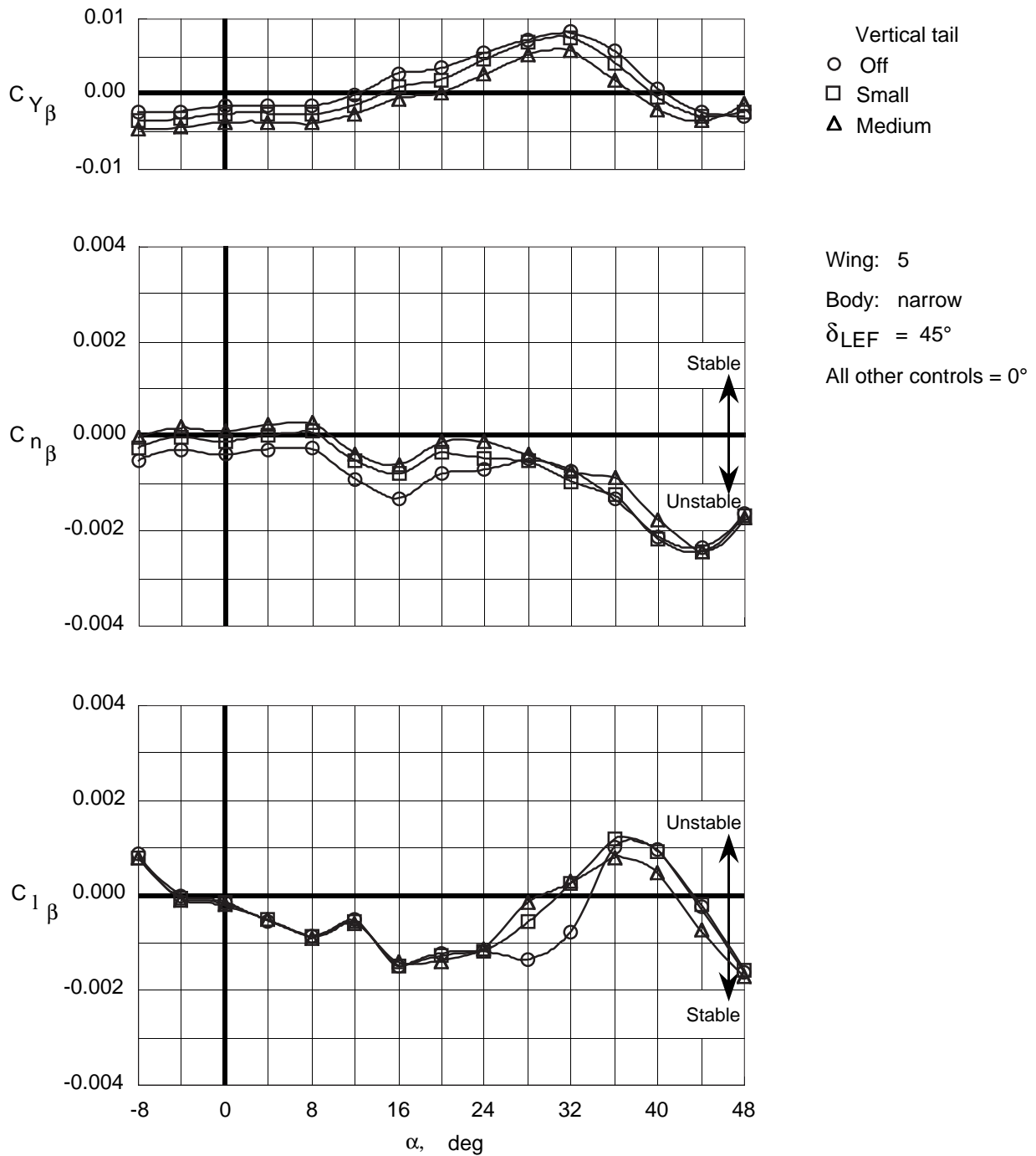


Figure 94. Effect of vertical tails on lateral-directional stability characteristics of Wing 5 with narrow top body on and leading-edge flaps deflected.

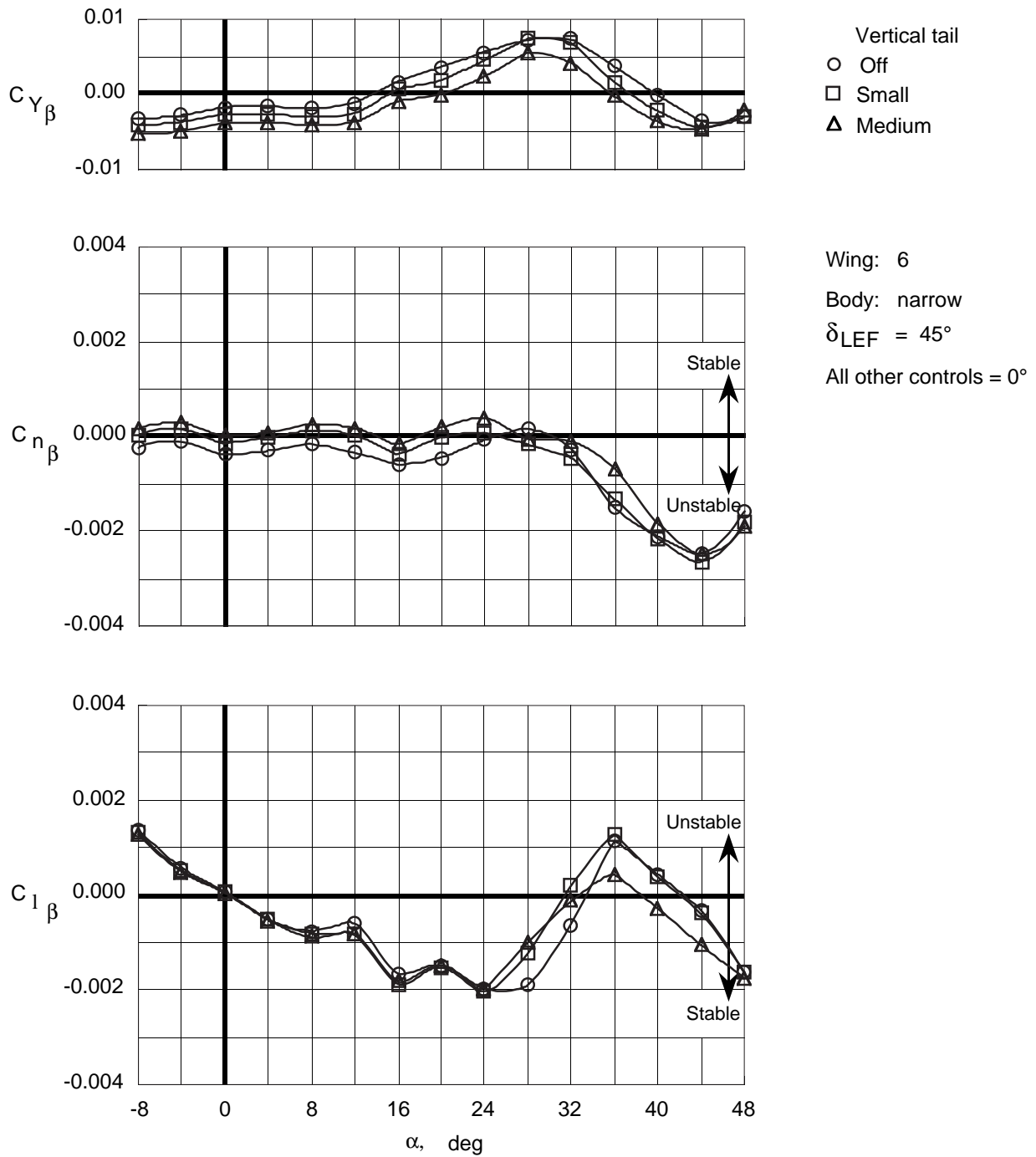


Figure 95. Effect of vertical tails on lateral-directional stability characteristics of Wing 6 with narrow top body on and leading-edge flaps deflected.

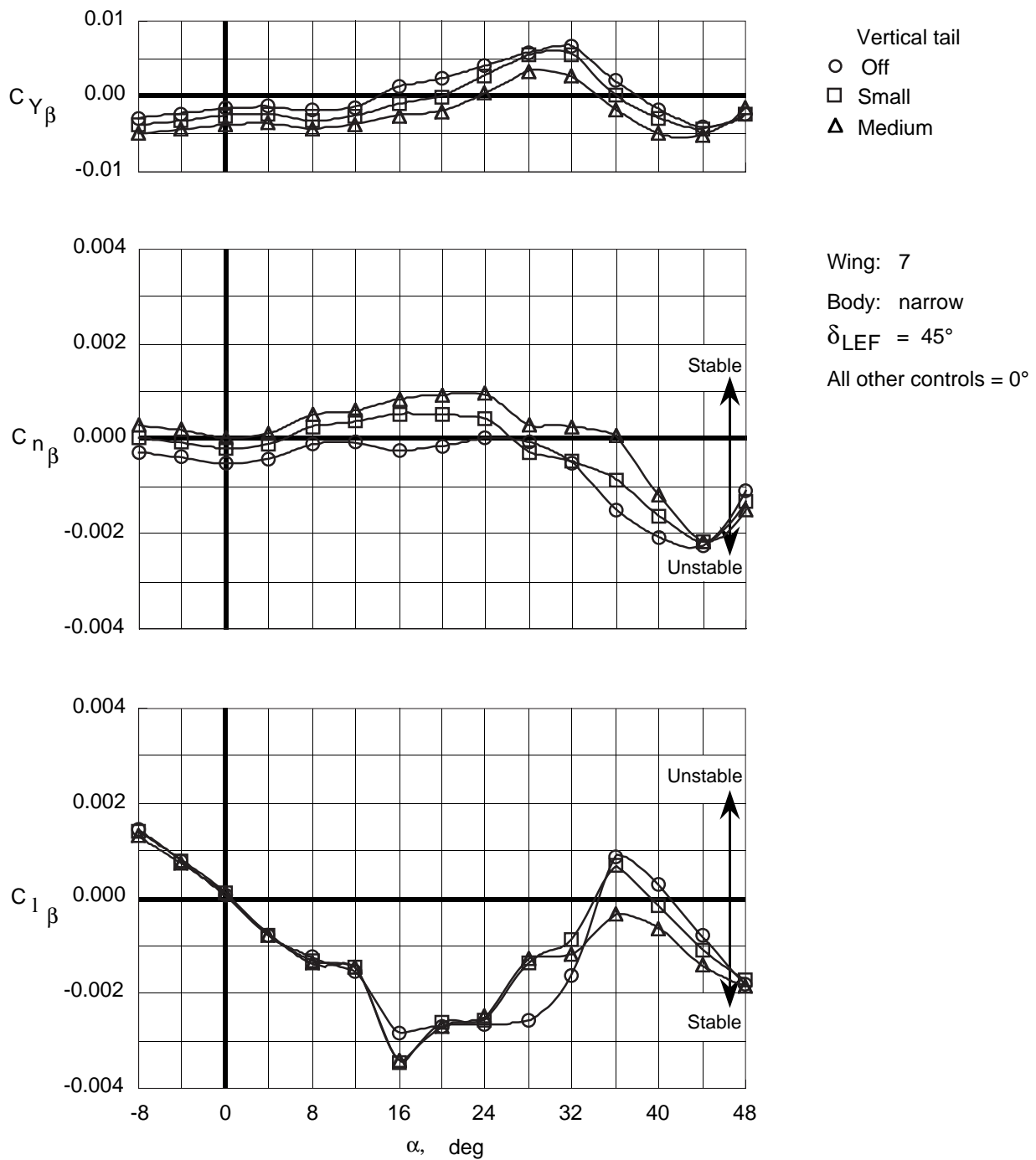


Figure 96. Effect of vertical tails on lateral-directional stability characteristics of Wing 7 with narrow top body on and leading-edge flaps deflected.

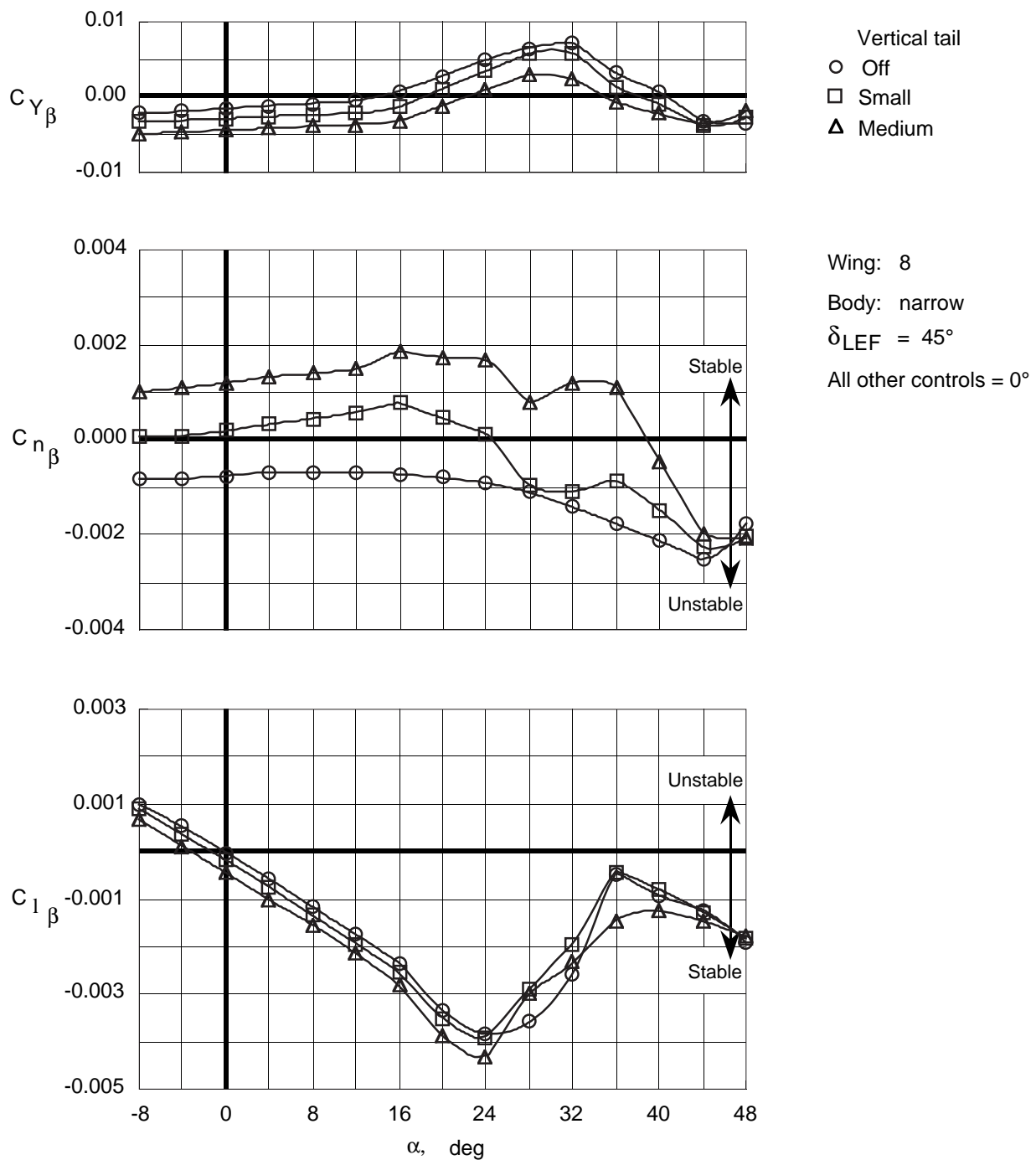


Figure 97. Effect of vertical tails on lateral-directional stability characteristics of Wing 8 with narrow top body on and leading-edge flaps deflected.

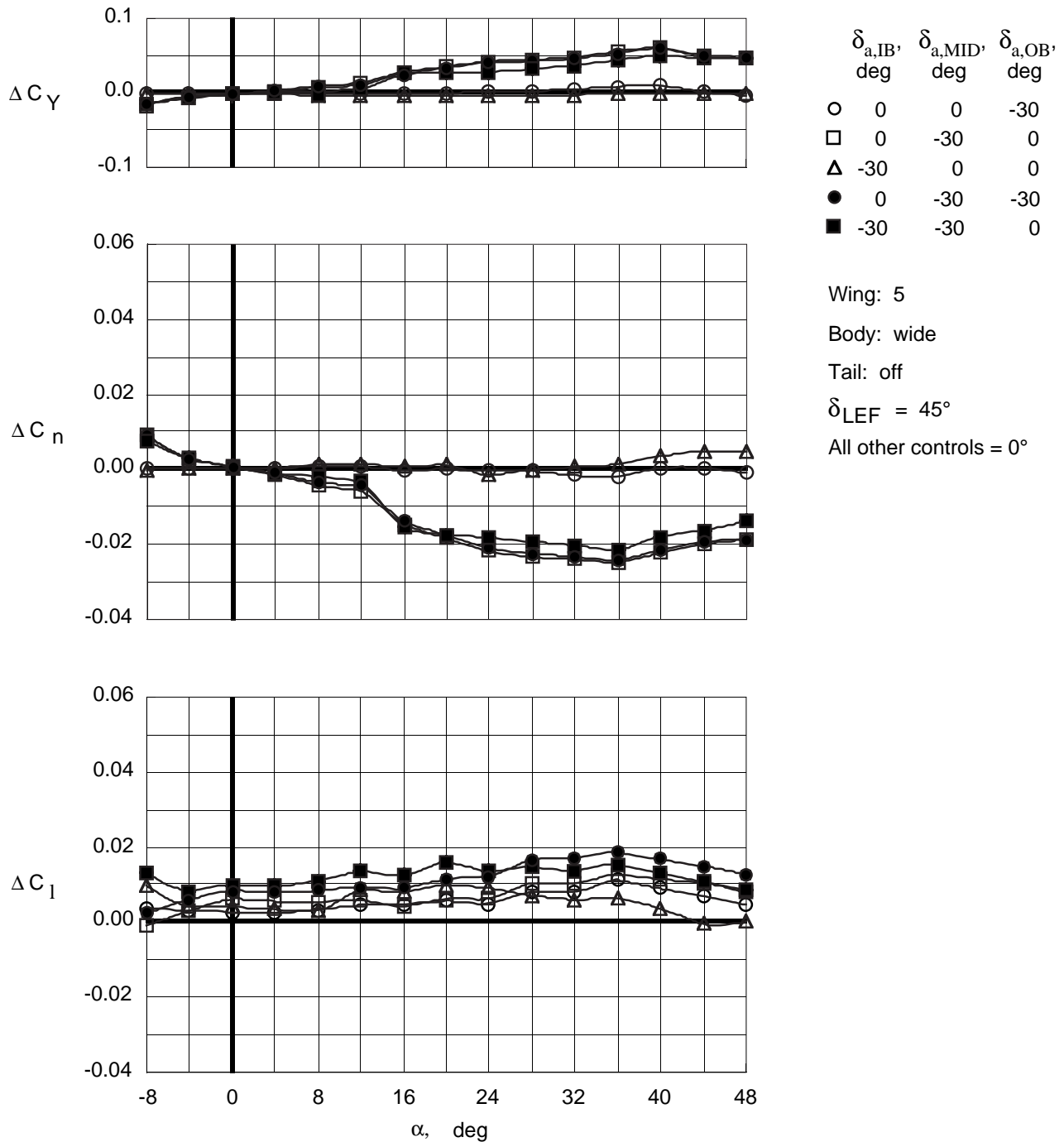


Figure 98. Control effectiveness of differential deflections of trailing-edge flaps on Wing 5 with wide top body on and leading-edge flaps deflected.

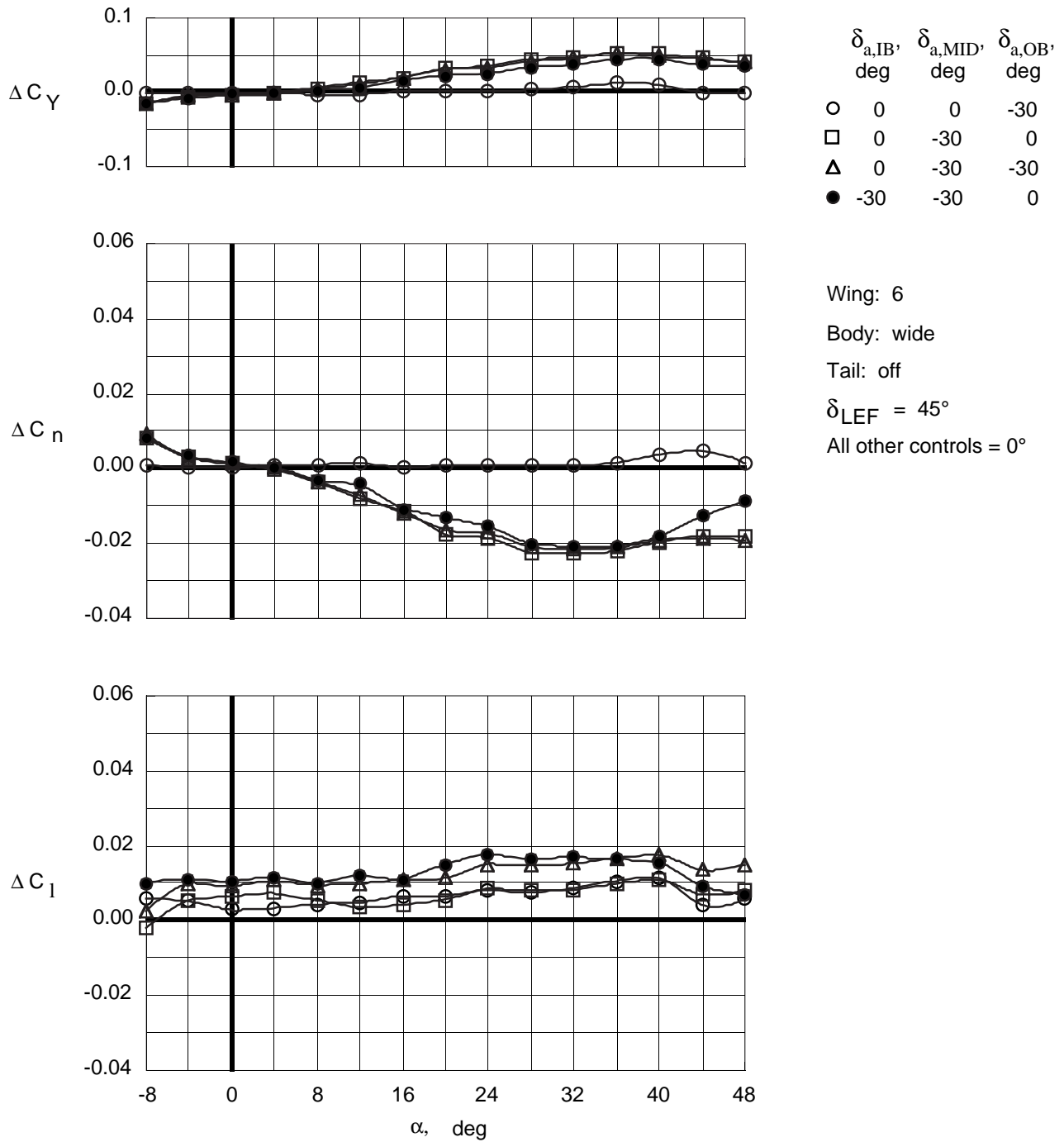


Figure 99. Control effectiveness of differential deflections of trailing-edge flaps on Wing 6 with wide top body on and leading-edge flaps deflected.

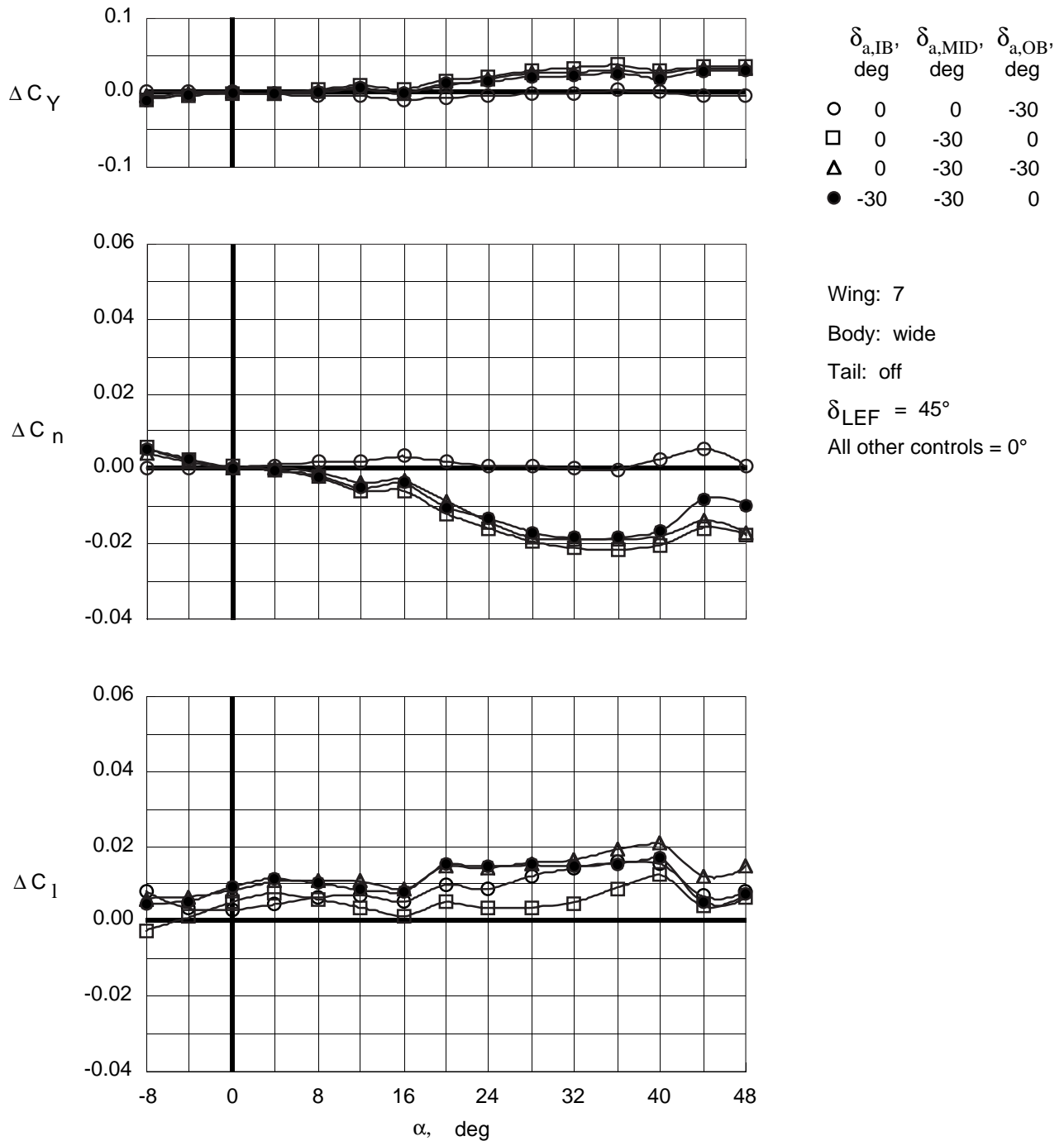


Figure 100. Control effectiveness of differential deflections of trailing-edge flaps on Wing 7 with wide top body on and leading-edge flaps deflected.

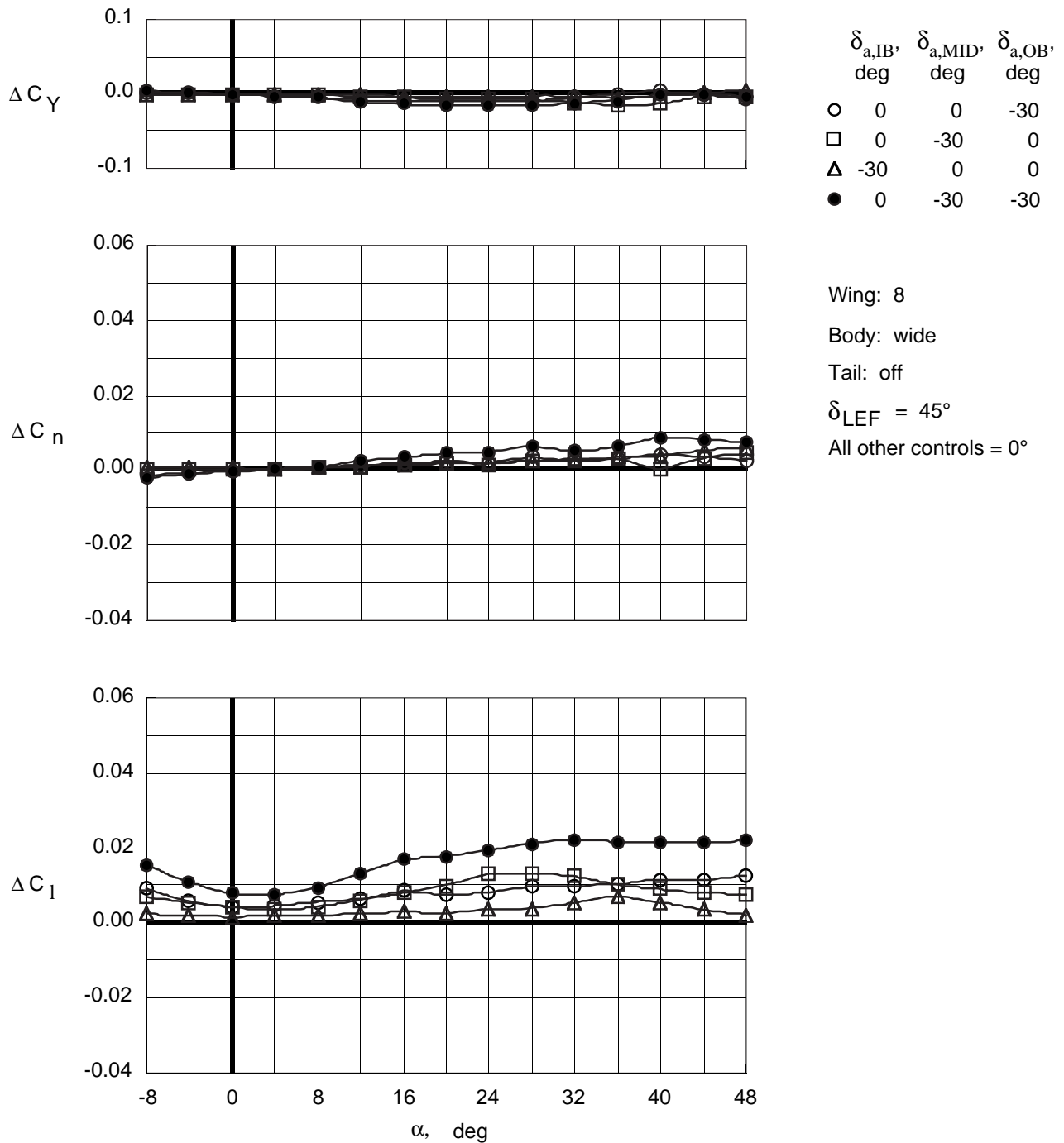


Figure 101. Control effectiveness of differential deflections of trailing-edge flaps on Wing 8 with wide top body on and leading-edge flaps deflected.

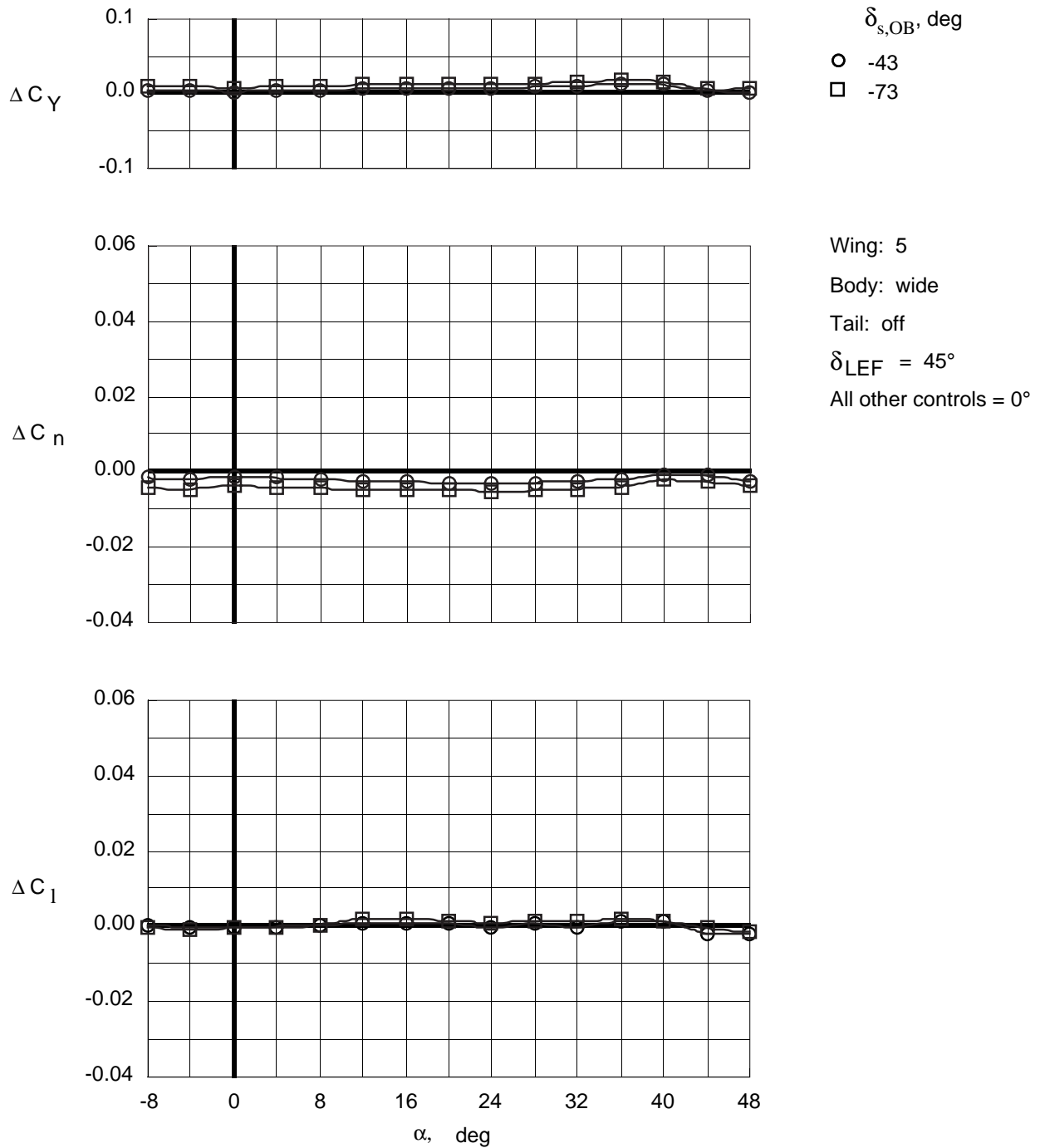


Figure 102. Control effectiveness of split deflections of right outboard trailing-edge flap on Wing 5 with wide top body on and leading-edge flaps deflected.

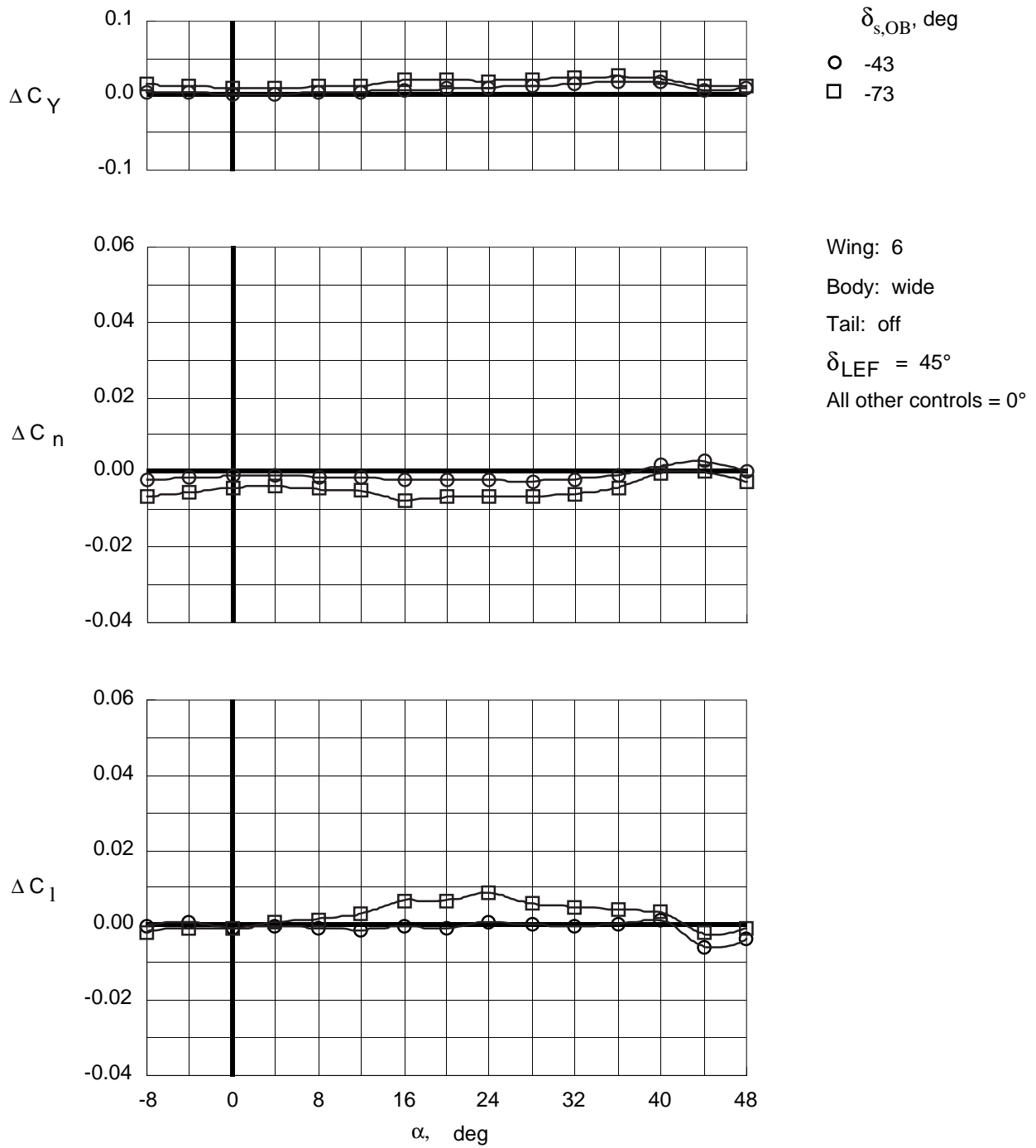


Figure 103. Control effectiveness of split deflections of right outboard trailing-edge flap on Wing 6 with wide top body on and leading-edge flaps deflected.

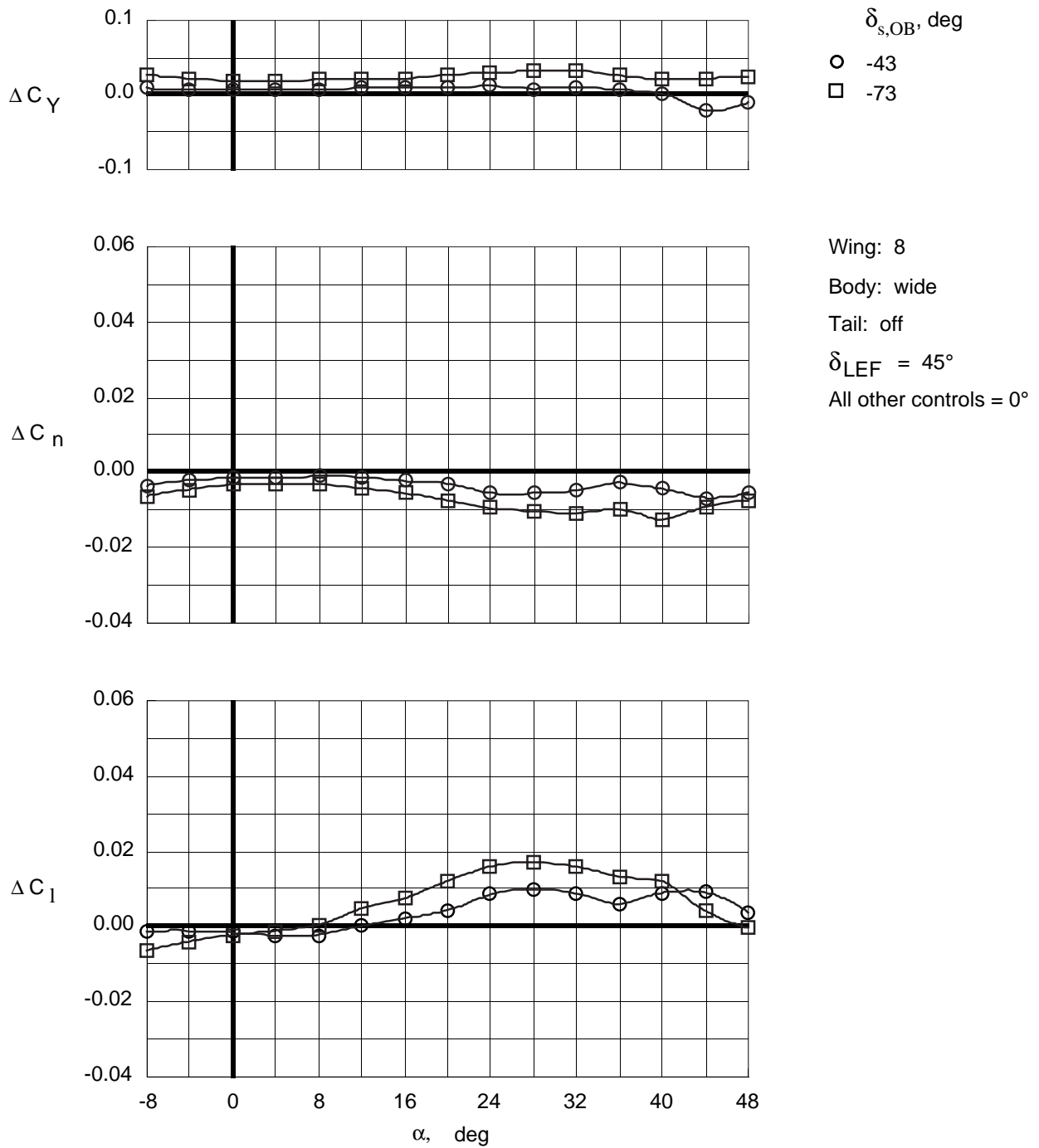


Figure 104. Control effectiveness of split deflections of right outboard trailing-edge flap on Wing 8 with wide top body on and leading-edge flaps deflected.

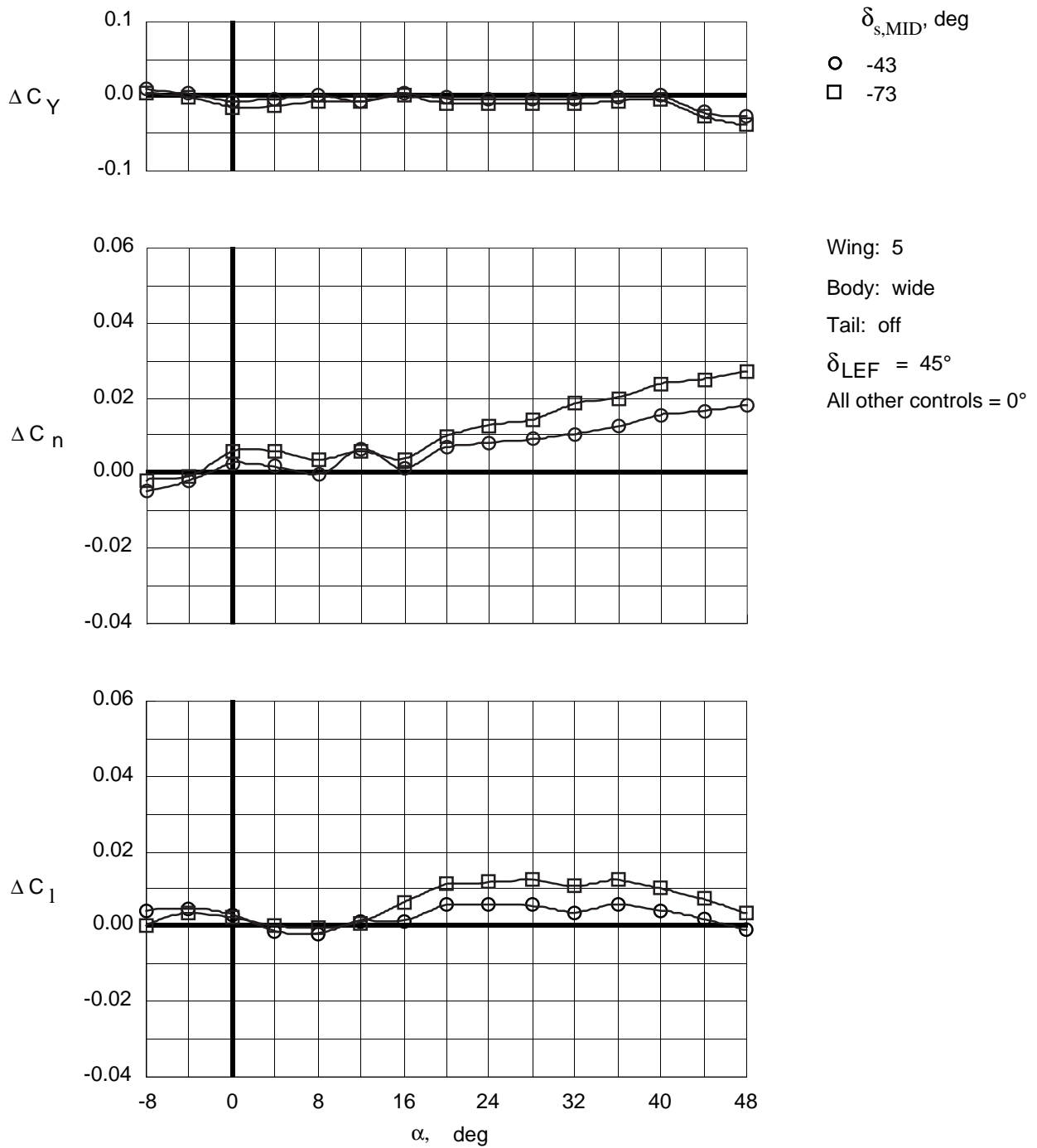


Figure 105. Control effectiveness of split deflections of right middle trailing-edge flap on Wing 5 with wide top body on and leading-edge flaps deflected.

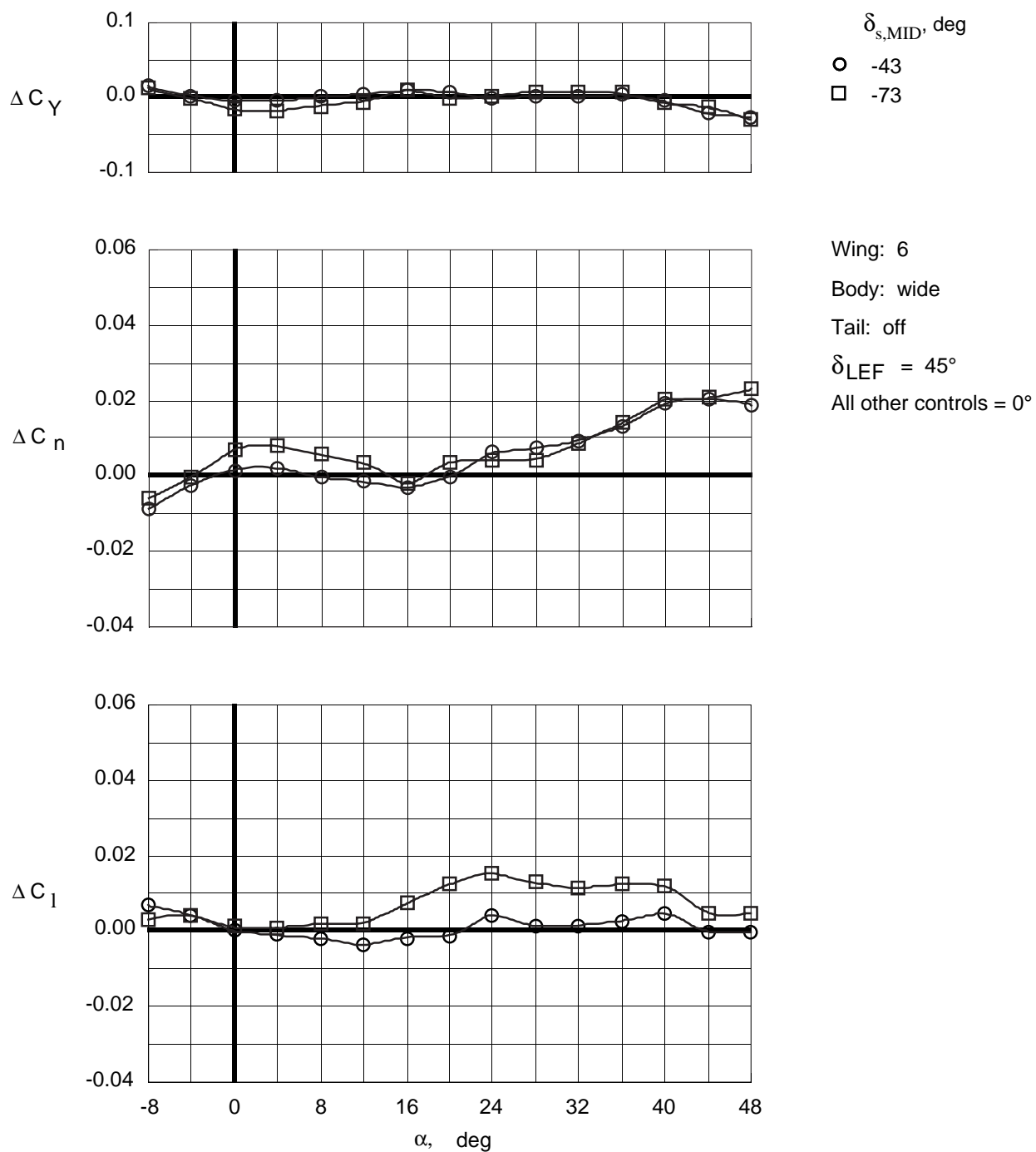


Figure 106. Control effectiveness of split deflections of right middle trailing-edge flap on Wing 6 with wide top body on and leading-edge flaps deflected.

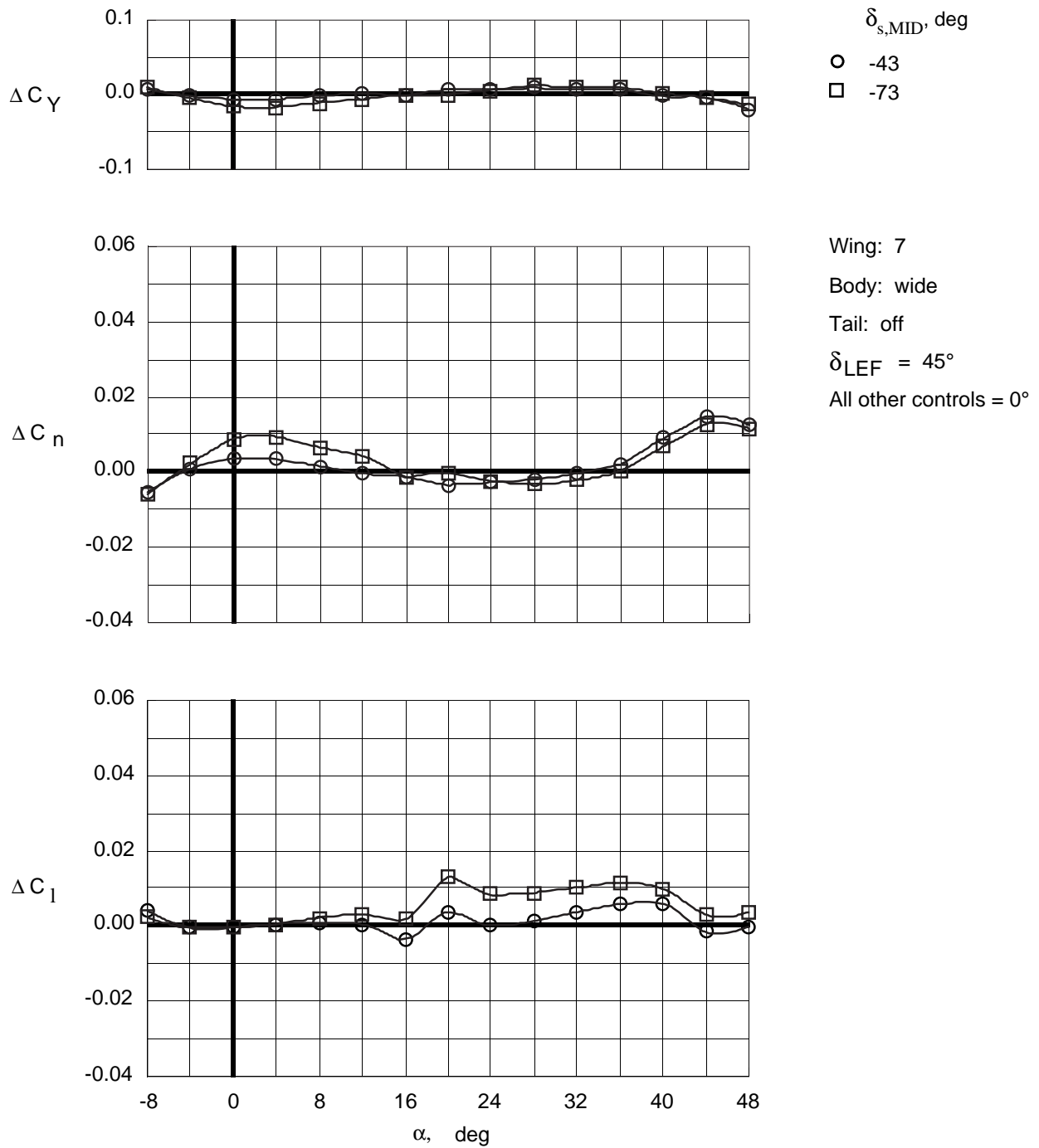


Figure 107. Control effectiveness of split deflections of right middle trailing-edge flap on Wing 7 with wide top body on and leading-edge flaps deflected.

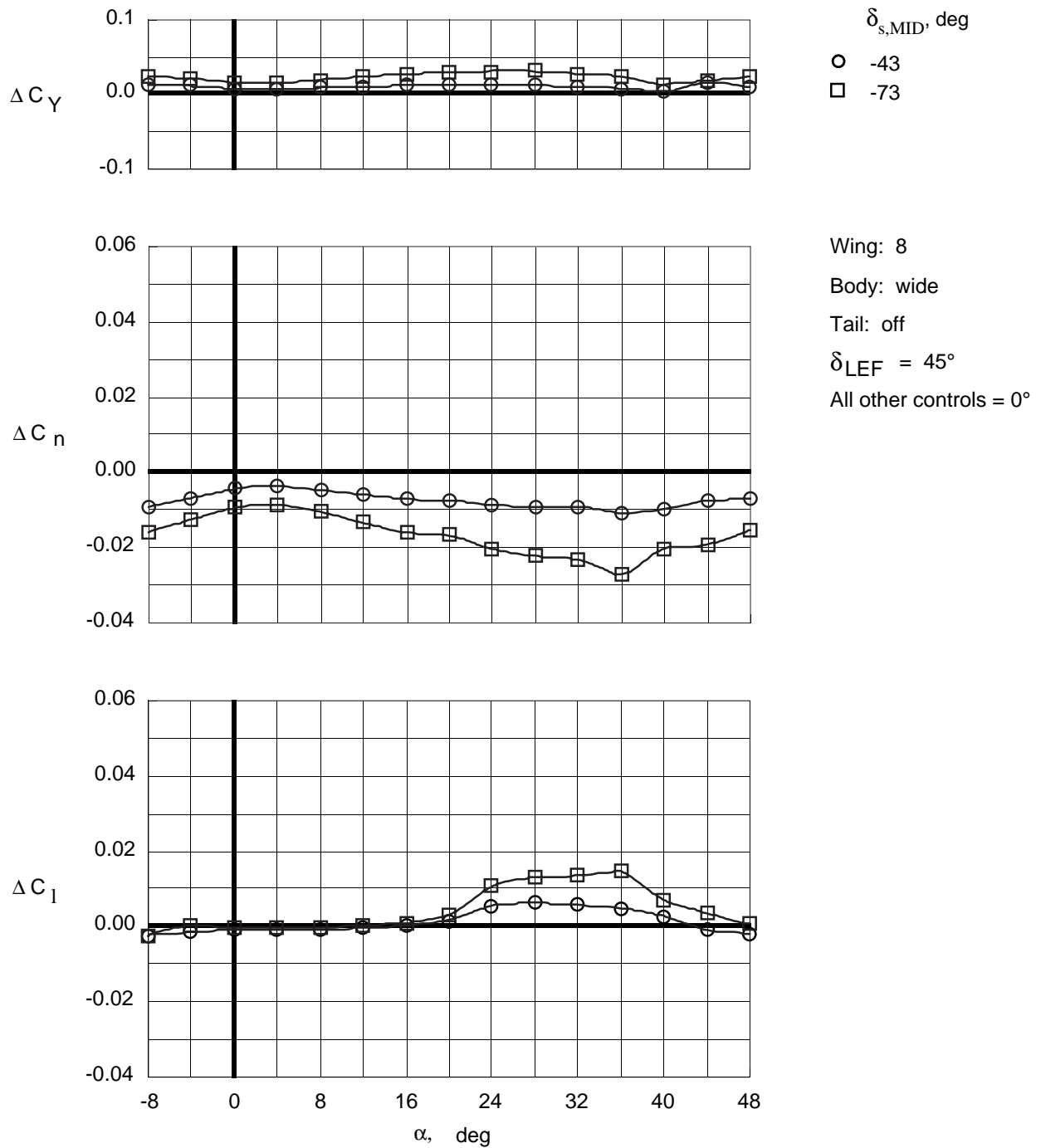


Figure 108. Control effectiveness of split deflections of right middle trailing-edge flap on Wing 8 with wide top body on and leading-edge flaps deflected.

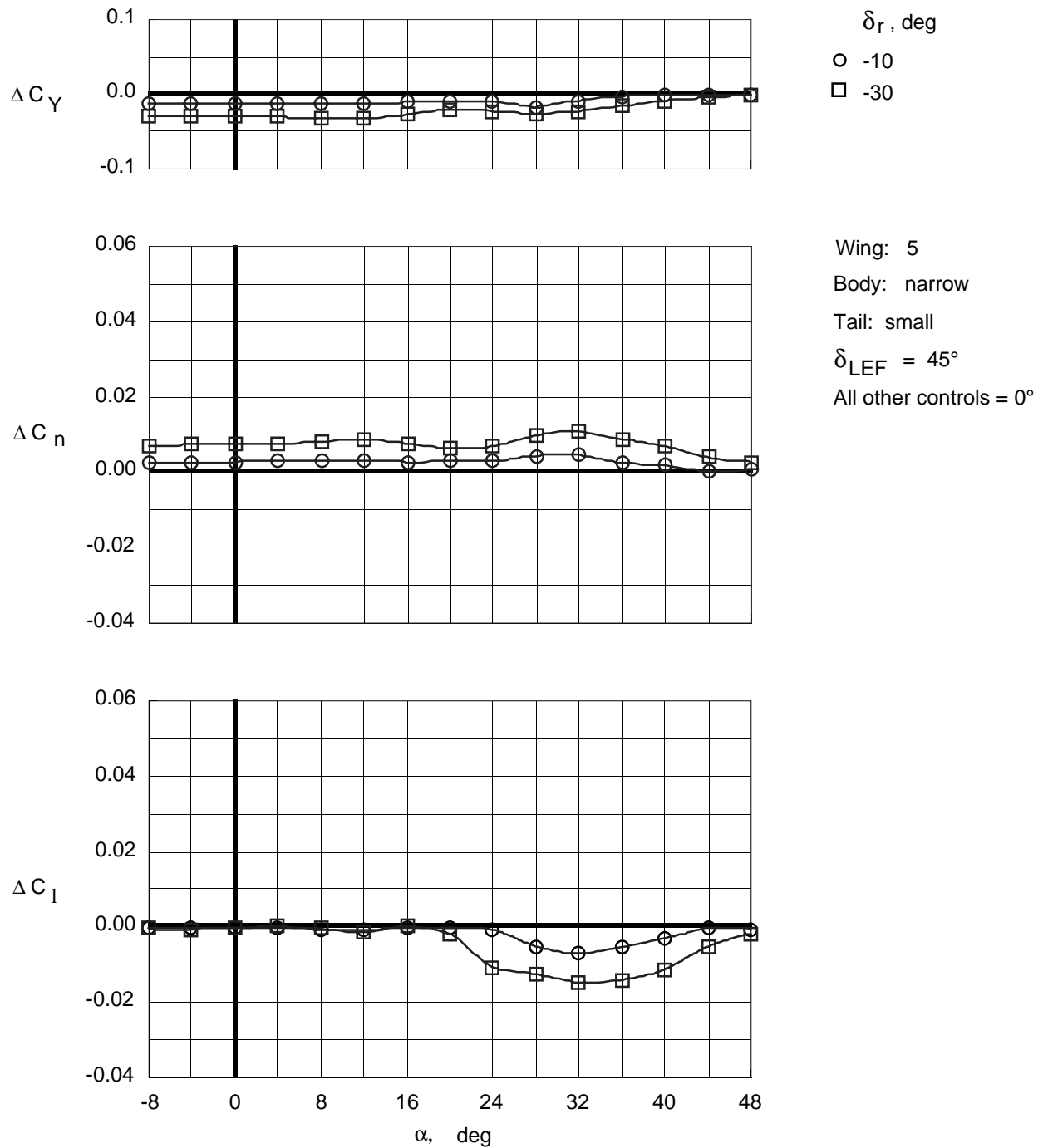


Figure 109. Control effectiveness of deflections of small vertical tails on Wing 5 with narrow top body on and leading-edge flaps deflected.

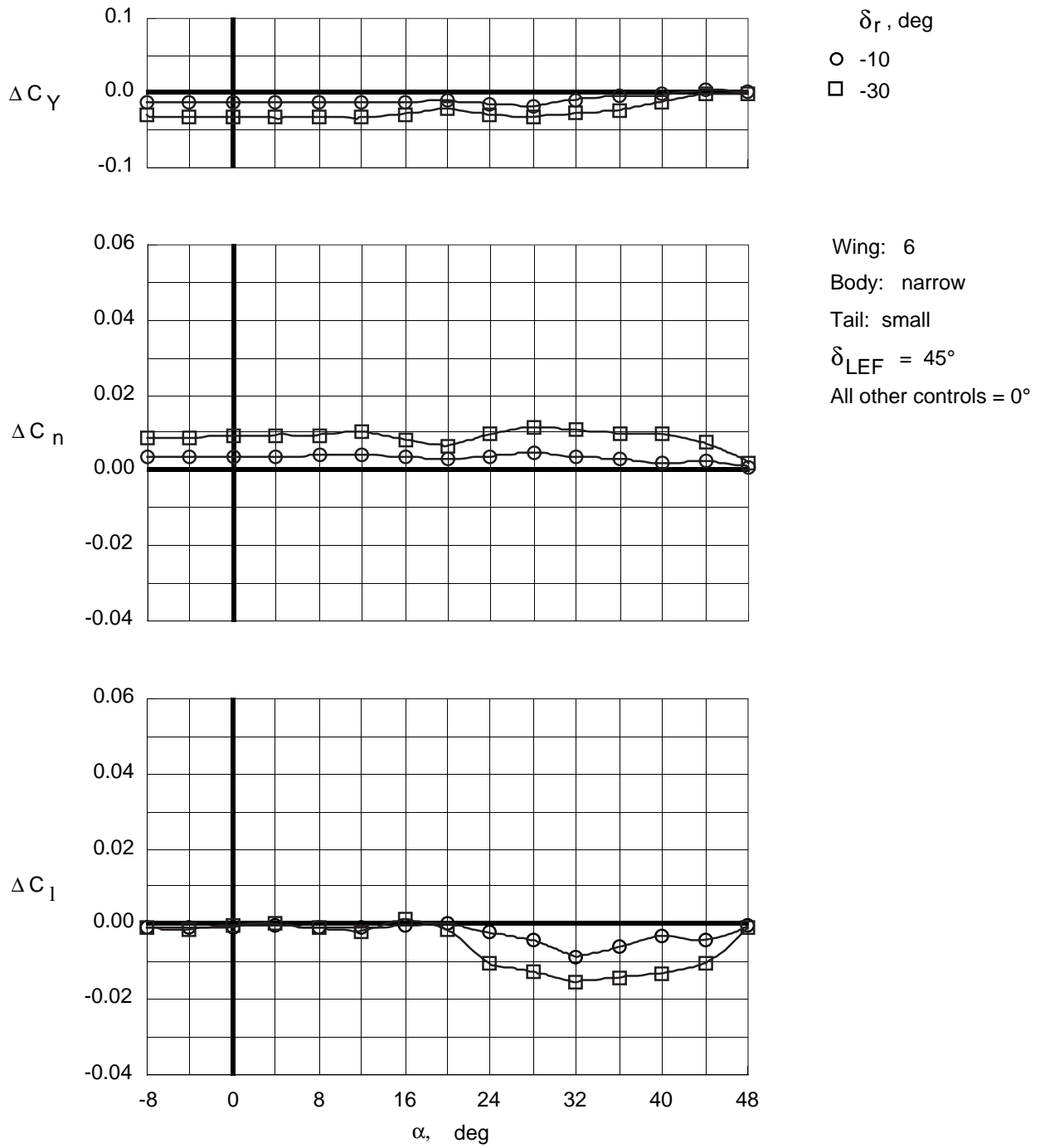


Figure 110. Control effectiveness of deflections of small vertical tails on Wing 6 with narrow top body on and leading-edge flaps deflected.

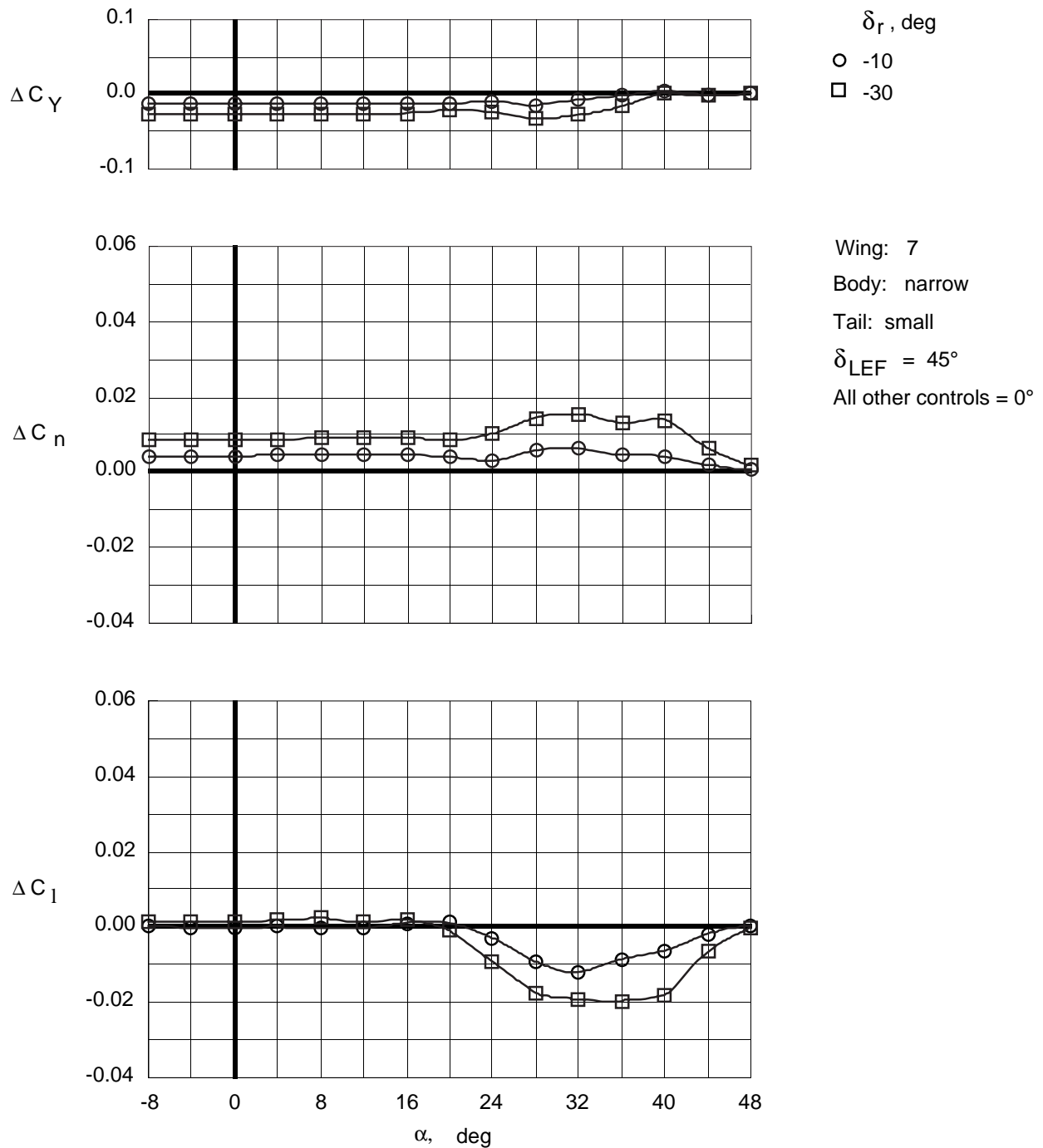


Figure 111. Control effectiveness of deflections of small vertical tails on Wing 7 with narrow top body on and leading-edge flaps deflected.

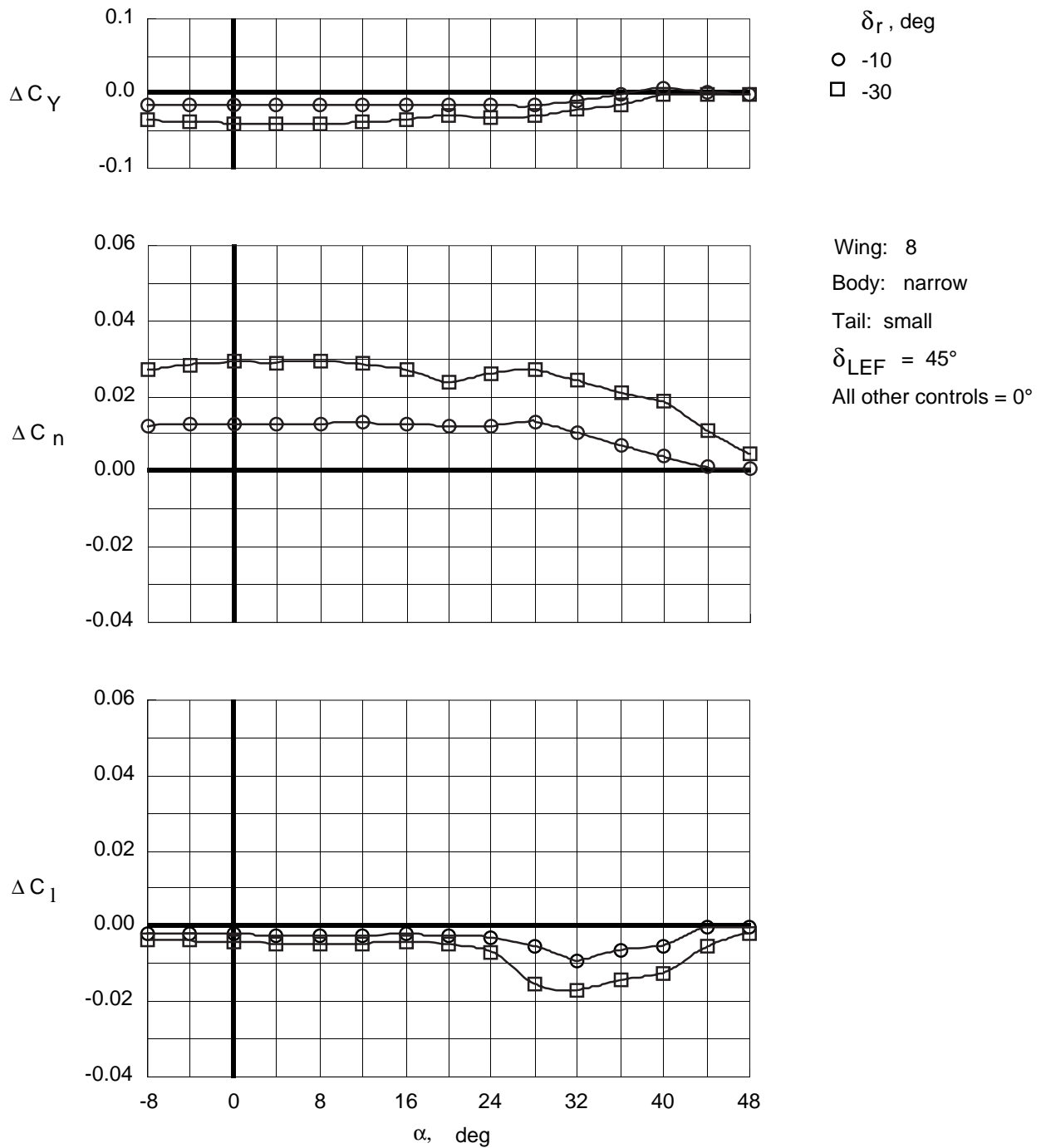


Figure 112. Control effectiveness of deflections of small vertical tails on Wing 8 with narrow top body on and leading-edge flaps deflected.

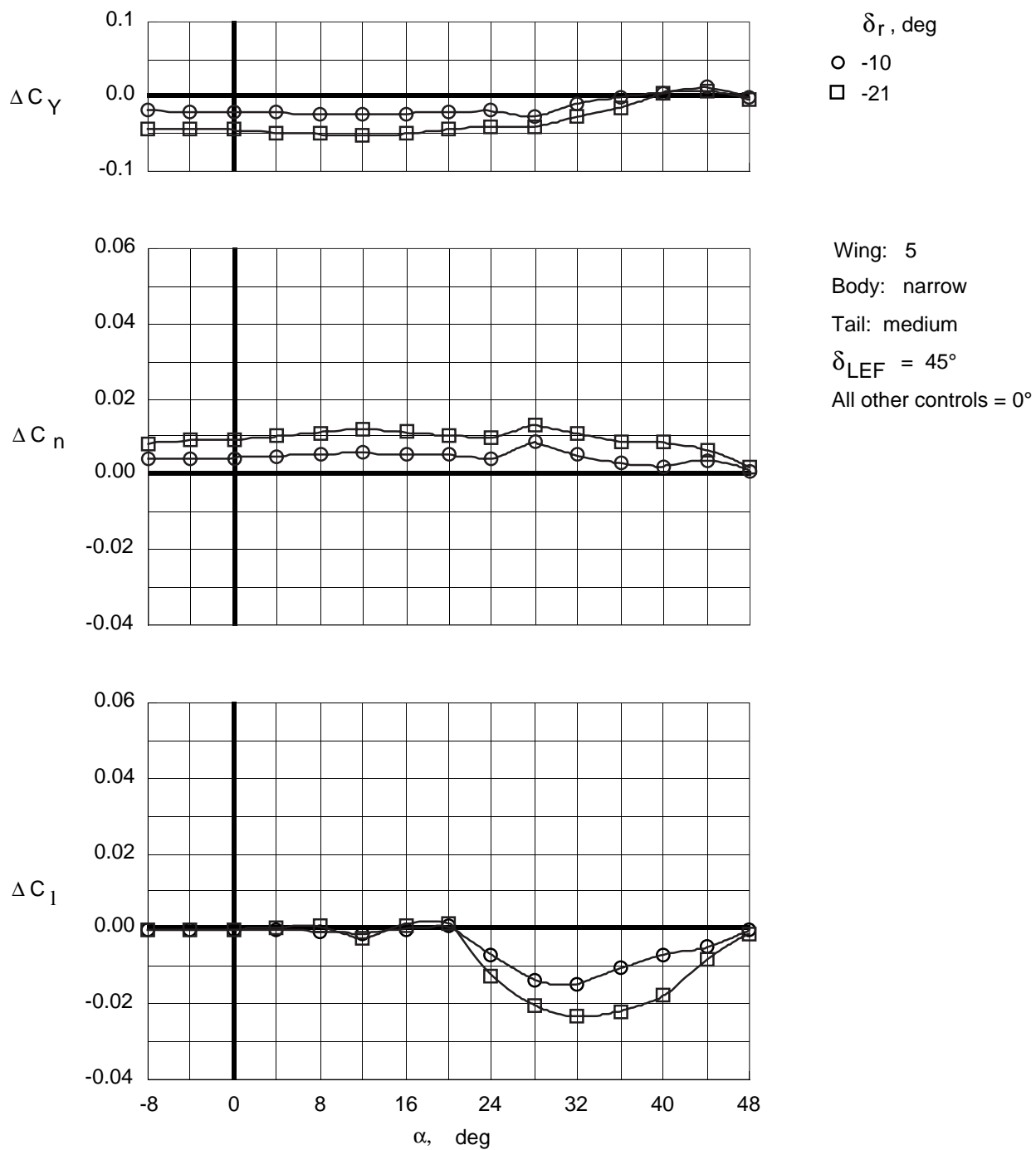


Figure 113. Control effectiveness of deflections of medium vertical tails on Wing 5 with narrow top body on and leading-edge flaps deflected.

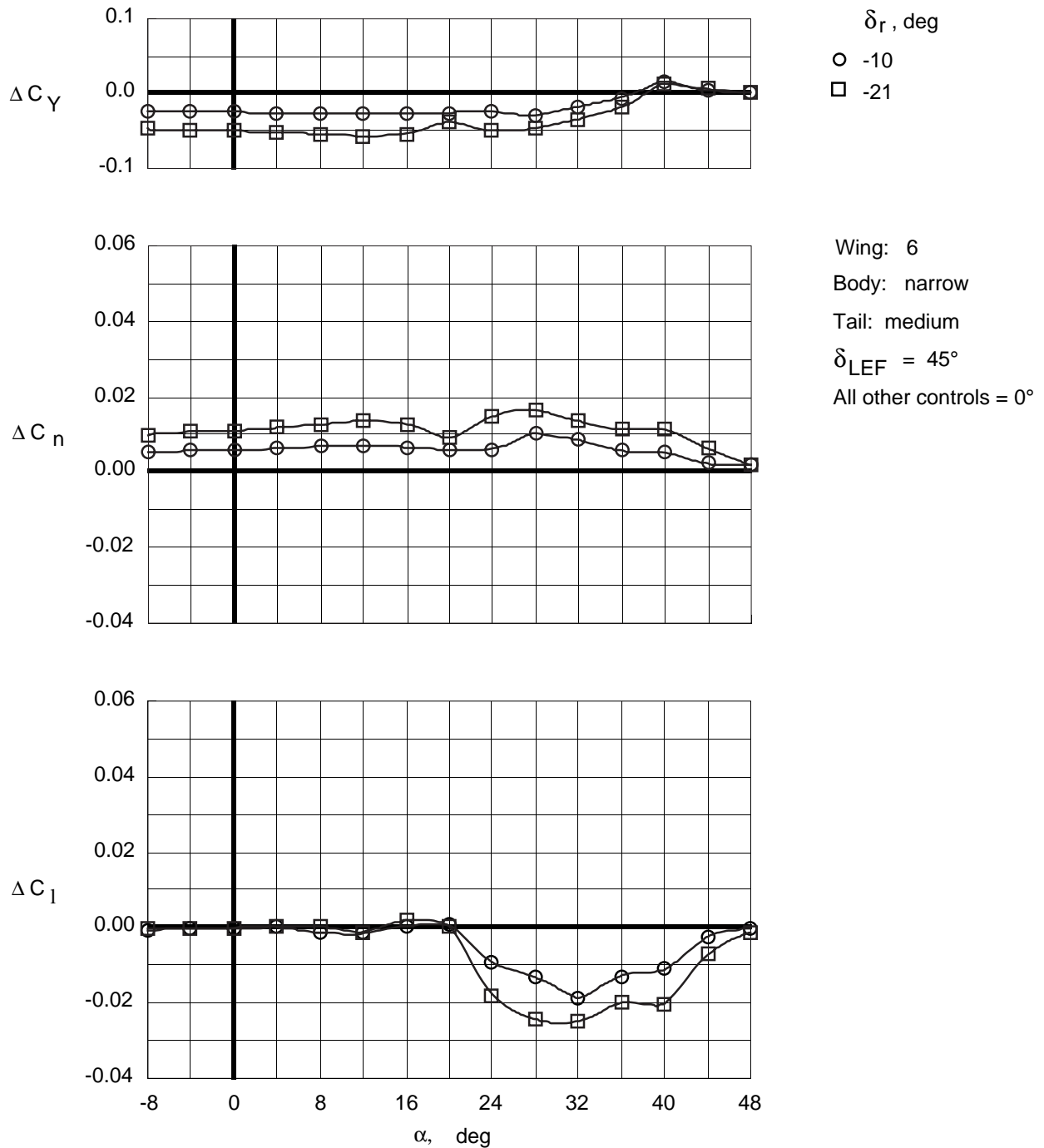


Figure 114. Control effectiveness of deflections of medium vertical tails on Wing 6 with narrow top body on and leading-edge flaps deflected.

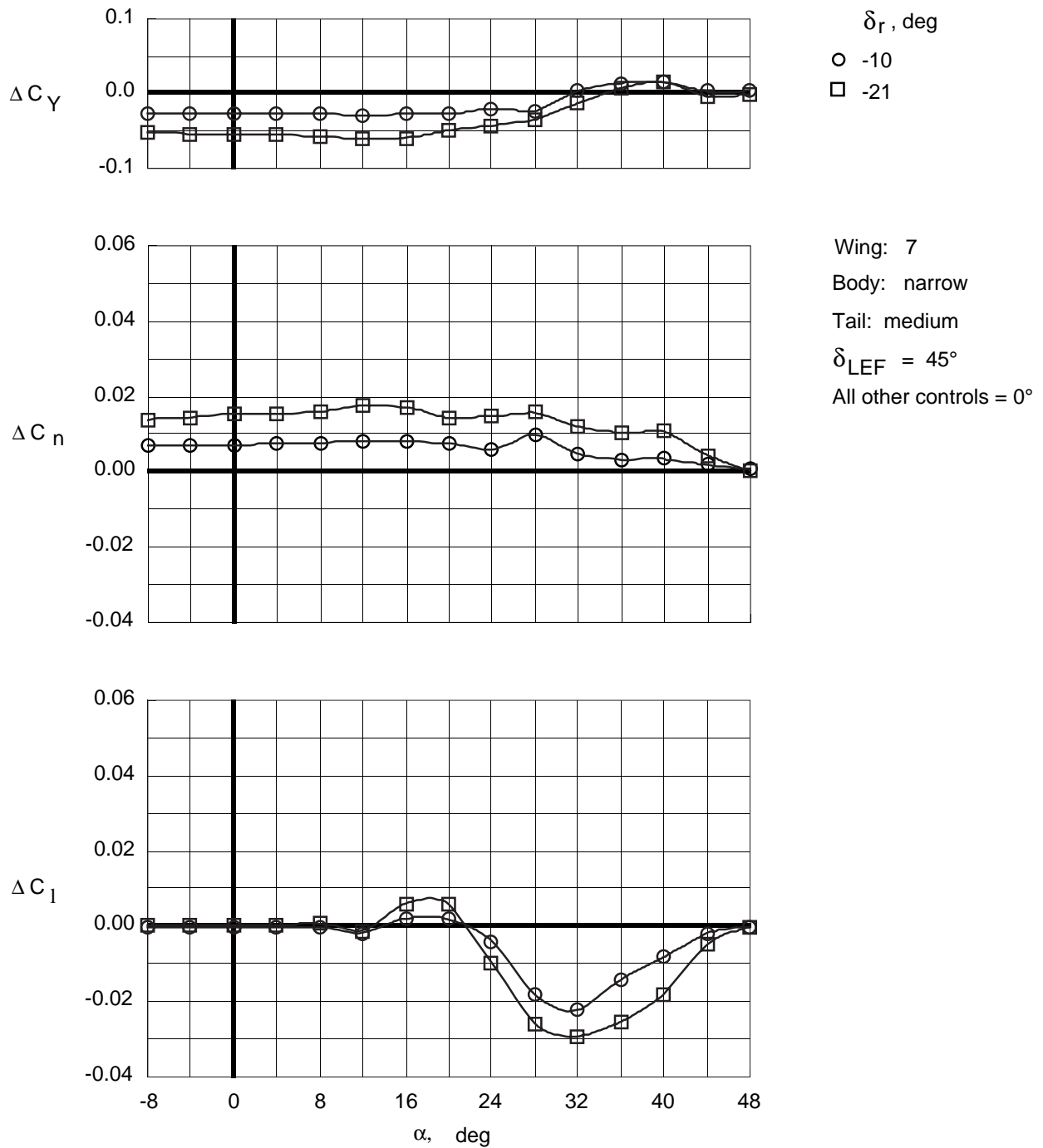


Figure 115. Control effectiveness of deflections of medium vertical tails on Wing 7 with narrow top body on and leading-edge flaps deflected.

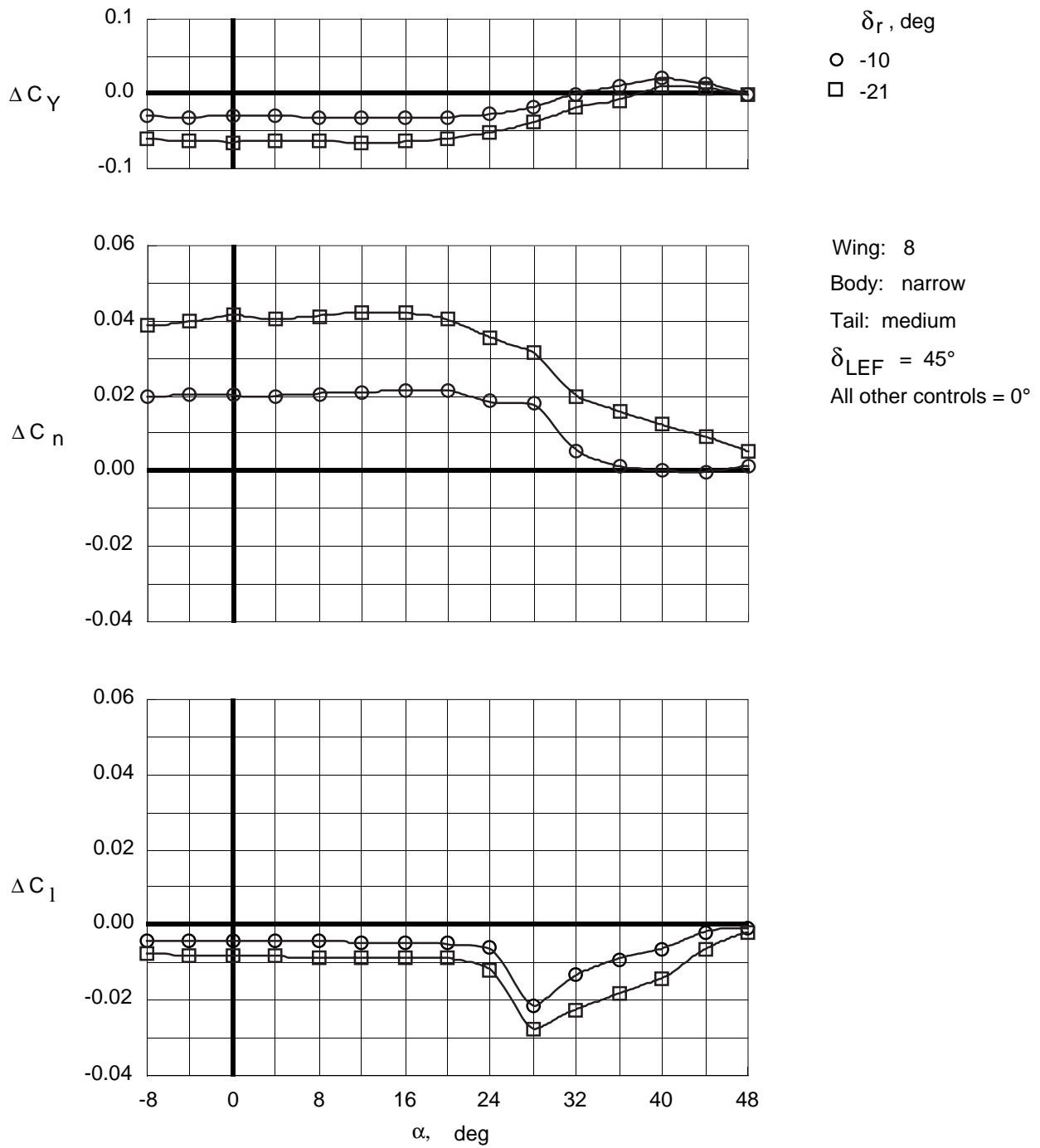
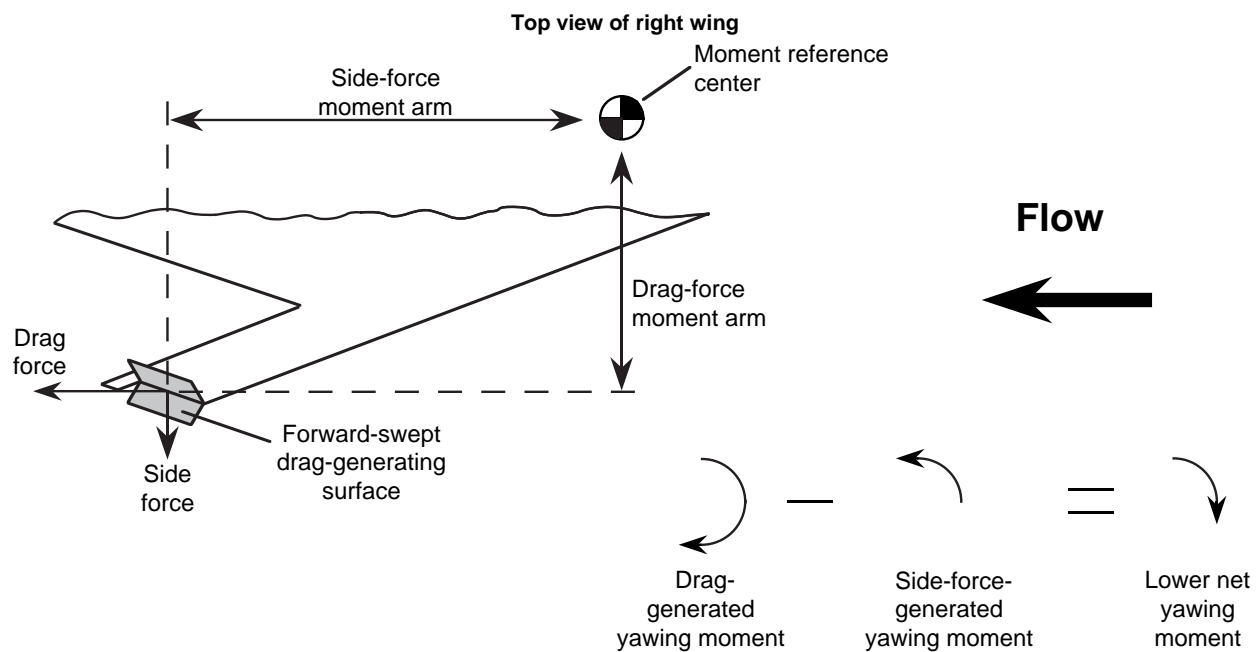
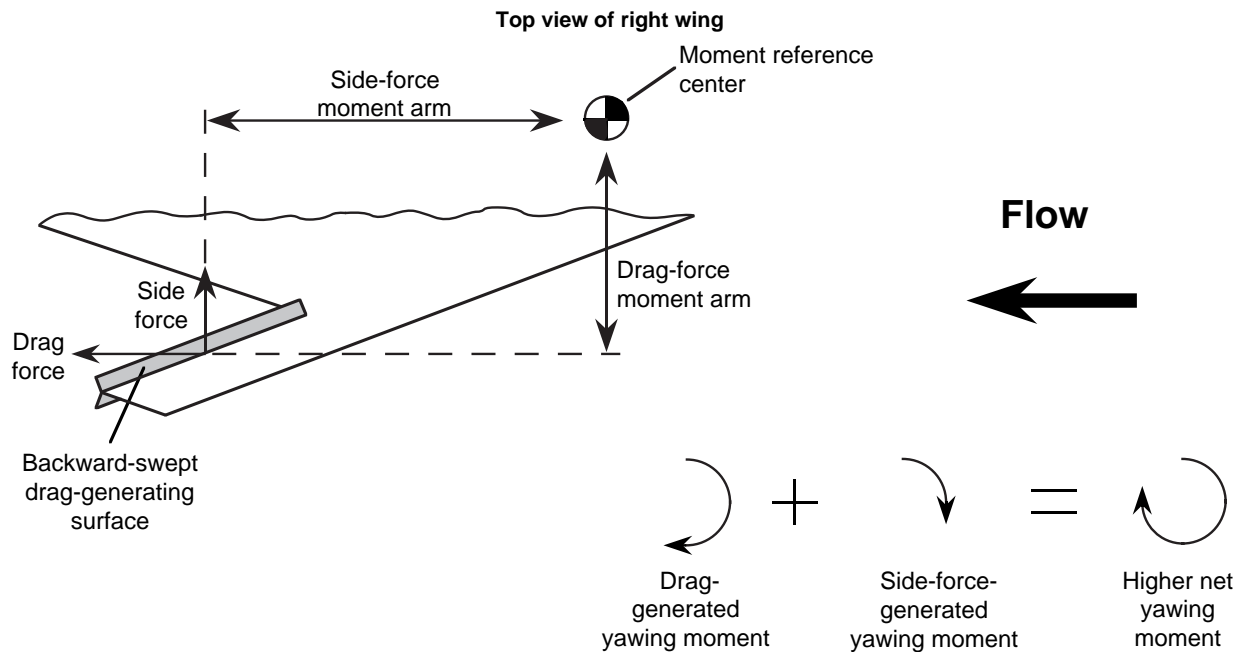


Figure 116. Control effectiveness of deflections of medium vertical tails on Wing 8 with narrow top body on and leading-edge flaps deflected.



(a) Forward-swept drag-generating surface.



(b) Backward-swept drag-generating surface.

Figure 117. Effect of hinge line sweep of drag-generating yaw control on side force and associated yawing moment generated by control deflection.



REPORT DOCUMENTATION PAGE			Form Approved OMB No. 0704-0188	
Public reporting burden for this collection of information is estimated to average 1 hour per response, including the time for reviewing instructions, searching existing data sources, gathering and maintaining the data needed, and completing and reviewing the collection of information. Send comments regarding this burden estimate or any other aspect of this collection of information, including suggestions for reducing this burden, to Washington Headquarters Services, Directorate for Information Operations and Reports, 1215 Jefferson Davis Highway, Suite 1204, Arlington, VA 22202-4302, and to the Office of Management and Budget, Paperwork Reduction Project (0704-0188), Washington, DC 20503.				
1. AGENCY USE ONLY (Leave blank)	2. REPORT DATE September 1995	3. REPORT TYPE AND DATES COVERED Technical Memorandum		
4. TITLE AND SUBTITLE Low-Speed Wind-Tunnel Investigation of the Stability and Control Characteristics of a Series of Flying Wings With Sweep Angles of 70°			5. FUNDING NUMBERS WU 505-68-30-01	
6. AUTHOR(S) Holly M. Ross, Scott P. Fears, and Thomas M. Moul				
7. PERFORMING ORGANIZATION NAME(S) AND ADDRESS(ES) NASA Langley Research Center Hampton, VA 23681-0001			8. PERFORMING ORGANIZATION REPORT NUMBER L-17460	
9. SPONSORING/MONITORING AGENCY NAME(S) AND ADDRESS(ES) National Aeronautics and Space Administration Washington, DC 20546-0001			10. SPONSORING/MONITORING AGENCY REPORT NUMBER NASA TM-4671	
11. SUPPLEMENTARY NOTES Ross and Moul: Langley Research Center, Hampton, VA, Fears: Lockheed Engineering & Sciences Company, Hampton, VA.				
12a. DISTRIBUTION/AVAILABILITY STATEMENT Unclassified-Unlimited Subject Category 05 Availability: NASA CASI (301) 621-0390			12b. DISTRIBUTION CODE	
13. ABSTRACT (Maximum 200 words) A wind-tunnel investigation was conducted in the Langley 12-Foot Low-Speed Tunnel to study the low-speed stability and control characteristics of a series of four flying wings over an extended range of angle of attack (-8° to 48°). Because of the current emphasis on reducing the radar cross section (RCS) of new military aircraft, the planform of each wing was composed of lines swept at a relatively high angle of 70°, and all the trailing edges and control surface hinge lines were aligned with one of the two leading edges. Three arrow planforms with different aspect ratios and one diamond planform were tested. The models incorporated leading-edge flaps for improved longitudinal characteristics and lateral stability and had three sets of trailing-edge flaps that were deflected differentially for roll control, symmetrically for pitch control, and in a split fashion for yaw control. Three top body widths and two sizes of twin vertical tails were also tested on each model. A large aerodynamic database was compiled that could be used to evaluate some of the trade-offs involved in the design of a configuration with a reduced RCS and good flight dynamic characteristics.				
14. SUBJECT TERMS Flying wings; Arrow wings; Diamond wings; Reduced radar cross section; Stability and control; High angle of attack			15. NUMBER OF PAGES 141	
			16. PRICE CODE A07	
17. SECURITY CLASSIFICATION OF REPORT Unclassified	18. SECURITY CLASSIFICATION OF THIS PAGE Unclassified	19. SECURITY CLASSIFICATION OF ABSTRACT Unclassified	20. LIMITATION OF ABSTRACT	